ifo
BEITRÄGE
zur Wirtschaftsforschung

81
2019

# Geography Matters: Spatial Dimensions of Trade, Migration and Growth

*Thomas Steinwachs*

ifo INSTITUTE
Leibniz Institute for Economic Research
at the University of Munich

ifo
BEITRÄGE
zur Wirtschaftsforschung

81
2019

# Geography Matters: Spatial Dimensions of Trade, Migration and Growth

*Thomas Steinwachs*

*Herausgeber der Reihe: Clemens Fuest*
*Schriftleitung: Chang Woon Nam*

ifo INSTITUTE
Leibniz Institute for Economic Research
at the University of Munich

**Bibliografische Information der Deutschen Nationalbibliothek**

Die Deutsche Nationalbibliothek verzeichnet diese Publikation
in der Deutschen Nationalbibliografie; detaillierte bibliografische
Daten sind im Internet über
http://dnb.d-nb.de
abrufbar.

ISBN: 978-3-95942-056-3



Druck: ifo Institut, München

ifo Institut im Internet:
http://www.cesifo-group.de

# Preface

This volume was prepared by Thomas Steinwachs while he was working at the ifo Center for International Economics. It was completed in September 2018 and accepted as a doctoral dissertation by the Department of Economics at the University of Munich (LMU). It is a collection of four self-contained essays which are included as separate chapters.

Each chapter considers the spatial dimension of economic processes in applied empirical work, concerning measurement, data handling and econometric methodology. Chapter 1 applies an econometric gravity analysis to bilateral trade flows to assess how successful the European Schengen Agreement has been in boosting international trade. It proposes a new indicator variable to account for the plurilateral agreement's spatial dimension. Chapter 2 provides a gravity analysis of international migration flows to investigate the impact of natural disasters on the movement of people between countries. It employs spatially mapped geographic data on the physical intensity of natural disasters. Chapter 3 zooms in on the local growth effects of natural disasters and assesses the associated diversion of economic activity across space. For this purpose, it introduces a new database combining physical intensities of geological and meteorological events with night-light emissions at spatially disaggregated grid cells. Chapter 4 further investigates the role of spatial connectivity for spillover transmission, exploiting geographic information on country borders and road networks.

Keywords: Trade Integration, European Integration, Schengen Agreement, Gravity Model, Natural Disasters, International Migration, Income Group Heterogeneity, Weather Shocks, Night-Light Emission, Growth, Spatial Spillovers, Grid Cell Analysis

JEL-No: F10, F15, F22, N74, N94, O15, O18, O44, Q54, R12

# Acknowledgments

I would like to express my sincere gratitude to the people who supported me along the way and who made this work possible.

Above all, I am deeply grateful to my supervisor Gabriel Felbermayr, who gave me the opportunity to become a part of his team. Gabriel has always been an inexhaustible source of knowledge and inspiration. His outstanding guidance has been driving my scientific progress from the very beginning. With his trust in my abilities and judgment, he greatly encouraged my pursuit to invest in new skills and to incorporate new technical advances into my work. In addition, Gabriel pulled out all the stops in facilitating scientific exchange and creating a fruitful environment.

Moreover, I am grateful to Carsten Eckel for agreeing to co-supervise this thesis and to Ilan Noy for accepting to serve on my committee. Both have shown interest in my research, asked the right questions and provided helpful advice. Special appreciation also applies to Jasmin Gröschl for countless stimulating discussions and very productive and successful collaborations on our joint publications and ongoing projects. Her mentoring has been an invaluable source of support. Also, I thank Mark Sanders and Vincent Schippers for being committed coauthors. Finally, I owe thanks to Wilhelm Kohler for sparking my passion for the field when it was needed the most.

Over the years, I have received vast encouragement from friends and colleagues at the Universities of Tübingen, Adelaide and Munich and at ifo Institute, particularly in my department. I am very grateful for all the inspiring conversations at day and night, for brilliant comments on my research and for many enjoyable breaks.

Shoreless gratitude goes to my beloved wife, to my parents and family and to my closest friends. They always put their faith in me and my capabilities, even when I misplaced mine. With their unconditional support, patience and understanding, they have had my back at all times and have a great share in this work. You folks rock!

∞

# Geography Matters: Spatial Dimensions of Trade, Migration and Growth

## Inaugural-Dissertation

zur Erlangung des Grades Doctor oeconomiae publicae (Dr. oec. publ.)

an der Ludwig-Maximilians-Universität München

**2018**

vorgelegt von

Thomas Steinwachs

Referent: Prof. Gabriel Felbermayr, Ph.D.
Korreferent: Prof. Dr. Carsten Eckel

Promotionsabschlussberatung: 30.01.2019

Datum der mündlichen Prüfung: 24.01.2019
Namen der Berichterstatter: Prof. Gabriel Felbermayr, Ph.D.
Prof. Dr. Carsten Eckel
Prof. Ilan Noy, Ph.D.

# Contents

# List of Figures

# List of Tables

# Introduction

This dissertation is a collection of four self-contained essays which are included as separate chapters. Each chapter addresses a distinct research question in the area of international economics and provides an independent piece of research, including its own introduction, conclusion and appendix. Despite this independence, all chapters emerge from a continuous research agenda and feature numerous links regarding methodology, research objectives and findings.

The overarching theme is to consider the spatial dimension of economic processes in applied empirical work, concerning measurement, data handling and econometric methodology. In a nutshell, Chapter 1 provides a new indicator to account for the spatial dimension of the plurilateral Schengen agreement in bilateral trade flow analysis. Chapter 2 employs spatially mapped geographic data on natural disasters in a gravity analysis of international migration. Chapter 3 introduces a new database combining physical intensities of geological and meteorological events with night-light emissions at spatially disaggregated grid cells and assesses the importance of spatial spillover effects. Finally, Chapter 4 exploits geographic information on country borders and road networks to investigate the role of spatial connectivity for spillover transmission. All chapters make heavy use of geographic information systems (GIS) to enrich the existing academic literature by exploring and providing new sources of geographic data. Moreover, they all share the guiding idea of exploiting exogenous treatment variation in large panel data analysis to obtain insights on fundamental economic mechanisms.

Methodologically, the first two essays both fall into the category of empirical gravity analysis and investigate trade and migration flows between country pairs. Metaphorically named after Newton's Law of Universal Gravitation, the gravity model of international economics explains bilateral transactions between observational units based on their economic masses and the transaction frictions between them. Dating back to Tinbergen (1962), the empirical gravity model was long lacking theoretical foundations. Over the last two decades, a large body of literature successively added structural underpinning, most influentially Eaton and Kortum (2002) and Anderson and Van Wincoop (2003). Finally, Arkolakis et al. (2012) show that a wide range of trade models with constant elasticity of substitution can give rise to an

empirically testable gravity equation. Head and Mayer (2014) describe the gravity model as *the* workhorse model for empirical analysis in the field of international economics. A very detailed best-practice guide to structural gravity model applications has recently been provided by Yotov et al. (2016).

The second two essays share a different methodological foundation, relying on spatial econometric panel modeling techniques to analyze local economic growth impacts and spillover effects at a very fine spatial resolution. Following Costinot et al. (2016), the globe is partitioned into fields along latitude and longitude. This leads to an arbitrary grid cell layout which may intersect true economic units. If the resolution of these cells is sufficiently high, this arbitrary intersection of *economic* units may give rise to substantial interdependencies between nearby *observational* units. As a result, the no-interference (Cox, 1958) component of the stable unit treatment value assumption (SUTVA; Rubin, 1980), according to which the potential outcomes of any observational unit are unaffected by treatment assignment to every other unit by assumption, is very likely violated. One class of models addressing this issue is provided by the field of Spatial Econometrics and has hitherto mostly been applied in the area of Economic Geography. The general idea is to define a spatial weights matrix which models relationships between neighboring observational units. This matrix can then be used to explicitly control for the treatment of neighbors as well as for spatially autoregressive processes in the dependent variable, in the residuals, or both. A very comprehensive overview is provided by LeSage and Pace (2009). In particular, Chapters 3 and 4 of this dissertation hold cases of application for the Spatial Lag of X (SLX) and the Spatial Durbin (Error) Model (Anselin, 2013; Halleck Vega and Elhorst, 2015), which share the advantage that they allow an explicit assessment of spillover effects induced by the treatment of neighboring observational units.

Chapter 1 explores the trade effects of the European Schengen Agreement. The Schengen Agreement is an important milestone in the European integration process. By successively abolishing border controls between member countries, its purpose is to facilitate the free movement of people and the unobstructed flow of goods and services across intra-European borders. The European refugee crisis of 2015 has led to temporary suspensions of the Schengen Agreement at a number of border crossings, especially along the so-called Balkan Route. In the associated policy debate on the Agreement's overall adequacy, it is important to consider the economic gains caused by the agreement, which would be at stake if it were abolished permanently.

To contribute to this debate, Chapter 1 applies an econometric gravity analysis to bilateral trade flows to assess how successful the Schengen Agreement has been in achieving its goals. Unlike earlier analyses, this study respects that Schengen has an important geographic component. A country's Schengen membership status does not only concern its own cross-border transactions. In addition, it also affects trade between third countries passing its territory in transit, by altering the relative number of checked borders crossed en route. Thus, by introducing a count variable of Schengen border crossings associated with bilateral trade flows, this study acknowledges that Schengen may treat different country pairs differently, depending on their relative geographical location. Moreover, it is shown that it is crucial to carefully control for other elements of European integration, such as membership in the customs union, the single market or the currency union, and to factor in countries' trade with themselves. Findings suggest that Schengen has boosted trade by about 2.81% on average, on top of the EU's trade effects (equivalent to a drop in tariffs between 0.46 and 1.02 percentage points). Trade creation effects for services are stronger than for goods, but estimates feature larger parameter uncertainty. Peripheral countries benefit more than central ones and even outsiders to the agreement gain if their trade routes are affected. While the Schengen Agreement has economically significant trade effects, this chapter also shows that other aspects of EU integration matter even more. Estimates establish a clear hierarchy, with the customs union and single market being the most important contributors, followed by other regional trade agreements (RTAs), then the Euro currency union and finally Schengen.

While the first chapter focuses on trade flows and is motivated by a policy response to the cross-border movement of people, Chapter 2 is dedicated to international migration itself. More specifically, it investigates the impact of natural disasters on bilateral migration flows between countries. In line with the Chapter 1, it employs a structural gravity analysis. Climate research suggests that global warming will increasingly lead to more frequent and more extreme natural disasters (e.g., IPCC, 2012). According to Oxfam figures, an estimated 243 million people are affected by natural disasters per year. One potential adaptation strategy to the humanitarian and economic consequences of natural disasters is migration. While not all of the affected move across borders, intra-national migration towards urban areas (e.g., as a response to rural aridification or crop failure) may put urban wages under pressure and thus also induce international migration as a secondary effect. While developing economies tend to be heavily affected by natural disasters, inhabitants are often liquidity constrained and least able to insure themselves or adopt alternative adaptation strategies. Moreover, migration

towards industrialized nations often is not feasible for people from developing countries due to increasingly strict immigration policies. For these reasons, it is ex-ante unclear whether and under what circumstances natural disasters induce international migration from a macro perspective.

The aim of Chapter 2 is to address this question empirically. A stylized theoretical gravity model of migration is constructed which includes natural disasters as random shocks. To estimate this model, exogenous data on the physical intensities of geological and meteorological events at the country level from 1980 to 2010 is deployed. This data is combined with the World Bank's Global Bilateral Migration Database which provides decennial migrant stocks from census data for all countries in the world. Estimates suggest that disaster events at origin on average lead to a 1.7% increase in bilateral migration. Considering heterogeneity across income groups, findings show that particularly middle-income countries experience significant push and pull effects of natural disasters on migration: Disasters at origin on average lead to an increase of outward international migration by 1.4%, while disasters at potential destinations reduce inward migration by 11.5%, evaluated at the mean. For low income countries, there is no evidence that natural disasters induce people to migrate internationally, potentially due to binding economic constraints. For high-income countries, estimates suggest that outmigration declines after natural disasters. This is in line with the hypothesis that typically high insurance penetration rates in these countries may cause incentives to stay as insured capital is upgraded after a disaster. All in all, comparing overall findings to studies on *intra*-national migration (e.g., Barrios et al., 2006; Beine and Parsons, 2015), the evidence that natural disasters affect international migration is relatively limited.

Chapter 3 therefore leaves the realm of country level analysis and zooms in on the effects of natural disasters and potential relocation mechanisms at spatially disaggregated grid cell units. The objective of this chapter is to analyze local growth effects of natural disasters and to assess the associated diversion of economic activity across space. Most disasters are very local events which should have specific effects on *local* economic growth. Hence, assessing their economic impacts in country-level analysis may lead to biased results. Moreover, correct identification of local average treatment effects is further complicated by the possibility that local shocks may shift production and consumption to neighboring locations. In Chapter 3, a new geo-coded database on geological and meteorological events (GAME) is introduced and matched with annual data on global night-light emissions, covering about 24,000 grid cells in

197 countries for the years 1992-2013.[1] Night-lights data has seen increasing popularity in recent economic literature and has become an established proxy for economic activity (cf. Chen and Nordhaus, 2011; Henderson et al., 2012). This chapter adopts this proxy as a dependent variable, interpreting variations in light emissions as reflecting changes in economic activity. Spatial econometric panel methods are applied to account for interdependencies between locations and to explicitly estimate spatial spillover effects.

Findings convey evidence for pronounced local average treatment effects and strong spatial spillovers, particularly for weather shocks: Main results show a reduction in night-time lights after storms, cold waves and extreme precipitation events. Evaluated at the average estimated lights-to-GDP growth elasticity, a one standard deviation increase in wind speeds, excessive precipitation or cold waves leads to a reduction in income growth of 0.33, 0.17 or 0.25 percentage points, respectively. Inter-temporal persistence of this effect is heterogeneous across disaster types. Moreover, these types exhibit strong evidence for positive local spillover effects towards nearby locations within an 80 km radius, suggesting that local specialization patterns are governed by substitution rather than by complementarity. Droughts exhibit a distinguished pattern. As they mostly affect agricultural outcomes, they do not seem to be negatively associated with growth in local light emissions. Instead, they exhibit negative spatial spillover effects. Using a Machine Learning approach to classify cells by land-use, it is shown that these spillovers are largely driven by the channel from rural towards nearby urban cells. Overall, results suggest that spatial shifts of economic activity after a natural disaster are a rather local phenomenon, stressing the importance of local adaptation policies. Moreover, findings provide evidence for substantial heterogeneity across income groups and world regions. In particular, results are mainly driven by cells in low- and middle-income economies. This finding is reminiscent of Chapter 2, which alluded to the possibility that high insurance penetration in high income countries might act as a hedging device against the need to relocate.

Chapter 4 dives deeper into the understanding of spillover propagation by examining the intermediating impact of spatial connectivity between locations. As shown in the third chapter, natural disasters may give rise to positive local spillover effects towards nearby locations, suggesting that substitution effects outweigh complementarity effects on average. The ability

[1] The underlying Gridded GAME database constructed by the author spans from 1979 to 2014 at monthly frequency. The time-scope and frequency chosen in this chapter is constrained by the availability of appropriate covariates.

to divert economic activity towards less affected surroundings has implications for a location's potential to mitigate or adapt to the humanitarian and economic consequences of natural disasters. Theory suggests that well-connected locations should find it easier to respond to shocks by importing more from other national regions or from abroad or by allowing people to escape the consequences of a disaster by relocating to less affected places.

While Chapter 3 largely ignores such connectivity considerations, they are the main objective of Chapter 4. Economic connectivity between grid cells can be driven by various aspects of economic life. A set of factors is provided by the gravity literature in international economics, to which the first two chapters of this dissertation contribute. Gravity models usually rely on bilateral proximity controls for given country pairs, such as distance. Moreover, international borders by themselves are a known obstacle to the free movement of goods and people (cf. Chapter 1). Another potential intermediating factor suggested by the literature on transport networks is the availability of roads infrastructure.

To explicitly examine potential transmission channels governing a location's connectivity with its neighbors, the empirical spatial panel framework introduced in Chapter 3 is extended. For this purpose, available geographic data on country borders and roads networks is exploited. Estimates suggest that short run relocation of economic activity is subject to a border effect. Spatial spillovers in the base period are driven by cells within national boundaries, whereas after one year there is no evidence for statistically significant differences between domestic and foreign spillovers. For wind and extreme precipitation events, domestic neighbors are on average the exclusive source of statistically significant spillover effects. For droughts and cold waves, spillovers from foreign locations also matter, but magnitudes of domestic spillovers are about 2.5 times and 1.5 times the size respectively. This suggests that international borders imply higher trade and migration costs, hampering the short-run relocation of economic activity across international borders compared to relocation within countries. Concerning the movement of goods, this finding is reminiscent of Chapter 1 which explicitly examines the trade effects of border controls. With respect to the movement of people, the finding that diversion of economic activity after natural disasters is largely confined within national boundaries is in line with Chapter 2 which only finds limited evidence for international migration due to natural disasters.

In addition to national borders, estimates suggest that the overall availability of roads, and major roads connectivity differences play a very important role for the propagation of spatial

spillover effects and hence potentially matter for the mitigation of disaster consequences. Spillovers from cells that feature a connection by at least one major road are the sole driver of spatial spillovers for extreme precipitation events and feature spillover effects for droughts and cold waves that are 1.9 times and 3.5 times as strong as spillovers from cells that lack such a connection. Exploiting heterogeneity in the roads connectivity in terms of distance and the number of connections available, results suggest that connectivity differences at smaller margins seem less crucial, whereas the overall availability of roads as well as connectivity differences at larger margins (i.e., upper vs. lower 50%) play a very important role.

# 1 The Trade Effects of Border Controls: Evidence from the European Schengen Agreement*

## 1.1 Introduction

The Schengen Agreement is seen as an important milestone in the European integration process. In this paper, it is tested econometrically whether the agreement has indeed fulfilled the promises. More precisely, it is asked whether Schengen has significantly spurred trade in goods and services amongst its members.

The agreement has abolished regular identity checks at internal EU borders, allowing them only in emergency situations and for limited periods of time. Schengen also sets out the modalities of cooperation in border-related police work. The agreement was signed in 1985 in the Luxembourg town of Schengen by Belgium, the Netherlands, Luxembourg, France, and Germany. In 1995, it was first enforced amongst seven countries (the above-mentioned five plus Spain and Portugal). The Schengen area has grown over time and today covers 26 countries. The EU members Bulgaria, Croatia, Cyprus, Ireland, Romania and the United Kingdom do not participate in Schengen while the non-EU countries Iceland, Norway, and Switzerland are part of it.

The Schengen Agreement is part and parcel of the complex European integration process. It complements the European customs union and single market, and the monetary union. By ending border controls, Schengen facilitates and accelerates the crossing of borders within Europe and delivers very tangible benefits for millions of travelers and commuters. Ademmer

*This chapter is based on joint work with Gabriel Felbermayr and Jasmin Gröschl. It is based on the published article *"The Trade Effects of Border Controls: Evidence from the European Schengen Agreement"*, JCMS: Journal of Common Market Studies 56(2), 2018, 335–351. This is a revised version of a joint working paper that circulated under ERIA Discussion Paper 2016-36, 2017 and ifo Working Paper No. 213, 2016. This Article has emanated from the authors' policy consulting work commissioned in parts by the German Federal Ministry for Economic Affairs and Energy, published in ifo Forschungsberichte 73, 2016. Findings have been featured in *"Handelseffekte von Grenzkontrollen"*, ifo Schnelldienst 69(05), 2016 and the blog article *"Trade costs of border controls in the Schengen area"*, VOX – CEPR Policy Portal, January 27, 2016, `https://voxeu.org/article/trade-costs-border-controls-schengen-area`. Grateful thanks apply to Hans-Werner Sinn, Yoto Yotov and Jeromin Zettelmeyer and seminar participants in Munich, Vienna and Yogyakarta for comments and suggestions.

et al. (2015) argue that the reduction of waiting times at borders reduces trade costs, which should stimulate cross border exchange and the mobility of service providers as well as of consumers.[1] Tighter regional integration should yield welfare benefits for citizens. Conversely, the reintroduction of identity checks at internal Schengen borders as one consequence of the European refugee crisis of 2015 may jeopardize these gains.[2] The goal of this paper is to estimate the trade-creating effects of Schengen in order to shed light on the size of the benefits at stake when ending the agreement as a whole.[3]

To this end, it is important to acknowledge a special characteristic of the Schengen Agreement. Unlike the customs union, the single market, Eurozone membership or other regional trade agreements (RTAs), which all have a clear bilateral scope, the Schengen Agreement has an obvious and important spatial dimension. Land-borne trade flows between two countries in Europe may cross only one internal border (e.g., France - Germany) or up to eight of them (e.g., Portugal - Finland). Hence, Schengen membership treats country pairs heterogeneously, depending on the number of internal Schengen borders crossed. This feature is ignored in the small existing literature, which treats Schengen analogously to trade agreements and currency unions, e.g., Davis and Gift (2014) or Chen and Novy (2011).

Moreover, land-borne trade between two Schengen outsiders (e.g., Romania and the UK) or between Schengen outsiders and insiders (e.g., Turkey and Germany) can also benefit from the agreement as goods transit through Schengen space.[4] Combining GIS data with information from Google Maps, the number of Schengen borders crossed by truck (and ferry) along the shortest road distance between trading partners are counted. This count variable is the measure of interest.

[1] Clearly, trade gains are not the only motivation for Schengen or European integration more broadly (see Baldwin et al., 2008).

[2] Monar (2014) offers a discussion of the *'Regulation (EU) 1051/2013 on common rules for the temporary re-introduction of border control at internal borders in exceptional circumstances'*. Trauner and Ripoll Servent (2016) argue that it is unclear whether the refugee crisis will strengthen or weaken the Schengen area in the long run.

[3] The estimates presented in this work imply long-run effects of undoing Schengen, assuming that check point conditions equivalent to the pre-Schengen era are re-established. The data used does not allow isolating the effects of temporary exemptions. Since the Agreement's implementation, border infrastructure and personnel have been built back whereas trade flows have grown considerably. Enforcing temporary exemptions where check-point conditions are worse than before Schengen suggests higher short-run effects than the presented long-run estimates suggest.

[4] Typically, econometric analysis of bilateral trade data assumes that third countries are affected only through general equilibrium effects by bilateral trade integration. Schengen is an example where third countries are directly affected through shorter transit times. The authors are grateful to a referee for pointing this out.

In contrast to existing studies, services trade or internal trade flows are not excluded. This study makes progress by (i) using a more accurate definition of treatment, (ii) employing the most recent and most adequate data, and (iii) making full use of newest methodological advances, while strictly adhering to the predicaments of structural gravity theory as laid out in Head and Mayer (2014).

The contribution of this paper is threefold: First, applying state-of-the art methods, an accurate partial equilibrium quantification of the trade (and trade cost) effects of Schengen can be provided. Flows of goods crossing a single Schengen border increase by 2.6% while services flows go up by 4.1% on average (equivalent to a drop in a tariff by 0.37 and 0.80 percentage points, respectively). Second, the trade effects of subsequent steps of European regional integration are consistently compared. Mutual EU membership increases trade in goods by 122.6% (53.2% for the Customs Union and 69.4% for the Single Market) and in services by 39.8% for all countries that have joined the EU after 1995. Other RTAs established after 1995 boost trade by an additional 35.3% in goods and 20.2% in services. The common adoption of the Euro in addition to EU membership is again more important for goods trade (15.3%) than for services trade (8.8%). So, Schengen is comparatively less important. Third, exploiting its spatial dimension, this study shows that the trade cost effects of Schengen vary between 0.17 percentage points for Ireland to 0.83 percentage points for Estonia, and that Schengen outsiders such as Turkey or Russia can benefit substantially (0.51 and 0.36 percentage points, respectively).

## 1.2 Empirical Model

Head and Mayer (2014) show that for a broad class of general equilibrium trade models with constant elasticity of substitution aggregation gives rise to a gravity equation of the following form:

$$X_{ij,t}^{s} = \frac{Y_{i,t}^{s} E_{j,t}^{s}}{Y_{t}^{s}} \cdot \left(1 + \tau_{ij,t}^{s}\right)^{-\sigma^{s}} \left(\frac{\phi_{ij,t}^{s}}{\Omega_{i,t}^{s} \Omega_{j,t}^{s}}\right)^{1-\sigma^{s}}, \tag{1.1}$$

where $X_{ij,t}^{s}$ is the value of exports of country $i$ to country $j$ in sector $s$ at time $t$, $Y_{i,t}^{s}$ is country $i$'s value of production in sector $s \in \{G, S, T\}$ for goods, services, and total trade, respectively. $E_{j,t}^{s}$ is country $j$'s expenditure in sector $s$, $Y_{t}^{s}$ is the value of global output, $1 + \tau_{ij,t}^{s}$ is an ad valorem tariff factor, $\phi_{ij,t}^{s} \geq 1$ measures bilateral non-tariff "iceberg" trade costs, and $\sigma^{s} > 1$ is

the sectoral elasticity of substitution.[5] In the literature, $1-\sigma^s$ is often referred to as "the trade elasticity". The terms $\Omega^s_{i,t}$ and $\Omega^s_{j,t}$ are called "multilateral resistance" terms. They account for the effects of third countries' trade costs on $i$'s exporting and on $j$'s importing behavior. These terms are generally unobserved and depend on bilateral trade costs between all trading partners worldwide.

Non-tariff trade costs $\phi^s_{ij,t}$ cannot be directly measured in the data but must be estimated. Suppressing sectoral indices to avoid cluttering, common practice is followed to specify

$$\phi_{ij,t} = \prod\nolimits_{\ell} \left(T^{\ell}_{ij,t}\right)^{\tilde{\delta}^{\ell}} \cdot \exp\left(\tilde{\beta}\text{Schengen}_{ij,t} + \sum\nolimits_{k} \tilde{\alpha}^{k} Z^{k}_{ij,t}\right), \tag{1.2}$$

where $T^{\ell}_{ij,t}$ denotes a trade cost shifter $\ell$ unrelated to policy (such as geographical or cultural distance). $Z^{k}_{ij,t}$ is an indicator variable capturing whether $i$ and $j$ are both taking part in an integration program $k$ (such as the customs union, the single market, the monetary union, or any other RTAs.

Substituting (1.2) into (1.1) and assuming that other trade costs $\mathbf{T}^s_{ij}$ are time-invariant, the estimation equation can be written

$$X_{ij,t} = \exp\left[\beta\text{Schengen}_{ij,t} - \sigma \ln\left(1+\tau_{ij,t}\right) + \sum\nolimits_{k} \alpha^{k} Z^{k}_{ij,t} + \nu_{ij} + \nu_{i,t} + \nu_{j,t}\right] + \varepsilon_{ij,t}, \tag{1.3}$$

where $\beta \equiv (1-\sigma)\,\tilde{\beta}$, $\alpha^k \equiv (1-\sigma)\,\tilde{\alpha}^k$, and $\varepsilon_{ij,t}$ is a random disturbance. The terms $\nu_{ij}$, $\nu_{i,t}$, and $\nu_{j,t}$ are country-pair, and year specific importer and exporter fixed effects, respectively. Their presence implies that time-invariant country-pair specific determinants of sectoral trade flows drop out of the equation. Moreover, they fully control for all exporter- and importer-specific time-varying determinants of trade (such as $Y_{i,t}, E_{j,t}, \Omega_{i,t}, \Omega_{j,t}$).

Except Russia and China, all countries in the sample are WTO members. Therefore, they apply the same tariff to all trade partners (most-favored nation principle, MFN), except in the case of a preferential trade agreement. Since those are controlled for explicitly, in principle, the MFN tariff $t_{j,t}$ could be included into the regression. $\sigma^G$ could be identified even in the

[5] Tariffs and non-tariff trade costs enter expression 1.1 with different exponents. The reason is that iceberg trade costs assume that $\phi^s_{ij,t} \geq 1$ units of a good must be produced in country $i$ for one unit to arrive for consumption in country $j$. The fraction $\phi^s_{ij,t} - 1$ melts away in transit (Samuelson, 1954). Hence, in contrast to tariffs, higher non-tariff trade costs increase the physical quantity of goods to be shipped. This lowers (in absolute values) the elasticity of exports (price times quantity) with respect to $\phi^s_{ij,t}$ compared to the one with respect to $1+\tau^s_{ij,t}$.

presence of the $\nu_{j,t}$ fixed effects due to the presence of intranational trade (for which $\tau_{j,t} = 0$); see Piermartini and Yotov (2016). The regressions presented go one step further. It is set $t_{ij,t} = \tau_{j,t} \times EXTRA_{ij}$, where $EXTRA_{ij}$ is a binary variable taking value 1 except if $j = i$ or when $i$ and $j$ are both part of the EU. This way, $\sigma^G$ is identified on the variance between intra- and international trade flows, and between EU and non-EU flows. As a side effect, this specification extracts the tariff-component of EU integration (the customs union effect), leaving the non-tariff component (the single market effect). The authors refrain from doing the same for other RTAs.[6]

The use of such a saturated model has several advantages. First, it provides some immunization against omitted variable bias as time-invariant bilateral or time-dependent country-level factors affecting trade, which are not modeled by (1.1), are accounted for. Second, it takes away the need to approximate (or iteratively simulate) the multilateral resistance terms and to collect sectoral output data (which are not always available in good quality). Third, the inclusion of bilateral fixed effects $\nu_{ij}$ is a defense against possible endogeneity concerns; see below.

This study is interested in unbiased estimates of $\sigma, \alpha^k$ and, in particular, $\beta$. Contrary to the literature, $\text{Schengen}_{ij,t}$ is *not* defined as a binary variable taking value 1 if country $i$ and country $j$ have both ratified the Schengen Agreement. Such a definition mis-measures the treatment and misses systematic treatment heterogeneity: A land-borne trade flow in Europe from $i$ to $j$ may cross one, two, or up to eight internal Schengen borders.[7] Moreover, the pair $ij$ may benefit from lower transit costs, even if $i$ and/or $j$ are outsiders to Schengen. Therefore, a count variable $\text{Schengen}_{ij,t} = \{1, \ldots, 8\}$ is used, registering the number of Schengen border crossings that land-borne trade between $i$ and $j$ involves.[8]

The existing literature (e.g., Davis and Gift, 2014) is largely silent on the possibility that selection of country pairs into Schengen may not be random. The estimate of $\beta$ would be upward biased if trade shocks $\varepsilon_{ij,t} > 0$ increase the odds of a trade route connecting $i$ and $j$ to be

[6] Clearly, the elasticity $\sigma^s$ can be estimated for goods trade only since services trade is not subject to any tariffs. It should not be over-interpreted, because its identification rests only on very few observations.

[7] Evidence from France suggests that about three quarters of intra-European trade is land-borne; see `www.statistiques.developpementdurable.gouv.frntransportsn873.html`.

[8] Rather than assuming linearity in the effect of Schengen borders, an array of indicator variables could have been specified, each taking the value of unity if one, two, three, ..., Schengen borders are crossed and zero else. However, it turns out that this strategy makes clean identification harder as the effects of a further seven variables would have to be estimated.

affected by Schengen. However, joining a plurilateral agreement such as Schengen is not a bilateral decision, and transportation costs between countries $i$ and $j$ depend on the Schengen status of transit countries. Thus, reverse causality may not be a major issue (for further treatment of potential endogeneity see the robustness section). Nonetheless, country-pair fixed effects $\nu_{ij}$ are included to account for all time-invariant determinants that might jointly affect Schengen$_{ij,t}$ and $X_{ij,t}$. This also addresses omitted variable bias and the endogeneity of other policy variables $Z^k_{ij,t}$, such as EU, Eurozone, or RTA membership, – controls that are crucial to identify an unconfounded treatment effect $\beta$ (see, e.g., Baier and Bergstrand, 2007).

It is important to acknowledge that the structural gravity equation (1.1) implies that the analysis should not only include *inter*national trade but also *intra*national trade, for which $i = j$ (see, e.g., Anderson and Yotov, 2015). Inference based on international flows alone is likely to lead to biased estimates. Yotov (2012), Dai et al. (2014), and Bergstrand et al. (2015) prove the importance of this issue in theory and also document the quantitative relevance of including own trade in the *ex post* evaluation of trade policy.

Equation (1.1) is estimated by Poisson Pseudo Maximum Likelihood (PPML) methods as recommended by Santos Silva and Tenreyro (2006, 2011) and Head and Mayer (2014). Standard errors allow for clustering at the country-pair level. Identification relies on the time variation within country pairs with different exposure to mutual EU, RTA, or EMU membership and the number of Schengen borders relative to the total number of borders crossed (the latter is captured by the bilateral fixed effect $\nu_{ij}$).

Before moving on, expectations about the trade effects of Schengen are briefly sketched. If border controls are abolished, waiting times and associated uncertainty are reduced such that international trade costs decline. Hence, trade-creating effects of Schengen are expected to be larger, the more Schengen borders a trade flow crosses. Other steps of European integration – customs union, single market, monetary union – target trade costs more directly, are more comprehensive, and therefore have more pronounced trade effects than Schengen. Ideally a clear ranking of trade-creating effects should emerge. Moreover, the services sector is more strongly affected by Schengen than manufacturing, as easing the movement of people is a necessary precondition for many services to be provided.

## 1.3 Data

The data used comprise yearly bilateral information on goods and services trade flows between and within countries, and sectoral output and expenditure data from the World Input-Output Database (WIOD), described by Timmer et al. (2015). The data capture 40 countries and the years 1995 to 2011, resulting in $40 \times 40 \times 17 = 27,200$ observations per sector. Geographical and historical variables stem from CEPII. Information on RTAs come from the WTO.[9] MFN tariffs are taken from the World Integrated Trade Solutions (WITS-TRAINS) database.

Data on the successive accession of countries to the Schengen Agreement stem from the European Commission.[10] GIS data are combined with information from Google Maps to count the number of Schengen borders crossed by truck (and ferry) moving from economic centers of $i$ to $j$ in year $t$.

From an econometric point of view, the often bemoaned variable geometry of Europe is an advantage. It allows using panel econometrics to disentangle the different trade effects of EU, Eurozone, and Schengen membership and of other trade agreements (e.g., EU-Turkey customs union, or pre-accession treaties). While all EMU countries are EU members and estimated EMU effects must therefore be interpreted as additional to EU effects, this relationship constitutes the only strict subset to consider. First, not all EU members belong to Schengen or the EMU. Second, not all EMU members are part of Schengen and vice versa, and they have ratified the agreement at different times. Third, some Schengen countries are not part of the EU and, the way the Schengen variable is constructed, it directly affects also outsiders to both Schengen and the EU (e.g., Turkey and Russia).[11] While variable geometry helps with separately identifying the trade effects of overlapping integration steps, one caveat must be kept in mind: the effects are identified through country pairs switching status; e.g., the single market coefficient reflects the effects of new members joining the EU in the period of observation (e.g., the 10 middle and eastern European countries, plus Romania and Bulgaria.)

[9] The RTA gateway is accessible via `http://rtais.wto.org/UI/PublicMaintainRTAHome.aspx`.

[10] Starting with seven countries in 1995, the agreement was joined by Italy and Austria in 1997, Greece in 2000, Denmark, Finland, Iceland, Norway, and Sweden in 2001, the Czech Republic, Estonia, Hungary, Latvia, Lithuania, Malta, Poland, Slovakia, and Slovenia in 2007, Switzerland in 2008. The EU members Bulgaria, Croatia, Cyprus, Ireland, Romania and the United Kingdom do not participate in Schengen, while the non-EU countries Iceland, Norway, and Switzerland do.

[11] Note that the estimated Schengen effect can be interpreted individually even if non-EU Schengen countries are not included in WIOD.

Since WIOD goes back exactly until 1995, the effects Schengen has on its founding members are absorbed by the country pair fixed effects, such that estimates are driven exclusively by the 19 countries that have joined the Agreement over time. Similarly, the EU estimate is driven by those countries that have joined the EU after 1995. The same logic applies to the effects of RTAs that have entered into force before the period of investigation. The Euro became a real currency subject to a single monetary policy only in 1999 such that the EMU estimate fully captures the Euro effect.

Figure 1.1 : Total EU-27 Trade in bn. US Dollar along the Number of Schengen Borders Crossed, 2011

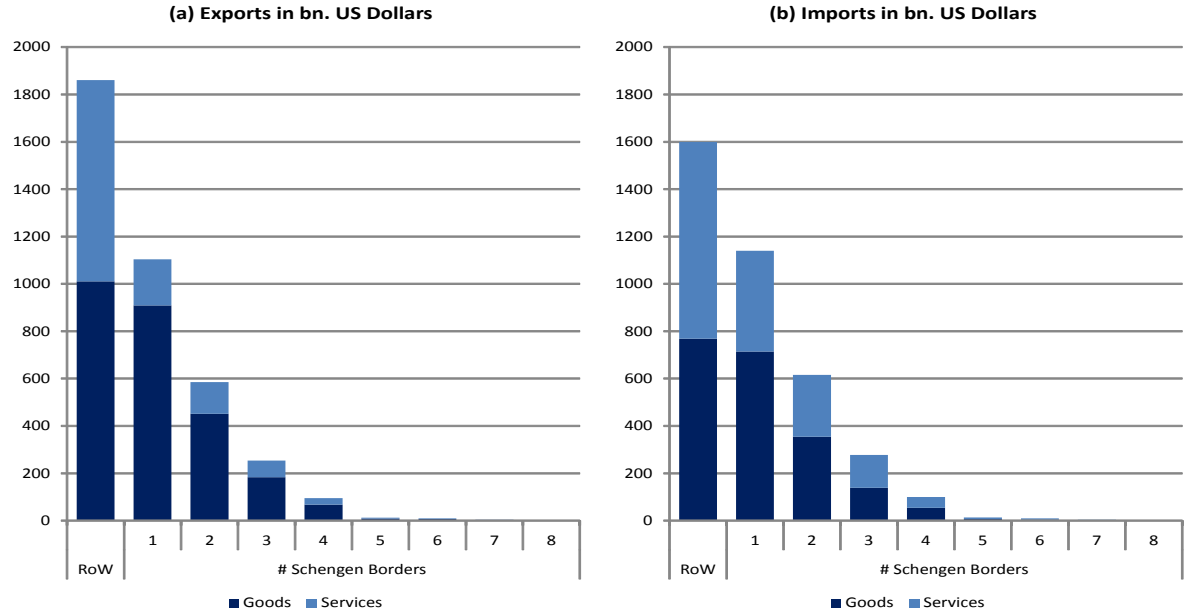


*Note:* Distribution of EU members' trade according to number of Schengen borders crossed in a bilateral relation. RoW denotes rest of the world.

Figure 1.1 shows how exports and imports of EU-27 countries are distributed across country-pairs involving the crossing of one to eight Schengen borders.

In 2011, 35% of goods trade of EU-27 countries crosses one Schengen border. The shares are 17%, 7%, and 3% for two, three or more than three borders, respectively. For services trade the shares are 21%, 13%, 7%, and 3%, respectively. The residual originates from outside the EU-27.[12] Extra-Schengen air-borne trade is unlikely to benefit from the Schengen Agreement;

[12] Note that RoW includes all trade beyond the 40 countries distinguished by WIOD. This comprises countries such as Norway, Switzerland, Iceland, and the Balkan, including Croatia. Gravity estimation results are thus slightly downward biased. Not considering RoW in calculating ad-valorem tariff equivalents would induce an upward bias. Including WIOD's RoW aggregate in ad-valorem tariff analysis implies opting for the more conservative approach given the null that Schengen does not affect trade flows.

sea-borne trade, however, may well benefit, as goods are shipped from major seaports to consumers (see robustness checks).

## 1.4 Results

### 1.4.1 Baseline Results

Table 1.1 provides results for total, goods, and services trade. The regression models follow equation (1.1). They show that the effect of Schengen is substantially overestimated when failing to control for other elements of EU integration. Moreover, controlling for MFN tariffs in regressions for goods trade, an estimate of the tariff elasticity equal to -2.4 is obtained. By construction, explicitly controlling for MFN tariffs only changes the effect of EU integration. Column (4) provides the effect of the EU inclusive of tariff elimination, column (5) exclusive of it. This difference can be exploited to separate the effects of the customs union from that of the single market.

Table 1.1 : The Impact of Schengen on Bilateral Exports (1995 - 2011)

**Dependent Variable:** Bilateral Exports

| | Total Trade | | Goods | | | Services | |
|---|---|---|---|---|---|---|---|
| | (1) | (2) | (3) | (4) | (5) | (6) | (7) |
| Schengen | 0.054*** | 0.0003 | 0.106*** | 0.026*** | 0.026*** | 0.067*** | 0.040* |
| | (0.01) | (0.01) | (0.02) | (0.01) | (0.01) | (0.02) | (0.02) |
| Both EU | | 0.617*** | | 0.800*** | 0.527*** | | 0.335*** |
| | | (0.07) | | (0.07) | (0.11) | | (0.08) |
| Both Euro | | 0.030 | | 0.137*** | 0.142*** | | 0.084* |
| | | (0.02) | | (0.03) | (0.03) | | (0.04) |
| Other RTA | | 0.250*** | | 0.294*** | 0.302*** | | 0.184** |
| | | (0.07) | | (0.06) | (0.07) | | (0.07) |
| Tariff | | | | | −2.443*** | | |
| | | | | | (0.57) | | |

*Note:* ***, **, * denote significance at the 1%, 5%, 10% levels, respectively. All models estimated using Poisson Pseudo Maximum Likelihood (PPML) methods. Robust standard errors (in parentheses) allow for clustering at the country-pair level. Pair as well as year specific importer and exporter fixed effects included but not reported. Number of observations: 27,200.

Figure 1.2 provides a quantitative interpretation based on the results on Table 1.1. The effect of a *single* Schengen border between a country pair leads, on average, to an increase in goods trade of about 2.6% and in services trade of 4.1%.[13]

[13] Estimated coefficients are translated by calculating $\%\Delta X^s = 100 \times [e^{\beta^s} - 1]$.

The figure shows very clearly that other steps of EU integration have led to substantially more trade creation than Schengen. Mutual EU membership proves most important for trade integration. The cumulative effects of the customs union and the single market increased trade in services by 39.8% and goods trade by 122.6%. The latter can be split up into a customs union effect of 53% and a single market effect of 69%.[14] Other RTAs boost trade in services by 20.2% and trade in goods by 35.3%. The mutual adoption of the Euro in addition to EU membership is more important for goods trade (15.3%) than for services trade (8.8%).

Figure 1.2 : Trade Creation Effects and Implied Ad Valorem Tariff Equivalents of Integration Policies

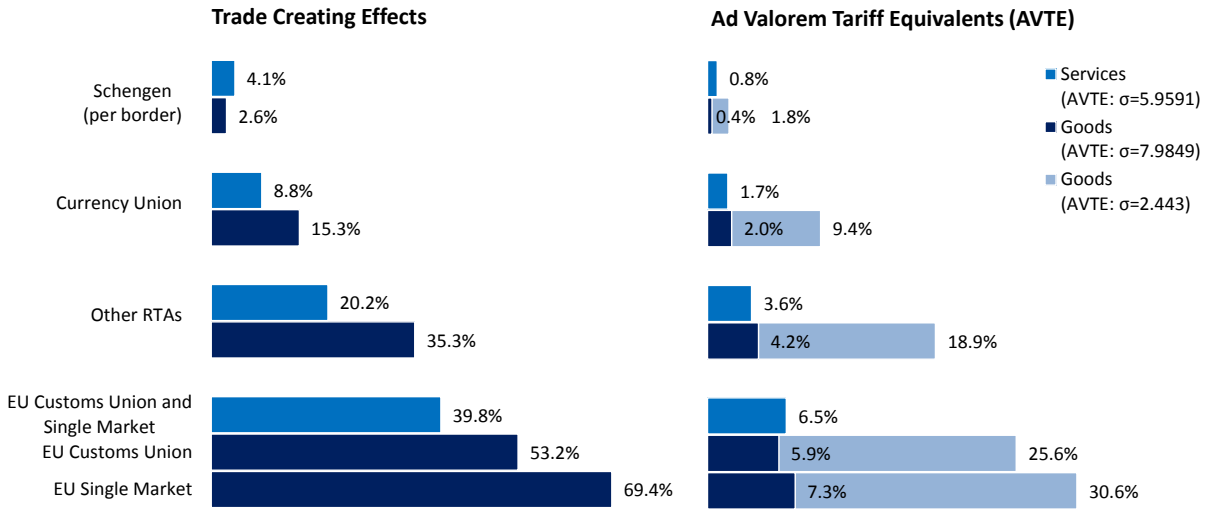


*Note:* Calculations based on Table 1.1

To express these estimates as *ad valorem* tariff equivalents (AVTEs), the elasticity of substitution $\sigma^s$ is needed.[15] Two consistent external estimates are borrowed from Egger et al. (2012), who report $\hat{\sigma}^G = 7.9849$ and $\hat{\sigma}^S = 5.9591$. For goods trade, the MFN result also suggests an internal elasticity of substitution estimate $\hat{\sigma}^G = 2.443$ ; for services, however, $\sigma^S$ cannot be estimated due to the lack of tariffs. Note that the internal elasticity estimate is identified only via a relatively low number of observations. Its magnitude is thus substantially smaller compared to the literature and yields high AVTEs. Moreover, it cannot be compared consistently to the external services elasticity of substitution. It therefore will only be used for illustrative purposes, calculating intervals for ad valorem tariff equivalents for the baseline results, but resort to the consistent external estimates by Egger et al. (2012) for any further analyses.

[14] Egan and Guimarães (2017) show that the Single Market still holds unrealized potential, as trade impediments continue to elicit business complaints and governments shield specific domestic industries from increased competition.

[15] $\%\text{AVTE}^s = 100 \times [(e^{\beta^s})^{(1/(1-\sigma^s))} - 1]$.

The right hand side of Figure 1.2 depicts ad valorem tariff equivalents to the estimated trade effects. The combined EU effect equals a tariff reduction of 6.5 percentage points for services. The corresponding combined EU effect for goods trade (not depicted) ranges from 10.8 (using the elasticity of substitution by Egger et al., 2012) to 42.6 (using own estimate) percentage points. The separated customs union effect on goods trade corresponds to an AVTE between 5.9% and 25.6%, and the single market implied AVTE lies between 7.3% and 30.6%, depending on the chosen elasticity. The RTA effects are equivalent to a tariff reduction of 3.6 percentage points for services and between 4.2 and 18.9 percentage points for goods. Common membership in the Euro Area implies trade effects equivalent to a reduction in tariffs of 1.7 percentage points for trade in services and 2.0 to 9.4 percentage points for trade in goods. Finally, one additional Schengen border is equivalent to a reduction in tariffs of 0.8 percentage points for trade in services and 0.37 to 1.8 percentage points for trade in goods.

Obtained findings add to the literature on the trade effects of European integration. However, this literature often does not control for the effects of the Schengen Agreement, which may bias the estimated effects of EU or Eurozone membership. To the largest extent, it also neither disaggregates between goods and services trade, nor does it incorporate domestic trade flows. The literature has produced very heterogeneous estimates of the trade effects of the Euro.[16] As pointed out by Baldwin et al. (2008), earlier papers suffered from misspecified econometric models; avoiding these pitfalls and applying state-of-the-art modeling techniques, very plausible estimates are generated.

To compare the overall trade effect of the Schengen Agreement to those of the EU, the Eurozone, or other RTAs, it must be considered that the total pair-level effect of the Schengen Agreement increases with the number of borders crossed between trade partners. To evaluate this in more detail, it is taken into account that country pairs differ with respect to the number of Schengen borders crossed by bilateral land-borne trade. When two internal borders are involved, the AVTE for goods amounts to 0.74%;[17] with three border crossings, the AVTE is 1.11%, and so forth; analogously for services trade. Accounting for the different trade structures of all EU-27 country pairs, the total average trade creating effect of Schengen is 2.81%, corresponding to an AVTE of between 0.46% and 1.02% (applying $\sigma_1^T = 7.1948$ and $\sigma_2^T = 3.8144$,

[16] See the work of Micco et al. (2003), Flam and Nordström (2006) Baldwin and Taglioni (2007), Bun and Klaassen (2007). Berger and Nitsch (2008), Bergin and Lin (2012) and Camarero et al. (2014).

[17] $100 \times [(e^{2 \cdot \beta})^{(1/(1-\sigma))} - 1]$, using the elasticity of substitution by Egger et al. (2012). Applying an own elasticity estimate for goods trade increases goods AVTEs about fivefold.

an EU-27 sector-share weighted mean of $\sigma^S$ and $\sigma_1^G$ or $\sigma_2^G$ respectively.).[18] Hence, the average trade creation induced by the Schengen Agreement alone is relatively low compared to the EU, the Euro, and other RTAs.[19]

### 1.4.2 Heterogeneity Across Member States

Clearly, diverse countries will be affected differently by Schengen, simply because geography, history, and specialization patterns imply that countries are heterogeneous with respect to the average number of Schengen borders that typical trade flows need to cross. To illustrate this, every country has its own break-down analogous to Figure 1.1. Calculating average AVTEs for available (geographically) European countries,[20] findings show that peripheral countries such as Estonia, Latvia, and Finland display the highest AVTEs (0.83%, 0.81%, and 0.80% respectively, see Appendix Table A.5 for details). These countries typically trade across several internal Schengen borders. At the lower end, geographically central economies such as Germany or France display smaller AVTEs (0.34% each). Ireland, whose main trade partners are the Schengen outsiders UK and US, features the lowest AVTE with 0.17%. Interestingly, Figure 1.3 shows that Schengen outsiders such as Russia or Turkey benefit from the removal of internal border controls, too. Their average trade costs savings from Schengen amount to 0.20% and 0.32% for goods and 0.57% and 1.08% for services trade, respectively.

Obviously, the overall magnitude of reported AVTEs depends on the assumed underlying trade elasticities, which have been taken from Egger et al. (2012) to ensure comparability across sectors. As a sensitivity check, a uniform elasticity of substitution of 6 is assumed instead and AVTEs are calculated again. Clearly, assuming a higher (lower) elasticity of substitution for services (goods and total) trade, leads to lower (higher) AVTEs. Qualitatively, the key findings remain unchanged; see Table A.6 in the Appendix for details.

Overall, results suggest an ad valorem tariff equivalent markedly below the 3% assumed by Aussilloux and Le Hir (2016) or Boehmer et al. (2016), and Schengen effects for goods trade are

[18] In the data used, 61% of EU-27 trade is in goods, 39% in services.

[19] The authors believe that a Schengen AVTE of below 1% is entirely plausible. Schengen does speed up the flow of traffic, but effects should not be overstated. Evidence from the US-Canadian border suggests that waiting times for trucks are about 20 minutes on average (see Appendix, Table A.4). With an average transportation cost margin of about 10% (Anderson and Van Wincoop, 2004), such a tariff equivalent implies that identity checks increase transportation costs by at most 10%. The 3% tariff equivalent used in Aussilloux and Le Hir (2016) and Boehmer et al. (2016) would, in turn, imply an increase in transportation costs by an implausible 30%.

[20] Numbers are averages across sectors and trade partners.

Figure 1.3 : Average Share of Trade Affected by Schengen and Associated Tariff Equivalents

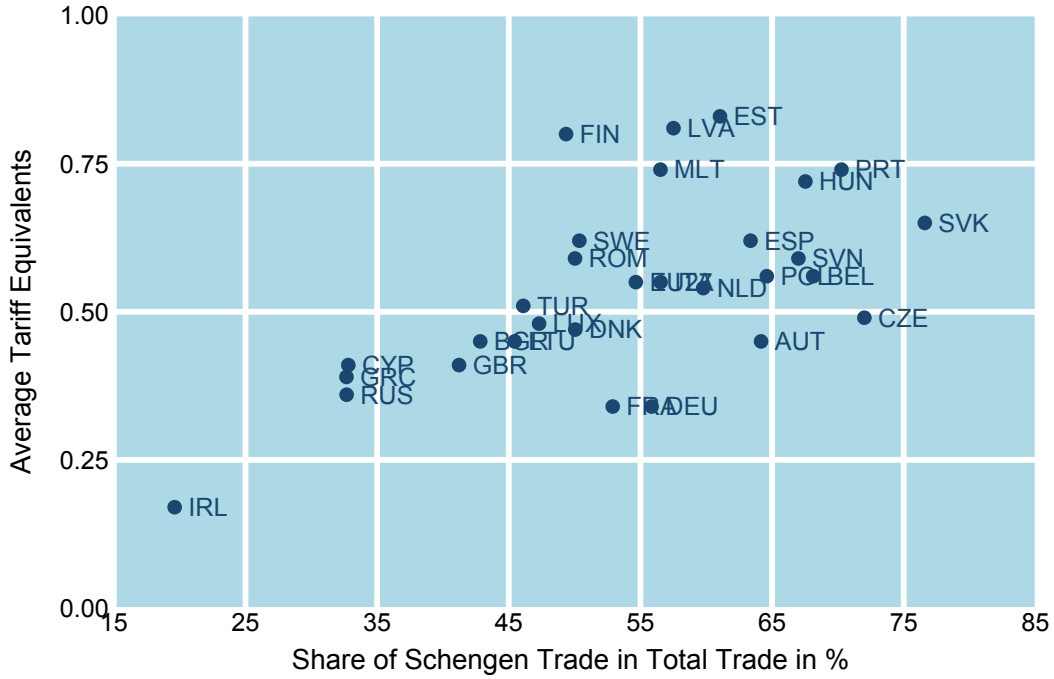


*Note:* Average tariff equivalents of membership to the Schengen Agreement, assuming sectoral trade elasticities provided by Egger et al. (2012).

clearly below the significantly larger long-run gravity estimates of previous studies such as Chen and Novy (2011), Davis and Gift (2014), or Aussilloux and Le Hir (2016). This implies that the spatial dimension and thus the number of Schengen borders to cross along the transit route matters for the identification of the Schengen effect and is preferable over using a simple indicator variable.

## 1.5 Robustness Analysis

Table 1.2 reports a number of robustness checks. Each row shows the estimated Schengen effects obtained by departing from some of the choices made in the baseline specification underlying the results reported in Table 1.1.[21] For goods trade, column (2) does not control for MFN tariffs, while column (3) does.

First, Panel A of Table 1.2 varies the sample. In the baseline model, products which are most likely transported by pipeline, ship or train (gas, petrol, mining & quarrying products) have

[21] Tables A.7 - A.16 in the Appendix provide full details.

Table 1.2 : Robustness: Schengen Effects in Alternative Models

**Dependent Variable:** Bilateral Exports

| | Total Trade | Goods (S1) | Goods (S2) | Services |
|---|---|---|---|---|
| | (1) | (2) | (3) | (4) |
| **PANEL A: Alternative Sample Composition** | | | | |
| [1] Including mining, gas, petrol | 0.007 | 0.035*** | 0.034*** | 0.040* |
| | (0.01) | (0.01) | (0.01) | (0.02) |
| [2] Excluding main bilateral trade partners | −0.003 | 0.017*** | 0.017*** | 0.043** |
| | (0.01) | (0.01) | (0.01) | (0.02) |
| [3] Intracontinental trade only (European Sample) | 0.005 | 0.034*** | 0.034*** | 0.057*** |
| | (0.01) | (0.01) | (0.01) | (0.02) |
| **PANEL B: Alternative Measurement of Treatment** | | | | |
| [4] Treating intercontinental trade flows | 0.024** | 0.050*** | 0.048*** | 0.073*** |
| | (0.01) | (0.01) | (0.01) | (0.03) |
| [5] Schengen as binary variable [0;1] | 0.030** | 0.070*** | 0.072*** | 0.065 |
| | (0.01) | (0.02) | (0.02) | (0.04) |
| [6] Chen and Novy (2011) indicator [0;0.5;1] | 0.161*** | 0.254*** | 0.247*** | 0.300*** |
| | (0.03) | (0.03) | (0.03) | (0.06) |
| **PANEL C: Alternative Econometric Choices** | | | | |
| [7] Pooled over sectors | 0.0003 | 0.026*** | 0.026*** | 0.040** |
| | (0.01) | (0.01) | (0.01) | (0.02) |
| [8] Baier and Bergstrand (2009) MR-Terms | 0.005 | 0.037*** | 0.038*** | 0.034 |
| | (0.01) | (0.01) | (0.01) | (0.02) |
| [9] No bilateral fixed effects | −0.130 | −0.084 | −0.128*** | −0.148 |
| | (0.08) | (0.07) | (0.06) | (0.09) |
| **PANEL D: Heterogeneity** | | | | |
| [10] Schengen Bin [1] | 0.026 | 0.084*** | 0.089*** | −0.048 |
| | (0.02) | (0.02) | (0.02) | (0.06) |
| Schengen Bin [2] | 0.036 | 0.113*** | 0.117*** | −0.012 |
| | (0.02) | (0.03) | (0.03) | (0.07) |
| Schengen Bin [3; 8] | 0.054* | 0.140*** | 0.138*** | 0.169* |
| | (0.03) | (0.03) | (0.03) | (0.09) |

*Note:* Specification 1 (S1) does not explicitly control for tariffs, while specification 2 (S2) does. ***, **, *, denote significance at the 1%, 5%, and 10% level, respectively. Robust clustered standard errors reported in parentheses. For details see Tables A7 - A16 in the Appendix. Default estimation technique is PPML (unless stated otherwise).

been excluded. Including them, the effect of a Schengen border on bilateral goods exports increases from an AVTE of 0.37% to an AVTE of 0.50% (0.49%) in column (2) (column (3)); see row [1].[22] This can be taken as evidence that at least some of the sectoral trade is carried by trucks (e.g., coal, earths, metal). The AVTEs of the EU, the Eurozone, and other RTAs remain very similar to the previous findings.

[22] Assuming $\sigma^G = 7.9849$.

In row [2], potential endogeneity concerns are addressed by excluding the three most important trade partners of each country from the sample, as trade shocks pertaining to them could have driven the decision to join the Schengen area. The results support the previous findings. The exclusion of important trade partners reduces the magnitude of a Schengen border on goods trade to an AVTE of 0.24%, while it slightly increases the magnitude on services trade to 0.87%.[23] The magnitudes of the EU, the Eurozone, or other RTA effects are reduced.[24]

Row [3] focuses on *intra*continental European trade only (treating Turkey and Russia as geographical Europe). Results remain very similar to the baseline results. As expected, coefficients increase slightly in magnitude, as all extra-continental trade flows are excluded from the sample. Focusing on intra-continental European trade only leads to an AVTE on goods trade of 0.49% and 1.14% on services trade. Similarly, the EU, the Euro area, and further RTA effects increase in magnitude.

Second, Panel B looks at alternative measurements of treatment. In row [4], *inter*continental trade of third countries with Schengen members is assumed to cross, on average, one internal Schengen border. While extra-Schengen air-borne trade is unlikely to benefit from Schengen, sea-borne trade may well benefit, as goods are transported from major seaports to the interior of the continent.[25] As expected, treating intercontinental trade by one Schengen border on average slightly inflates estimates and leads to statistically significant estimates for total trade. Findings suggest AVTEs of 0.39% for total trade,[26] 0.71% (0.68%) for goods in column (2) (column (3)), and 1.46% for services. All other controls remain similar in magnitude relative to the baseline results.

Row [5] employs a binary Schengen indicator as in Davis and Gift (2014) or Aussilloux and Le Hir (2016). This more than doubles the estimated Schengen effect. In addition, the trade

[23] Assuming $\sigma^S = 5.9591$.

[24] Note that these estimates are subject to sample selection bias. The direction of the bias depends on the systematic characteristics of the trade partners dropped.

[25] Note that no information on transport modes for global trade, or even trade within Europe, is available. Hence, assuming an average of one border crossing for trade that does not originate in geographical Europe only provides an approximation of treated intercontinental trade values.

[26] Assuming $\sigma^T = 7.1948$.

effect on services trade is now less accurately measured.[27] The trade effects of the EU, the Euro, and other RTAs remain close to the baseline findings.

Similarly, coding whether both, one or none of the trade partners are Schengen members $(Schengen = 0, 0.5, 1)$, as in Chen and Novy (2011), strongly inflates the Schengen estimates (row [6]), suggesting an AVTE of 3.6% (3.5%) for goods in column (2) (column (3)) and of 5.9% for services trade. Comparing these estimates to the ones obtained using the newly introduced treatment measure suggests that ignoring the geographic features of the Schengen area leads to an overestimation of the Schengen Agreement's trade effects. Recall that, accounting for the different trade structures of all EU-27 country pairs, the total average trade creating effect of Schengen obtained using the more exact measure of treatment is 2.81%, i.e., an AVTE of only 0.46%.

Panel C varies econometric choices. Row [7] pools over all 35 sub-sectors (see Table A.3 in the Appendix) instead of aggregating trade, with standard errors allowing for clustering at the country-pair–subsector level.[28] This increases the number of observations from 27,200 to 380,800 for goods and to 514,539 for services trade. Next to country pair fixed effects, year specific importer, exporter, and sector fixed effects are applied.[29] This choice leaves the baseline results given in Table 1.1 virtually unchanged in terms of sign, magnitude, and level of significance.

In the following, the consequences of deviating from the preferred and state-of-the-art methodology is examined. Findings show that these choices make it harder to disentangle the trade effects of integration, not only for Schengen but also for other measures such as the EU or RTAs. In row [8], a different approach in controlling for multilateral resistance is pursued. Instead of using year specific importer and exporter fixed effects, Baier and Bergstrand (2009) are followed by using a Taylor Series expansion to explicitly control for unobserved multilateral resistances. This strategy requires controlling additionally for exporter supply and importer demand, which is extracted from WIOD. A vector $\mathbf{MR}^{s}_{ij,t}$ is constructed that contains

[27] Note that this binary Schengen indicator disregards the geographical component of Schengen but simply measures the average trade effect of both trade partners being Schengen members, whereas the study at hand measures the average trade effect of one Schengen border en route between two countries. By accounting for the spatial distribution of Schengen borders, the introduced treatment measure allows a more sophisticated disentanglement of the actual border effects at work.

[28] Multi-way clustering addresses intraclass correlation at the subsectoral and at the country pair level, hedging against the risk of inflating Type I error rates.

[29] Choosing country pair-sector fixed effects and year specific importer and exporter fixed effects instead does not change the results.

first-order approximations of the terms $\Omega^s_{i,t}$ and $\Omega^s_{j,t}$ for all types of trade costs.[30] This change in methodology only marginally increases the estimated Schengen effect for goods trade and slightly decreases that for services trade, leading to a lower level of significance on the latter. This is also true for the EU, the Euro, and the RTA trade effects. Nevertheless, the overall order of magnitude of the estimated coefficients remains very similar and thus leaves the key findings unchanged.

Failure to control for time-invariant determinants that might jointly affect trade integration (i.e., Schengen, EU, Euro, RTAs) and export volumes gives rise to omitted variable bias and potential endogeneity of policy variables. In row [9], bilateral fixed effects are replaced by explicit trade cost proxies, such as bilateral distance, dummies for adjacency, intranational trade, and common language. As expected, this leads to implausible effects not only on Schengen membership, but also on all other trade policy variables – except for the Eurozone. This result is reminiscent of Baier and Bergstrand (2007), who show that bilateral fixed effects are a crucial ingredient in the identification of causal effects of trade agreements because common but unobserved time-invariant determinants of both trade and the conclusion of agreements lead to biased estimates if they are not accounted for.

Finally, Panel D actually tests the heterogeneous effects of the Schengen Agreement, additionally to calculating them for all countries in the sample in the previous section. To approach this, the Schengen variable is broken into subsets based on the number of borders crossed. Bins are taken, containing observations with one Schengen border, observations with two Schengen borders, and those with three or more (up to eight) Schengen borders.[31] Zero Schengen borders are the reference category. Similar to the baseline specification, the heterogeneity across the number of Schengen borders to be crossed is best identified for goods trade, as these are generally the most stable results – total trade faces an aggregation bias and services trade results are only marginally statistically significant. Positive effects are found for total trade, but only the effect on three or more Schengen borders is statistically significant on the

[30] More precisely, multilateral resistance terms are calculated based on a linearized version of the canonical trade model that underlies equation (1.1). They are calculated for any trade cost proxy $\phi_{ij}$ as $MR\_\phi^s_{ij,t} = \left[\left(\sum_{k=1} \lambda^s_{k,t}\phi_{ik}\right) + \left(\sum_{m=1} \delta^s_{m,t}\phi_{mj}\right) - \left(\sum_{k=1}\sum_{m=1} \lambda^s_{k,t}\delta^s_{m,t}\phi_{km}\right)\right]$, where $\delta^s_{m,t}$ denotes country $m$'s share in total world supply, $S^s_{m,t}/S^s_t$ in sector $s$, and $\lambda^s_{k,t}$ is an analogously defined sectoral demand share. $\phi_{ij}$ can be the log of distance, an adjacency dummy, a dummy for intranational trade, or various trade policy dummies governing the membership of a pair in Schengen, the EU, the Eurozone, or other RTAs.

[31] The data include relatively little observations with more than 3 Schengen borders. This leads to issues when trying to identify effects empirically for these observations. They are thus combined in one bin, which can be seen as an additional exercise to calculate the heterogeneous effects separately.

10% level. Similarly, positive and statistically significant effects are found on goods trade, the size of them monotonically depending on the number of borders crossed. While Schengen increased trade for pairs with one border by 9.2%, those with two borders already experience a trade increase by 12.3% and the trade of country pairs with three or more borders increased on average by 15%. For services this again looks different. While a statistically significant effect for one or two borders relative to zero borders cannot be identified, three or more borders exert a statistically significant effect and increase services trade for these pairs by 18.4%. The stronger effect on services than on goods for many Schengen borders is again not surprising, as Schengen also promotes the mobility of individuals, which is more important for the cross-border provision of services than of goods and might be even more relevant for pairs with many Schengen borders. Overall, this shows that – due to the skewed distribution of the number of Schengen borders – it is not easy to empirically identify the heterogeneity across countries, particularly for services trade.

## 1.6 Conclusion

This paper analyzes the impact of the Schengen Agreement on trade in goods and services. It contributes to the literature by recognizing the spatial structure of the Schengen treatment, fully accounting for other European integration steps, and taking transit routes and the number of Schengen borders to be crossed *en route* into account.

Using a more accurate definition of the Schengen treatment and making full use of the newest methodological advances, obtained PPML results imply a ranking of trade policy effects. Schengen significantly helps fostering trade integration in goods and services trade, namely by 2.6% and 4.1% per Schengen border, respectively, in the preferred specification. Drawing on structural estimates of the sectoral elasticity of substitution by Egger et al. (2012), this equals an ad valorem tariff equivalent of 0.37% in goods trade and 0.80% in services trade. The total average trade creation effect of Schengen is about 2.81%, corresponding to a drop in tariffs of about 0.46 percentage points.

Quite plausibly, in comparison with EU and Eurozone membership, and with other RTAs, the average trade creation induced by the Schengen Agreement alone is relatively low. EU membership boosts trade in goods by 122.6% (53.2% due to the customs union and 69.4% due to the single market) and in services by 39.8%, respectively. Other RTAs increase trade in

goods by an additional 35.3% and in services by 20.2%. Common membership in the Eurozone is again more important for goods trade than for services trade, 15.3% and 8.8%, respectively.

Substantial heterogeneity is found across countries, because geography, history, and specialization patterns imply that countries are heterogeneous with respect to the average number of Schengen borders that their trade flows need to cross. Peripheral countries benefit most from Schengen. Interestingly, through transit effects, Schengen outsiders also benefit from the removal of border controls within the Schengen area.

Finally, although the trade promoting effects of Schengen seem relatively small compared to other integration measures, abolishing the Schengen area implies bearing further cost which are not as easily quantifiable. The free movement of people can be considered a climax in the ongoing process of European integration which, if forfeited, might jeopardize the European idea and many of its political achievements. In this context, a question to be addressed in future research should be whether an ongoing European integration process could be ensured *in spite of* (rather than because of) ending the Schengen Agreement.

# Appendix A.1 Supplementary Appendix

## A.1.1 Supplementary Tables

Table A.1 : Summary Statistics

| variable | N | mean | sd | max | min |
|---|---|---|---|---|---|
| Exports$_{ij,t}$ | 27,200 | 20.39 | 272.13 | 12,385.98 | 0.00 |
| Schengen$_{ij,t}$ | 27,200 | 0.79 | 1.31 | 8.00 | 0.00 |
| Schengen$_{ij,t}$ (S = 1) | 27,200 | 0.99 | 1.25 | 8.00 | 0.00 |
| Schengen$_{ij,t}$ [0;1] | 27,200 | 0.13 | 0.34 | 1.00 | 0.00 |
| Schengen$_{ij,t}$ [0;0.5;1] | 27,200 | 0.34 | 0.35 | 1.00 | 0.00 |
| Both EU$_{ij,t}$ | 27,200 | 0.26 | 0.44 | 1.00 | 0.00 |
| Both Euro$_{ij,t}$ | 27,200 | 0.08 | 0.27 | 1.00 | 0.00 |
| Other RTA$_{ij,t}$ | 27,200 | 0.23 | 0.42 | 1.00 | 0.00 |
| $\ln$(Supply$_{i,t}$) | 27,200 | 13.03 | 1.82 | 17.06 | 8.78 |
| $\ln$(Demand$_{j,t}$) | 27,200 | 12.33 | 1.82 | 16.54 | 8.26 |
| $\ln$(Distance$_{ij}$) | 27,200 | 8.03 | 1.14 | 9.81 | 2.13 |
| Adjacency$_{ij}$ | 27,200 | 0.06 | 0.23 | 1.00 | 0.00 |
| Common Language$_{ij}$ | 27,200 | 0.05 | 0.22 | 1.00 | 0.00 |
| Colony$_{ij}$ | 27,200 | 0.04 | 0.19 | 1.00 | 0.00 |
| Colony post 1945$_{ij}$ | 27,200 | 0.01 | 0.12 | 1.00 | 0.00 |
| Same Country$_{ij}$ | 27,200 | 0.02 | 0.14 | 1.00 | 0.00 |
| $\ln$(MFN$_{ij,t}$) | 27,200 | 0.08 | 0.09 | 0.50 | 0.00 |

*Note:* Summary statistics for the complete sample and total trade.

Table A.2 : WIOD Country List

| ISO Code | Country |
|---|---|
| AUS | Australia |
| AUT | Austria |
| BEL | Belgium |
| BGR | Bulgaria |
| BRA | Brazil |
| CAN | Canada |
| CHN | China, People's Rep. of |
| CYP | Cyprus |
| CZE | Czech Republic |
| DEU | Germany |
| DNK | Denmark |
| ESP | Spain |
| EST | Estonia |
| FIN | Finland |
| FRA | France |
| GBR | United Kingdom |
| GRC | Greece |
| HUN | Hungary |
| IDN | Indonesia |
| IND | India |
| IRL | Ireland |
| ITA | Italy |
| JPN | Japan |
| KOR | Korea |
| LTU | Lithuania |
| LUX | Luxembourg |
| LVA | Latvia |
| MEX | Mexico |
| MLT | Malta |
| NLD | Netherlands |
| POL | Poland |
| PRT | Portugal |
| ROM | Romania |
| RUS | Russia |
| SVK | Slovak Republic |
| SVN | Slovenia |
| SWE | Sweden |
| TUR | Turkey |
| TWN | Taiwan |
| USA | United States |

Table A.3 : WIOD Sector List

| Sector | ISIC rev.3 | Description |
|---|---|---|
| C01 | AtB | Agriculture, Hunting, Forestry and Fishing |
| C02 | C | Mining and Quarrying |
| C03 | 15t16 | Food, Beverages and Tobacco |
| C04 | 17t18 | Textiles and Textile Products |
| C05 | 19 | Leather, Leather and Footwear |
| C06 | 20 | Wood and Products of Wood and Cork |
| C07 | 21t22 | Pulp, Paper, Paper , Printing and Publishing |
| C08 | 23 | Coke, Refined Petroleum and Nuclear Fuel |
| C09 | 24 | Chemicals and Chemical Products |
| C10 | 25 | Rubber and Plastics |
| C11 | 26 | Other Non-Metallic Mineral |
| C12 | 27t28 | Basic Metals and Fabricated Metal |
| C13 | 29 | Machinery, Nec |
| C14 | 30t33 | Electrical and Optical Equipment |
| C15 | 34t35 | Transport Equipment |
| C16 | 36t37 | Manufacturing, Nec; Recycling |
| C17 | E | Electricity, Gas and Water Supply |
| C18 | F | Construction |
| C19 | 50 | Sale, Maintenance and Repair of Motor Vehicles and Motorcycles; Retail Sale of Fuel |
| C20 | 51 | Wholesale Trade and Commission Trade, Except of Motor Vehicles and Motorcycles |
| C21 | 52 | Retail Trade, Except of Motor Vehicles and Motorcycles; Repair of Household Goods |
| C22 | H | Hotels and Restaurants |
| C23 | 60 | Inland Transport |
| C24 | 61 | Water Transport |
| C25 | 62 | Air Transport |
| C26 | 63 | Other Supporting and Auxiliary Transport Activities; Activities of Travel Agencies |
| C27 | 64 | Post and Telecommunications |
| C28 | J | Financial Intermediation |
| C29 | 70 | Real Estate Activities |
| C30 | 71t74 | Renting of M&Eq and Other Business Activities |
| C31 | L | Public Admin and Defense; Compulsory Social Security |
| C32 | M | Education |
| C33 | N | Health and Social Work |
| C34 | O | Other Community, Social and Personal Services |
| C35 | P | Private Households with Employed Persons |

Table A.4 : Waiting time for commercial vehicles and traffic volume at US–Canadian border checkpoints, 2014

| | Waiting time (minutes) | | | | |
|---|---|---|---|---|---|
| Border Station | mean | min | max | # vehicles | Station share |
| ME: Calais | 0 | 0 | 0 | 62,352 | 1.1% |
| ME: Houlton | 1 | 0 | 6 | 84,043 | 1.4% |
| ME: Jackman | 0 | 0 | 0 | 84,755 | 1.5% |
| ME: Madawaska | 3 | 0 | 15 | 19,238 | 0.3% |
| MI: Detroit | 20 | 10 | 30 | 1,600,000 | 27.6% |
| MI: Port Huron | 7 | 0 | 37 | 778,268 | 13.4% |
| MI: Sault Ste. Marie | 5 | 0 | 15 | 38,932 | 0.7% |
| MN: Intertiol Falls | 0 | 0 | 0 | 16,528 | 0.3% |
| MT: Sweetgrass | 20 | 10 | 45 | 145,803 | 2.5% |
| ND: Pembi | 18 | 12 | 36 | 229,079 | 3.9% |
| NY: Alexandria Bay | 15 | NA | NA | 192,551 | 3.3% |
| NY: Buff.-Niagara Falls | 24 | 11 | 36 | 962,076 | 16.6% |
| NY: Champ.-Rouses Pt. | 45 | NA | NA | 285,195 | 4.9% |
| NY: Massena | 0 | 0 | 0 | 23,188 | 0.4% |
| NY: Ogdensburg | 10 | NA | NA | 37,726 | 0.7% |
| VT: Derby Line | 20 | NA | NA | 97,836 | 1.7% |
| VT: Highgate Springs | 15 | NA | NA | 93,914 | 1.6% |
| VT: Norton | 0 | 0 | 0 | 11,161 | 0.2% |
| WA: Blaine | 8 | 0 | 0 | 367,994 | 6.3% |
| WA: Lynden | 10 | NA | NA | 41,580 | 0.7% |
| WA: Point Roberts | 10 | NA | NA | 18,121 | 0.3% |
| WA: Sumas | 25 | 10 | 100 | 149,361 | 2.6% |
| Other | NA | NA | NA | 462,508 | 8.0% |
| Weighted Mean / Sum | 18 | | | 5,802,209 | 100% |

Table A.5 : Ad Valorem Tariff Equivalents due to Schengen, by Country

| Country | Ad Valorem Tariff Equivalents | | | | | Share of Schengen Trade | | |
|---|---|---|---|---|---|---|---|---|
| | Goods | | Services | Total Trade | | Goods | Services | Total Trade |
| | $\sigma_1^G = 7.9849$ | $\sigma_2^G = 2.443$ | $\sigma^S = 5.9591$ | $\sigma_1^T = 7.1948$ | $\sigma_2^T = 3.8144$ | | | |
| EST | 0.63% | 3.08% | 1.20% | 0.83% | 1.83% | 68.87% | 52.50% | 61.04% |
| LVA | 0.64% | 3.15% | 1.09% | 0.81% | 1.80% | 67.76% | 50.20% | 57.51% |
| FIN | 0.67% | 3.26% | 1.12% | 0.80% | 1.76% | 52.29% | 43.26% | 49.35% |
| MLT | 0.42% | 2.05% | 1.15% | 0.74% | 1.65% | 51.16% | 59.95% | 56.52% |
| PRT | 0.64% | 3.14% | 0.97% | 0.74% | 1.64% | 79.40% | 58.41% | 70.27% |
| HUN | 0.60% | 2.94% | 1.03% | 0.72% | 1.60% | 73.13% | 55.39% | 67.53% |
| SVK | 0.53% | 2.60% | 0.96% | 0.65% | 1.43% | 79.37% | 69.53% | 76.60% |
| SWE | 0.58% | 2.84% | 0.73% | 0.62% | 1.38% | 60.83% | 36.08% | 50.36% |
| ESP | 0.47% | 2.29% | 0.94% | 0.62% | 1.37% | 67.12% | 58.03% | 63.36% |
| ROM | 0.48% | 2.36% | 0.80% | 0.59% | 1.30% | 57.13% | 42.77% | 50.03% |
| SVN | 0.51% | 2.47% | 0.78% | 0.59% | 1.30% | 73.98% | 53.29% | 67.00% |
| BEL | 0.44% | 2.14% | 0.81% | 0.56% | 1.24% | 74.40% | 59.89% | 68.12% |
| POL | 0.47% | 2.30% | 0.77% | 0.56% | 1.24% | 72.23% | 49.66% | 64.60% |
| ITA | 0.44% | 2.13% | 0.83% | 0.55% | 1.22% | 60.68% | 48.83% | 56.53% |
| NLD | 0.47% | 2.29% | 0.69% | 0.54% | 1.19% | 72.05% | 45.39% | 59.77% |
| TUR | 0.32% | 1.58% | 1.08% | 0.51% | 1.13% | 40.60% | 59.00% | 46.10% |
| CZE | 0.40% | 1.97% | 0.76% | 0.49% | 1.08% | 75.69% | 60.18% | 72.01% |
| LUX | 0.46% | 2.26% | 0.60% | 0.48% | 1.06% | 86.06% | 42.98% | 47.30% |
| DNK | 0.44% | 2.17% | 0.56% | 0.47% | 1.03% | 69.89% | 38.09% | 50.05% |
| LTU | 0.57% | 2.80% | 0.44% | 0.45% | 1.00% | 78.92% | 28.26% | 45.45% |
| BGR | 0.35% | 1.73% | 0.63% | 0.45% | 0.99% | 47.00% | 37.70% | 42.83% |
| AUT | 0.37% | 1.80% | 0.62% | 0.45% | 0.99% | 72.71% | 50.68% | 64.16% |
| CYP | 0.36% | 1.75% | 0.52% | 0.41% | 0.91% | 44.87% | 28.53% | 32.81% |
| GBR | 0.30% | 1.46% | 0.58% | 0.41% | 0.90% | 45.58% | 38.03% | 41.22% |
| GRC | 0.36% | 1.75% | 0.48% | 0.39% | 0.86% | 45.04% | 28.27% | 32.67% |
| RUS | 0.20% | 0.99% | 0.57% | 0.36% | 0.81% | 30.71% | 33.99% | 32.68% |
| DEU | 0.30% | 1.46% | 0.43% | 0.34% | 0.75% | 60.02% | 42.55% | 55.85% |
| FRA | 0.29% | 1.42% | 0.44% | 0.34% | 0.74% | 58.87% | 39.88% | 52.89% |
| IRL | 0.14% | 0.69% | 0.22% | 0.17% | 0.37% | 23.79% | 15.96% | 19.62% |
| EU 27 Mean | 0.46% | 2.23% | 0.75% | 0.55% | 1.21% | 63.66% | 45.71% | 54.65% |
| EU 27 Median | 0.46% | 2.26% | 0.76% | 0.55% | 1.22% | 67.76% | 45.39% | 56.52% |
| EU 27 | 0.38% | 1.86% | 0.64% | 0.46% | 1.02% | 62.03% | 43.92% | 54.96% |

*Note:* Sorted by Total AVTE in descending order. AVTEs have been calculated dependent on each country's trade volumes of goods and services trade across the number of Schengen borders. The counterfactual trade volumes have been calculated respective of estimated Schengen effects from the gravity estimation. AVTEs result from the difference in counterfactual (cf) to observed (obs) trade, assuming $\sigma_1^G = 7.9849$, $\sigma_1^S = 5.9591$ structurally estimated by Egger et al. (2012), $\sigma_2^G = 2.443$ (goods elasticity of substitution estimate from own analysis) and $\sigma_1^T = 7.1948$, $\sigma_2^T = 3.8144$ (EU-27 sector-share weighted mean of $\sigma^S$ and $\sigma_1^G$ or $\sigma_2^G$ respectively), for goods, services, and total trade: $(X^{s,cf}/X^{s,obs})^{(1/\sigma^s)} - 1 \, \forall \, s \in \{G, S, T\}$.

Table A.6 : Average Tariff Equivalents due to Schengen, by Country

| Country | Average Tariff Equivalents ($\sigma = 6$) | | | Share of Schengen Trade in Total Trade | | |
|---|---|---|---|---|---|---|
| | Goods | Services | Total Trade | Goods | Services | Total Trade |
| EST | 0.88% | 1.19% | 1.03% | 68.87% | 52.50% | 61.04% |
| LVA | 0.90% | 1.08% | 1.01% | 67.76% | 50.20% | 57.51% |
| FIN | 0.93% | 1.11% | 0.99% | 52.29% | 43.26% | 49.35% |
| MLT | 0.59% | 1.14% | 0.92% | 51.16% | 59.95% | 56.52% |
| PRT | 0.90% | 0.96% | 0.92% | 79.40% | 58.41% | 70.27% |
| HUN | 0.84% | 1.02% | 0.90% | 73.13% | 55.39% | 67.53% |
| SVK | 0.74% | 0.95% | 0.80% | 79.37% | 69.53% | 76.60% |
| SWE | 0.81% | 0.72% | 0.77% | 60.83% | 36.08% | 50.36% |
| ESP | 0.66% | 0.93% | 0.77% | 67.12% | 58.03% | 63.36% |
| ROM | 0.68% | 0.79% | 0.73% | 57.13% | 42.77% | 50.03% |
| SVN | 0.71% | 0.78% | 0.73% | 73.98% | 53.29% | 67.00% |
| BEL | 0.61% | 0.80% | 0.69% | 74.40% | 59.89% | 68.12% |
| POL | 0.66% | 0.77% | 0.69% | 72.23% | 49.66% | 64.60% |
| ITA | 0.61% | 0.83% | 0.69% | 60.68% | 48.83% | 56.53% |
| NLD | 0.66% | 0.69% | 0.67% | 72.05% | 45.39% | 59.77% |
| TUR | 0.45% | 1.07% | 0.63% | 40.60% | 59.00% | 46.10% |
| CZE | 0.57% | 0.75% | 0.61% | 75.69% | 60.18% | 72.01% |
| LUX | 0.65% | 0.59% | 0.60% | 86.06% | 42.98% | 47.30% |
| DNK | 0.62% | 0.55% | 0.58% | 69.89% | 38.09% | 50.05% |
| LTU | 0.80% | 0.44% | 0.56% | 78.92% | 28.26% | 45.45% |
| BGR | 0.50% | 0.63% | 0.55% | 47.00% | 37.70% | 42.83% |
| AUT | 0.52% | 0.61% | 0.55% | 72.71% | 50.68% | 64.16% |
| CYP | 0.50% | 0.51% | 0.51% | 44.87% | 28.53% | 32.81% |
| GBR | 0.42% | 0.57% | 0.51% | 45.58% | 38.03% | 41.22% |
| GRC | 0.50% | 0.48% | 0.48% | 45.04% | 28.27% | 32.67% |
| RUS | 0.28% | 0.57% | 0.45% | 30.71% | 33.99% | 32.68% |
| DEU | 0.42% | 0.43% | 0.42% | 60.02% | 42.55% | 55.85% |
| FRA | 0.41% | 0.43% | 0.42% | 58.87% | 39.88% | 52.89% |
| IRL | 0.20% | 0.22% | 0.21% | 23.79% | 15.96% | 19.62% |
| EU 27 Mean | 0.64% | 0.74% | 0.68% | 63.66% | 45.71% | 54.65% |
| EU 27 Median | 0.65% | 0.75% | 0.69% | 67.76% | 45.39% | 56.52% |
| EU 27 | 0.53% | 0.63% | 0.57% | 62.03% | 43.92% | 54.96% |

*Note:* Sorted by Total AVTE in descending order. AVTEs have been calculated dependent on each country's trade volumes of goods and services trade across the number of Schengen borders. The counterfactual trade volumes have been calculated respective of estimated Schengen effects from the gravity estimation. AVTEs result from the difference in counterfactual (cf) to observed (obs) trade, assuming $\sigma = 6$: $(X^{cf}/X^{obs})^{(1/\sigma)} - 1$.

Table A.7 : The Impact of Schengen on Bilateral Exports, including all Sectors (1995 - 2011)

**Dependent Variable:** Bilateral Exports

| | Total Trade | | Goods | | | Services | |
|---|---|---|---|---|---|---|---|
| | (1) | (2) | (3) | (4) | (5) | (6) | (7) |
| Schengen$_{ij,t}$ | 0.061*** | 0.007 | 0.109*** | 0.035*** | 0.034*** | 0.067*** | 0.040* |
| | (0.01) | (0.01) | (0.02) | (0.01) | (0.01) | (0.02) | (0.02) |
| Both EU$_{ij,t}$ | | 0.592*** | | 0.744*** | 0.475*** | | 0.335*** |
| | | (0.07) | | (0.07) | (0.10) | | (0.08) |
| Both Euro$_{ij,t}$ | | 0.054** | | 0.147*** | 0.152*** | | 0.084* |
| | | (0.02) | | (0.03) | (0.03) | | (0.04) |
| Other RTA$_{ij,t}$ | | 0.236*** | | 0.268*** | 0.268*** | | 0.184** |
| | | (0.06) | | (0.06) | (0.07) | | (0.07) |
| MFN$_{ij,t}$ | | | | | −2.342*** | | |
| | | | | | (0.50) | | |

*Note:* ***, **, * denote significance at the 1%, 5%, 10% level, respectively. Robust clustered standard errors reported in parentheses. Pair as well as year specific importer and exporter fixed effects included but not reported. Number of observations: 27,200.

Table A.8 : Endogeneity of Schengen and Bilateral Exports, excluding Gas, Fuel, Coke, Mining & Quarrying and the 3 Most Important Trade Partners (1995 - 2011)

**Dependent Variable:** Bilateral Exports

| | Total Trade | | Goods | | | Services | |
|---|---|---|---|---|---|---|---|
| | (1) | (2) | (3) | (4) | (5) | (6) | (7) |
| Schengen$_{ij,t}$ | 0.041*** | −0.003 | 0.085*** | 0.017** | 0.017** | 0.075*** | 0.043** |
| | (0.01) | (0.01) | (0.01) | (0.01) | (0.01) | (0.02) | (0.02) |
| Both EU$_{ij,t}$ | | 0.607*** | | 0.710*** | 0.493*** | | 0.342*** |
| | | (0.07) | | (0.07) | (0.09) | | (0.07) |
| Both Euro$_{ij,t}$ | | −0.026 | | 0.067** | 0.071** | | 0.087* |
| | | (0.03) | | (0.03) | (0.03) | | (0.05) |
| Other RTA$_{ij,t}$ | | 0.250*** | | 0.170*** | 0.163*** | | 0.144** |
| | | (0.07) | | (0.06) | (0.06) | | (0.06) |
| MFN$_{ij,t}$ | | | | | −1.818*** | | |
| | | | | | (0.50) | | |

*Note:* ***, **, * denote significance at the 1%, 5%, 10% level, respectively. Robust clustered standard errors reported in parentheses. Pair as well as year specific importer and exporter fixed effects included but not reported. All specifications exclude the 3 most important trade partners of each country. Number of observations: 25,160.

Table A.9 : The Impact of Schengen on Bilateral Exports, excluding Gas, Fuel, Coke, Mining & Quarrying, European Sample (1995 - 2011)

**Dependent Variable:** Bilateral Exports

| | Total Trade | | Goods | | | Services | |
|---|---|---|---|---|---|---|---|
| | (1) | (2) | (3) | (4) | (5) | (6) | (7) |
| Schengen$_{ij,t}$ | 0.061*** | 0.005 | 0.120*** | 0.034*** | 0.034*** | 0.081*** | 0.057*** |
| | (0.01) | (0.01) | (0.02) | (0.01) | (0.01) | (0.02) | (0.02) |
| Both EU$_{ij,t}$ | | 0.993*** | | 1.380*** | 1.423*** | | 0.471*** |
| | | (0.10) | | (0.10) | (0.10) | | (0.16) |
| Both Euro$_{ij,t}$ | | 0.033 | | 0.155*** | 0.155*** | | 0.081** |
| | | (0.02) | | (0.03) | (0.03) | | (0.04) |
| Other RTA$_{ij,t}$ | | 0.617*** | | 0.843*** | 0.843*** | | 0.342** |
| | | (0.10) | | (0.09) | (0.09) | | (0.16) |
| MFN$_{ij,t}$ | | | | | 0.361 | | |
| | | | | | (0.36) | | |

*Note:* ***, **, * denote significance at the 1%, 5%, 10% level, respectively. Robust clustered standard errors reported in parentheses. Pair as well as year specific importer and exporter fixed effects included but not reported. Number of observations: 14,297.

Table A.10 : The Impact of Schengen on Bilateral Exports, excluding Gas, Fuel, Coke, Mining & Quarrying, Intercontinental Trade with one Schengen Border (1995 - 2011)

**Dependent Variable:** Bilateral Exports

| | Total Trade | | Goods | | | Services | |
|---|---|---|---|---|---|---|---|
| | (1) | (2) | (3) | (4) | (5) | (6) | (7) |
| Schengen$_{ij,t}$ | 0.072*** | 0.024*** | 0.122*** | 0.050*** | 0.048*** | 0.094*** | 0.073*** |
| | (0.01) | (0.01) | (0.02) | (0.01) | (0.01) | (0.02) | (0.02) |
| Both EU$_{ij,t}$ | | 0.594*** | | 0.779*** | 0.508*** | | 0.298*** |
| | | (0.07) | | (0.07) | (0.11) | | (0.09) |
| Both Euro$_{ij,t}$ | | 0.021 | | 0.129*** | 0.135*** | | 0.074* |
| | | (0.02) | | (0.03) | (0.03) | | (0.04) |
| Other RTA$_{ij,t}$ | | 0.249*** | | 0.293*** | 0.301*** | | 0.181** |
| | | (0.07) | | (0.06) | (0.07) | | (0.07) |
| MFN$_{ij,t}$ | | | | | −2.433*** | | |
| | | | | | (0.57) | | |

*Note:* ***, **, * denote significance at the 1%, 5%, 10% level, respectively. Robust clustered standard errors reported in parentheses. Pair as well as year specific importer and exporter fixed effects included but not reported. Number of observations: 27,200.

Table A.11 : The Impact of Schengen on Bilateral Exports, excluding Gas, Fuel, Coke, Mining & Quarrying, Dummy (1995 - 2011)

**Dependent Variable:** Bilateral Exports

| | Total Trade | | Goods | | | Services | |
|---|---|---|---|---|---|---|---|
| | (1) | (2) | (3) | (4) | (5) | (6) | (7) |
| Schengen [0;1] | 0.148*** | 0.030** | 0.252*** | 0.070*** | 0.072*** | 0.134*** | 0.065 |
| | (0.02) | (0.01) | (0.03) | (0.02) | (0.02) | (0.04) | (0.04) |
| Both EU$_{ij,t}$ | | 0.602*** | | 0.788*** | 0.514*** | | 0.344*** |
| | | (0.07) | | (0.07) | (0.11) | | (0.08) |
| Both Euro$_{ij,t}$ | | 0.023 | | 0.130*** | 0.134*** | | 0.083* |
| | | (0.02) | | (0.03) | (0.03) | | (0.04) |
| Other RTA$_{ij,t}$ | | 0.250*** | | 0.295*** | 0.302*** | | 0.184** |
| | | (0.07) | | (0.06) | (0.07) | | (0.07) |
| MFN$_{ij,t}$ | | | | | −2.444*** | | |
| | | | | | (0.57) | | |

*Note:* ***, **, * denote significance at the 1%, 5%, 10% level, respectively. Robust clustered standard errors reported in parentheses. Pair as well as year specific importer and exporter fixed effects included but not reported. Number of observations: 27,200.

Table A.12 : The Impact of Schengen on Bilateral Exports, excluding Gas, Fuel, Coke, Mining & Quarrying, Indicator (1995 - 2011)

**Dependent Variable:** Bilateral Exports

| | Total Trade | | Goods | | | Services | |
|---|---|---|---|---|---|---|---|
| | (1) | (2) | (3) | (4) | (5) | (6) | (7) |
| Schengen [0;0.5;1] | 0.306*** | 0.161*** | 0.493*** | 0.254*** | 0.247*** | 0.346*** | 0.300*** |
| | (0.03) | (0.03) | (0.05) | (0.03) | (0.03) | (0.05) | (0.06) |
| Both EU$_{ij,t}$ | | 0.559*** | | 0.738*** | 0.469*** | | 0.260*** |
| | | (0.07) | | (0.07) | (0.11) | | (0.09) |
| Both Euro$_{ij,t}$ | | 0.011 | | 0.118*** | 0.124*** | | 0.065 |
| | | (0.02) | | (0.03) | (0.03) | | (0.04) |
| Other RTA$_{ij,t}$ | | 0.247*** | | 0.291*** | 0.299*** | | 0.177** |
| | | (0.07) | | (0.06) | (0.07) | | (0.07) |
| MFN$_{ij,t}$ | | | | | −2.426*** | | |
| | | | | | (0.57) | | |

*Note:* ***, **, * denote significance at the 1%, 5%, 10% level, respectively. Robust clustered standard errors reported in parentheses. Pair as well as year specific importer and exporter fixed effects included but not reported. Number of observations: 27,200.

Table A.13 : The Impact of Schengen on Bilateral Exports, excluding Gas, Fuel, Coke, Mining & Quarrying, Pooled over Sectors (1995 - 2011)

**Dependent Variable:** Bilateral Exports

| | Total Trade | | Goods | | | Services | |
|---|---|---|---|---|---|---|---|
| | (1) | (2) | (3) | (4) | (5) | (6) | (7) |
| Schengen$_{ij,t}$ | 0.054*** | 0.0003 | 0.106*** | 0.026*** | 0.026*** | 0.067*** | 0.040* |
| | (0.01) | (0.01) | (0.01) | (0.01) | (0.01) | (0.02) | (0.02) |
| Both EU$_{ij,t}$ | | 0.617*** | | 0.800*** | 0.527*** | | 0.335*** |
| | | (0.08) | | (0.10) | (0.11) | | (0.08) |
| Both Euro$_{ij,t}$ | | 0.030 | | 0.137*** | 0.142*** | | 0.084* |
| | | (0.02) | | (0.03) | (0.03) | | (0.04) |
| Other RTA$_{ij,t}$ | | 0.250*** | | 0.294*** | 0.302*** | | 0.184** |
| | | (0.08) | | (0.09) | (0.10) | | (0.07) |
| MFN$_{ij,t}$ | | | | | −2.443*** | | |
| | | | | | (0.40) | | |
| Observations | 897,600 | 897,600 | 380,800 | 380,800 | 380,800 | 514,539 | 514,539 |

*Note:* ***, **, * denote significance at the 1%, 5%, 10% level, respectively. Robust clustered standard errors reported in parentheses. Pair as well as year specific importer, exporter, and sector fixed effects included but not reported.

Table A.14 : The Impact of Schengen on Bilateral Exports, excluding Gas, Fuel, Coke, Mining & Quarrying, Baier and Bergstrand (2009) MR-Terms (1995 - 2011)

**Dependent Variable:** Bilateral Exports

| | Total Trade | | Goods | | | Services | |
|---|---|---|---|---|---|---|---|
| | (1) | (2) | (3) | (4) | (5) | (6) | (7) |
| Schengen$_{ij,t}$ | 0.060*** | 0.005 | 0.118*** | 0.037*** | 0.038*** | 0.060*** | 0.034 |
| | (0.01) | (0.01) | (0.02) | (0.01) | (0.01) | (0.02) | (0.02) |
| Both EU$_{ij,t}$ | | 0.651*** | | 0.818*** | 0.653*** | | 0.330*** |
| | | (0.09) | | (0.09) | (0.11) | | (0.09) |
| Both Euro$_{ij,t}$ | | 0.029 | | 0.124*** | 0.126*** | | 0.079* |
| | | (0.03) | | (0.03) | (0.03) | | (0.05) |
| Other RTA$_{ij,t}$ | | 0.275*** | | 0.322*** | 0.313*** | | 0.168** |
| | | (0.08) | | (0.08) | (0.08) | | (0.08) |
| MFN$_{ij,t}$ | | | | | −1.350** | | |
| | | | | | (0.55) | | |
| $\ln$ Supply$_{i,t}$ | 0.651*** | 0.649*** | 0.740*** | 0.736*** | 0.751*** | 0.554*** | 0.550*** |
| | (0.07) | (0.07) | (0.07) | (0.07) | (0.06) | (0.09) | (0.09) |
| $\ln$ Demand$_{j,t}$ | 0.438*** | 0.439*** | 0.407*** | 0.401*** | 0.394*** | 0.445*** | 0.453*** |
| | (0.07) | (0.07) | (0.08) | (0.08) | (0.07) | (0.09) | (0.09) |

*Note:* ***, **, *, denote significance at the 1%, 5%, and 10% level, respectively. Robust clustered standard errors reported in parentheses. Pair, country, and time fixed effects included but not reported. All specifications include Baier and Bergstrand (2009) multilateral resistance terms for all trade costs. Number of observations: 25,857.

Table A.15 : The Impact of Schengen on Bilateral Exports, excluding Gas, Fuel, Coke, Mining & Quarrying, PPML without bilateral fixed effects (1995 - 2011)

**Dependent Variable:** Bilateral Exports

| | Total Trade | | Goods | | | Services | |
|---|---|---|---|---|---|---|---|
| | (1) | (2) | (3) | (4) | (5) | (6) | (7) |
| Schengen$_{ij,t}$ | −0.437*** | −0.130 | −0.196*** | −0.084 | −0.139** | −0.655*** | −0.148 |
| | (0.06) | (0.08) | (0.05) | (0.07) | (0.06) | (0.09) | (0.09) |
| Both EU$_{ij,t}$ | | −1.098*** | | −0.496*** | −0.923*** | | −1.661*** |
| | | (0.19) | | (0.16) | (0.15) | | (0.22) |
| Both Euro$_{ij,t}$ | | 0.299*** | | 0.212** | 0.252*** | | 0.277 |
| | | (0.12) | | (0.09) | (0.09) | | (0.19) |
| Other RTA$_{ij,t}$ | | −1.415*** | | −0.975*** | −0.449** | | −2.376*** |
| | | (0.16) | | (0.15) | (0.20) | | (0.21) |
| MFN$_{ij,t}$ | | | | | −8.873*** | | |
| | | | | | (1.74) | | |
| $\ln$ Distance$_{ij}$ | −2.314*** | −2.211*** | −2.011*** | −1.957*** | −1.569*** | −2.723*** | −2.537*** |
| | (0.06) | (0.06) | (0.06) | (0.06) | (0.06) | (0.09) | (0.07) |
| Adjacency$_{ij}$ | −1.710*** | −0.888*** | −0.970*** | −0.518*** | −0.402*** | −3.209*** | −1.616*** |
| | (0.12) | (0.15) | (0.10) | (0.16) | (0.14) | (0.26) | (0.19) |
| Common Language$_{ij}$ | 0.064 | 0.279* | 0.194 | 0.336** | 0.062 | 0.513* | 0.686*** |
| | (0.25) | (0.16) | (0.24) | (0.15) | (0.18) | (0.26) | (0.19) |
| Colony$_{ij}$ | 0.318 | 0.039 | 0.142 | −0.023 | −0.135 | 0.713*** | 0.210 |
| | (0.21) | (0.18) | (0.18) | (0.17) | (0.17) | (0.25) | (0.20) |
| Colony post 1945$_{ij}$ | −0.877** | −0.758* | −0.732* | −0.644 | 0.751* | −1.395*** | −1.172** |
| | (0.43) | (0.40) | (0.43) | (0.41) | (0.43) | (0.52) | (0.46) |
| Same Country$_{ij}$ | −0.757* | −0.504** | −0.855** | −0.618*** | 0.254 | −1.207** | −0.931* |
| | (0.40) | (0.22) | (0.41) | (0.23) | (0.23) | (0.56) | (0.50) |

*Note:****, **, * denote significance at the 1%, 5%, 10% level, respectively. Robust clustered standard errors reported in parentheses. Pair as well as year specific importer and exporter fixed effects included but not reported. Number of observations: 27,200.

Table A.16 : The Impact of Schengen on Bilateral Exports estimated in Bins (1995 - 2011)

**Dependent Variable:** Bilateral Exports

| | Total Trade | Goods | | Services |
|---|---|---|---|---|
| | (1) | (2) | (3) | (4) |
| Schengen Bin [1] | 0.026 | 0.084*** | 0.089*** | −0.048 |
| | (0.02) | (0.02) | (0.02) | (0.06) |
| Schengen Bin [2] | 0.036 | 0.113*** | 0.117*** | −0.012 |
| | (0.02) | (0.03) | (0.03) | (0.07) |
| Schengen Bin [3; 8] | 0.054* | 0.140*** | 0.138*** | 0.169* |
| | (0.03) | (0.03) | (0.03) | (0.09) |
| Both EU | 0.601*** | 0.778*** | 0.504*** | 0.331*** |
| | (0.07) | (0.07) | (0.11) | (0.08) |
| Both Euro | 0.024 | 0.129*** | 0.134*** | 0.088** |
| | (0.02) | (0.03) | (0.03) | (0.04) |
| Other RTA | 0.250*** | 0.294*** | 0.302*** | 0.184** |
| | (0.07) | (0.06) | (0.07) | (0.07) |
| Tariff | | | −2.450*** | |
| | | | (0.57) | |

*Note:* ***, **, * denote significance at the 1%, 5%, 10% level, respectively. Robust clustered standard errors reported in parentheses. Pair as well as year specific importer and exporter fixed effects included but not reported. Number of observations: 27,200.

# 2 Do Natural Disasters Cause International Migration?*

## 2.1 Introduction

According to the UN-DESA 2016 report on migration, 244 million international migrants are living in the world in 2015. 157 million of these stem from middle-income countries, with their numbers rising more rapidly than those from other income groups. Related to this, the amount of people affected by natural disasters stands at an estimated number of 243 million per year.[1] The reports by the IPCC (2012), by the World Bank (2012) and the Stern Review (Stern, 2006) particularly accentuate that climate change and natural disasters have become serious issues that are global in their consequences. If global warming progresses, it will become increasingly impossible to sustain livelihoods in some regions so that the numbers of those needing to relocate permanently will continue to increase (Stern, 2006; Marchiori and Schumacher, 2011; IPCC, 2012; Economist, 2012). Historically, the vast bulk of relocation of people caused by natural disasters has occurred within nations.[2] Even though not all of the affected move across borders, international migration might provide a potential adaptation mechanism in the presence of natural disasters (McLeman and Smit, 2006; Tacoli, 2009; Barnett and Webber, 2010; Marchiori and Schumacher, 2011).

On these grounds, the impact of increasingly extreme natural disasters on the worldwide relocation of people is one of the major potentially problematic issues that need scrutiny. Knowledge remains limited on the factors at work involving disasters as a cause of interna-

*This chapter is based on joint work with Jasmin Gröschl. It is based on the published article *"Do Natural Hazards Cause International Migration?"*, CESifo Economic Studies 63(4), 2017, 445–480. This is a revised version of a joint working paper that circulated under CESifo Working Paper No. 6145, October 2016. Parts of this article are based on the chapter "Climate Change and the Relocation of Population" in Jasmin Gröschl (2013), "Gravity Model Applications and Macroeconomic Perspectives", ifo Beiträge zur Wirtschaftsforschung 48. Thanks apply to Michel Beine, Ilan Noy, Max Steinhardt, and workshop participants of the CESifo Venice Summer Institute on Climate Change and Migration, EEA 2016 in Geneva, ETSG 2016 in Helsinki and the International Economics workshop 2016 in Göttingen for comments and suggestions.

[1]This figure is provided by Oxfam (2009), "Forecasting the numbers of people affected annually by natural disasters up to 2015". Other studies suggest even higher numbers, finding that 135 million are at risk due to desertification alone (INCCCD, 1994), while 200 million are at jeopardy due to sea-level rise (Myers and Myers, 2002).

[2]In this context, previous research found an effect of disasters in particular on migration from rural to urban areas within national boundaries (Barrios et al., 2006; Beine and Parsons, 2015).

tional migration. One potential strategy in coping with temporary events, such as earthquakes, might be temporary relocation. However, disasters related to climate change might lead to more permanent migration, as these events may strip individuals from their basis of existence. Two channels advocated by Marchiori and Schumacher (2011) may cause permanent relocation as an adaptation mechanism. First, if amenities at home change or more infectious diseases occur, this may directly lead to higher emigration abroad. Second, crop failure or aridification in rural areas force people to migrate to urban regions, which puts urban wages under pressure and might thus lead to higher international migration. The rural poor in developing economies are most affected by natural disasters. By contrast, they are often liquidity constrained and least able to insure themselves or adopt alternative adaptation strategies. Moreover unfettered migration to the global North is not always possible as industrialized nations get increasingly tough on migrants with stricter immigration policies (Boeri and Brücker, 2005).[3]

The aim of this paper is to assess whether natural disasters induce international migration from a macro perspective. It relates to the literature on the determinants of migration[4], to the general empirical literature on bilateral migration[5], and to the more specific subcategory on the relation between migration and natural disasters or climate change. Empirical research is often regionally constrained. Naudé (2010) and Drabo and Mbaye (2015) investigate the relation between disasters and international migration from Sub-Saharan Africa or developing countries to OECD economies, respectively. They find that disasters cause outmigration. Other studies look at single extreme disasters to evaluate their impact on migration. Ambrosetti and Petrillo (2016) examine intra-national migration flows after L'Aquila's earthquake of 2009, finding a strong increase of outflows from L'Aquila to other provinces and close regions. Yet another branch of literature focuses only on certain disaster types. Reuveny and Moore (2009), Coniglio and Pesce (2015), and Backhaus et al. (2015) use a gravity framework to analyze the role of origin country climate anomalies on international migration to OECD countries. Their results suggest that an increase in weather-related shocks in the origin increases outmigration. Beine and Parsons (2015) use a comprehensive data set of global migration for 1960 to 2000. They find little direct effects of climate anomalies or disasters on international migration, but rather on migration from rural to urban areas. In a more recent paper, Beine and Parsons

[3] For a survey on the measurement, determinants and outcomes of migration policies, see Ortega and Peri (2015) and further contributions in that issue.

[4] Important contributions are Sjaastad (1962); Borjas (1987, 1989); Mincer (1978); Stark (1991).

[5] Studies include Lewer and Van den Berg (2008); Pedersen et al. (2008); Letouzé et al. (2009); Ortega and Peri (2009); Mayda (2010); Beine et al. (2011), to name a few.

(2017) find some evidence of weather conditions on the variation in bilateral migrant stocks, suggesting that disasters affect credit constraints of individuals, deterring emigration from all origin countries but spurring emigration to neighboring countries. For middle-income origins, they find that natural disasters foster emigration to former colonial powers. Notably, Beine and Parsons (2017) highlight the importance of how differences in modeling climate change can lead to differing results.

A range of promising approaches to identify the link between disasters and migration exists, but the underlying data used in seeking answers often has its drawbacks[6], which makes it difficult to generalize results and policy implications. As recapitulated by Mbaye and Zimmermann (2015) in a literature review, effects of environmental disasters on migration range from positive to neutral to negative outcomes. Above all, most of the empirical literature suffers from two major problems. First, they exclude migration towards non-OECD countries, which might induce a large measurement error. According to the Global Bilateral Migration Database, migration to non-OECD countries accounts for 51% of international migration. Piguet et al. (2011) note that disasters are unlikely to affect migration in rich and politically stable economies. Exceptions that also include non-OECD destinations are Beine and Parsons (2015, 2017), who find little effect of climate change on migration, and Cattaneo and Peri (2016), who find in a monadic regression that higher temperature increases migration to urban areas and middle-income countries, while poor countries are liquidity constrained. Second, studies have often used information on the incidence of disasters from databases drawn from insurance records or news. This introduces severe reporting and endogeneity biases, as both, insurance penetration and damage caused are correlated with development, which in turn affects migration patterns (for a detailed discussion, see Felbermayr and Gröschl, 2014).

In this paper, a stylized theoretical gravity model of migration is constructed based on derivations by Anderson (2011) and natural disasters are included as random shocks. To estimate the implications of this model, a conditional fixed effects Poisson Pseudo Maximum Likelihood approach advocated by Santos Silva and Tenreyro (2006) is followed. This paper offers two contributions beyond recent work: (i) it explicitly estimates the time-variant part of multilateral resistance (MR)[7] in bilateral migration, thereby allowing disasters in the origin *and* the destination to vary in impact; and (ii) it deploys updated and extended natural disaster

[6] Empirical economists face a lack of observational data and definitions for migration and disasters.

[7] MR terms are adapted to the setup from the derivations of Baier and Bergstrand (2009) using a Taylor series expansion.

data from *ifo GAME*, based on exogenous intensity measures, solving the endogeneity and reporting problems of insurance- and news-based disaster data.

Bilateral migration data provided by the World Bank is constructed from decennial census information which captures temporary migration only to a very limited extend. Any kind of migration that takes place and is reverted within the ten years between two census rounds is excluded, as these short-term migrants do not show up in census stocks. Moreover, the data extends almost exclusively to legal immigrants.[8] Therefore, the presented results hold almost only for legal medium to long-run international migration. Even though temporary or short-term migration present a very valid coping strategy in face of natural disasters, it cannot be captured with the available world-wide data.

Obtained results suggest little evidence for an impact of natural disasters on medium to long-term international migration. Using the full sample and considering the timing of events combined with migration decisions, findings suggest that a mean event at origin leads to 1.7% more bilateral migration. The identification of statistically significant effects becomes very noisy if timing is not considered. Moreover, decomposing disasters by type does not yield evidence for a clear pattern. When countries are distinguished by income levels, heterogeneity across groups is found. There is no evidence that individuals from low-income countries migrate internationally if struck by natural disasters. International migration or other adaptation strategies may not be feasible for financially constrained individuals (see also Cattaneo and Peri, 2016 and Beine and Parsons, 2017). If high-income countries experience disasters, their outmigration declines, possibly due to high insurance penetration rates. These may cause incentives to stay as insured capital is upgraded after a disaster. Middle-income countries show a clear pattern of migration due to disasters - which lead to international migration of 1.4%, while those at potential destinations decrease migration by 11.5%, both evaluated at the mean. Hence, examining the effect of natural disasters on migration using a full sample may lead to aggregation bias.

The remainder of the paper is structured as follows. Section 2.2 provides a theoretical gravity model of migration. Section 2.3 describes details on the empirical strategy and section 2.4 addresses the data. Section 2.5 provides results and a sensitivity analysis. The last section concludes.

[8] The exact implications of this for the results remain unclear: Undocumented migrants may be more mobile after an exogenous shock but are also more likely to be financially constrained, potentially favoring less costly internal migration.

## 2.2 A Gravity Model of Migration

To provide a simple theoretical motivation for estimating bilateral migration in a gravity framework, Anderson (2011) is followed. The decision to migrate is, in contrast to the decision to export, characterized by the choice over a discrete number of alternative locations on a global scale. The costs of migration are common to all migrants within a particular bilateral link, albeit migration costs may have an idiosyncratic component reflecting individual costs or utility from moving.

Consider a multi-country framework where $i, j = 1, \cdots, C$ denote countries, $h = 1, \cdots, H$ denotes individuals, and $t$ denotes time. Each individual $h$ has an idiosyncratic component of utility from migrating, $\xi_{ijh,t}$, which is unobservable and independently distributed across individuals with an $iid$ extreme value distribution. In addition, individuals face costs of migration, which are the same for all workers that migrate in a particular migration corridor, $\kappa_{ij,t} = \kappa_{ji,t}$.[9] Migration costs constitute an iceberg cost factor $\kappa_{ij,t} \geq 1$ and $\kappa_{ii,t} = 1$ at time $t$. Migration costs are a function of several factors, comprising time-invariant costs from the move, such as cultural proximity (common language, common colonizer), or geographic location (distance, common border), and time-variant factors, such as networks (stock of migrants), regional networks (regional trade agreements), immigration policies, political ties between country-pairs, or benevolence of welfare states in receiving countries. Moreover, migration costs may also follow a common time trend $t$.

When a natural disaster strikes, it damages and destroys both physical and human capital. It follows that disasters affect the migration decision by reducing the productivity of labor. By this they affect wages and eventually also the movement of population.[10] Natural disasters are formally introduced as random shocks $\Phi$, where $\Phi \geq 1$.[11] The occurrence of random

[9] Note that migration costs may as well vary by skill levels. Migration costs could be lower for skilled workers and increase with decreasing skill level. Individuals with low skill levels may benefit more from migrating but also face relatively higher migration costs given their lower income and potential liquidity constraints they face in situations where they cannot save or borrow enough to pay the costs of migration. On the other hand, migrant networks may increase with skill and thus lead to lower migration costs for the more highly skilled. This implies selection mechanisms by skill, which this model abstracts from due to a disability to test implications empirically on the basis of available global migration data that does not allow distinguishing migrants by skill level.

[10] Note that natural disasters could also affect migration costs directly, such that migration costs would increase with natural disasters as, for instance, infrastructure or amenities get destroyed. This would make migration more costly and less likely. Here, it is abstained from modeling a direct effect; instead it is considered that disasters change multilateral resistance of countries, thus assuming an implicit effect on migration costs.

[11] Random shocks may also incorporate civil or international war, changes in governance from autocracy to democracy or vice versa, etc.

shocks and the damage they cause are assumed to be idiosyncratic across locations. Random shocks have a transitive effect on labor productivity as they suddenly shift demand and/or supply structures. Let the wage net of migration costs and net of random shocks to labor productivity in the destination be $w_{j,t}/(\kappa_{ij,t}\Phi_{j,t})$, where $w_{j,t}$ denotes the wage in destination $j$ at time $t$, and wage net of the labor productivity shock at home is $w_{i,t}/\Phi_{i,t}$, where $w_{i,t}$ denotes the wage at origin $i$ at time $t$ and $\kappa_{ii,t} = 1$. Then, an individual $h$ migrates if the utility from migrating to some destination $j$ at time $t$ is larger than from staying at home, $(w_{j,t}/(\kappa_{ij,t}\Phi_{j,t}))\,\xi_{ijh,t} \geq w_{i,t}/\Phi_{i,t}$.[12]

To evaluate migration, suppose expected utility is a logarithmic constant relative risk aversion (CRRA) CES function.[13] Specifically, the observable component of log-linear utility from migrating is

$$\ln u_{ij,t} = \ln w_{j,t} - \ln \kappa_{ij,t} - \ln \Phi_{j,t} - [\ln w_{i,t} - \ln \Phi_{i,t}].^{14} \tag{2.1}$$

Note that individual decisions can be aggregated up to a representative individual (McFadden, 1974), as migrants are assumed to be homogeneous except for the random term $\xi_{ijh,t}$. To retrieve a tractable gravity equation, it is assumed that the aggregated level of the discrete choice probability is equal to migration flows from source $i$ to destination $j$ at time $t$. Aggregate bilateral migration is then given as

$$M_{ij,t} = P(u_{ij,t})N_{i,t}, \tag{2.2}$$

[12] The average expected gain in utility from not migrating (remaining in $i$) is zero for individuals that choose to stay in the origin (Ortega and Peri, 2009). $w_{i,t}$ and $\Phi_{i,t}$ are constant across all destinations.

[13] The CES utility function is given as $u_{ij,t} = \frac{1}{\sigma-1}\left(\frac{w_{j,t}/(\kappa_{ij,t}\Phi_{j,t})}{w_{i,t}/\Phi_{i,t}}\right)^{\sigma-1}$, where $\sigma$ is the elasticity of substitution for wages in different locations (also called the coefficient of relative risk aversion). Compared to partial equilibrium Random Utility Maximization (RUM) models – an alternative theoretical foundation used widely in the migration literature (see Beine et al. (2016) for a discussion and related literature) –, the approach presented in this paper features a similar setup, yields a similarly tractable gravity equation, but allows theoretically tracing the wage effects of natural disasters, which drive the migration decision. Simultaneously, it allows accounting for countervailing general equilibrium labor market effects induced by changes in the labor stocks.

[14] Utility may also be derived from country characteristics $C$ that denote benefits such as public infrastructure, amenities, the welfare state etc. (see for instance Beine and Parsons (2015) for a more detailed discussion). Here, these benefits are not specifically modeled as no particular attention is devoted to country specific factors which do not alter the prediction of the random shock variable. The role of these factors for migration is considered by country dummies (time-invariant) and by controls and MR terms (time-varying) in the empirical section.

where the population in the source country takes a decision on migration and, with $\xi_{ijh,t}$ following an iid extreme value distribution, the probability $P(u_{ij,t})$[15] is given by

$$P(u_{ij,t}) = P(u_{ij,t} = \max_{\mathrm{k}} u_{ik,t}) = \frac{e^{u_{ij,t}}}{\sum_k e^{u_{ik,t}}} \quad \text{for} \quad ik \neq ij. \tag{2.3}$$

Since the $\Phi$'s and $\kappa$'s enter the model multiplicatively through their effect on wages, they combine into a shock-cost measure $\theta_{ij,t}$ that represents both migration costs and random shocks from natural disasters or similar factors on labor productivity.[16] Both migration costs and random shocks to labor productivity operate in combination with given wages to generate the allocation of migrants. The combined shock-cost measure is then given as $\theta_{ij,t} = \kappa_{ij,t}\Phi_{j,t}/\Phi_{i,t}$.

With logarithmic utility, the structure of the migration equation corresponds to

$$M_{ij,t} = \frac{(w_{j,t}/\theta_{ij,t})^{\sigma-1}}{\sum_k (w_{k,t}/\theta_{ik,t})^{\sigma-1}} N_{i,t}. \tag{2.4}$$

To derive a tractable gravity equation, define $\Gamma_{i,t} \equiv \sum_k (w_{k,t}/\theta_{ik,t})^{\sigma-1}$ and specify the aggregated labor market clearing condition as $N_{j,t} \equiv \sum_i M_{ij,t}$. The clearing condition is then $N_{j,t} = w_{j,t}^{\sigma-1} \sum_i (\theta_{ij,t}^{1-\sigma}/\Gamma_{i,t}) N_{i,t}$. In equilibrium, wages are

$$w_{j,t}^{\sigma-1} = \frac{N_{j,t}}{N_t \Gamma_{j,t}} \tag{2.5}$$

with total world population $N_t \equiv \sum_i N_{i,t} \equiv \sum_j N_{j,t}$ and $\Gamma_{j,t} = \sum_i \frac{\theta_{ij,t}^{1-\sigma}}{\Gamma_{i,t}} \frac{N_{i,t}}{N_t}$. Substituting for the equilibrium wage in equation (2.4) using equation (2.5) yields the tractable gravity specification of migration

$$M_{ij,t} = \frac{N_{i,t} N_{j,t}}{N_t} \left( \frac{\theta_{ij,t}}{\tilde{\Gamma}_{i,t} \tilde{\Gamma}_{j,t}} \right)^{1-\sigma}, \tag{2.6}$$

with the outward migration friction price index $\tilde{\Gamma}_{i,t} = \left[ \sum_j \frac{N_{j,t}}{N_t} \left( \frac{\theta_{ij,t}}{\tilde{\Gamma}_{j,t}} \right)^{1-\sigma} \right]^{1/1-\sigma}$ and the inward migration friction price index of $\tilde{\Gamma}_{j,t} = \left[ \sum_i \frac{N_{i,t}}{N_t} \left( \frac{\theta_{ij,t}}{\tilde{\Gamma}_{i,t}} \right)^{1-\sigma} \right]^{1/1-\sigma}$.

[15] For examples of bilateral migration discrete choice models that build on a multinomial logit function, see Beine et al. (2011), Grogger and Hanson (2011), Gibson and McKenzie (2011) or Beine and Parsons (2015).

[16] This useful simplification follows Anderson (2009) and is exploited in what follows. It can be decomposed at any point into its components.

To make the impact of random shocks visible in the gravity equation of migration, $\theta_{ij}$ is decomposed. This gives

$$M_{ij,t} = \frac{N_{i,t}N_{j,t}}{N_t}\left(\frac{\kappa_{ij,t}}{\tilde{\Gamma}_{i,t}\tilde{\Gamma}_{j,t}}\right)^{1-\sigma}\Phi_{i,t}^{\sigma-1}\Phi_{j,t}^{1-\sigma}, \tag{2.7}$$

and multilateral resistance terms are $\tilde{\Gamma}_{i,t} = \left[\sum_j \frac{N_{j,t}}{N_t}\left(\frac{\kappa_{ij,t}}{\tilde{\Gamma}_{j,t}}\right)^{1-\sigma}\left(\frac{\Phi_{j,t}}{\Phi_{i,t}}\right)^{1-\sigma}\right]^{1/1-\sigma}$ and $\tilde{\Gamma}_{j,t} = \left[\sum_i \frac{N_{i,t}}{N_t}\left(\frac{\kappa_{ij,t}}{\tilde{\Gamma}_{i,t}}\right)^{1-\sigma}\left(\frac{\Phi_{j,t}}{\Phi_{i,t}}\right)^{1-\sigma}\right]^{1/1-\sigma}$.

The first term of equation (2.7) denotes bilateral migration in a world without frictions, where migrants are found in equal shares relative to the population in all destinations. The second term denotes the impact of frictions in a world that entails costs to migration. The larger bilateral migration costs $\kappa_{ij,t}$, the lower are migration flows. Albeit, in a world in which migrants choose from a set of alternative destinations, migration also depends on multilateral resistance, which captures worldwide bilateral migration costs. The third term indicates that random shocks to labor productivity in the origin and in the receiving country affect migration. The larger the shock in the origin $\Phi_{i,t}$, the higher are migration flows. The larger the shock in the destination $j$ at time $t$, the lower are migration flows.

## 2.3 Empirical Strategy

To test the predictions of the previous section regarding the effect of disasters on bilateral migration patterns, a fully fledged gravity model is outlined on a panel of bilateral migration and primary disaster data. Estimating an augmented gravity specification, it is examined how natural disasters in the origin ($\Phi_{i,t}$) and in the destination ($\Phi_{j,t}$) affect bilateral migration rates ($M_{ij,t}/N_{ii,t}$).

To get an estimable equation on migration rates, logs are taken of equation (2.7) to obtain

$$\ln\frac{M_{ij,t}}{N_{ii,t}} = (1-\sigma)\ln\kappa_{ij,t} + (\sigma-1)\ln\tilde{\Gamma}_{i,t} + (\sigma-1)\ln\tilde{\Gamma}_{j,t} + (\sigma-1)\ln\Phi_{i,t} + (1-\sigma)\ln\Phi_{j,t}.^{17} \tag{2.8}$$

[17] Note that $N_t$ is constant, $\ln N_{j,t}$ is omitted, and $\ln N_{i,t}$ is transformed to $\ln N_{ii,t}$ (the non-migrant population of $i$) to obtain migration rates as the dependent variable rather than migration flows. Mayda (2010); Beine and Parsons (2015) are followed by using migration rates.

As discussed earlier in Section 2.2, migration costs comprise time-invariant and time-variant components. The cost function is modeled empirically as

$$\kappa_{ij,t} = g(\ln(\text{DIST}_{ij}), \text{ADJ}_{ij}, \text{LAN}_{ij}, \text{COL}_{ij}, \text{RTA}_{ij,t}, \text{MigStock}_{ij,t-1}, \nu_t, \nu_i, \nu_j) \tag{2.9}$$

which is a function of controls for time-invariant historical or cultural country characteristics, such as bilateral distance $\ln(\text{DIST}_{ij})$, adjacency $\text{ADJ}_{ij}$, common language $\text{LAN}_{ij}$, and colonial heritage $\text{COL}_{ij}$. The cost function also comprises time-varying components, such as regional trade agreements $\text{RTA}_{ij,t}$ that account for the fact that more integrated countries or regions might also experience higher migration flows.[18] $\text{MigStock}_{ij,t-1}$ is the stock of migrants from country $i$ residing in $j$ at time $t-1$, which captures network effects.[19] $\nu_t$ are time specific dummies that account for common trends. $\nu_i$ and $\nu_j$ are a complete collection of origin and destination country dummies which account for all time-invariant country characteristics. Multilateral resistance (MR) terms have a time-invariant and a time-variant component. While the time-invariant component of MR is fully captured by origin and destination country fixed effects, the time-variant component of MR is captured by $\tilde{\Gamma}_{i,t}$ and $\tilde{\Gamma}_{j,t}$ in equation (2.8).[20] As in the traditional gravity model, price indexes are computable once migration costs $\kappa_{ij,t}$ are constructed econometrically.

Zero bilateral migration flows make up about 65% of observations. To account for these zero migration flows and to correct for heteroskedastic error terms, a conditional fixed effects (FE) Poisson Pseudo Maximum Likelihood (PPML) approach is chosen, as advocated by Santos Silva and Tenreyro (2006).[21] Based on equation (2.8), a gravity equation is estimated of the form

[18] The RTA variable incorporates free trade agreements, currency unions and customs unions.

[19] The recent literature on migration is followed, which identifies migrant networks to promote bilateral migration flows, trade and capital flows (Rauch and Trindade, 2002; Munshi, 2003; Kugler and Rapoport, 2007; Docquier and Lodigiani, 2010; Bertoli and Fernández-Huertas Moraga, 2012; Patel and Vella, 2013; Docquier et al., 2014). In particular, Beine et al. (2011) find that migrant networks significantly increase migration flows to OECD countries. To address potential endogeneity concerns pointed out by Munshi (2014), lagged migration stocks are excluded as a robustness check from the baseline specification.

[20] Ideally, the time-variant component of MR is controlled for using time-varying country fixed effects. Since the disaster variables are country-time specific, this approach is unfeasible. The fixed effects would pick up the variation in the variables of interest.

[21] If zeros are prevalent in the data and error terms are heteroskedastic, PPML generates consistent estimates even when the underlying distribution is not strictly Poisson.

$$\frac{M_{ij,t}}{N_{ii,t}} = \exp[\alpha_1 \Phi_{i,t} + \alpha_2 \Phi_{j,t} + \alpha_3 \ln(\text{GDP}_{j,t}/\text{GDP}_{i,t}) + \alpha_4 \text{Civil War}_{i,t} + \alpha_5 \text{Civil War}_{j,t} + \boldsymbol{\alpha_6 \kappa_{ij,t}} + \boldsymbol{\alpha_7 \mathbf{MR}_{\mathbf{ij,t}}}] + \varepsilon_{ij,t} \tag{2.10}$$

where $\frac{M_{ij,t}}{N_{ii,t}}$ is the decennial bilateral migration rate calculated as the migration flow from $i$ to $j$ at decade $t$ divided by the domestic non-migrant population in country $i$. $\Phi_{i,t}$ ($\Phi_{j,t}$) capture the physical intensity of natural disasters in the origin (destination) in a given decade. These may be included as an index variable or separately for specific types (see data section for more detail). As common in the migration-disaster literature, two country specific controls that vary over time are included directly. $\text{GDP}_{j,t}/\text{GDP}_{i,t}$ is the ratio of destination to origin decennial average per capita GDP and proxies average wage differences. $\text{Civil War}_{n,t}$ with $n = i, j$ are count variables of the number of years in which civil wars took place in the source or the receiving country, respectively, within the last 10 years of observation. $\boldsymbol{\kappa_{ij,t}}$ is a vector of migration costs as outlined in equation (2.9). It represents time constant and time-varying costs including a complete collection of origin and destination country dummies and time specific fixed effects. The constructed MR terms $\mathbf{MR_{ij,t}} = \tilde{\Gamma}_{i,t}, \tilde{\Gamma}_{j,t}$ capture the time-variant component of multilateral resistance (e.g., immigration policies or benevolence of the welfare state). MR indices are derived from a first-order Taylor series expansion of the gravity equation following Baier and Bergstrand (2009). MR terms are approximated based on distance ($\text{MRDIST}_{ij,t}$), adjacency ($\text{MRADJ}_{ij,t}$), common language ($\text{MRLAN}_{ij,t}$), colonial relationship ($\text{MRCOL}_{ij,t}$), and RTAs ($\text{MRRTA}_{ij,t}$) which are weighted by population over world population (a proxy for a country's relative migrant potential). For details see Appendix B.1.1. This econometric approach allows controlling simultaneously for the direct effects of disasters in the source and the destination country and for time-varying country characteristics absorbed in the MR terms. $\varepsilon_{ij,t}$ is an additive error term.

The model suggests that $\alpha_1$ is positive such that disasters in the origin induce migration out of affected countries, while $\alpha_2$ is negative indicating that disasters in potential destinations reduce migration. This theoretical prediction is brought to the data in the next section.

## 2.4 Data

### 2.4.1 International Migration

Two data sets are combined. The *Global Migrant Origin Database* (Version 4, 2007) provided by the World Bank reports bilateral migration stocks (based primarily on the foreign-born concept) in intervals of 10 years from 1960 to 2000 for 226 countries. The data set combines census and population register records to construct decennial matrices corresponding to the last five completed census rounds. Data for 2010 are also provided by the World Bank and updates data by Ratha and Shaw (2007) as described in the Migration and Remittances Factbook 2011 (see Canuto and Ratha, 2011). The 2010 data set also uses the foreign-born concept and similar sources and methods as the 1960-2000 data.

To calculate bilateral decennial migration rates, the difference between contiguous bilateral migrant stocks are taken to approximate migration flows, which are then divided by the non-migrant origin population (following Beine and Parsons, 2015). Non-migrant origin population is constructed as the country's total population (according to WDI) minus the sum of immigrants in that country. In some cases, migration stocks shrink over the observed time period, which leads to negative values. As the exact reason of the decrease in migration stocks is not clear, all negative values are ignored by setting them to zero, implicitly assuming that migrant stocks decrease due to mortality.[22]

In the sample, zero bilateral migration flows make up about 65% of observations. To account for these zero migration flows and a potentially heteroskedastic error structure, a FE PPML model is estimated. Still, observations are lost due to missing data for migration rates, control variables and natural disasters, preserving 66,673 observations for estimation. These preserved observations spread over all three decades (17,556 observations for 1981–1990, 24,806 for 1991–2000, and 24,311 for 2001–2010) and across 162 countries as listed in Appendix B.1.2, Table B.3. Hence, sufficient variation can be expected in the data.[23]

[22] This strategy is in line with the literature. The actual reasons for negative differences between subsequent bilateral migrant stocks are related to the underlying issue that migration flows converted from stocks do not factor out stock changes due to mortality, return migration or migration to a third country (see Beine et al., 2016). The data does not allow disentangling the true drivers of negative stock differences.

[23] The loss of data is commonly known in the literature. For example Beine and Parsons (2015), the paper most closely related to this study, have similar observation numbers spread over four decades from 1960-2000.

Table B.1 in Appendix B.1.2 includes summary statistics for the migration rate. The decennial migration rate ranges between 0% and 50% of the total non-migrant origin population at the beginning of the respective decade. Due to the large number of zero migration flows, the mean migration rate is 0.02%. For a deeper understanding of the dimension of international migration, the table also includes figures for the underlying decennial migration flows, ranging from 0 to 4,705,677 people, with a mean of 1,726. The maximum migration flow is observed from Mexico to the United States between 1990 and 2000 and corresponds to a migration rate of 6% of the Mexican non-migrant population at the beginning of 1990. The maximum migration rate of 50% is observed from Brunei to India between 1980 and 1990 and corresponds to a decennial migration flow of 71,089 people.

While temporary international migration may pose a valid mechanism for adapting to transitory natural disasters, it must be emphasized that the decennial World Bank data includes such short-term migrants only to a very limited extent. Results almost exclusively rely on medium to long-run international migration, which excludes any kind of migration that takes place and is reverted within the ten years between two census rounds, as these short-term migrants are not captured in the census stocks. The data does not allow identifying the share of temporary vs. long-run migrants. Moreover, the World Bank data relies on official census data, hence undocumented migrants are not included. Finally, note that a large number of bilateral migrant stocks in the data are estimated rather than observed, such that attenuation due to measurement error may pose an inherent issue.[24]

### 2.4.2 Natural Disasters

This study uses natural disaster data from the ifo GAME database on geological and meteorological events, first introduced by Felbermayr and Gröschl (2014). The database contains physical intensities of earthquakes, volcanic explosions, storms, droughts, floods, and temperature anomalies on a monthly basis from 1979 to 2014 for 232 countries.[25] The data included in ifo GAME stem from various primary sources and come in two different types of geo-coding requiring different treatment: (a) non-gridded disasters (volcanoes, hurricanes, and earth-

[24] This implies that presented results only hold for more permanent (long-term) migration, whereas no claims can be inferred about temporary or short-term migration, which still might present a very valid coping strategy in face of transit natural disasters.

[25] An earlier version of the Ifo GAME data base ranging from 1979 to 2010, covering 188 countries, and using slightly different mapping procedures is currently available at `http://www.cesifo-group.de/ifoHome/research/Departments/International-Trade/Ifo_GAME.html`.

quakes) are aggregated to the country level by directly mapping the data to all countries within a radial geodesic buffer around the exact disaster geo-location;[26] (b) gridded data (temperatures, precipitation, SPEI) are aggregated to the country level by calculating area-weighted arithmetic means. The exact data sources as well as the respective spatio-temporal aggregation procedures and index choices are described in detail below; descriptive statistics are shown in Figure 2.2.

**Earthquakes.** A country's earthquake hazard is measured by its maximum earthquake magnitude. Physical earthquake magnitudes from the Incorporated Research Institutions for Seismology (IRIS) are mapped to each country within 150 km of the respective epicenter. The data is aggregated to the decennial level by collapsing maximum earthquake magnitudes across all months. The resulting earthquake magnitude is distributed between 0 and 10, with a mean of 5.9 and a standard deviation of 1.9 (compare Figure 2.2).

**Volcanic Explosions.** A country's volcanic activity is measured by its maximum volcanic explosivity index (VEI). The VEI is obtained from the Smithsonian Global Volcanism Program and mapped to each country within 50 km of the respective volcano's geo-location. It is aggregated to the decennial level for each country by collapsing it to its respective maximum across all months. Resulting VEIs are distributed between 0 and 6, with a mean of around 0.4 and a standard deviation of 1.1 (compare Figure 2.2).

**Storms.** In order to measure storms, a country's maximum combined wind speed from two data sources is used. Hurricane wind speeds in knots at the exact locations and paths of hurricane centers come from the International Best Track Archive for Climate Stewardship (IBTrACS) v03r07, provided by the World Meteorological Organization (WMO) and the US National Oceanic and Atmospheric Administration (NOAA). Hurricane wind speeds are mapped to each country within a 100 km range of the respective hurricane eye. Wind speeds of winter or summer storms in knots stem from weather station data of the Global Summary of the

[26] Not knowing the true spatial extent of natural disasters poses a potential problem. Volcanoes are very local events, but gas plumes can have extensive impact. Also, the true geographic extent of earthquakes and hurricanes is not easy to predict given only their magnitude and location at center. In addition, geological, meteorological and surface characteristics matter. This study thus relies on approximations from the literature, as the prediction of the true spatial extent of disaster events lies beyond the scope of this paper.

Day (GSOD) statistics, which report wind speeds measured at terrestrial weather stations worldwide by the exact geo-location of the respective station. To obtain a decennial measure for each country, maximum wind speeds are collapsed across all months. Resulting combined wind speed is distributed between 16 and 165 knots, with a mean of 78.3 and a standard deviation of 29.8 (compare Figure 2.2).

**Temperature.** Extreme temperature is measured by the absolute mean temperature difference from the long-run monthly mean. Monthly mean land surface air temperatures in degrees Celsius at 0.5° x 0.5° latitude-longitude grid cell levels come from the Climate Prediction Center of the National Centers for Environmental Prediction. The data combine and interpolate information collected from the Global Historical Climatology Network Version 2 (GHCN) and the Climate Anomaly Monitoring System (CAMS). Spatially aggregating grid cell data addresses two caveats. First, coordinates of measuring points are located at grid cell centers which means that (a) small countries may not have any measuring points within their geographic boundaries, and (b) for larger countries, measuring points in border regions may concern only a relatively small aerial fraction. Second, fixed-degree grid cells feature varying metric area along latitudes due to the earth's curvature. Hence, measuring points more remote from the equator affect smaller land area. The following procedure is applied to address both caveats: First, each country $i$ is split into fractions $frac$ by grid cells. Second,

Figure 2.1 : 2.5° Grid Cell Aggregation Example

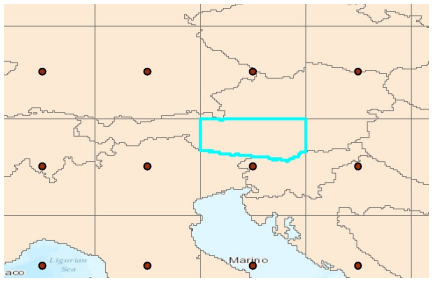

*Source:* Esri, own calculations.

geodesic land area $a$ in km$^2$ is calculated for each fraction in a cell. At any point in time $t$, values of each measuring point are added to all fractions within its respective cell, as they constitute the best proxy available in their respective grid cell (compare Figure 2.1). Finally, gridded observations are aggregated to the country level by calculating a weighted mean using each country's geodesic land area within a grid cell as analytic weights:

$$\bar{x}^{*^{i,t}} = \frac{\sum_{frac \in i} a^i_{frac} \cdot x^{i,t}_{frac}}{\sum_{frac \in i} a^i_{frac}} \tag{2.11}$$

Then, the differences between monthly mean temperatures and the long-run (1979-2014) monthly mean is calculated for each country. To match the decennial data, temperature differences are collapsed across all months in a decade. In order to treat heat and cold waves alike, absolute values of the measure are taken (see also Felbermayr and Gröschl, 2014). The absolute temperature difference is distributed between 0 and 1.4 degrees Celsius, with a mean of 0.3 and a standard deviation of 0.2 (compare Figure 2.2).

**Precipitation.** Excessive precipitation, which might exceed percolation and sewage capacities, is captured by the positive maximum precipitation difference from the long-run monthly mean. Monthly mean precipitation in mm/day at 2.5° x 2.5° latitude-longitude grid cell level are obtained from the National Aeronautics and Space Administration (NASA) Global Monthly Merged Precipitation Analyses of the Global Precipitation Climatology Project (GPCP) Version 2.2, which combines and harmonizes observations from satellites and weather stations (gauges). The gridded observations are aggregated to the country level in the same way as for temperatures (see equation (2.11)). For each country, the differences between monthly mean precipitation and the long-run (1979-2014) monthly mean is calculated. For the decennial level, maximum precipitation differences across all months in a decade are used. To avoid picking up the effect of potential droughts, only positive maxima are considered. The resulting indicator is distributed between 0.1 and 21.2, with a mean of 4.2 and a standard deviation of 2.9 (compare Figure 2.2).

**Droughts.** Droughts are approximated by the negative mean of the Standardized Precipitation-Evapotranspiration Index (SPEI) computed at a time-scale of 9 months.[27] Monthly mean precipitation in mm/day at 0.5° x 0.5° latitude-longitude grid cell level are obtained from the Climatic Research Unit of the University of East Anglia (CRU TS v3.23). While this data set is based on weather stations, its longer time-scope and the availability of information

[27] The SPEI is specifically designed to quantify and monitor droughts according to their intensity and duration (Vicente-Serrano et al., 2010). It takes the amount of rainfall at given locations as well as the evapotranspiration into account and thus is an advancement of the Standardized Precipitation Index (compare McKee et al., 1993).

on evapotranspiration are necessary ingredients to calculate the SPEI. The climatic water balance (precipitation minus potential evapotranspiration) is calculated at grid cell level for each month. The water balance is then standardized for each grid cell by use of a log-logistic distribution function (applying an unbiased Probability Weighted Moments method).[28] The SPEI is standardized with zero mean and a standard deviation of one, where negative values indicate a drought. The gridded SPEIs are aggregated to the country level by use of equation (2.11). To get to the decennial level, SPEI values are collapsed to their mean across all months, taking only negative values in absolute terms into account. The resulting SPEI indicator is distributed between 0 and 1.2, with a mean of 0.1 and a standard deviation of 0.2 (compare Figure 2.2).

Figure 2.2 : Kernel Densities of Disaster Indicators

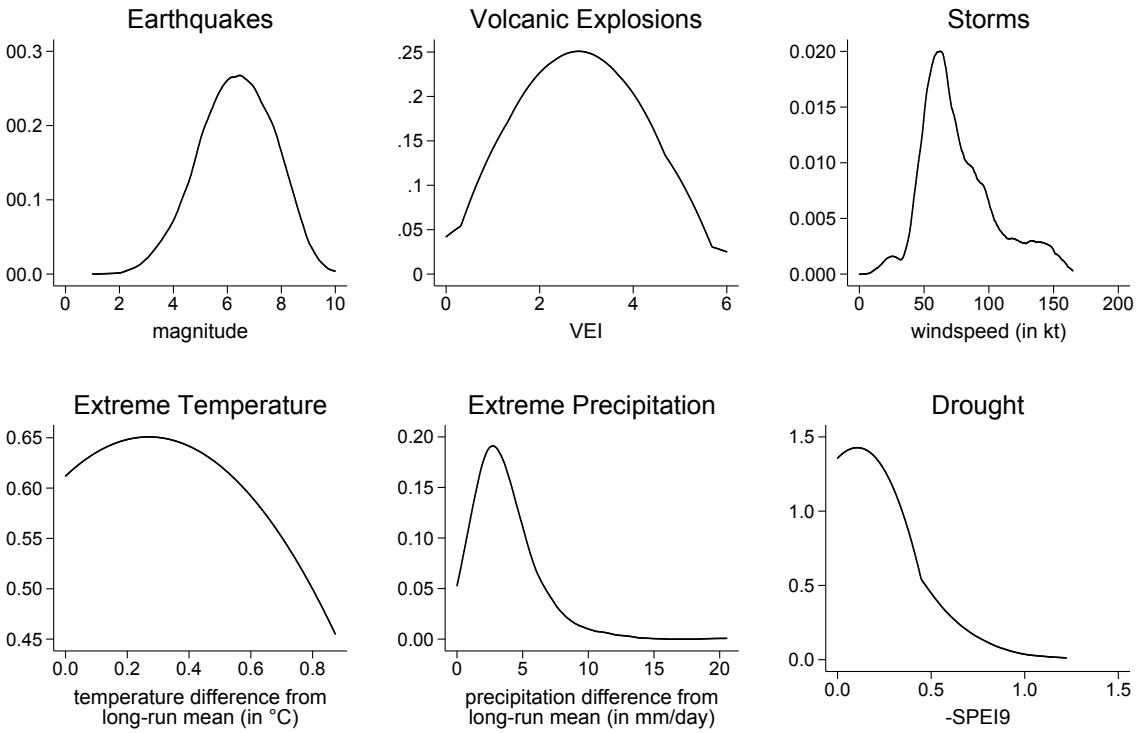


*Note:* Zeros excluded for earthquakes and volcanic explosions

[28] Data from the current month and of the respective past nine months are used, giving all months the same weight and taking 1901-2014 as a reference period for obtaining the distribution parameters.

**Distribution Across Income Groups.** The above indicators are compared across income groups in Figure B.1 in the Appendix. It can be seen that earthquakes are more common among middle-income countries with a mean magnitude of 6.5, than in high- or low-income regions. Volcanic explosions also mostly spread across middle-income countries, while there is very little volcanic activity in low-income countries, but quite some activity in high-income groups with a lower standard deviation but a higher mean of 0.5. Storms have the lowest mean density (61.8 knots) in low-income regions with some spread especially at the higher end (>100 knots). Middle-income countries have a higher mean (75.7) but experience more storms in the upper tail, while high-income countries have the highest mean with 85.4 knots. Contrasting this, temperature differences are quite evenly distributed across income groups, as are differences in excess precipitation where middle-income and especially high-income countries experience a long tail. Droughts measured at absolute negative SPEI levels are more prevalent in low-income countries with a mean of 0.3 but less spread than in middle-income regions (standard deviation of 0.2).

**Disaster Index.** A combination of four different disaster indices is used. The simplest one combines all types of disaster intensity measures into an index variable, Disaster Index$_{i,t}$ = Quake$_{i,t}$ + Volcano$_{i,t}$ + Storm$_{i,t}$ + $\Delta$ Precipitation$_{i,t}$ + Drought$_{i,t}$+ $\Delta$ Temperature$_{i,t}$, using an equal weights scheme. Moreover, an index weighted by the inverse of the standard deviation of each disaster type within a country is considered (compare Felbermayr and Gröschl, 2014). This is guided by the idea of precision weights, such that no one disaster component dominates the movement of the index. Finally, the time dimension is also taken into account by weighting each physical intensity with a probability obtained from a normal distribution $f(x) = N(0; 1)$ which is fit over 120 months in a decade.[29] This way, disaster magnitudes are onset weighted at the monthly level, such that events which occur earlier or later within a decade get a smaller weight than events occurring in the middle of a decade when aggregating to the decennial level. The rational for using a bell-shaped onset weighting scheme is that the effect of natural disasters that occurred at the beginning of the decade may already have smoothed out before the next census, whereas events occurring at the very end of a decade might not yet show an effect in the census as it takes some time for people to adjust. This approach is adapted to this framework based on an idea by Noy (2009), who studies the impact of disasters on macroeconomic output over a year and linearly adjusts disasters by onset month to account

[29] The distribution is shifted such that the first and the last month each correspond to f(-3) and f(3) respectively and then re-scale such that $max[f(x)] = 1$, ensuring a maximum probability-weight of 1.

for their occurrence during the observed year. Again, the simple and the inverse standard deviation weighted index are used with and without with onset weighting.

As the impact of a disaster on the economy might depend on the disaster intensity relative to the size of the economy, Skidmore and Toya (2002) are followed by scaling all respective disaster variables by land area. This is potentially important, because it alleviates biases resulting from spatial aggregation. On the one hand, larger countries ceteris paribus have a higher chance of being hit by a disaster of a given magnitude. On the other hand, the larger a country is the less likely will a natural disaster at a given location within that country have a statistically significant impact on inward or outward migration. Descriptive statistics on the various disaster indices can be found in Table B.1 in the Appendix.

### 2.4.3 Controls

Data on population size and GDP per capita stem from the World Bank's World Development Indicators (WDI). Information on civil wars are taken from the Intra-State War Data (v4.1) of the Correlates of War Project. The measure used is the total number of years involving civil wars within the last 10 years of the reported migration observation. Geographic and cultural linkages – distance, common border, common language, colonial relation – as well as land area in square kilometers are taken from the CEPII Geographic and Bilateral Distance Database (2011). Information on regional trade agreements comes from the RTA-Gateway of the WTO.[30] Countries' income groups are defined along 2014 World Bank Gross National Income per capita, using the World Bank Atlas Method.

## 2.5 Results

This section presents results on the impact of aggregated natural disasters and disaggregated disaster types on medium to long-run migration patterns. An examination of heterogeneity across income groups and a sensitivity analysis are also provided.

### 2.5.1 Baseline Results

Table 2.1 reports the baseline results. All regressions include origin and destination country fixed effects, year dummies and respective MR terms. Each column uses a different specifica-

[30] The RTA gateway is accessible via `http://rtais.wto.org/UI/PublicMaintainRTAHome.aspx`.

tion of the physical disaster intensity index as described in Section 2.4. All disaster indicators are divided by the log land area to account for size differences of countries.[31]

Across all four specifications, control variables are consistent in sign, overall magnitude, and level of significance. According to column (1), one additional year of civil war at the origin country implies an increase in the bilateral migration rate by 5.7% over a decade.[32] Conversely, one additional year of civil war at destination leads to a decline in the bilateral inward migration rate by 23% over a decade. Presence of a mutual regional trade agreement, a proxy for regional networks, increases the bilateral migration rate by 31.3%. The controls for cultural proximity are also in line with the gravity literature on migration. If bilateral distance increases by 10%, bilateral migration decreases by 7.5%. The presence of a common official language or common colonial history boost bilateral migration by 65.7% or 60% respectively. Wage differences, proxied by the log ratio of destination over origin GDP per capita, show a positive but not statistically significant effect. Moreover, a 10% increase in the lagged bilateral migrant stock, a proxy for network effects, implies an increase in the bilateral migration rate by 3.6%. The effect is slightly smaller than the estimated 4% by Beine and Parsons (2015) and lower than the 6.5% estimated by Beine et al. (2011), who use different time and country samples.[33]

The physical intensity disaster index itself shows mixed results across specifications. In column (1), the simple physical intensity disaster index is used, which sums up the physical intensities across all disaster types. Using this indicator, no statistically significant evidence for a causal effect of natural disasters on the bilateral migration rate is found. In column (2), the disaster index weighted by its inverse standard deviation is used to ensure that the entire index is not driven by variation in only one disaster type. Using this indicator, estimates imply a counter-intuitive negative push effect, suggesting that natural disasters at origin have overall led to a decline in the decennial bilateral migration rate.[34] Timing of the migration decision related to natural disasters might play an important role. Hence, disasters happening at the beginning

[31] Note that similar results are obtained without scaling by log land area.

[32] $\%\Delta$Mig.Rate $= 100 \times [e^{\beta} - 1]$

[33] Munshi (2014) points at endogeneity concerns of using the lagged bilateral migration stock as a network variable, since it could, for example, reflect unobserved demand shocks or matching skills available at the origin and needed at the destination. Bilateral fixed effects are not used in the preferred specification, since the migration data only covers three decennial waves and thus within-group variation is limited. Instrumental variable methods are not considered because network effects are not the focus of this paper. As a robustness check, it is therefore shown that the exclusion of lagged migration stocks does not affect the results on the natural disaster variables, see Appendix B.1.2, Table B.4.

[34] As shown in part 2.5.3 of this section, this effect is driven by high-income origin countries.

Table 2.1 : Baseline Results

**Dependent Variable:** Migration Rate$_{ij,t}$

| | **basic** | | **onset weighted** | |
|---|---|---|---|---|
| | simple (1) | sd weighted (2) | simple (3) | sd weighted (4) |
| Disaster Index$_{i,t}$ | −0.111 | −0.009*** | −0.060 | 0.004*** |
| | (0.09) | (0.00) | (0.11) | (0.00) |
| Disaster Index$_{j,t}$ | 0.025 | −0.002 | 0.012 | −0.013 |
| | (0.11) | (0.01) | (0.14) | (0.01) |
| **Controls** | | | | |
| $\ln\left(\text{GDP p.c.}_{j,t}/\text{GDP p.c.}_{i,t}\right)$ | 0.168 | 0.206 | 0.175 | 0.201 |
| | (0.23) | (0.23) | (0.23) | (0.23) |
| Civil War$_{i,t}$ | 0.055** | 0.058** | 0.042* | 0.060** |
| | (0.03) | (0.03) | (0.03) | (0.03) |
| Civil War$_{j,t}$ | −0.261** | −0.259** | −0.258** | −0.258** |
| | (0.11) | (0.11) | (0.11) | (0.11) |
| RTA$_{ij,t}$ | 0.272** | 0.290** | 0.291** | 0.294** |
| | (0.12) | (0.12) | (0.12) | (0.12) |
| $\ln\left(\text{Mig. Stock}_{ij,t-1}+1\right)$ | 0.357*** | 0.357*** | 0.358*** | 0.357*** |
| | (0.03) | (0.03) | (0.03) | (0.03) |
| $\ln\left(\text{Distance}_{ij}\right)$ | −0.748*** | −0.747*** | −0.743*** | −0.744*** |
| | (0.08) | (0.08) | (0.08) | (0.08) |
| Contiguity$_{ij}$ | 0.381** | 0.380** | 0.371** | 0.377** |
| | (0.16) | (0.16) | (0.16) | (0.16) |
| Common Language$_{ij}$ | 0.505*** | 0.505*** | 0.501*** | 0.508*** |
| | (0.11) | (0.11) | (0.11) | (0.11) |
| Colony$_{ij}$ | 0.470*** | 0.467*** | 0.463*** | 0.471** |
| | (0.17) | (0.17) | (0.17) | (0.17) |
| Log-Likelihood | −73.980 | −74.024 | −73.895 | −74.013 |
| Observations | 66,673 | 66,673 | 66,673 | 66,673 |

*Note:* ***, **, * denote significance at the 1%, 5% and 10% level, respectively. Constant, origin, destination and decade fixed effects and MR terms are included but not reported. Natural disasters are scaled by log land area. Robust standard errors reported in parentheses.

or towards the end of the decade might not induce migration counting into the decennial census rounds. In columns (3) and (4), the time dimension is thus taken into account, using a bell-shaped onset-weighting scheme as explained in Section 2.4. Using the simple onset weighted index still does not yield any statistically significant evidence (column 3). However, if onset weighting is combined with the disaster index weighted by inverse standard deviations in column (4), a positive and statistically significant push effect emerges, suggesting that natural disasters at origin have overall led to an increase in the bilateral migration rate by 1.68% (evaluated at the mean). Pull effects are negative but not statistically significant.

The latter finding implies that the timing of migration decisions combined with natural disaster events plays an important role for the identification of migration responses to natural disasters. Column (4) is thus taken as the default specification.[35]

### 2.5.2 Heterogeneity Across Disaster Types

As a next step, intensities of all disaster types are used simultaneously.[36] Again, all physical intensity measures are weighted by log land area, but very similar results are obtained if not done so.

Table 2.2 shows the coefficients for each physical intensity type. If basic intensity measures are used, no statistically significant evidence for causal effects is found (column (1)). Using onset weighting in column (2) reveals positive push effects of volcanic explosions, suggesting that volcanic events at origin boost the decennial bilateral outward migration rate by 7.9% (evaluated at the mean). Also, a counter-intuitive positive pull effect for earthquakes in destinations is obtained, suggesting that people migrate more towards earthquake-prone countries. This result may be driven by middle-income countries, which are more prone to earthquakes (compare Figure B.1) but are also preferred destinations for migrants from low- and other middle-income countries. One reasoning might be that even though earthquakes destroy a lot of capital, the migrants might still be better off due to reconstruction purposes that might create new jobs (particularly in high- or top-middle income countries with high insurance and investment rates). Evidence for the effects of other disaster types cannot be pinned down. Findings on controls (not shown in the Table) are similar with respect to signs, magnitudes, and levels of significance as in the baseline specification in Table 2.1.

### 2.5.3 Heterogeneity Across Origin Country Groups

Migration responses of individuals are likely to differ systematically across countries depending on income characteristics. On the one hand, individuals in poor countries may not migrate internationally after a disastrous event, because they are liquidity constrained (see Cattaneo and Peri, 2016). On the other hand, high-income countries usually feature high insurance

[35] While onset weighting can only proxy for the timeliness of adjustment, the exact shape of the actual onset response function requires further research, which lies beyond the scope of this paper.

[36] Using all physical intensities simultaneously might induce multicollinearity into the regression as, e.g., temperature is also used as a component of potential evapotranspiration in calculating the SPEI. However, if temperature events are omitted from the regression, this does not change the results.

Table 2.2 : Heterogeneity Across Disaster Types

| **Dependent Variable:** Migration Rate$_{ij,t}$ | | |
|---|---|---|
| | **basic** | **onset weighted** |
| | (1) | (2) |
| Earthquake$_{i,t}$ | 0.643 | −0.451 |
| | (0.48) | (0.65) |
| Earthquake$_{j,t}$ | 0.631 | 2.434*** |
| | (0.77) | (0.71) |
| Volcanic Explosion$_{i,t}$ | 2.144 | 2.452** |
| | (1.46) | (1.24) |
| Volcanic Explosion$_{j,t}$ | 1.565 | −1.442 |
| | (2.06) | (1.09) |
| Windspeed$_{i,t}$ | −0.120 | −0.044 |
| | (0.08) | (0.11) |
| Windspeed$_{j,t}$ | 0.038 | 0.000 |
| | (0.10) | (0.13) |
| $\Delta$ Precipitation$_{i,t}$ | 0.235 | 0.384 |
| | (0.36) | (0.50) |
| $\Delta$ Precipitation$_{j,t}$ | −1.058 | −0.797 |
| | (1.05) | (0.76) |
| $\Delta$ Temperature$_{i,t}$ | 0.120 | 4.373 |
| | (3.96) | (7.44) |
| $\Delta$ Temperature$_{j,t}$ | −2.434 | −15.279 |
| | (6.95) | (15.70) |
| Drought (SPEI)$_{i,t}$ | −5.300 | 2.076 |
| | (3.42) | (6.63) |
| Drought (SPEI)$_{j,t}$ | −1.014 | 6.467 |
| | (4.94) | (8.97) |
| Log-Likelihood | −73.882 | −73.743 |
| Observations | 66,673 | 66,673 |

*Note:* ***, **, * denote significance at the 1%, 5% and 10% level, respectively. Constant, origin, destination and decade fixed effects and MR terms are included but not reported. Natural disasters are scaled by log land area. Robust standard errors reported in parentheses. Controls included as in Table 2.1.

penetration rates. Thus, individuals from high-income countries may not see the need to migrate if losses from natural disasters are insured. In fact, crop yield destruction can easily be compensated by high-income countries via imports (as they are often financially open), whereas insured damages in built structures and capital assets may even result in a growth-propagating replacement with new, higher quality or more innovative substitutes. This might in turn boost individuals' expected earnings and therefore may lead to a decline in outward migration. In line with this reasoning, finding evidence for a significant migration response to natural disasters by liquidity constrained low-income countries should not be expected, whereas insured high-income countries may either show no or even a negative effect for disas-

ters at origin. Middle-income countries, where individuals have the financial means to migrate but insurance penetration rates are rather low are thus most likely to exhibit international migration in case of natural disasters. Consequently, pooling over all country pairs across all origin income groups might induce aggregation bias in the baseline regression.

Table 2.3 : Heterogeneity Across Origin Country Income Groups

**Dependent Variable:** Migration Rate$_{ij,t}$

| | **Low-Income Origins** | | **Middle-Income Origins** | | **High-Income Origins** | |
|---|---|---|---|---|---|---|
| | basic | onset weighted | basic | onset weighted | basic | onset weighted |
| | (1) | (2) | (3) | (4) | (5) | (6) |
| Disaster Index$_{i,t}$ | −0.011 | 0.039 | −0.001 | 0.003*** | −0.010** | −0.037 |
| | (0.03) | (0.08) | (0.02) | (0.00) | (0.00) | (0.04) |
| Disaster Index$_{j,t}$ | 0.005 | −0.001 | −0.015** | −0.030* | −0.001 | −0.015 |
| | (0.02) | (0.01) | (0.01) | (0.02) | (0.01) | (0.02) |
| **Controls** | | | | | | |
| $\ln$ (GDP p.c.$_{j,t}$/GDP p.c.$_{i,t}$) | 0.895** | 0.801* | 0.370 | 0.369 | −0.322 | −0.540 |
| | (0.45) | (0.45) | (0.23) | (0.23) | (0.42) | (0.41) |
| Civil War$_{i,t}$ | −0.052 | −0.050 | 0.050* | 0.043 | 0.172 | 0.158 |
| | (0.04) | (0.04) | (0.03) | (0.03) | (0.21) | (0.20) |
| Civil War$_{j,t}$ | −0.179* | −0.177* | −0.019 | −0.027 | −0.477*** | −0.484*** |
| | (0.10) | (0.10) | (0.04) | (0.04) | (0.13) | (0.13) |
| RTA$_{ij,t}$ | 0.577** | 0.523** | 0.173 | 0.213 | 0.705*** | 0.714*** |
| | (0.27) | (0.26) | (0.17) | (0.18) | (0.23) | (0.23) |
| $\ln$ (Mig. Stock$_{ij,t-1}+1$) | 0.386*** | 0.390*** | 0.372*** | 0.371*** | 0.249*** | 0.247*** |
| | (0.04) | (0.04) | (0.05) | (0.04) | (0.05) | (0.05) |
| $\ln$ (Distance$_{ij}$) | −0.488*** | −0.481*** | −0.780*** | −0.776*** | −0.694*** | −0.696*** |
| | (0.12) | (0.12) | (0.10) | (0.10) | (0.11) | (0.11) |
| Contiguity$_{ij}$ | 1.111*** | 1.103*** | 0.521*** | 0.506*** | 0.130 | 0.121 |
| | (0.22) | (0.21) | (0.16) | (0.16) | (0.36) | (0.35) |
| Common Language$_{ij}$ | 0.240* | 0.243* | 0.881*** | 0.876*** | 0.139 | 0.141 |
| | (0.14) | (0.15) | (0.14) | (0.14) | (0.29) | (0.29) |
| Colony$_{ij}$ | 0.580 | 0.543 | 0.313 | 0.346* | 0.709*** | 0.723*** |
| | (0.39) | (0.38) | (0.21) | (0.21) | (0.25) | (0.25) |
| Log-Likelihood | −8.183 | −8.179 | −38.895 | −38.905 | −24.749 | −24.759 |
| Observations | 11,302 | 11,302 | 33,080 | 33,080 | 22,291 | 22,291 |

*Note:* ***, **, * denote significance at the 1%, 5% and 10% level, respectively. Constant, origin, destination, and decade fixed effects and MR terms are included but not reported. Natural disaster indicator components are weighted with their inverse standard deviation. Natural disasters are scaled by log land area. Robust standard errors reported in parentheses.

Table 2.3 tests this hypothesis and shows estimates by origin country income groups.[37] Columns (1) and (2) contain the results for low-income origin countries only. In line with the liquidity-constraint hypothesis (see also Beine and Parsons, 2017), no statistically significant evidence for migration effects of the disaster indices is found. Columns (3) and (4) contain the results for middle-income origins. Evaluated at the mean, the basic result in

[37] For descriptives on the distributions of natural disaster types across low-, middle- and high-income countries see Figure B.1 in Appendix B.1.2.

column (3) suggests a negative and statistically significant pull effect of disasters in potential destinations of -7.3%; $(100 \times [e^{-0.015 \cdot 5.075} - 1])$. If the time dimension is considered in column (4), disasters in the origin increase migration by 1.4% (evaluated at the mean; $(100 \times [e^{0.003 \cdot 4.529} - 1])$ whereas disasters in the destination have a negative pull effect of -11.5% at the mean; $(100 \times [e^{-0.030 \cdot 4.085} - 1])$. Thus, push and pull effects are largely in line with priors for the group of middle-income origin countries. Again, timing is important to identify causal effects. Columns (5) and (6) show results for high-income origins. A negative and statistically significant push effect of natural disasters is observed for the basic index in column (5). This finding is in line with the hypothesis that natural disasters might potentially hamper outward migration from high-income countries due to positive income effects resulting from the replacement of insured losses. Moreover, given the absence of evidence for significant push effects for low- and middle-income country groups in columns (1) and (3), it follows that high income origin countries do drive the negative push effects in column (4) of Table 2.1. If weighting by onset month in column (6), the evidence for this effect again vanishes.

The result that middle-income countries show a positive and statistically significant push effect of natural disasters on bilateral migration is in line with findings from monadic regressions by Cattaneo and Peri (2016). Interestingly, control variables also show heterogeneity across income groups: While there is no evidence that overall wage differences, proxied by relative GDP per capita, play a significant role for the decision to migrate from middle- and high-income countries, they significantly drive migration from low-income countries. A 10% increase in the per capita GDP ratio implies a nearly proportionate increase in the bilateral migration rates from low-income countries by 8–9%. Moreover, armed conflicts in the destination have a very strong deterring effect on potential migrants from high-income countries (who seem to have a strong preference for safety), a small but significantly positive effect for low-income countries (for whom other motives, like escaping poverty, might be dominant), and a negative but non-significant effect for middle-income countries. A similar ranking, albeit with less pronounced differences in magnitude, arises for RTAs. Contiguity, on the other hand, plays the strongest role for low-income countries, with more than three times the effect on the migration rate than for middle-income countries. There is no evidence for adjacency to play a role for high-income countries. This finding supports the hypothesis that migrants from poorer countries are on average more financially constrained, as moving to neighboring countries implies lower migration cost. Common language is important for middle-income countries, more than doubling the bilateral migration rate, but there is no evidence that it

affects migration for high-income economies. On the other hand, colonial relationships are of major importance for high-income origins, but less so for low- and middle-income economies. Finally, diasporas are equally important for low- and middle-income, but less for high-income countries.

It can be concluded that heterogeneity in migration behavior exists across income groups of countries. This leads to aggregation bias if considered jointly and may be responsible for some counterintuitive or absent evidence (effects level out) presented earlier in this paper.

## 2.6 Robustness Analysis

Migration might only take place if major events drive people out of their home country, while small scale events may not exert an effect on international migration. As a first check, the disaster intensity index is thus re-constructed using only the top two standard deviations of the disaster type indicators while setting smaller events to zero. This way, the disaster variable captures major events only. Table 2.4 column (1) shows that this modification does not lead to statistically significant estimates.[38]

As noted earlier, it might take some time for people to react to disasters and to come up with the decision to migrate, particularly across international borders. Thus, an alternative approach is chosen as a second check. Instead of applying a bell-shaped onset weighting scheme, all disasters that took place within two years before each census are excluded from the disaster index. The results are shown in Table 2.4 column (2). Again, the disaster index does not show evidence for a significant impact on the bilateral migration rate, but might also not consider timing properly.[39]

The frequency rather than the intensity might matter for the migration decision. The disaster variable is changed from physical intensities capturing the strength of disastrous events to a count variable capturing their frequency. For each disaster type, the number of months within a decade is counted in which an event beyond a specified threshold[40] has occurred. This number is then summed up over all types and transformed into an inverse weighted

[38] If the simple instead of the sd-weighted index is used, results do not change.
[39] Again, using the simple instead of the sd-weighted index does not change this result.
[40] Chosen thresholds are given in Appendix B.1.2, Table B.2.

Table 2.4 : Sensitivity Analysis

**Dependent Variable:** Migration Rate$_{ij,t}$ (log in OLS)

| | **Exclude Disasters (Intensity)** | | **Disaster Frequency (Count)** | | **OLS (Intensity)** | | **Heckman Selection (Intensity)** | |
|---|---|---|---|---|---|---|---|---|
| | < Max -2 sd | Census -2 Years | basic | onset weighted | basic | onset weighted | Probit, onset weighted | OLS, onset weighted |
| | (1) | (2) | (3) | (4) | (5) | (6) | (7) | (8) |
| Disaster Index$_{i,t}$ | −0.334 | −0.005 | −0.038 | −0.013 | 0.000 | 0.000 | 0.000 | 0.000 |
| | (0.38) | (0.02) | (0.05) | (0.12) | (0.00) | (0.00) | (0.00) | (0.00) |
| Disaster Index$_{j,t}$ | 0.028 | 0.001 | 0.018 | −0.039 | −0.002 | −0.006 | −0.002*** | −0.006 |
| | (0.07) | (0.01) | (0.06) | (0.14) | (0.00) | (0.00) | (0.00) | (0.00) |
| **Controls** | | | | | | | | |
| $\ln\left(\text{GDP p.c.}_{j,t}/\text{GDP p.c.}_{i,t}\right)$ | 0.210 | 0.238 | 0.216 | 0.214 | 0.117** | 0.117** | 0.008 | 0.109** |
| | (0.23) | (0.22) | (0.24) | (0.23) | (0.05) | (0.05) | (0.03) | (0.05) |
| Civil War$_{i,t}$ | 0.052** | 0.056** | 0.055** | 0.059** | 0.005 | 0.006 | 0.006 | 0.005 |
| | (0.03) | (0.03) | (0.03) | (0.03) | (0.01) | (0.01) | (0.00) | (0.01) |
| Civil War$_{j,t}$ | −0.260** | −0.277** | −0.259** | −0.259** | 0.015 | 0.015 | −0.022*** | 0.018* |
| | (0.12) | (0.11) | (0.11) | (0.11) | (0.01) | (0.01) | (0.00) | (0.01) |
| RTA$_{ij,t}$ | 0.290** | 0.310** | 0.290** | 0.279** | −0.066** | −0.064** | 0.064*** | −0.065** |
| | (0.12) | (0.12) | (0.12) | (0.12) | (0.03) | (0.03) | (0.02) | (0.03) |
| $\ln\left(\text{Mig. Stock}_{ij,t-1}+1\right)$ | 0.358*** | 0.354*** | 0.357*** | 0.357*** | 0.590*** | 0.590*** | 0.033*** | 0.584*** |
| | (0.03) | (0.03) | (0.03) | (0.03) | (0.01) | (0.01) | (0.00) | (0.01) |
| $\ln\left(\text{Distance}_{ij}\right)$ | −0.745*** | −0.719*** | −0.746*** | −0.748*** | −0.521*** | −0.520*** | −0.283*** | −0.475*** |
| | (0.08) | (0.08) | (0.08) | (0.08) | (0.02) | (0.02) | (0.01) | (0.02) |
| Contiguity$_{ij}$ | 0.373** | 0.450*** | 0.379** | 0.378** | 0.457*** | 0.458*** | 0.027 | 0.454*** |
| | (0.17) | (0.15) | (0.16) | (0.16) | (0.07) | (0.07) | (0.06) | (0.07) |
| Common Language$_{ij}$ | 0.506*** | 0.480*** | 0.504*** | 0.506*** | 0.384*** | 0.383*** | 0.167*** | 0.349*** |
| | (0.11) | (0.11) | (0.11) | (0.11) | (0.03) | (0.03) | (0.02) | (0.03) |
| Colony$_{ij}$ | 0.469*** | 0.488*** | 0.472*** | 0.467*** | 0.007 | 0.009 | −0.014 | 0.011 |
| | (0.17) | (0.17) | (0.17) | (0.17) | (0.09) | (0.09) | (0.07) | (0.09) |
| Common Religion$_{ij}$ | | | | | | | 0.234*** | |
| | | | | | | | (0.03) | |
| $\rho$ | | | | | | | −0.239*** | |
| | | | | | | | (0.07) | |
| $\sigma$ | | | | | | | 0.352*** | |
| | | | | | | | (0.01) | |
| Log-Likelihood/$R^2$ | −74.013 | −73.122 | −74.019 | −74.022 | 0.783 | 0.783 | -68,899.91 | |
| Observations | 66,673 | 66,048 | 66,673 | 66,673 | 23,255 | 23,255 | 65,386 | |

*Note:* ***, **, * denote significance at the 1%, 5% and 10% level, respectively. Physical intensity indicator components are weighted with their inverse standard deviation. Natural disasters are scaled by log land area. Constant, origin, destination, and decade fixed effects and MR terms are included but not reported. Robust standard errors reported in parentheses.

index. Columns (3) and (4) in Table 2.4 show that the disaster frequency does not imply any evidence for statistically significant push or pull effects, whether or not timing is considered.

Fourth, deviating from using FE PPML as the preferred estimation technique, FE OLS results are presented. Estimating OLS causes a loss of 43,418 observations for which the dependent variable is zero. Columns (5) and (6) show that disasters do not exert a significant effect on migration.[41] One peculiarity of the OLS results is that significant negative effects are obtained for RTAs. This finding occurs in OLS due to the lack of country-pair fixed effects, which causes omitted variable bias (for an overview of the large body of trade gravity literature on this topic, see Head and Mayer, 2014). If bilateral fixed effects are included, RTA effects become insignificant, but the network variable reverses (see Appendix B.1.2, Table B.5). Since the migration data only covers three decennial waves, the inclusion of bilateral fixed effects is problematic as within-group variation is limited. This problem is aggravated by OLS compared to PPML due to zero migration flows. Hence, Beine and Parsons (2015) are followed by excluding bilateral fixed effects and using direct gravity controls for common country characteristics in all previous and prospective specifications.

Finally, a Heckman selection model is estimated to explore potential heterogeneity in the adaptation mechanism at the extensive versus the intensive margin. In the absence of a better instrument, the Helpman et al. (2008) common religion measure is used as a selection variable. Results suggest that natural disasters in the destination country negatively affect the probability to observe a non-zero migration rate between a country pair (column (7)), whereas, conditional on the probability that bilateral migration takes place, there is no evidence that disasters have any statistically significant push or pull effects (column (8)). Conclusively, natural disasters rather tend to affect migration at the extensive margin whereas there is no evidence for an effect at the intensive margin.[42]

[41] Using the simple disaster index instead yields positive push and negative pull effects which are statistically significant. However, this finding is not robust, potentially due to heteroskedastic error terms. A White test proposed by Wooldridge (2003, pp. 268-269) for applications with lengthy regressors yields White's special Chi-Squared test statistic of 109.07 and a p-value of 2.1e-24. The Null hypothesis of homoskedasticity is rejected such that estimated variances under OLS are biased. PPML, beyond solving the problem of zero dependent variables, consistently estimates the gravity equation and is robust to measurement error and different patterns of heteroskedasticity (see Santos Silva and Tenreyro, 2006; Head and Mayer, 2014; Fally, 2015). Estimating FE PPML based on the smaller OLS sample does not yield statistically significant disaster estimates.

[42] Note that Heckman results are not directly comparable to PPML, which nest the intensive and extensive effects in one estimate while Heckman separates them.

## 2.7 Conclusion

This paper aims to provide an answer to the question on the impact of natural disasters on international migration. To motivate the empirical strategy, a stylized gravity framework of bilateral migration is constructed, introducing disasters as random shocks. To test the implications empirically, a full matrix of international migration available for increments of 10 years from 1980 to 2010 and disaster data based on intensity measures of geological and meteorological events are employed. A conditional fixed-effects PPML model is estimated to address the issue of zero migration flows and potentially heteroskedastic standard errors. The gravity estimations are augmented by the use of explicit MR terms to control for unobservable time-varying country characteristics.

PPML findings show little robust, if at all noisy evidence for push and pull effects of natural disasters on medium to long-run international relocation. Findings convey evidence that disaster intensity in the origin causes bilateral migration to increase by 1.7% (evaluated at the mean). This effect can be identified only when considering the timing of events with respect to the migration decision, using a bell-shaped onset weighting scheme. If timing is neglected or alternative disaster measures are applied, this finding turns out not to be robust. Decomposing natural disasters by type does not show evidence for a clear pattern of events. Nevertheless, when distinguishing between origin income groups, substantial heterogeneity can be found, suggesting that natural disasters have positive push and negative pull effects for middle-income countries. These are neither financially constrained (as low-income countries), nor do they show high insurance penetration rates (as high-income countries). As a result, examining the effects of natural disasters on migration using a full country sample may lead to aggregation bias.

Finally, it cannot be ruled out that the mere aggregation of ten-year data smooths out a big amount of information and makes identification of causal effects problematic. Above all, temporary international relocation, which is a potential mechanism for adapting to transient natural disasters, is not captured by the data. Also, a large number of bilateral migrant stocks is estimated rather than observed, giving rise to attenuation bias as a consequence of measurement error. These are potential reasons for the absence of causal evidence. Given these migration data restrictions, the outlined findings must therefore be taken with caution.

# Appendix B.1 Supplementary Appendix

## B.1.1 Supplementary Derivations

Details on the Taylor series expansion to obtain tractable MR terms estimated in the empirical specifications. From the theoretical derivations in section 2.2, MR terms are given by

$$\tilde{\Gamma}_{i,t} = \left[ \sum_{j} \delta_{j,t} \left( \frac{\theta_{ij,t}}{\tilde{\Gamma}_{j,t}} \right)^{1-\sigma} \right]^{\frac{1}{1-\sigma}}, \tag{B.1}$$

$$\tilde{\Gamma}_{j,t} = \left[ \sum_{i} \delta_{i,t} \left( \frac{\theta_{ij,t}}{\tilde{\Gamma}_{i,t}} \right)^{1-\sigma} \right]^{\frac{1}{1-\sigma}}, \tag{B.2}$$

where $\delta$ is $N_{i,t}/N_t$ or $N_{j,t}/N_t$, respectively.

The first order Taylor series expansion of any function $f(x_i)$, centered at $x$, is given by $f(x_i) = f(x) + [f'(x)](x_i - x)$. Baier and Bergstrand (2009) is followed by centering around symmetric migration frictions $\theta_{ij,t} = \theta$. Both sides of equation (B.1) are divided by a constant $\theta^{1/2}$:

$$\begin{aligned} \tilde{\Gamma}_{i,t}/\theta^{1/2} &= \left[ \textstyle\sum_j \delta_{j,t} \left( \theta_{ij,t}/\theta^{1/2} \right)^{1-\sigma} / \tilde{\Gamma}_{j,t}^{1-\sigma} \right]^{\frac{1}{1-\sigma}} \\ &= \left[ \textstyle\sum_j \delta_{j,t} \left( \theta_{ij,t}/\theta \right)^{1-\sigma} / \left( \tilde{\Gamma}_{j,t}/\theta^{1/2} \right)^{1-\sigma} \right]^{\frac{1}{1-\sigma}} \end{aligned} \tag{B.3}$$

Define $\hat{\Gamma}_{i,t} = \tilde{\Gamma}_{i,t}/\theta^{1/2}$, $\hat{\theta}_{ij,t} = \theta_{ij,t}/\theta$, and $\hat{\Gamma}_{j,t} = \tilde{\Gamma}_{j,t}/\theta^{1/2}$. Substituting these in the previous equation gives rise to

$$\hat{\Gamma}_{i,t} = \left[ \sum_{j} \delta_{j,t} \left( \hat{\theta}_{ij,t}/\hat{\Gamma}_{j,t} \right)^{1-\sigma} \right]^{\frac{1}{1-\sigma}}. \tag{B.4}$$

It will later be useful to rewrite equation (B.4) as

$$e^{(1-\sigma)\ln \hat{\Gamma}_{i,t}} = \sum_{j} e^{\ln \delta_{j,t}} e^{(\sigma-1)\ln \hat{\Gamma}_{j,t}} e^{(1-\sigma)\ln \hat{\theta}_{ij,t}}, \tag{B.5}$$

where $e$ is the natural logarithm operator. In a world with symmetric migration costs $\theta_{ij,t} = \theta$, connoting $\hat{\theta}_{ij,t} = 1$, the latter implies

$$\hat{\Gamma}_{i,t}^{1-\sigma} = \sum_{j} \delta_{j,t} \hat{\Gamma}_{j,t}^{\sigma-1} \tag{B.6}$$

multiplying both sides by $\hat{\Gamma}_{i,t}^{\sigma-1}$ yields

$$1 = \sum_{j} \delta_{j,t} (\hat{\Gamma}_{i,t} \hat{\Gamma}_{j,t})^{\sigma-1}. \tag{B.7}$$

As noted in Feenstra (2004, p.158, footnote 11), the solution to this equation is $\hat{\Gamma}_{i,t} = \hat{\Gamma}_{j,t} = 1$. For this reason, under symmetric migration costs $\hat{\theta}_{ij,t} = \hat{\Gamma}_{i,t} = \hat{\Gamma}_{j,t} = 1$ and $\Gamma_{i,t} = \Gamma_{j,t} = \theta^{1/2}$. A first-order log-linear Taylor series expansion of $\hat{\Gamma}_{i,t}$ from equation (B.5), analogue for $\hat{\Gamma}_{j,t}$, centered at $\hat{\theta} = \hat{\Gamma}_{i,t} = \hat{\Gamma}_{j,t} = 1$ yields

$$\ln \tilde{\Gamma}_{i,t} = -\sum_{j} \delta_{j,t} \ln \tilde{\Gamma}_{j,t} + \sum_{j} \delta_{j,t} \ln \theta_{ij,t} \tag{B.8}$$

and

$$\ln \tilde{\Gamma}_{j,t} = -\sum_{i} \delta_{i,t} \ln \tilde{\Gamma}_{i,t} + \sum_{i} \delta_{i,t} \ln \theta_{ij,t}. \tag{B.9}$$

Using $d\left[e^{(1-\sigma)\ln \hat{x}}\right] / d[\ln \hat{x}] = (1-\sigma) e^{(1-\sigma)\ln \hat{x}}$, some mathematical manipulation and assuming symmetry of migration costs, a solution to the above equations is

$$\ln \tilde{\Gamma}_{i,t} = \left[ \sum_{j} \delta_{j,t} \ln \theta_{ij,t} - \frac{1}{2} \sum_{k} \sum_{m} \delta_{k,t} \delta_{m,t} \ln \theta_{km,t} \right] \tag{B.10}$$

and

$$\ln \tilde{\Gamma}_{j,t} = \left[ \sum_{i} \delta_{i,t} \ln \theta_{ij,t} - \frac{1}{2} \sum_{k} \sum_{m} \delta_{k,t} \delta_{m,t} \ln \theta_{km,t} \right], \tag{B.11}$$

where multilateral resistances are normalized by (the square root of) population weighted average migration frictions (the combined shock-cost measure).
In the empirical specification MR terms are calculated as

$$\begin{aligned}\text{MRDIST}_{ij,t} = \Bigg[ &\left( \sum_{k=1}^{C} \delta_{k,t} (\ln \text{Dist}_{ik} + \Phi_{k,t} - \Phi_{i,t}) \right) \\ &+ \left( \sum_{m=1}^{C} \delta_{m,t} (\ln \text{Dist}_{mj} + \Phi_{j,t} - \Phi_{m,t}) \right) \\ &- \left( \sum_{k=1}^{C} \sum_{m=1}^{C} \delta_{k,t} \delta_{m,t} (\ln \text{Dist}_{km} + \Phi_{m,t} - \Phi_{k,t}) \right) \Bigg] ,\end{aligned} \tag{B.12}$$

$$\begin{aligned}\text{MRADJ}_{ij,t} = \Bigg[ &\left( \sum_{k=1}^{C} \delta_{k,t} (\text{Adj}_{ik} + \Phi_{k,t} - \Phi_{i,t}) \right) \\ &+ \left( \sum_{m=1}^{C} \delta_{m,t} (\text{Adj}_{mj} + \Phi_{j,t} - \Phi_{m,t}) \right) \\ &- \left( \sum_{k=1}^{C} \sum_{m=1}^{C} \delta_{k,t} \delta_{m,t} (\text{Adj}_{km} + \Phi_{m,t} - \Phi_{k,t}) \right) \Bigg] ,\end{aligned} \tag{B.13}$$

where $\delta$ denotes a states' share of population over 'total' world population, $\text{N}_{k,t}/\text{N}_t$ and $\text{N}_{m,t}/\text{N}_t$.

MR terms for RTA, Colony and Common Language are calculated analogously.

### B.1.2 Supplementary Tables

Table B.1 : Summary Statistics, PPML, Full Sample

| | mean | sd | min | max |
|---|---|---|---|---|
| Migration Rate$_{ij,t}$ | 0.0002 | 0.003 | 0 | 0.500 |
| Migration Flow$_{ij,t}$ | 1,726 | 28,712 | 0 | 4,705,677 |
| **Aggregate Disaster Indices** | | | | |
| Disaster Index$_{i,t}$ | 7.370 | 2.842 | 1.616 | 19.557 |
| Disaster Index$_{j,t}$ | 7.421 | 2.855 | 1.616 | 19.557 |
| Disaster Index$_{i,t}$, onset weighted | 5.777 | 2.247 | 0.767 | 15.522 |
| Disaster Index$_{j,t}$, onset weighted | 5.813 | 2.256 | 0.767 | 15.522 |
| Disaster Index$_{i,t}$, sd weighted | 5.096 | 21.526 | 0 | 322.040 |
| Disaster Index$_{j,t}$, sd weighted | 5.102 | 22.082 | 0 | 322.040 |
| Disaster Index$_{i,t}$, onset, sd weighted | 4.156 | 14.855 | 0 | 533.030 |
| Disaster Index$_{j,t}$, onset, sd weighted | 4.196 | 15.113 | 0 | 533.030 |
| Disaster Index$_{i,t}$, major | 1.873 | 4.061 | 0 | 17.709 |
| Disaster Index$_{j,t}$, major | 1.896 | 4.101 | 0 | 17.709 |
| Disaster Index$_{i,t}$, census -2yrs | 7.130 | 2.749 | 1.621 | 19.305 |
| Disaster Index$_{j,t}$, census -2yrs | 7.182 | 2.764 | 1.621 | 19.305 |
| Disaster Counts$_{i,t}$ | 14.137 | 6.144 | 2.565 | 33.542 |
| Disaster Counts$_{j,t}$ | 14.152 | 6.199 | 2.565 | 33.542 |
| Disaster Counts$_{i,t}$, onset | 5.880 | 2.528 | 0.710 | 13.827 |
| Disaster Counts$_{j,t}$, onset | 5.886 | 2.550 | 0.710 | 13.827 |
| **Disaster Types (basic)** | | | | |
| Earthquake$_{i,t}$ | 0.511 | 0.158 | 0 | 0.947 |
| Earthquake$_{j,t}$ | 0.510 | 0.160 | 0 | 0.947 |
| Volcanic Explosion$_{i,t}$ | 0.042 | 0.093 | 0 | 0.476 |
| Volcanic Explosion$_{j,t}$ | 0.043 | 0.093 | 0 | 0.476 |
| Windspeed$_{i,t}$ | 6.455 | 2.641 | 1.133 | 17.709 |
| Windspeed$_{j,t}$ | 6.502 | 2.649 | 1.133 | 17.709 |
| $\Delta$ Precipitation$_{i,t}$ | 0.329 | 0.278 | 0.008 | 2.936 |
| $\Delta$ Precipitation$_{j,t}$ | 0.333 | 0.282 | 0.008 | 2.936 |
| $\Delta$ Temperature$_{i,t}$ | 0.023 | 0.018 | 2.1e-05 | 0.115 |
| $\Delta$ Temperature$_{j,t}$ | 0.023 | 0.018 | 2.1e-05 | 0.115 |
| Drought (SPEI)$_{i,t}$ | 0.012 | 0.018 | 0 | 0.127 |
| Drought (SPEI)$_{j,t}$ | 0.012 | 0.018 | 0 | 0.127 |

Continued on next page

Table B.1 – continued from previous page

| | mean | sd | min | max |
|---|---|---|---|---|
| **Disaster Types (onset weighted)** | | | | |
| Earthquake$_{i,t}$ | 0.418 | 0.155 | 0 | 0.792 |
| Earthquake$_{j,t}$ | 0.418 | 0.155 | 0 | 0.792 |
| Volcanic Explosion$_{i,t}$ | 0.031 | 0.072 | 0 | 0.311 |
| Volcanic Explosion$_{j,t}$ | 0.0315 | 0.073 | 0 | 0.311 |
| Windspeed$_{i,t}$ | 5.094 | 2.127 | 0.119 | 13.899 |
| Windspeed$_{j,t}$ | 5.127 | 2.135 | 0.119 | 13.899 |
| $\Delta$ Precipitation$_{i,t}$ | 0.218 | 0.198 | 0.006 | 1.404 |
| $\Delta$ Precipitation$_{j,t}$ | 0.221 | 0.199 | 0.006 | 1.404 |
| $\Delta$ Temperature$_{i,t}$ | 0.011 | 0.008 | 9.9e-05 | 0.048 |
| $\Delta$ Temperature$_{j,t}$ | 0.011 | 0.008 | 9.9e-05 | 0.048 |
| Drought (SPEI)$_{i,t}$ | 0.005 | 0.009 | 0 | 0.072 |
| Drought (SPEI)$_{j,t}$ | 0.005 | 0.009 | 0 | 0.072 |
| **Controls** | | | | |
| $\ln$ (GDP p.c.$_{j,t}$/GDP p.c.$_{i,t}$) | 0.028 | 2.187 | −6.149 | 6.149 |
| Civil War$_{i,t}$ | 0.729 | 1.947 | 0 | 10 |
| Civil War$_{j,t}$ | 0.721 | 1.948 | 0 | 10 |
| RTA$_{ij,t}$ | 0.169 | 0.375 | 0 | 1 |
| $\ln$ (Mig. Stock$_{ij,t-1}+1$) | 2.608 | 3.084 | 0 | 16.053 |
| $\ln$ (Distance$_{ij}$) | 8.718 | 0.774 | 2.349 | 9.894 |
| Contiguity$_{ij}$ | 0.021 | 0.143 | 0 | 1 |
| Common Language$_{ij}$ | 0.147 | 0.354 | 0 | 1 |
| Colony$_{ij}$ | 0.013 | 0.114 | 0 | 1 |

*Note:* 66,673 Observations, all disaster variables are land area weighted.

Figure B.1 : Kernel Densities of Disaster Indicators by Country Income Groups

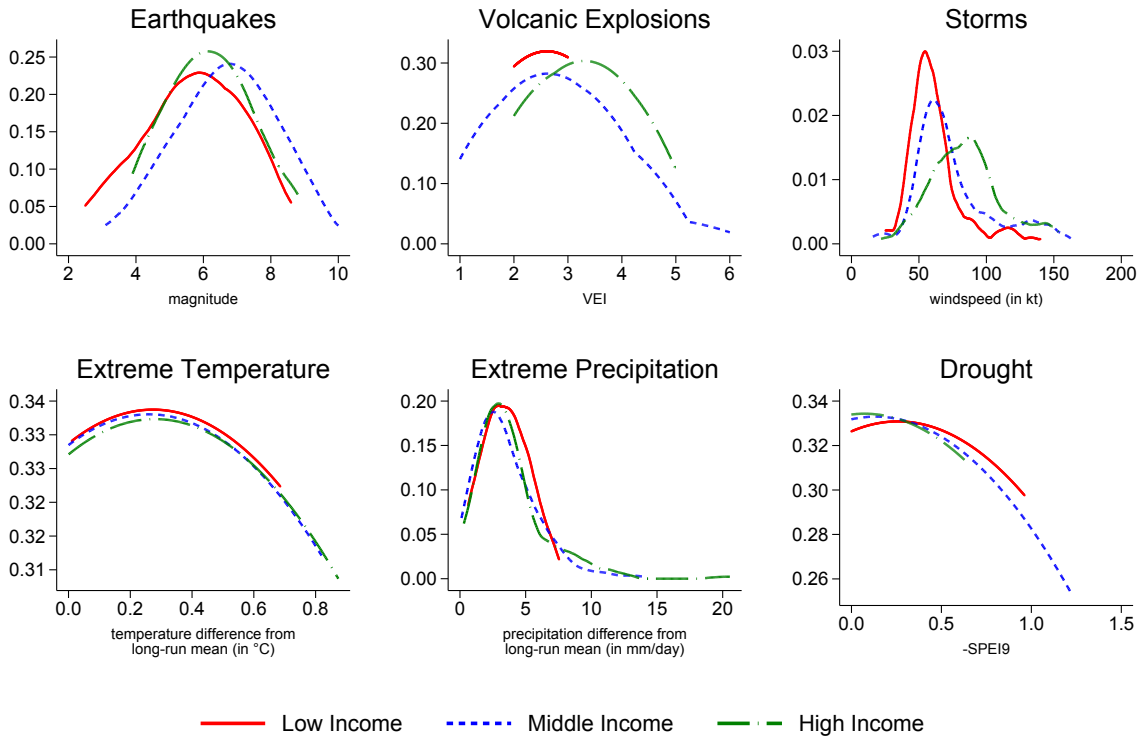


*Note:* Observations are at decennial level. Zeros excluded for earthquakes and volcanic explosions.

Table B.2 : Standard Thresholds for Disaster Count Variables

| **Count Indicator** | **Intensity Measure** | **Bound** | **Minimum Event Type** |
|---|---|---|---|
| Earthquakes | maximum magnitude | $\geq 4$ | felt shaking of the earth with light damage caused to buildings and structures |
| Storms | maximum sustained wind speed | $\geq 64$ knots | some damage to buildings and trees, extensive damage to to power lines and poles (Cat. 1 on Saffir-Simpson Hurricane Scale) |
| Volcanoes | maximum Volcanic Explosivity Index (VEI) | $\geq 1$ | light eruption with ejecta volume $>$ 10,000 $m^3$ |
| Extreme Precipitation | positive difference of monthly mean precipitation from monthly long-run mean | $\geq 1.5$ mm/day | excess-rain anomaly |
| Extreme Temperatures | absolute difference of monthly mean temperature from monthly long-run mean | $\geq 1.5$°C | temperature anomaly |
| Droughts | mean Standardized Precipitation Evapotranspiration Index (SPEI) | $\leq 0$ | mild drought (Vicente-Serrano et al., 2010) |

Table B.3 : Countries in PPML Specification

| | Case numbers | | | Case numbers | |
|---|---|---|---|---|---|
| | **Origin** | **Destination** | | **Origin** | **Destination** |
| Afghanistan | 151 | 0 | Kuwait | 307 | 318 |
| Albania | 439 | 450 | Kyrgyzstan | 439 | 450 |
| Algeria | 440 | 289 | Lao People's Democratic Rep. | 439 | 450 |
| Angola | 439 | 450 | Latvia | 307 | 318 |
| Argentina | 439 | 450 | Lebanon | 440 | 289 |
| Armenia | 307 | 318 | Lesotho | 439 | 450 |
| Australia | 439 | 450 | Liberia | 439 | 450 |
| Austria | 439 | 450 | Libya | 307 | 318 |
| Azerbaijan | 307 | 318 | Lithuania | 307 | 318 |
| Bahamas | 439 | 450 | Luxembourg | 439 | 450 |
| Bahrain | 439 | 450 | Madagascar | 439 | 450 |
| Bangladesh | 439 | 450 | Malawi | 439 | 450 |
| Belarus | 307 | 318 | Malaysia | 439 | 450 |
| Belgium | 439 | 450 | Mali | 439 | 450 |
| Belize | 439 | 450 | Mauritania | 439 | 450 |
| Benin | 439 | 450 | Mauritius | 439 | 450 |
| Bhutan | 150 | 161 | Mexico | 439 | 450 |
| Bolivia (Plurinational State) | 439 | 450 | Mongolia | 439 | 450 |
| Bosnia and Herzegovina | 307 | 318 | Morocco | 440 | 289 |
| Botswana | 440 | 289 | Mozambique | 439 | 450 |
| Brazil | 439 | 450 | Namibia | 439 | 450 |
| Brunei Darussalam | 439 | 450 | Nepal | 439 | 450 |
| Bulgaria | 439 | 450 | Netherlands | 439 | 450 |
| Burkina Faso | 439 | 450 | New Zealand | 439 | 450 |
| Burundi | 439 | 450 | Nicaragua | 439 | 450 |
| Cambodia | 307 | 318 | Niger | 439 | 450 |
| Cameroon | 439 | 450 | Nigeria | 439 | 450 |
| Canada | 439 | 450 | Norway | 439 | 450 |
| Central African Rep. | 439 | 450 | Oman | 439 | 450 |
| Chad | 439 | 450 | Pakistan | 440 | 289 |
| Chile | 439 | 450 | Panama | 439 | 450 |
| China | 440 | 289 | Papua New Guinea | 439 | 450 |
| China, Hong Kong (SAR) | 439 | 450 | Paraguay | 439 | 450 |
| Colombia | 439 | 450 | Peru | 439 | 450 |

Continued on next page

Table B.3 – continued from previous page

| | Case numbers | | | Case numbers | |
|---|---|---|---|---|---|
| | **Origin** | **Destination** | | **Origin** | **Destination** |
| Congo | 439 | 450 | Philippines | 439 | 450 |
| Costa Rica | 439 | 450 | Poland | 307 | 318 |
| Croatia | 307 | 318 | Portugal | 439 | 450 |
| Cuba | 439 | 450 | Puerto Rico | 439 | 450 |
| Cyprus | 439 | 450 | Qatar | 150 | 161 |
| Czech Rep. | 307 | 318 | Rep. of Korea | 439 | 450 |
| Côte d'Ivoire | 439 | 450 | Rep. of Moldova | 439 | 450 |
| Democratic Rep. of the Congo | 440 | 289 | Romania | 307 | 318 |
| Denmark | 439 | 450 | Russian Federation | 439 | 450 |
| Djibouti | 307 | 318 | Rwanda | 439 | 450 |
| Dominican Rep. | 439 | 450 | Saudi Arabia | 439 | 450 |
| Ecuador | 439 | 450 | Senegal | 439 | 450 |
| Egypt | 439 | 450 | Sierra Leone | 439 | 450 |
| El Salvador | 439 | 450 | Singapore | 439 | 450 |
| Equatorial Guinea | 307 | 318 | Slovakia | 307 | 318 |
| Eritrea | 308 | 157 | Slovenia | 307 | 318 |
| Estonia | 307 | 318 | Solomon Islands | 307 | 318 |
| Ethiopia | 439 | 450 | South Africa | 439 | 450 |
| Fiji | 439 | 450 | Spain | 439 | 450 |
| Finland | 439 | 450 | Sri Lanka | 439 | 450 |
| France | 439 | 450 | Sudan | 439 | 450 |
| Gabon | 439 | 450 | Suriname | 439 | 450 |
| Gambia | 439 | 450 | Swaziland | 439 | 450 |
| Georgia | 439 | 450 | Sweden | 439 | 450 |
| Germany | 439 | 450 | Switzerland | 439 | 450 |
| Ghana | 440 | 289 | Tajikistan | 439 | 450 |
| Greece | 439 | 450 | Thailand | 439 | 450 |
| Guatemala | 439 | 450 | TFYR of Macedonia | 307 | 318 |
| Guinea | 439 | 450 | Togo | 439 | 450 |
| Guinea-Bissau | 439 | 450 | Trinidad and Tobago | 439 | 450 |
| Guyana | 439 | 450 | Tunisia | 439 | 450 |
| Haiti | 307 | 318 | Turkey | 439 | 450 |
| Honduras | 439 | 450 | Turkmenistan | 439 | 450 |
| Hungary | 307 | 318 | Uganda | 439 | 450 |
| Iceland | 439 | 450 | Ukraine | 439 | 450 |

Continued on next page

Table B.3 – continued from previous page

| | Case numbers | | | Case numbers | |
|---|---|---|---|---|---|
| | **Origin** | **Destination** | | **Origin** | **Destination** |
| India | 439 | 450 | United Arab Emirates | 150 | 161 |
| Indonesia | 439 | 450 | United Kingdom | 439 | 450 |
| Iran (Islamic Rep.) | 439 | 450 | United Rep. of Tanzania | 439 | 450 |
| Iraq | 439 | 450 | United States of America | 439 | 450 |
| Ireland | 439 | 450 | Uruguay | 439 | 450 |
| Israel | 439 | 450 | Uzbekistan | 439 | 450 |
| Italy | 439 | 450 | Vanuatu | 439 | 450 |
| Jamaica | 439 | 450 | Venezuela (Bolivarian Rep.) | 439 | 450 |
| Japan | 439 | 450 | Viet Nam | 440 | 289 |
| Jordan | 439 | 450 | Yemen | 307 | 318 |
| Kazakhstan | 307 | 318 | Zambia | 439 | 450 |
| Kenya | 439 | 450 | Zimbabwe | 439 | 450 |

*Note:* Case numbers extracted from post-estimation sample tabulation.

Table B.4 : Baseline Results, Not Controlling for Migrant Networks

**Dependent Variable:** Migration Rate$_{ij,t}$

| | **basic** | | **onset weighted** | |
|---|---|---|---|---|
| | simple | sd weighted | simple | sd weighted |
| | (1) | (2) | (3) | (4) |
| Disaster Index$_{i,t}$ | −0.112 | −0.010*** | −0.061 | 0.004*** |
| | (0.09) | (0.00) | (0.11) | (0.00) |
| Disaster Index$_{j,t}$ | 0.018 | −0.001 | 0.001 | −0.008 |
| | (0.10) | (0.01) | (0.14) | (0.01) |
| **Controls** | | | | |
| $\ln$ (GDP p.c.$_{j,t}$/GDP p.c.$_{i,t}$) | 0.239 | 0.282 | 0.240 | 0.271 |
| | (0.22) | (0.22) | (0.22) | (0.22) |
| Civil War$_{i,t}$ | 0.037 | 0.039 | 0.025 | 0.042 |
| | (0.03) | (0.03) | (0.03) | (0.03) |
| Civil War$_{j,t}$ | −0.203** | −0.200** | −0.198** | −0.199** |
| | (0.08) | (0.08) | (0.08) | (0.08) |
| RTA$_{ij,t}$ | 0.617*** | 0.629*** | 0.634*** | 0.632*** |
| | (0.12) | (0.12) | (0.12) | (0.12) |
| $\ln$ (Distance$_{ij}$) | −1.309*** | −1.311*** | −1.309*** | −1.309*** |
| | (0.08) | (0.08) | (0.08) | (0.08) |
| Contiguity$_{ij}$ | 0.903*** | 0.901*** | 0.897*** | 0.900*** |
| | (0.18) | (0.18) | (0.18) | (0.18) |
| Common Language$_{ij}$ | 1.017*** | 1.016*** | 1.015*** | 1.019*** |
| | (0.16) | (0.16) | (0.16) | (0.16) |
| Colony$_{ij}$ | 1.434*** | 1.436*** | 1.435*** | 1.438*** |
| | (0.20) | (0.20) | (0.20) | (0.20) |
| Log-Likelihood | −76.644 | −76.685 | −76.577 | −76.675 |
| Observations | 66,673 | 66,673 | 66,673 | 66,673 |

*Note:* ***, **, * denote significance at the 1%, 5% and 10% level, respectively. Constant, origin, destination and decade fixed effects and MR terms are included but not reported. Natural disasters are scaled by log land area. Robust standard errors reported in parentheses.

Table B.5 : OLS, Full Sample, 1980-2010, Bilateral Fixed Effects

**Dependent Variable:** Migration Rate$_{ij,t}$

| | **basic** | | **onset weightd** | |
|---|---|---|---|---|
| | simple | sd weighted | simple | sd weighted |
| | (1) | (2) | (3) | (4) |
| Disaster Index$_{i,t}$ | 0.059** | −0.062 | 0.070* | 0.106 |
| | (0.03) | (0.08) | (0.04) | (0.08) |
| Disaster Index$_{j,t}$ | −0.174*** | −0.196** | −0.070* | 0.269*** |
| | (0.03) | (0.08) | (0.04) | (0.09) |
| **Controls** | | | | |
| $\ln$ (GDP p.c.$_{j,t}$/GDP p.c.$_{i,t}$) | 0.371*** | 0.398*** | 0.419*** | 0.415*** |
| | (0.06) | (0.06) | (0.06) | (0.06) |
| Civil War$_{i,t}$ | 0.011 | 0.010 | 0.008 | 0.012 |
| | (0.01) | (0.01) | (0.01) | (0.01) |
| Civil War$_{j,t}$ | 0.027*** | 0.026*** | 0.032*** | 0.033*** |
| | (0.01) | (0.01) | (0.01) | (0.01) |
| RTA$_{ij,t}$ | −0.052 | −0.049 | −0.050 | −0.043 |
| | (0.06) | (0.06) | (0.06) | (0.06) |
| $\ln$ (Mig. Stock$_{ij,t-1}+1$) | −0.114*** | −0.121*** | −0.122*** | −0.125*** |
| | (0.01) | (0.01) | (0.01) | (0.01) |
| $R^2$(within) | 0.079 | 0.071 | 0.071 | 0.071 |
| Observations | 23,255 | 23,255 | 23,255 | 23,255 |

*Note:* ***, **, * denote significance at the 1%, 5% and 10% level, respectively. Constant, bilateral and decade fixed effects, and MR terms are included but not reported. Robust standard errors reported in parentheses.

# 3 Shedding Light on the Spatial Diffusion of Disasters*

## 3.1 Introduction

A large body of research suggests that global warming is a reality and that it will result in more frequent and more extreme natural disasters; see IPCC (2014) for a synthesis report. Hence, it is important to improve the understanding of the economic consequences of natural disasters around the globe. This paper provides an attempt at measuring the average impact on local economic activity of various types of meteorological and geological events and their spatial spillovers.

While the direct material destruction and the toll on human lives caused by disasters are all too evident, measuring their economic consequences is prone to difficulties. Early papers have investigated the relation between direct disaster damages, deaths, and economic development (see e.g. Kahn, 2005; Anbarci et al., 2005). Building on these, a growing literature predominantly uses aggregated cross-country data to investigate the effect of natural disasters on economic growth.[1] Findings depend heavily on the type of disaster data, country sample, and the types of disasters studied (Raddatz, 2007; Cavallo et al., 2013; Felbermayr and Gröschl, 2014).

Several data and specification issues explain the ambiguity of findings. First, many studies use information on the incidence of natural disasters from databases drawn from insurance records or news.[2] This introduces severe reporting, selection and endogeneity biases, as both insurance penetration and damage caused are correlated with development (Felbermayr and Gröschl, 2014). In addition, such data lack information on physical intensities of events

*This chapter is based on joint work with Gabriel Felbermayr, Jasmin Gröschl, Mark Sanders and Vincent Schippers. It is based on the article *"Shedding Light on the Spatial Diffusion of Disasters"*, CESifo Working Paper No. 7146, July 2018. Grateful thanks apply to Ilan Noy, Wouter Botzen and participants at FIW Workshop on International Economic Networks Vienna, Development Economics and Policy Conference Zurich, IOSE St.Petersburg, EGIT Düsseldorf, ETSG Florence, IO and Trade Seminar at LMU Munich, Seminar at Victoria University Wellington, Workshop on Geodata and Economics Braunschweig and the Conference on Environmental Economics in Orléon for useful comments and suggestions.

[1] For comprehensive literature reviews, see Cavallo and Noy (2011) and Klomp and Valckx (2014).

[2] For example, this is the case for the often used EM-DAT data base or the data provided by Munich-Re, the world's largest reinsurance firm.

that have not caused sufficient damage to qualify as a disaster (Strömberg, 2007). To tackle these issues, Felbermayr and Gröschl (2014) proposed and collected a database with information on the exogenous physical intensities of geological and meteorological events from primary sources at the country-level.[3] Their evidence clearly suggests a negative impact, with a substantial growth penalty for the worst 5% of shocks.

Most papers conduct their analysis at the country level. However, mapping natural events to countries of heterogeneous size can result in measurement error and attenuation bias (Noy, 2009). By aggregating local events data to the country level, important information is lost. First, similar events causing similar damage and impact on income show up as a major shock in a small island state's gross domestic product (GDP), whereas they might go unnoticed in a large country.[4] Second, the difference between an event striking a densely populated coastal region or an empty desert is lost, particularly in countries with a large territory. Third, in large economies, geographic spillover effects may disguise the full local treatment effect. Hence, regressing country level GDP (growth) on aggregate indicators of local natural events might yield biased estimates.

The challenge is to find a proxy of local economic activity at the same level of geographical detail as the meteorological and geological data.[5] Satellite technology has produced numerous data products that contain information on human presence and activity at a very fine level of spatial resolution. Recent papers have started to explore these data; for a survey see Donaldson and Storeygard (2016). Night-time light emissions have been shown to strongly correlate with economic activity (see Henderson et al., 2012; Nordhaus and Chen, 2015; Pinkovskiy and Sala-i Martin, 2016). While Henderson et al. (2012) investigate the informational value of night-lights in estimating economic growth at the country level, an emerging literature investigates even smaller sub-national units: Michalopoulos and Papaioannou (2013, 2014) focus on ethnic homelands, Hodler and Raschky (2014) on sub-national administrative units,

[3] `https://www.cesifo-group.de/ifoHome/facts/EBDC/Ifo-Research-Data/Ifo_GAME_Dataset.html`.

[4] For example, Strobl (2011) illustrates that, in the United States, hurricane effects wash out at the state level and even more so at the national level, leaving no trace in economic growth rates.

[5] While industrialized countries record income and production for sub-national administrative units, the same data is scarce for most other countries. The G-Econ project provides gross product per capita data at a 1° ×1° cell level. It uses gross product data for the lowest available political subdivision. For most low-income countries, this unit remains the national level, such that regional income estimates are largely driven by (an often estimated) population distribution. This methodology leaves serious GDP measurement problems unaddressed for a substantial part of the globe. As discussed by Henderson et al. (2012), national accounts are particularly weak in low-income countries.

Storeygard (2016) on cities, Henderson et al. (2017) on uniform grid cells and Bleakley and Lin (2012) on locations along rivers as natural features. The broad consensus is that growth in remotely sensed night-time light provides a very useful proxy for GDP growth over the long-run but also accurately tracks short-run fluctuations in economic growth.

Using night-lights as a proxy for economic activity has at least three benefits for this research: First, while growth in lights reflects growth in economic activity, measurement error in night-lights is not correlated with the level of income per capita.[6] Second, night-light information is available for all countries at a standard geographic resolution.[7] Third, GDP per capita statistics fail to account for an often sizable informal economy.[8] In addition, natural disasters tend to affect the poorest members of society, who are often active in the informal economy and whose activity is hard to measure (for an excellent discussion, see World Bank and United Nations, 2010). Yet, being able to capture (part of) the informal sector is important to identify the true effect of natural extreme events.

This study is not the first one using night-lights to assess disaster impacts at the local level. Bertinelli and Strobl (2013) and Elliott et al. (2015) study direct hurricane and typhoon impacts on light emission. They find reduced local light growth caused by hurricanes in the Caribbean and typhoons in coastal China, respectively, where the size of the effect found is twice as large compared to using GDP data at the country level. Although both papers are limited in regional focus and evaluate the impact of a specific disaster type, their findings strengthen the case for assessing disaster impacts at the local level and and propose night-light emissions as a suitable proxy. In this paper, the empirical analysis is extended to 24,000 geographical units of 0.5°×0.5° in 197 countries over 22 years and a wide array of different natural events is studied.

Zooming in on the grid cell level risks violating the standard assumption that errors are uncorrelated across units of observation. Especially weather shocks have a spatial extent, often affecting multiple locations at once. Even though there is variation across these locations, exogenous treatment is potentially spatially correlated. If spatial spillover effects exist between

[6] This is especially relevant for studying economic impacts in developing countries, where measurement error on the official GDP statistics is large. Henderson et al. (2012) use night-lights to find improved measures of income growth statistics for countries with low quality national accounts.

[7] Thus a number of low-income countries can be included that provide no national account GDP statistics (i.e., Myanmar or Somalia), while these countries frequently do experience extreme natural events. This avoids selection bias stemming from samples limited by availability of national accounts for GDP statistics.

[8] See, e.g., Schneider and Enste (2000); Schneider (2005) for worldwide estimates on the informal economy and Tanaka and Keola (2017) for a study using night lights data to identify the informal sector.

neighboring locations, the treatment of neighbors may have explanatory power, such that not explicitly modeling the spatial relationship gives rise to correlated errors and causes omitted variable bias. Another issue arises if exogenous shocks had a spatial correlation structure which is imperfectly captured by the disaster data. While some measurement error is certainly present, there is no evidence for a systematic spatial pattern. However, there may still be other omitted variables such as trade or migration between cells which imply that errors may be spatially correlated even if the treatment of neighbors is controlled for and the intensity of natural disasters has no systematic measurement error. Hence, the grid cell approach requires an explicit modeling of spatial treatment spillovers and of spatial autocorrelation in the residuals. The direction of these spatial spillovers depends, amongst other things, on specialization patterns: if a neighboring region specializes in similar industries, economic activity may shift towards it. If a neighboring region specializes in down-stream or up-stream industries, it may well be hurt by the shock. Hence, the relationship between the two regions may be governed by complementarity or by substitution effects.[9] This paper does not explore the exact mechanisms through which such spillovers arise, but makes a first attempt to empirically measure them.

In sum, this paper takes the analysis of economic impacts of natural disasters to global uniform grid cell data and evaluates the local economic effects of natural shocks. For this, a large data set of geological and meteorological events (ifo GAME Database) is updated and matched with available data on night-time light emissions as a proxy for economic activity. Following Costinot et al. (2016), the globe is partitioned into fields along latitude and longitude. Along with economic variables, various disaster types (storms, extreme precipitation, droughts, cold waves, and earthquakes) are mapped to specific grid cells using geographical information systems. In this paper, a balanced panel of 24,184 grid cells is created with a resolution of 0.5°×0.5° (approximately 55×55 km at the equator) spread across 197 countries from 1992 to 2013. Using spatial econometric panel techniques, the impact of various types of events on the growth of night-time light emissions is estimated, controlling for cell population, a set of year- and cell fixed effects and accounting for spatial autocorrelation in the error term.

Main results show a reduction in night-time lights after storms, cold waves and extreme precipitation events. For these types of events, there is strong evidence for positive spatial spillover effects within an 80 km radius. At the mean, effects are moderate and range in

[9] This logic is well known from the international trade literature, see Hsieh and Ossa (2016) for a recent application.

the order of 0.1-0.3 percentage points. At the extremes of the disaster measures, effects are pronounced and amount to several percentage points reduction in light growth in the short run. More specifically, evaluated at the average estimated lights-to-GDP growth elasticity, a one standard deviation increase in wind speeds leads to a reduction in income growth of 0.33 percentage points. With a time lag, the local effect is four times as large and spillovers from *one* cell increase local lights growth by 0.08 percentage points, corresponding to an income growth spillover of 0.13 percentage points for a one standard deviation increase in wind. Similarly, a one standard deviation increase in excessive precipitation and cold waves decrease income growth by 0.17 and 0.25 percentage points, respectively. With a time lag, excessive precipitation *increases* income growth by 0.12 percentage points, while the effect of cold spells persists to be negative by 0.11 percentage points. Associated contemporaneous spillovers amount to 0.03 and 0.07 percentage points, respectively. As droughts mostly affect agricultural outcomes, they do not seem to be associated with light emissions. Short-run negative spatial spillovers of these events are largely driven by rural rather than urban cells, suggesting that droughts cause indirect damages in rural economies.

Assessment of alternative spillover specifications indicates that disaster spillovers are a rather local phenomenon. This implies that adaptation policies aiming at supporting the temporary relocation of economic activity after a natural disaster should appreciate the very local nature of shock effects and associated spillovers. An extension to the empirical framework shows that there is evidence for heterogeneity across income groups and world regions. In particular, results are mainly driven by cells in low- and middle-income economies.

Results are robust to top- and bottom-coding, increasing the spatial radius, the temporal aggregation method, and controlling for time-varying country characteristics.

The remainder of the paper is organized as follows: Section 3.3 describes the econometric methodology. In section 3.2, data sources and the construction of the data set are discussed. Section 3.4 presents baseline results and shows the existence of both local treatment effects as well as spillovers to neighboring cells. Section 3.5 assesses the relevance of disaster spillovers across longer distances. Section 3.7 offers an extension to the baseline framework, zooming in on the heterogeneity of effects across income groups and world regions. Finally, results are tested with respect to a number of measurement and specification variations in Section 3.6. The last section concludes.

## 3.2 Measuring Economic Activity and Natural Disasters at the Cell Level

### 3.2.1 Light Emissions

First, the dependent variable, growth in night-time light emissions, which is taken as a proxy for local economic activity, is described. The data stem from the US Air Force Defense Meteorological Satellite Program (DMSP). They comprise yearly composite satellite images from which the yearly mean luminosity of each pixel can be extracted as a digital number (DN).[10] To align the data with the overall setup, all lights pixels that do not cover land surface are excluded[11] and the literature is followed by masking all pixels within gas flaring zones identified by Elvidge et al. (2009b).[12] Similarly, areas around volcanoes are masked.[13]

In addition, years in which more than one composite night-light image is available are dealt with. As the on-board sensors degrade over time, the DMSP launches a new satellite every 3 to 6 years. In 12 of the 22 available years, two satellites were in orbit simultaneously. In these cases, the satellite with the best coverage of valid nights per pixel in a given year is selected on the basis of each respective satellite-year layer's summary statistics.[14] If the number of

[10] Appendix C.1.1 provides supplementary information on data generation and graphical illustration.

[11] Even though substantial presence of light at sea exists (e.g., fishing boats or oil rigs), this economic activity cannot directly be attributed to any location on land and is therefore excluded. Further, natural disasters affect light emission at sea differently from that on land. At sea, lights may be mobile and seafaring may be ceased temporarily.

[12] The DMSP Operational Linescan System instruments record gas flares (typically resulting from gas disposal at oil production sites) as heavily over-glowing areas that differ markedly from areas with lights of electric origin. This affects approximately 2,300 grid cells; 0.89% of global land area.

[13] Volcanic eruptions show up in light data if they involve prolonged lava flows. If they are short-lived, they are excluded from the annual stable lights products by default. Some volcanoes (e.g., Etna in Italy and Popocatepetl in Mexico), however, show presence of lava flows throughout the entire period observed (1992-2013). Persistent light at all known volcanic locations is approximately circular with a consistent radius of 3 to 5 km. Consequently, these zones are masked from the light data. Two areas with lava flows near to Kilauea (Hawaii) and Nyiranongo (Congo, DRC) are masked manually to account for their spatial size and shape.

[14] Typically, the lights literature takes the simple average of these images (see, e.g., Chen and Nordhaus, 2011; Henderson et al., 2012; Pinkovskiy and Sala-i Martin, 2016). However, data availability (the number of valid nights that led to pixel construction) can be quite different across satellite-years. This introduces missing observations even if one satellite contains valid information. It also generates potentially spurious mean pixel values in which underlying valid nights enter the final mean with inconsistent weight or may be double-counted. Satellite-year inspection leads to selecting the layer from the respective youngest satellite with only one exception. There is a clear time-trend in the average number of valid nights, which steadily improves as new satellites are launched (see Table C.3 in the Appendix).

valid nights for a radiance pixel is zero, it is masked from the data. The prepared night-light layers are aggregated to mean light intensity for the 0.5°×0.5° grid cells.[15]

To translate light changes into economic magnitudes, Henderson et al. (2012) and Storeygard (2016) estimate lights-to-GDP growth elasticities at the country and the Chinese prefecture level, respectively. For both levels of aggregation, they find an elasticity of approximately 0.3. Following their approach allows obtaining an elasticity for the specific sample used in this research: Grid-cell data can be aggregated to the country level using area-weights for the spatial aggregation. Then, the natural logarithm of country level GDP in real currency units is regressed on the log of aggregate night-light intensity and a full set of country and time fixed effects.

Using the full time-span from 1992 to 2013 and the set of 197 countries, estimates suggest an aggregate lights-to-GDP growth elasticity of 0.37. The within $R^2$ is equal to 0.273, so that time variation in light emissions explains more than a quarter of the variation in GDP within a country over time. Moreover, the country level elasticity of lights to the population density (0.10) is not significantly different from the elasticity of GDP to the population density (0.13).[16] In line with recent literature connecting population density to total factor productivity (TFP) at the grid cell level (Desmet et al., 2018), this finding fosters the adequacy of light emissions as a proxy for gridded economic activity. Figure 3.1 compares grid cell level lights growth to country level GDP growth over time. Even without adjusting for potential systematic measurement error in the lights data, which will be taken care of econometrically, the plots indicate substantial variation across time and provide suggestive evidence for the co-movement of light and economic activity across the world.

### 3.2.2 Natural Disasters

The independent variables of interest measure the physical intensities of geological and meteorological events. Starting from Felbermayr and Gröschl (2014), a new data set of monthly observations is compiled from various sources at 0.5° by 0.5° grid cell resolution for the entire globe, named the Gridded GAME (geological and meteorological events) Database. The

[15] Additionally the number of top-coded (DN63) and bottom-coded (DN0) pixels in each cell are recorded. For robustness, top- or bottom-coded pixels are excluded in Section 3.6.1.

[16] One needs to bear in mind that this correlation is obtained by aggregating data to the country-level; this biases the strength of the lights-GDP link downwards. Detailed results are shown in Table C.4 in the Appendix. If the regression is restricted to the same time frame as Henderson et al. (2012), the obtained elasticity is 0.35 and the within $R^2$ is 0.240.

Figure 3.1 : Growth in Lights vs. Growth in GDP

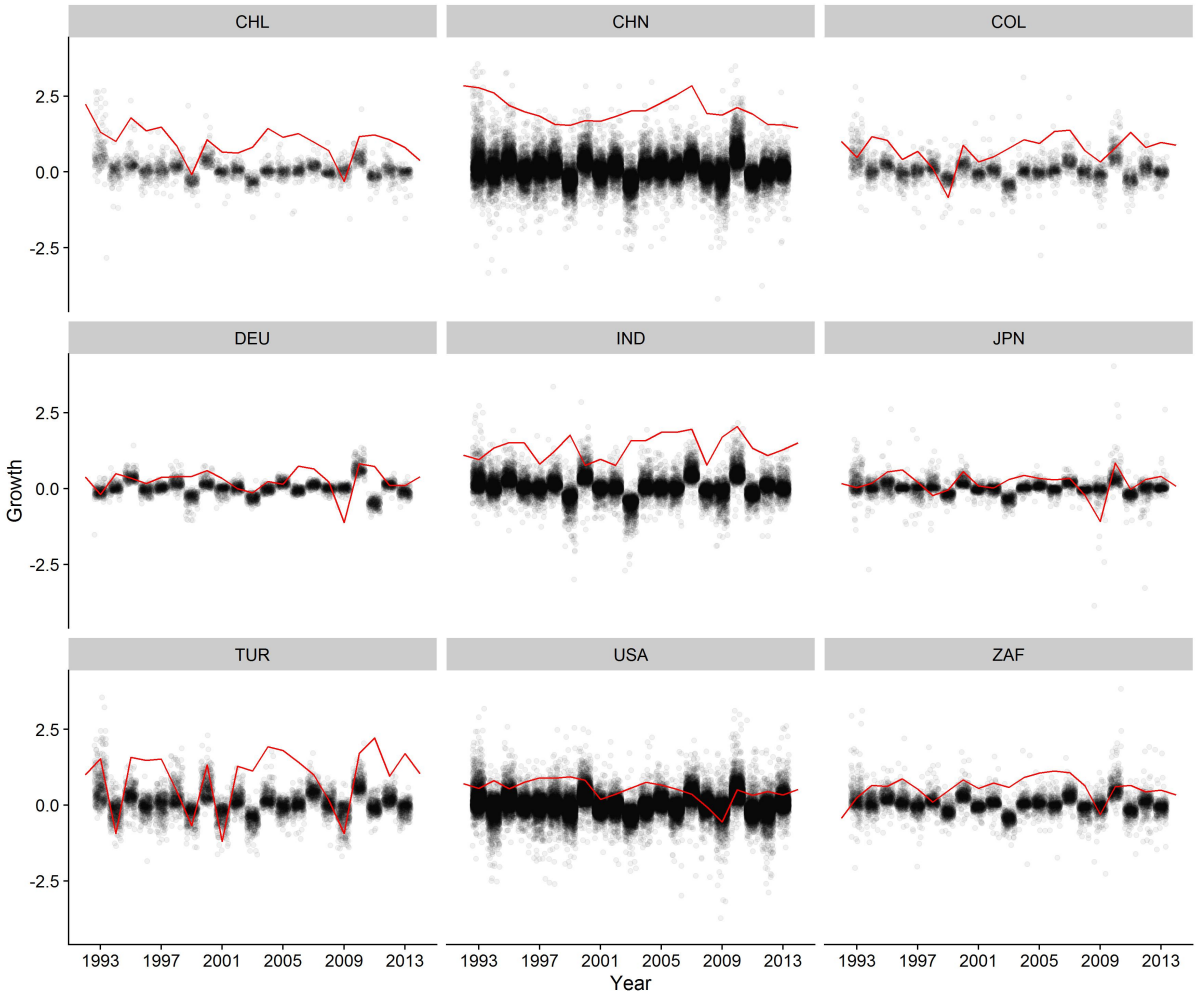


*Note:* Jitter-plots represent annual light growth at the cell level by country. Line-plots represent annual country level GDP growth, scaled by factor 0.2.

database covers the period 1979–2014 and captures earthquakes, storms, droughts, extreme precipitation and extreme temperature events.[17] While this research will ultimately be at the annual level, it is quintessential to collect primary intensity data at the monthly level for climatic and meteorological events, the lowest common level of disaggregation. This allows accounting for local seasonality in meteorological and climatic patterns. The main objective is to identify extreme events, which by construction implies identifying anomalies from local conditions. The climate science literature is followed in defining anomalies as

[17] Note that the Gridded GAME data includes records on volcanic eruptions and accompanying Volcanic Explosivity Index (VEI), but since continuous presence of lava at the surface emits light that is captured in the night-light data, no use can be made of this measure in the present study.

(extreme) deviations from monthly means for an individual cell (see Kraus, 1977; Nicholson, 1986).

Data from the Incorporated Research Institutions for Seismology (IRIS)[18] is used to measure the locations of epicenters and magnitudes of **earthquakes**.[19] IRIS collects data from a vast number of seismological institutions around the world and provides global coverage. Maximum earthquake magnitudes observed at epicenter locations are mapped to the respective grid cell within a given month. As IRIS provides global coverage, any missing values are set to zero.

Data on **extreme precipitation** events is also collected. These events may cause damage, when precipitation exceeds the local percolation capacities.[20] Monthly precipitation in millimeters stems from the University of East Anglia Climatic Research Unit Time-Series (CRU TS 3.23).[21] The data set is based on gauge data by weather stations. As precipitation can be discontinuous in time and fractal in space, climate scientists apply sophisticated reanalysis methods to produce high-quality estimates for monthly precipitation covering all land areas (excluding Antarctica) at 0.5° resolution (see Harris et al., 2014). CRU compiles and homogenizes station data from numerous sources into a consistent format, assessing global precipitation variability and additional variables that allow the derivation of drought indices, such as the Standardized Precipitation-Evapotranspiration Index (SPEI). To identify extreme precipitation events by cell at the monthly level, location-specific seasonality and systematic spatial differences are taken into account. Following the climatological literature, standardized anomalies are calculated by subtracting the long-run (1979-2014) mean precipitation observed in a cell for a given month and standardizing it with the corresponding cellular long-run standard deviation for that month:

$$\gamma_{i,m,y}^{prec} = \frac{x_{i,m,y}^{prec} - \bar{x}_{i,m}^{prec}}{\sigma_{i,m}^{prec}}, \text{ where } i = \text{cell}, m = \text{month}, y = \text{year}.$$

[18] `http://service.iris.edu/fdsnws/event/docs/1/builder/`

[19] Magnitudes provided (e.g., Richter Scale, Moment Magnitude) differ across earthquakes, but all follow a logarithmic scale, are valid in their respective range and can be compared with each other.

[20] Information on flood events (their extent and depth) at the grid cell level, as provided by the Dartmouth Flood Observatory, would be preferred, but no such data is available with global and consistent coverage. Kocornik-Mina et al. (2015) use maps of 53 selected large floods to study their impact on economic activity at a very fine 1×1 km resolution. Their estimates suggest economic effects in a similar order of magnitude as the ones found by this study and exhibit the same dynamic pattern.

[21] `http://browse.ceda.ac.uk/browse/badc/cru/data/cru_ts/cru_ts_3.23/data`.

This indicator measures both positive and negative precipitation extremes. As extreme precipitation events which potentially exceed local percolation capacities are of particular interest, the constructed monthly precipitation indicator is censored at zero.[22] The resulting measure records the positive deviation of precipitation from the long-run monthly mean in a cell accounted in units of standard deviation from its mean.

To capture **droughts**, the SPEI is calculated from gridded data on precipitation (PRE) and potential evapotranspiration (PET) contained in the CRU TS 3.23 data set. This takes into account the amount of water coming in (precipitation) and the amount lost (evapotranspiration), resulting in a climatic water balance for each cell in a given month. (Vicente-Serrano et al., 2010) is followed[23] to construct a cell-specific monthly SPEI that has a zero mean, a standard deviation of one and is theoretically unbounded. Negative values indicate drought events, hence, a zero-censored version of the constructed indicator is used.[24] Hot weather conditions enter the SPEI as part of potential evapotranspiration. The drought indicator therefore includes heat waves to the extent that they are accompanied by dry conditions.

**Cold waves** can cause major disruption to both social and economic activity. To capture these events, gridded 0.5° resolution land surface temperature in degrees Celsius is used[25], compiled by the Climate Prediction Center (CPC) of the National Oceanic and Atmospheric Administration (NOAA). This data set combines two large sources of station observations collected from the Global Historical Climatology Network (GHCN) v2 and the Climate Anomaly Monitoring System (CAMS).[26] To obtain global spatio-temporal coverage and consistency, unique reanalysis methods are applied to the source data (see Fan and Van den Dool, 2008). Again, the grid cell resolution is perfectly consistent with Gridded GAME such that observations are merged by longitude and latitude of cells' geographic centers. Cell-specific low temperature events at the monthly level are identified as standardized anomalies, analogous to extreme precipitation events, by taking location-specific seasonality and systematic spatial differences in the climatology into account. Hence, temperature is normalized by subtracting the long-run

[22] The uncensored precipitation measure is recorded in the Gridded GAME database. While negative index values might hint at droughts, a more sophisticated index proposed in the hydrological literature is used.

[23] The climatic water balance (PRE$-$PET) is standardized for each cell with a log-logistic distribution function, applying the unbiased probability weighted moments method to data from the current and the respective past $n-1$ months with $n \in [1, 3, 6, 9, 12]$. The reference period to obtain the distribution parameter is 1901–2014.

[24] The converse argument that positive values represent extreme precipitation events is, however, not true.

[25] Mean surface temperatures provided in Kelvin is converted to Celsius: °C $=$ °K $- 273.1$

[26] `http://www.esrl.noaa.gov/psd/data/gridded/data.ghcncams.html`.

(1979-2014) mean temperature observed in a cell for a given month and standardizing this deviation by the cell long-run standard deviation for that month:

$$\gamma_{i,m,y}^{temp} = \frac{x_{i,m,y}^{temp} - \bar{x}_{i,m}^{temp}}{\sigma_{i,m}^{temp}}, \text{ where } i = \text{cell}, m = \text{month}, y = \text{year}.$$

This indicator reflects both positive and negative temperature extremes. To isolate information on cold wave treatment, positive monthly anomalies are censored and negative ones are expressed in absolute terms. The resulting cold wave indicator records negative deviations of surface temperature from the long-run monthly mean at the cell, accounted in units of standard deviation from this mean.

To examine **storms**, a combined measure is created using information on maximum monthly sustained wind speeds from two distinct sources. The International Best Track Archive for Climate Stewardship (IBTrACS) Version v03r09[27] conveys information on moving center-locations with respective wind speeds of tropical cyclones. The Global Summary of the Day (GSOD) statistics[28] contain wind speeds measured at weather stations. The lack of gridded data poses a challenge: The spatial spillover analysis requires a panel which is balanced and provides at least one neighbor per grid cell. Given the impermanence of cyclones and both the uneven spatial distribution and inter-temporal fluctuation of stations, readily available wind speed data is insufficient to provide these ingredients.[29] Moreover, available point-location data does not accommodate the spatial dimension of storms. Consequently, two types of spatial interpolation techniques are applied. A wind field model provided and described in detail by Geiger et al. (2017) is used to generate continuous gridded wind field cells from IBTrACS, which provides distributions of surface wind speeds around hurricane centers. The model uses all available information on wind speed, pressure and direction to compute sustained winds speeds that most likely occurred in cells surrounding available data points. Figure 3.2 presents hurricane Katrina as an example of how raw data are transformed to a wind field. To capture summer and winter storms, cells are filled with gridded non-cyclone wind speeds. GSOD

[27] `http://www.ncdc.noaa.gov/oa/ibtracs/index.php?name=ibtracs-data`.

[28] `ftp://ftp.ncdc.noaa.gov/pub/data/gsod`.

[29] Balancing reduces the sample to cells with at least one station or hurricane center in every period. Simply setting cells with missing wind speed information to zero induces measurement error as a true monthly maximum wind speed of zero is very unlikely. Figure C.2 in the Appendix visualizes observational losses resulting from balancing if wind speeds are not interpolated.

Figure 3.2 : Hurricane Katrina – IBTrACS (l.) vs. Wind Field (r.)

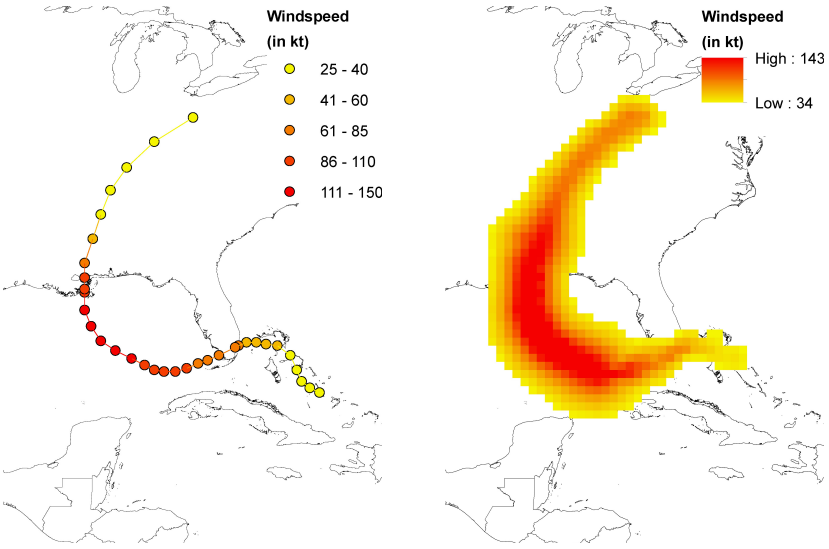


data are combined with a global kriging spatial interpolation algorithm (see Krige, 1951).[30] Finally, a combined wind speed measure is constructed, which prefers wind field information on hurricanes, cyclones or typhoons – if any such event has affected the cell – to the cell's kriged station wind speed. The resulting wind speed indicator is the maximum sustained wind speed for a cell-month combination, measured in knots.

As night-lights are provided annually, the monthly physical intensities are aggregated to an annual intensity indicator for each type. Indicators distributed around zero need to be split, such that extreme events from both tails do not cancel out. Measures of cold waves and droughts need no further adjustment, except censoring positive index values in the monthly data. To aggregate extreme precipitation, negative index values of the monthly precipitation measure are censored.

A straightforward aggregation approach would be to take the simple mean over all monthly observations in a cell for each calendar year. This would, however, introduce measurement error and bias, as all monthly observations within each year would be given the same weight. Consequently, a disaster that occurred earlier in a year may have had a different impact, with

[30] Haslett and Raftery (1989) were the first to adopt kriging to a wind speed context by modeling the spatial distribution of Irish wind power resources using historical wind speed data. Using daily European climate data, Hofstra et al. (2008) show that kriging performs best out of six interpolation methods. Kriged predictions are based on the aerial (semi-)variance in wind speeds across locations in relation to the distance between locations. These predictions convey more information about the spatial persistence of observed values than alternative interpolation methods, e.g., inverse distance weighting, where a linear decay across space is imposed as a structural assumption. The exact procedure is described in detail in Appendix C.1.2.

respect to the number of months in which luminosity has been captured by the satellites after the event, than one that happened later. To take this dynamic relationship into account, a rolling-window weighted mean for each type is calculated, weighting it by the number of months it affected luminosity. This ensures a uniform take on potential disaster impacts, allowing all realizations to affect light growth for 12 consecutive months.[31] The final indicators capture weighted annual averages of the monthly indicator values from the Gridded GAME database, reflecting disaster intensity by cell and year. Figure 3.3 describes the distributions of aggregated variables.

Figure 3.3 : Kernel Densities of Annual Aggregate Physical Intensities

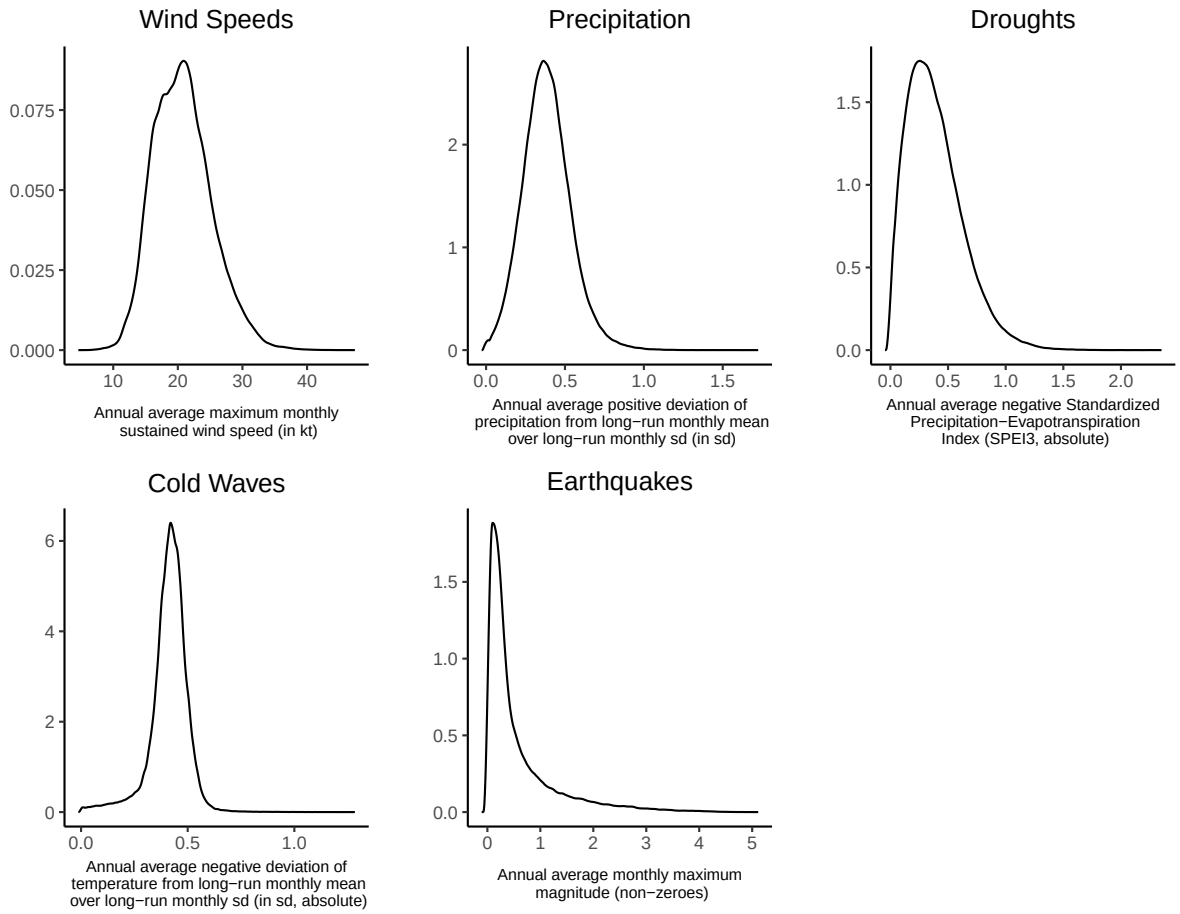


*Note:* Density distributions of aggregate annual physical intensities. All measures are reported over the full sample, except earthquakes, for which the density over the non-zero magnitudes is reported. Note that 80% of cell-years show zero earthquake magnitude in the full sample.

[31] It must be recognized that, in principle, longer lasting disaster impacts are possible. These are taken into account by including a temporal lag of the treatment variable into the regressions. In the robustness section, results are provided which use the simple annual mean as an alternative.

Note that by construction of the weighted annual average, the range of the distributions is smaller than at the monthly level. Table 3.1 provides examples of natural events and illustrates how these are reflected in the yearly aggregates in comparison to the monthly input data. Corresponding cell means and cell standard deviations of the yearly aggregate measure are provided. The examples show that extreme events lie way above the cell means and in the tail of the cell-specific distributions. Full summary statistics on yearly aggregates for the estimation sample are provided in Table C.2 in the Appendix.

Table 3.1 : Representation of Natural Events in the Monthly Data vs. the Yearly Aggregates

| Event | Date | Place | Lat | Lon | Month | Year | C-Mean | C-SD |
|---|---|---|---|---|---|---|---|---|
| Hurricane Katrina | 08/2005 | New Orleans, USA | 28.75 | -89.25 | 138 kt | 38.3 kt | 28.9 kt | 3.4 |
| Odisha Cyclone | 10/1999 | Odisha, India | 19.75 | 86.25 | 128 kt | 24.8 kt | 17.8 kt | 3.2 |
| Haiti Earthquake | 01/2010 | Haiti | 18.25 | -72.25 | 7.7 | 1.3 | 0.2 | 0.3 |
| Kobe Earthquake | 01/1995 | Kobe, Japan | 34.75 | 135.25 | 7.3 | 3.8 | 2.1 | 0.8 |
| Extreme Rain & Flash-Flood + Heavy Prec. (Ohio Winterstorm) | 06/2013 12/2013 | Maryville, Missouri, USA | 35.75 | -83.75 | 2.66 4.16 | 1.52 | 0.43 | 0.35 |
| Torrential Rains | 11/1994 | Kairo/Nile Valley, Egypt | 30.25 | 32.25 | 4.56 | 0.56 | 0.23 | 0.15 |
| UK Record Winter | 12/2010 | Country-Wide, UK | 55.25 | -2.25 | 2.30 | 0.67 | 0.43 | 0.09 |
| Heavy Coldwave | 07/2003 | Cuzco Region, Peru | -12.75 | -71.25 | 2.04 | 0.59 | 0.49 | 0.11 |
| Drought (prolonged) | 01/2012 | Country-Wide, Mexico | 20.25 | -104.25 | 1.63 | 0.80 | 0.52 | 0.17 |
| Drought (prolonged) | 02/1992 | Country-Wide, Zimbabwe | -21.25 | 31.75 | 2.89 | 1.38 | 0.44 | 0.40 |

*Note:* Columns *Lat* and *Lon* represent geographic coordinates of grid cell centroids for reported values. *Month* represents maximum index realizations of respective events in the monthly raw data, observed in the month of occurrence. *Year* represents the corresponding (simple mean) aggregate over 12 months of the year. *C-Mean* and *C-SD* refer to cell-specific distributions of yearly aggregates.

The structure of the disaster intensity variables combined with the fixed effects approach allows letting the data decide which cell-specific events are extreme.[32] It is indeed these (extreme) deviations that form disaster events this research is ultimately interested in.[33]

### 3.2.3 Population

A key control variable, population at the pixel level, stem from the Gridded Population of the World (GPW) collection provided by the Center for International Earth Science Information Network (CIESIN). The data contain 5-year target estimates based on census inputs gathered at the lowest administrative units available, which are redistributed from their administrative

[32] Note that the fixed effects essentially demean the measures, leaving deviations from the cell-mean as the source of disaster identification.

[33] Note that point estimates on the respective disaster variables cannot be directly compared as measures are based on different units of account.

census boundaries to a uniform pixel grid by using aerial weights.[34] Pixel data are aggregated to grid cell units by summing population numbers within each cell. To interpolate the years between the given 5-year periods, exponential population growth is assumed.

## 3.3 Empirical Strategy

The aim of this research is to identify the local average treatment effect of various types of natural events at the grid level. This requires accounting for the spatial structure of the data both conceptually and econometrically. A grid cell approach is taken with 0.5°×0.5° resolution. This coincides with primary data records on meteorological and climatological events and provides a natural starting point. Superimposing this arbitrary layout has the advantage that it intersects with actual economic units that may show a high connectivity and clustering. Observational units are therefore entirely exogenous.[35]

A first somewhat naive approach that ignores potential spillovers and the spatial structure of error terms is a simple panel fixed effects growth estimation, in which within-cell variation of year-to-year growth in average night-light emission is related to the intensity of events in that year:[36]

$$\Delta\boldsymbol{\ell}_t = \boldsymbol{\ell}_{t-1}\gamma + \boldsymbol{D}_t\boldsymbol{\beta^0} + \boldsymbol{X}_t\boldsymbol{\delta^0} + \boldsymbol{\nu} + \boldsymbol{\pi} + \boldsymbol{u}_t \tag{3.1}$$

where the $K \times 1$ vector $\Delta\boldsymbol{\ell}_t$ captures the growth rate in night-light emissions expressed in yearly changes of the logarithm of mean night-light intensity $\boldsymbol{\ell}_t \equiv \ln\left(\overline{\textbf{light}}_t\right)$ for each of the $K$ grid cells, $\Delta\boldsymbol{\ell}_t \equiv \boldsymbol{\ell}_t - \boldsymbol{\ell}_{t-1}$. The disaster treatment variable $\boldsymbol{D}_t$ is a $K \times P$ matrix of physical intensities (and temporal lags) and $\boldsymbol{X}_t$ is a $K \times N$ matrix of $N$ control variables (population) at the grid cell level in year $t$. $\boldsymbol{\pi}$ denotes a full set of year fixed effects to capture global trends, such

[34] Note that the GPW data applied here is *not* constructed using lights as an input factor; contrary to the widely-used GRUMP population data that make use of night-light emissions to redistribute population counts across pixels.

[35] An alternative would be to conduct estimations at the sub-national level on administrative divisions. Economic data (e.g., income inequality) are available as control variables for some countries. However, these variables are almost always correlated with night-lights, if not (partly) constructed using them. Moreover, administrative units across the globe differ tremendously in size and reflect geographic and demographic conditions as well as political decisions, which are often determinants of night-lights themselves or jointly determined with it.

[36] As more detailed data become available, a higher level of temporal detail may be an alternative. But studying annual averages ensures that not only short-run power outages are captured (a channel through which disaster events might affect night-light emissions) such that the focus is on longer lasting impacts on the emission of night-light throughout the year.

as technological progress, energy costs, and the global business cycle.[37] Moreover, year fixed effects address systematic time variation in the measurement of light emissions. On-board gain settings of sensors vary across and within satellites over time and with satellite age – yet, these effects are not documented. Accordingly, raw satellite data is not calibrated and direct comparison of light intensities over time would therefore be problematic. This issue is tackled by following Henderson et al. (2012) and Chen and Nordhaus (2011) who propose to include time fixed effects. $\nu$ denote cell fixed effects controlling for time-constant local unobservable variables. Cell fixed effects absorb location-specific baseline risk, which determines to what extent disasters occur unexpectedly and may thus affect economic responses to shocks. Consequently, identification relies on unexpected variation in the physical intensity measure. How night-light growth reflects GDP growth may be structurally related to historical, cultural and political differences in the use of light. In addition, night-light emission patterns may be systematically driven by land use. Areas dominated by agricultural use emit little to no light as they grow (Keola et al., 2015). To the extent that these differences and land use patterns are time-invariant, they are captured by cell fixed effects. Cell fixed effects also control for inherent systematic measurement error in night-lights across latitude (e.g., due to stray light, aurora, and the solar cycle) and for overall topography and other unobserved geographic determinants. This basic model is explored first to take the analysis from national to the grid cell level and to show very basic correlations.

However, the spatial dependence of both night-light growth and disaster intensity requires relaxing the traditional independence assumption, often implicitly applied in most work in this field. As cells intersect true economic units (e.g., cities or metropolitan areas), this makes them spatially dependent by construction. Also, weather shocks typically do not account to only single cells but have a spatial extent of their own. Thus, despite treatment variation across space within this extent, exogenous shocks are correlated with shocks in neighboring cells. In addition, night-light growth in one cell is not orthogonal to disasters occurring in neighboring cells due to potential spillover effects. Hence, treatment of neighbors may have explanatory power and is correlated with own treatment, which leads to omitted variable bias.

[37] In the sensitivity analysis, it is shown that results remain robust when including country-specific year-effects. While this allows to control for time-varying country characteristics (e.g. institutions, policies or overall infrastructure), it tremendously reduces the degrees of freedom and restricts identification to countries beyond a critical geographic size.

To avoid this bias and account for spatial dependence, the idea is to simultaneously model local treatment effects and spillover effects to neighboring cells. Therefore, a spatial Durbin error model (SDEM) (see Anselin, 2013; Halleck Vega and Elhorst, 2015) with cell and year fixed effects is chosen.[38] In this model, the dependent variable may not only depend on own covariates but also on the covariates of neighboring units. This implies that natural shock events not only affect light growth in the cells in which they are recorded, but also indirectly affect light growth in neighboring cells. A fully specified spatial panel model is estimated of the form:

$$\begin{aligned} \Delta \boldsymbol{\ell}_t &= \boldsymbol{\ell}_{t-1}\gamma + \boldsymbol{D}_t\boldsymbol{\beta}^{\mathbf{0}} + \boldsymbol{X}_t\boldsymbol{\delta}^{\mathbf{0}} + \boldsymbol{W}^r\boldsymbol{D}_t\boldsymbol{\beta}^{\mathbf{1}} + \boldsymbol{W}^r\boldsymbol{X}_t\boldsymbol{\delta}^{\mathbf{1}} + \boldsymbol{\nu} + \boldsymbol{\pi} + \boldsymbol{u}_t \\ \boldsymbol{u}_t &= \rho\boldsymbol{W}^r\boldsymbol{u}_t + \boldsymbol{\varepsilon}_t. \end{aligned} \tag{3.2}$$

where $\boldsymbol{W}^r$ is a time-invariant $K \times K$ dimensional spatial weights matrix, which allows accounting for spatial spillovers. It is specified as binary and isotropic, meaning that its elements are equal to one for all neighboring cells within the spatial radius $r$ around a given cell's center and discretely drop to zero for all cells beyond that radius, as recommended by Conley (2008).[39] In the baseline specification, a geodesic radius $r$ of 80 km is chosen. This implies that effectively eight adjacent cells are considered neighbors at the equator. Using a constant metric distance ensures that the geographic area of neighbors remains constant over latitude. This leads to the inclusion of a larger number of cells along the longitudinal axis the further one moves away from the equator.[40] Gibbons et al. (2015) discuss requirements of imposing structure on the spatial process to disentangle treatment effects from direct spillovers in the dependent variable. The cutoff choice is to some extent arbitrary and it is not formally testable.[41] By interacting determinants with $\boldsymbol{W}^r$, spatial lags are obtained. The inclusion of spatial lags – similar to the inclusion of temporal lags in time-series – allows local outcomes to depend not only on local treatment but also on the treatment of neighbors. $\boldsymbol{\beta}^{\mathbf{1}}$ and $\boldsymbol{\delta}^{\mathbf{1}}$ are

[38] As it is reasonable to assume that spatial spillovers from natural events are confined in their geographical extent, local rather than global spillovers are modeled explicitly. This study therefore prefers the SDEM over the more often used spatial Durbin model (SDM) specification. For a discussion, see Halleck Vega and Elhorst (2015). Section 3.5 discusses SDM as an alternative specification.

[39] This structure imposes a strict balancing restriction on the panel such that the same set of neighbors is used for a specific cell across all 21 years in the sample.

[40] Due to the curvature of the earth, the metric length of 0.5° longitude decreases with latitudinal distance to the equator, whereas the metric length of 0.5° latitude remains approximately constant.

[41] To test whether results are sensitive to the spatial radius chosen for the weights matrix, the distance cutoff is increased in Section 3.5 to $r$ = 160 km.

thus average local spillover effects of a marginal change in the respective explanatory variable in *one* neighboring cell.

Following the econometric literature, spatial clustering and spillovers in unobserved characteristics are accounted for by allowing for spatial auto-correlation in the error term $\boldsymbol{u_t}$. This is crucial due to potentially high connectivity and clustering of observed values in the spatially disaggregated data and to account for the fact that residual spatial auto-correlation (RSA) may reflect unobserved natural or economic processes. Superimposing an arbitrary grid cell layout implies that cells need not be independent from each other, as cell borders may intersect true economic units (i.e., urban settlements) and share national or regional business cycles and institutions. While the imposed spatial structure accounts partially for the true spatial dependence, it must still be corrected for RSA, which otherwise may bias the spatial estimates.

The Global Moran's $I$ test (Moran, 1950) allows testing for residual auto-regressive processes ($\boldsymbol{u_t} = \rho \boldsymbol{W}^r \boldsymbol{u_t} + \boldsymbol{\varepsilon_t}$).[42] In a spatial lag of X (SLX) regression with two-way cell and time fixed effects, a positive and statistically significant test is observed for all disaster categories, see Table C.5. Hence, the Null is rejected in favor of positive RSA (i.e., spatial clustering). Thus, the SDEM is preferred over the more parsimonious SLX specification. To account for RSA, Baltagi et al. (2007) type spatial auto-correlation in the residuals is applied.[43] To model RSA and to address non-linearity in $\rho$, the Maximum-Likelihood approach for spatial panel models provided by Millo and Piras (2012) and Millo (2014) is used. This allows consistent estimation of the local economic impact of natural disasters together with spillover effects to neighboring locations.

[42] It takes the following form

$$I = \frac{N}{W} \cdot \frac{\sum_c \sum_j w_{cj}(x_c - \bar{x})(x_j - \bar{x})}{\sum_c (x_c - \bar{x})^2}.$$

The Null of no residual spatial auto-correlation equals $E(I) = \frac{-1}{N-1}$.

[43] An SLX model excluding the spatial error component is also estimated. Results are shown in Tables C.6 to C.8 in the Appendix. Furthermore, an ordinary least squares (OLS) model is estimated with standard errors adjusted for spatial clustering following the procedure implemented by Hsiang (2010), see Table C.17.

## 3.4 Main Results

In this section, a parsimonious panel fixed effects model is taken as a starting point to then show how modeling the spatial dependence of grid cells changes local treatment effects. In later sections, robustness checks are presented and heterogeneity in income groups and across world regions is explored.

### 3.4.1 Explorative Results

Following Bertinelli and Strobl (2013) and Elliott et al. (2015), the point of departure is a simple ordinary least squares (OLS) model including cell and year fixed effects, as described in the methodology section. Extreme precipitation is taken as an example, as this shows most explicitly how modeling spatial spillovers affects the results. Results are presented in Table 3.2, columns (1) to (4). Not accounting for spatial dependence and spatial autocorrelation in the simple panel fixed effects setting suggests a positive and statistically significant effect of precipitation on night-light growth in column (1). This is a counterintuitive finding reminiscent of earlier results in the literature; see Felbermayr and Gröschl (2014) for a discussion. Controls, such as initial light levels and population show expected negative and positive results, respectively.

As spatial dependence between grid cells is present, spatial spillovers in production and consumption may affect surrounding locations. Thus, in column (2), Halleck Vega and Elhorst (2015) are followed by estimating an SLX model, which includes the spatial weights matrix but does not account for residual spatial autocorrelation. The local average treatment effect turns substantially negative and highly significant, while simultaneously a positive coefficient estimate for the spatial spillover of extreme precipitation is found. Hence, the local impact of extreme precipitation is negative, but a cell's night-light growth is positively affected by extreme precipitation events in neighboring cells.[44] Point estimates on lagged night-light intensity and population remain stable and highly significant. Next, a temporal lag is added to the SLX model to allow for dynamic effects in column (3). For lagged local treatment and

[44] Note that Bertinelli and Strobl (2013) and Elliott et al. (2015) investigate potential spatial spillovers. However, rather than allowing for direct spillovers, they average disaster intensity over the set of a cell and a range of its neighbors. Both studies find little evidence for spatial spillovers, while this study finds strong evidence in favor of their existence. Note that the the size of grid cells (0.5°compared to 1 $km^2$) is considerably larger. Spatial spillovers in this approach are thus estimated over a much longer distance, while their spillovers would be part of the local treatment effect in this approach.

spatial spillovers, highly significant point estimates suggest a reversal of respective effects in the year of occurrence. This indicates that spillovers are, on average, temporary and recovery occurs within two years.

Table 3.2 : Model Buildup: Impact of Precipitation and Wind on Light Growth

**Dependent Variable:** $\Delta \ln(\text{lights}_t)$

| | **precip.** | | | | **wind** | | | |
|---|---|---|---|---|---|---|---|---|
| | (1) | (2) | (3) | (4) | (5) | (6) | (7) | (8) |
| $\text{disaster}_t$ | 0.0115*** | −0.0613*** | −0.0752*** | −0.0310*** | −0.0051*** | −0.0102*** | −0.0010 | −0.0020** |
| | (0.0029) | (0.0078) | (0.0081) | (0.0070) | (0.0003) | (0.0009) | (0.0010) | (0.0009) |
| $\text{disaster}_{t-1}$ | | | 0.0481*** | 0.0219*** | | | −0.0143*** | −0.0090*** |
| | | | (0.0077) | (0.0069) | | | (0.0010) | (0.0009) |
| $W \cdot \text{disaster}_t$ | | 0.0114*** | 0.0138*** | 0.0049*** | | 0.0008*** | −0.0002 | 0.0000 |
| | | (0.0011) | (0.0011) | (0.0013) | | (0.0001) | (0.0001) | (0.0002) |
| $W \cdot \text{disaster}_{t-1}$ | | | −0.0079*** | −0.0021 | | | 0.0015*** | 0.0008*** |
| | | | (0.0011) | (0.0013) | | | (0.0001) | (0.0002) |
| $\ln(\text{pop}_t)$ | 0.0412*** | 0.0250*** | 0.0250*** | 0.0257*** | 0.0404*** | 0.0238*** | 0.0236*** | 0.0247*** |
| | (0.0028) | (0.0027) | (0.0027) | (0.0013) | (0.0028) | (0.0027) | (0.0027) | (0.0013) |
| $W \cdot \ln(\text{pop}_t)$ | | 0.0149*** | 0.0149*** | 0.0112*** | | 0.0145*** | 0.0143*** | 0.0108*** |
| | | (0.0009) | (0.0009) | (0.0006) | | (0.0008) | (0.0008) | (0.0006) |
| $\ln(\text{lights}_{t-1})$ | −0.4090*** | −0.4123*** | −0.4122*** | −0.4367*** | −0.4109*** | −0.4146*** | −0.4152*** | −0.4387*** |
| | (0.0032) | (0.0032) | (0.0032) | (0.0011) | (0.0032) | (0.0032) | (0.0032) | (0.0011) |
| $\rho$ | | | | 0.0672*** | | | | 0.0672*** |
| | | | | (0.0000) | | | | (0.0000) |
| Method | OLS | SLX | SLX | SDEM | OLS | SLX | SLX | SDEM |
| Observations | 502,026 | 502,026 | 502,026 | 502,026 | 507,864 | 507,864 | 507,864 | 507,864 |

*Note:* ***, **, * denote significance at the 1%, 5% and 10% level. Specifications (1) to (3) and (5) to (7) are estimated by panel OLS, (4) and (8) is estimated by Maximum Likelihood. Standard errors (in parentheses) allow for heteroskedasticity and clustering at the cell level in specifications (1) to (3) and (5) to (7). Cell and year fixed effects included but not reported. Spatial radius is r=80 km. Yearly disaster intensities reflect time-weighted rolling averages over 12 subsequent monthly observations.

The spatial spillovers modeled capture spatial dependence only partially due to the fact that grid cells may intersect with metropolitan areas along their arbitrary borders. Night-light growth is thus expected to be spatially correlated across contingent cells due to unobserved characteristics which also follow a spatial pattern, so residual spatial autocorrelation remains a concern.[45] Therefore, in column (4), the preferred SDEM model is estimated, which augments the SLX model with Baltagi-type spatial errors. Point estimates on both local and spillover effects are substantially reduced in size but remain qualitatively similar. Note that the lagged spillover effect of extreme precipitation turns insignificant in the SDEM specification. The spatially auto-regressive parameter $\rho$ is positive and highly statistically significant, which is in line with the results of Moran's $I$ test.

[45] Absence of RSA is rejected in the SLX model for all disaster types in a Moran's $I$ test, with evidence for positive spatial autocorrelation implying spatial clustering patterns.

To compare obtained estimates with existing grid level studies, the storm indicator is specifically taken under consideration (see Table 3.2, columns (5) to (8)). In line with Bertinelli and Strobl (2013) and Elliott et al. (2015), local average treatment effects remain consistently negative across all model specifications (also in the lags). Note, however, that the point estimate for the SDEM specification (column (8)) is more than half the size of that in the OLS specification (column (5)). Contrary to the aforementioned studies, this research finds evidence for positive and statistically significant spatial spillovers. The fact that spillovers show up significantly only in the lagged period may be consistent with results by Bertinelli and Strobl (2013) and Elliott et al. (2015) that suggest absence of spatial spillovers in the contemporaneous year.

Results for all other disaster categories are reported in Tables C.6 to C.8 in the Appendix. Substantial differences between the estimated local average treatment effect in OLS versus SLX models are found for all disaster categories, and they may vary qualitatively in terms of estimated signs and lagged effects. For all categories but earthquakes, evidence for the presence of spatial spillovers is found. For droughts, the mirror image of precipitation patterns is obtained, with a negative local treatment effect in the OLS, but a sign reversal when allowing for spatial spillovers. Cold waves behave like precipitation, with the sign of the effect reversing when moving from the simple framework to allowing for spatial spillovers. For earthquakes, the size of the positive estimate is reduced together with significance levels when moving from OLS to SLX and subsequently to SDEM, but a positive local treatment effect remains. There is no evidence for consistent spatial spillovers. A reason may be substantial measurement error in the spatial extent of earthquakes and in their precise location. Reported epicenters often lie at the outer edge of an earthquake's fault rather than at the center of distributed ground movement. Furthermore, capturing negative light growth effects of earthquakes in the yearly response variable might generally be unfeasible: Earthquakes are sudden and short-lived, while temporary relocation of activity into the open, such as evacuation to emergency camps, as well as reconstruction and building sites tend to increase rather than dampen light emissions. Post-impact stimuli to the reconstruction sector are common and are frequently reported (see, e.g., Chang, 2010; Hallegatte and Przyluski, 2010). In addition, duration of the reconstruction phase varies widely, depending on financial and technical constraints (see, e.g., Ghil et al., 2011). For these reasons, further discussion of earthquake results is disregarded in the following. Instead, focus is put on weather shocks, which can be measured with much higher precision in this setup.

### 3.4.2 Baseline Results

The previous section clearly established the SDEM model as the preferred specification. Table 3.3 presents results for each type of weather shock.

Table 3.3 : Baseline Results

**Dependent Variable:** $\Delta \ln(\text{lights}_t)$

| | **wind** | **precip.** | **drought** | **cold** |
|---|---|---|---|---|
| $\text{disaster}_t$ | −0.0020** | −0.0310*** | 0.0083* | −0.0762*** |
| | (0.0009) | (0.0070) | (0.0048) | (0.0153) |
| $\text{disaster}_{t-1}$ | −0.0090*** | 0.0219*** | 0.0005 | −0.0326** |
| | (0.0009) | (0.0069) | (0.0047) | (0.0149) |
| $W \cdot \text{disaster}_t$ | 0.0000 | 0.0049*** | −0.0044*** | 0.0218*** |
| | (0.0002) | (0.0013) | (0.0009) | (0.0027) |
| $W \cdot \text{disaster}_{t-1}$ | 0.0008*** | −0.0021 | 0.0010 | −0.0195*** |
| | (0.0002) | (0.0013) | (0.0009) | (0.0026) |
| $\ln(\text{pop}_t)$ | 0.0247*** | 0.0257*** | 0.0276*** | 0.0244*** |
| | (0.0013) | (0.0013) | (0.0014) | (0.0013) |
| $W \cdot \ln(\text{pop}_t)$ | 0.0108*** | 0.0112*** | 0.0115*** | 0.0106*** |
| | (0.0006) | (0.0006) | (0.0006) | (0.0006) |
| $\ln(\text{lights}_{t-1})$ | −0.4387*** | −0.4367*** | −0.4329*** | −0.4379*** |
| | (0.0011) | (0.0011) | (0.0011) | (0.0011) |
| $\rho$ | 0.0672*** | 0.0672*** | 0.0676*** | 0.0672*** |
| | (0.0000) | (0.0000) | (0.0000) | (0.0000) |
| Observations | 507,864 | 502,026 | 468,174 | 506,037 |

*Note:* ***, **, * denote significance at the 1%, 5% and 10% level. All specifications are SDEM and are estimated by Maximum Likelihood. Standard errors in parentheses. Cell and year fixed effects included but not reported. Spatial radius is r=80 km. Yearly disaster intensities reflect time-weighted rolling averages over 12 subsequent monthly observations.

Baseline results suggest that storms, extreme precipitation events and cold waves have negative and statistically significant local average treatment effects. Within a geodesic radius of 80 km, significantly positive spatial spillover effects of these event types are observed. This suggests that exogenous shocks lead to a deflection of economic activity towards less affected neighboring regions. Persistence or reversal of treatment effects over time is heterogeneous across disaster types.

Extreme winds that increase the yearly wind speed measure by one knot are associated with a decline in lights growth of 0.2 percentage points on average. Applying the light-to-GDP growth elasticity documented in Section 3.2.1, a one standard deviation increase in the yearly wind speed measure leads to a reduction of income growth below its local growth path by 0.33

percentage points on average.[46] Interestingly, a large proportion of the growth impact only kicks in with a time-lag. After one period, an increase in the yearly wind speed measure by one knot reduces lights growth by 0.9 percentage points. This implies that a one standard deviation increase in wind speeds reduces economic growth in affected cells by 1.49 percentage points. On average, spatial spillover effects of storms are insignificant in the baseline period. After one period, a positive spillover effect is found which suggests an increase in local lights growth by 0.08 percentage points if in *one* of the neighboring cells the yearly mean wind speed is driven up by one knot – implying an increase in income growth by 0.13 percentage points for a one standard deviation increase in wind.[47]

Monthly extreme precipitation may exceed local percolation capacities and potentially cause flooding. A precipitation event that increases the yearly precipitation measure by one standard deviation reduces local income growth by 0.17 percentage points. One period later, recovery leads to a higher growth in local income by 0.12 percentage point increase in local income growth for a one standard deviation increase in the yearly rainfall measure. A one standard deviation increase in extreme precipitation events in one neighboring cell within 80 km leads on average to spillovers increasing local income growth by 0.03 percentage points. Finally, there is no significant evidence that spatial spillovers persist longer than one period after an extreme precipitation event.

Given that droughts primarily affect agricultural outcomes but agricultural production is not associated with light emission in most parts of the world, finding evidence for a negative local impact of droughts on the light-based outcome proxy is not to be expected. In fact, while night-lights typically reflect industrial and services sectors (Doll et al., 2006; Ghosh et al., 2010), as mentioned earlier, agriculture (and forestry) emit less or no visible light as they grow (Keola et al., 2015). From a macroeconomic perspective, agricultural production also reflects intermediary inputs to light-emitting industry production and to general consumption.[48] However, while agriculture may be reflected through consumption and intermediary industry output at the country level, the observational units defined for this analysis are less likely to capture such negative secondary effects due to the high geographic resolution. Instead,

[46] The GDP growth effect of a one standard deviation increase in the annual wind measure (4.49) corresponds to a wind speed estimate of -0.0020, multiplied by 100 and translated using the lights-to-GDP growth rate elasticity of 0.37: $[-0.0020 \cdot 100] \cdot 0.37 \cdot 4.49 = -0.33$

[47] If a storm hits multiple cells simultaneously, aggregate spillovers from the neighborhood accumulate.

[48] Wu et al. (2013) use aggregate night-lights at country level to estimate the extent to which night-time lights implicitly reflect agricultural production. In a sample of 169 countries observed from 1995 to 2009, their results suggest that the agricultural sector accounts for 25% of total light radiance.

it is more likely that droughts in rural areas reduce consumption and intermediary industry output in nearby urban areas, located in neighboring cells. Consequently, negative spatial spillovers are expected to be driven by droughts in mostly rural rather than urban cells.

This hypothesis is supported by the data. Estimates suggest that income growth is reduced on average by 0.04 percentage points for each neighboring 0.5° grid cell within a range of 80 km that experiences a one standard deviation increase in drought.To test the hypothesis that this effect is driven by spillovers from rural to urban cells, an unsupervised machine learning algorithm is combined with the pixel-level land use data from the Moderate Resolution Imaging Spectroradiometer (MODIS) 500-m map of global urban extent (Schneider et al., 2009) provided by the Food and Agriculture Organization of the United Nations (FAO), to classify the data into 0.5°×0.5° cells that are predominantly urban (i.e., residential) or non-urban (see Appendix C.1.4 for more details).[49] Table C.1 in the Appendix shows a decomposition of the direct and spillover effects of droughts along this classification. Results suggest that negative spillovers from non-urban to urban cells drive the aggregate spillover, with magnitudes about twice as large as within non-urban neighborhoods. Spillovers within pairs of non-urban cells persist, however, potentially due to residual urban structures in cells classified as non-urban. As expected, no evidence is found for spillovers from urban to non-urban cells and only weak spillovers are found within urban neighborhoods. The positive direct effect is nearly three times as large in urban compared to non-urban cells.

A one standard deviation increase in cold waves reduces income growth by 0.25 percentage points in the base period and by 0.10 percentage points after one period. Corresponding spillovers suggest that economic activity is shifted to neighboring locations in the current year, increasing their income growth on average by 0.07 percentage points. The spillover effect of cold waves does not persist over time; instead a sign reversal in a similar order of magnitude is observed.

Control variables consistently show expected signs and significance levels for all weather shocks. A 1% population increase is associated with an increase in lights growth of 2.5 percentage points on average, which implies an increase in GDP growth of 0.9 percentage points.

[49] A simple classification approach is also provided, which does not depend on machine learning for classification. This classification gives a 10% share of urban cells, instead of 5% obtained by the clustering approach. It holds similar results. Note that in both cases classification provides an indication of a cell's key type, but does not imply that a cell is *exclusively* urban or non-urban.

If population in a neighboring cell increases by 1%, local lights grow by 1.1 percentage points, with an average increase in GDP growth of 0.4 percentage points.

Figure 3.4 : Percentile Light Growth Effects of Natural Disasters

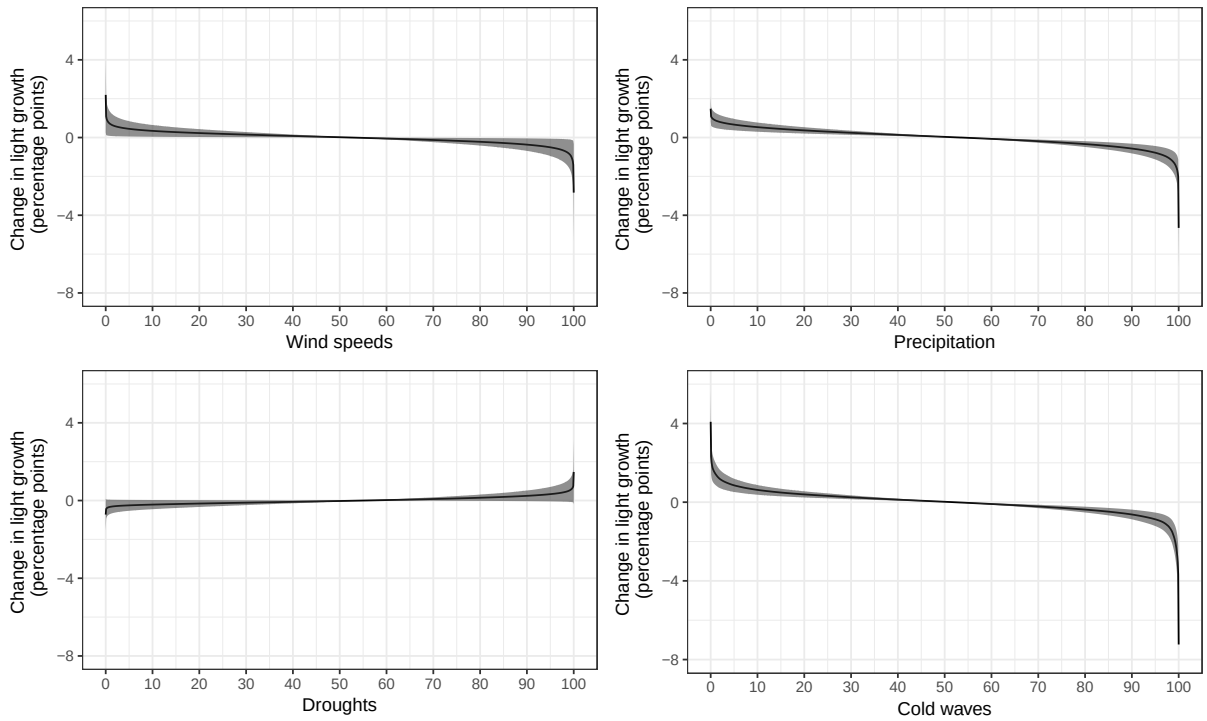


*Note:* Contemporaneous change in night-light growth as estimated in Table 3.3, as a function of percentile realizations of the respective demeaned intensity measures (i.e., surprise realizations). 95% confidence interval is plotted in shaded gray.

Next, the distribution of weather shocks is explored to evaluate growth effects at different realizations of respective indicators. Figure 3.4 shows contemporaneous growth effects along the difference in disaster intensity from its long run cell mean.[50] In line with Felbermayr and Gröschl (2014), a non-linear shape of growth effects is found for all disaster types. This strongly resembles modeling results on the non-linear relation between physical intensity and asset losses or output losses (Hallegatte et al., 2007; Hallegatte, 2008). For all types, the 95% smallest realizations of intensity measures imply a reduction in light growth of less than 1 percentage point.[51] The worst 5% of realizations show substantially larger effects, with extreme shocks being located in the top 1% of realizations. The top 1% of storms decrease light growth by

[50] Disaster intensities are demeaned to calculate quantile impacts. The empirical fixed effects strategy identifies on surprise realizations of treatment variables. Non-demeaned physical intensities exhibit clustering of non-surprises especially within the lower quantile. Since these do not contribute to identification, demeaning is used to avoid overdrawing growth effects.

[51] Lower percentiles ultimately constitute positive surprise events.

more than 1 percentage point, while the top 1% realizations of extreme precipitation are associated with a reduction in light growth of more than 2 percentage points. The top 1% of cold waves are associated with more than 3 percentage points lower light growth. Drought effects should be treated with caution due to the features discussed above. For completeness, positive drought effects are equally more sizable for the largest 1%, but only weakly significant.

## 3.5 Assessing spillovers across longer distances

The baseline specification models spillover effects from natural disasters as local phenomena that matter within a spatial radius of 80 km around a treated location. Knowing whether this local notion of disaster spillovers is appropriate matters for assessing the adequacy of the econometric strategy. Moreover, understanding if disaster spillovers are a local phenomenon most relevant across short distances or a global one showing repercussions also over long distances has important implications for policies targeted at strengthening a location's adaptation capacities. This section examines the relevance of spillovers across longer distances by conducting two exercises.

First, Panel A of Table 3.4 addresses the choice of the cutoff distance for the weighting matrix by doubling the spatial radius around treated locations to 160 km.[52] If spillovers from more remote locations matter less than those originating from closer ones, the spillover estimate should decline in magnitude relative to the baseline specification, suggesting a lower average spillover effect from treating one cell within the local neighborhood.

Results suggest that doubling the neighborhood radius has little effect on local average treatment effects. However, average local spillovers broadly show a substantial decline in magnitude.[53] Hence, adding cells beyond 80 km to the local neighborhood drives down the average spillover effect per cell observed within this neighborhood. This indicates that spatial spillovers of weather shocks are local phenomena that decline with distance, complying with Tobler's first law of geography (Tobler, 1970).

Second, Panel B of Table 3.4 turns to a *global* spillover model, allowing spillovers to occur also beyond a cell's local neighborhood. In principle, if a disaster strikes in a cell, this may have an impact on its direct surroundings, which in turn spills over to the surroundings'

[52] A radius of 160 km effectively captures the second order neighbors of a cell at the equator.
[53] Table C.9 in the Appendix shows full results.

surroundings. The mechanics of the global spillover model allow spillovers to propagate from one neighborhood to the next, as long as these neighborhoods are contiguously connected.

Thus far, *local* spillover effects have been estimated through SDEM or SLX models, which do not allow for such a spillover propagation beyond the local neighborhood. One advantage of these models is that estimated coefficients on spatially lagged explanatory variables can be interpreted directly and in terms of local spillover effects attributed exclusively to exogenous variation within a defined neighborhood. An alternative approach, which has often been used in the applied empirical literature, is the spatial Durbin model (SDM) with a spatially autocorrelated dependent variable rather than a spatial error structure. As discussed by Halleck Vega and Elhorst (2015) and Anselin (2013), this model class implies a *global* notion of spillover effects. With global spillovers, estimates on spatially lagged dependent variables do not reflect only exogenous spillovers from the defined neighborhood, but they structurally represent both exogenous and endogenous spillovers, with the latter resulting as general equilibrium (GE) effects from the propagation of external effects across all contiguous locations in the universe. The degree to which spillovers are propagated is captured by a spatial multiplier.[54]

A potential advantage of the latter approach is that it explicitly enforces "global" compliance with the stable unit treatment value assumption (SUTVA) by allowing observational units not only to interfere within an exogenously defined neighborhood, but across all contiguous locations.[55] The disadvantage, however, is that exogenous local and endogenous global GE spillover components cannot be disentangled. In this context, allowing for a propagation of exogenous weather shocks across all contiguous cells seems inadequate given the goal of explaining local phenomena at a very disaggregated level. Generally, SDM coefficients on the direct and the spatially lagged explanatory variables cannot be interpreted in a straightforward way.[56] Following this, an assessment is provided of how findings are affected in a global spillover model estimated by maximum likelihood techniques:

$$\Delta \boldsymbol{\ell}_t = \boldsymbol{\ell}_{t-1}\gamma + \lambda \boldsymbol{W}^r \Delta \boldsymbol{\ell}_t + \boldsymbol{D}_t\boldsymbol{\beta}^{\mathbf{0}} + \boldsymbol{X}_t\boldsymbol{\delta}^{\mathbf{0}} + \boldsymbol{W}^r\boldsymbol{D}_t\boldsymbol{\beta}^{\mathbf{1}} + \boldsymbol{W}^r\boldsymbol{X}_t\boldsymbol{\delta}^{\mathbf{1}} + \boldsymbol{\nu} + \boldsymbol{\pi} + \varepsilon_t \quad (3.3)$$

[54] Contiguity implies that some overlap between the spatial neighborhoods of two given cells in the $\boldsymbol{W}^r$ matrix must exist.

[55] Explicit SUTVA enforcement in local spillover models is confined to observational units defined as local neighbors, implying that SUTVA compliance beyond the local neighborhoods holds by assumption. The similarity of point estimates presented for SDM and SDEM specifications provides support that SUTVA violation is not a concern in the baseline model.

[56] As discussed by Halleck Vega and Elhorst (2015), this methodological peculiarity is mostly ignored in applied research.

Table 3.4, Panel B shows estimates consistent in sign and overall magnitude with the baseline specification but conveying a different meaning.[57] To properly disentangle direct and spillover effects, coefficients need to be translated applying the spatial multiplier $(\boldsymbol{I} - \lambda \boldsymbol{W})^{-1} = \boldsymbol{I} + \lambda \boldsymbol{W} + \lambda^2 \boldsymbol{W}^2 + \lambda^3 \boldsymbol{W}^3 + \ldots$, such that the direct effect is reflected in the diagonal and the spillover in the off-diagonal elements of $(\boldsymbol{I} - \lambda \boldsymbol{W})^{-1}[\beta^0 + \boldsymbol{W}\beta^1]$, where $\lambda$ is the spatial autoregressive coefficient from equation (3.3), governing the degree to which spillovers propagate across space. The mean direct effect, obtained by averaging over all diagonal elements, is provided in square brackets. This mean effect corresponds to the local average treatment effect obtained by the local spillover specification in the SDEM baseline.

For direct effects, translated coefficients are similar to point estimates. In contrast, the interpretation of translated spillover coefficients in square brackets is very different from the local spillover baseline. The row-wise mean across all connected (non-sparse) off-diagonal elements captures how a cell is affected on average by treatment of any other cell which is part of its contiguously connected spatial neighborhood, also beyond the imposed radius of 80 km.

If neighborhoods are spatially disconnected by gaps larger than 80 km, the desired propagation-effect is interrupted. This is often the case across oceans, seas, large mountain ranges, deserts, and other uninhabited areas. Comparison with Figures C.7-C.10 shows that, even though the term “global spillovers” might suggest otherwise, the cells in the sample are quite far from being contiguously connected around the world such that the global spillovers reported do not reflect a world-wide propagation but rather a “regional” one. Above all, the extent of such contiguous regions is heterogeneous across space and hardly tractable.

Nevertheless, for some parts of the world, contiguous areas are of considerable size. The small estimate for $\lambda$ indicates that spillovers phase out quickly across space when applying the spatial multiplier. As a consequence, the mean magnitude by which a cell is affected by *any* other cell in its contiguous neighboring region is, on average, vanishing across space compared to the local spillover effects from only the next-door neighbors, estimated in the baseline. These findings are in line with the conclusion drawn from Panel A and essentially support the choice of a local spillover specification to be adequate, both due to the lack of spatial contiguity in the data and given the strong phasing-out of effects across longer distances.

[57] Table C.10 in the Appendix shows full global spillover results.

Table 3.4 : Spillovers Across Longer Distances

**Dependent Variable:** $\Delta \ln(\text{lights}_t)$

| | **wind** | **precip.** | **drought** | **cold** |
|---|---|---|---|---|
| **PANEL A: Radius r=160km** | | | | |
| $\text{disaster}_t$ | −0.0016** | −0.0249*** | 0.0125*** | −0.0849*** |
| | (0.0007) | (0.0057) | (0.0041) | (0.0136) |
| $\text{disaster}_{t-1}$ | −0.0052*** | 0.0158*** | −0.0075* | −0.0129 |
| | (0.0007) | (0.0057) | (0.0040) | (0.0133) |
| $W \cdot \text{disaster}_t$ | 0.0000 | 0.0008** | −0.0015*** | 0.0061*** |
| | (0.0000) | (0.0004) | (0.0003) | (0.0009) |
| $W \cdot \text{disaster}_{t-1}$ | 0.0001* | 0.0000 | 0.0005* | −0.0060*** |
| | (0.0000) | (0.0004) | (0.0003) | (0.0008) |
| **PANEL B: Global Spillovers** | | | | |
| $\text{disaster}_t$ | −0.0046*** | −0.0279*** | −0.0016 | −0.0974*** |
| | [−0.0044] | [−0.0259] | [−0.0029] | [−0.0794] |
| | (0.0007) | (0.0060) | (0.0041) | (0.0122) |
| $\text{disaster}_{t-1}$ | −0.0095*** | 0.0198*** | 0.0017 | −0.0858*** |
| | [−0.0093] | [0.0189] | [0.0017] | [−0.0908] |
| | (0.0007) | (0.0059) | (0.0041) | (0.0119) |
| $W \cdot \text{disaster}_t$ | 0.0005*** | 0.0037*** | −0.0010* | 0.0217*** |
| | [0.0000] | [0.0001] | [−0.0001] | [0.0010] |
| | (0.0001) | (0.0009) | (0.0006) | (0.0017) |
| $W \cdot \text{disaster}_{t-1}$ | 0.0008*** | −0.0021** | −0.0001 | 0.0015 |
| | [0.0000] | [−0.0001] | [0.0000] | [−0.0003] |
| | (0.0001) | (0.0009) | (0.0006) | (0.0017) |
| $\lambda$ | 0.0671*** | 0.0671*** | 0.0675*** | 0.0671*** |
| | (0.0000) | (0.0000) | (0.0000) | (0.0000) |

*Note:* ***, **, * denote significance at the 1%, 5% and 10% level. All Panel A is SDEM, Panel B is SDM. All regressions are estimated by Maximum Likelihood. Standard errors in parentheses. Cell and year fixed effects included but not reported in all specifications. Spatial radius is r=160 km in Panel A and r=80km in Panel B. Yearly disaster intensities reflect time-weighted rolling averages over 12 subsequent monthly observations. Global Spillovers show average effects translated with spatial multiplier in square brackets. Full results are shown in Tables C.9 and C.10 in the Appendix.

Finally, the result that relocation of economic activity after a natural disaster is a rather local phenomenon disappearing over longer distances has policy implications. Policymakers might intend to increase a location's adaptation capacity by strengthening its economic linkages (e.g., via infrastructure investments) to allow for easier short term shifts of economic activity across space.[58] In this case, strengthening local links across shorter distances seems to be more relevant than policies targeted at longer distances.

[58] Identification of the the role of specific transmission channels for local spillovers are left for future research.

## 3.6 Robustness Analysis

Next, issues related to measurement and alternative specifications that may affect the baseline results are explored. A summary of robustness results is shown in Table 3.5.

### 3.6.1 Sensitivity to Top- and Bottom-Coding

DMSP satellite sensors are subject to saturation, resulting in top-coding of pixels for which light emission is at or above the sensor's detection saturation level.[59] Pixels are top-coded at DN63 and are mainly found in urban centers. The share of top-coded pixels ranges from zero in some low and middle income economies — but also in sparsely populated high income countries (e.g., Canada) — to around 2.5% for small but densely populated high income areas (e.g., the Netherlands, Belgium). Notable exceptions are Singapore and Hong Kong, both small and densely populated, and two small island states (Malta and Trinidad and Tobago). There, the share of top-coded cells runs close to or within the double digits as a substantial part is urban built-up area.[60]

Top-coding may be a concern for identification if the change in night-time lights due to a shock happens beyond the saturation level of the satellite sensor. To account for this, pixels which are top-coded at least once during the observed time period are masked. None of the 0.5° cells are fully top-coded, while 8% of cells in the sample contain some fraction of top-coded pixels. The mean degree of top-coding is 3.7% (sd 8.4%) and for 99% of these cells top-coding is below 50% of land area. As top-coded pixels are unresponsive to shocks as long as light levels remain beyond the satellite sensor saturation threshold, excluding these should – if anything – lead to larger point estimates. Table 3.5, Panel A shows that results are robust to excluding top-coding from the data, with all disaster models showing point estimates almost identical to the baseline results.[61]

Bluhm and Krause (2017) suggest that satellite sensor saturation starts already at pixel values as low as DN55. While changes in the DN55-DN62 range can still be measured, larger measurement error might be present in this range with a structural downward bias on recorded

[59] Bluhm and Krause (2017) propose a method to impute "true" light values for top-coded pixels by assuming a Pareto distribution on top lights. Although this approach may be of great value to the general literature, imputed measures cannot be used for studying shocks on its values.

[60] Gas flaring introduces areas with top-coded pixels into the raw data. These are masked by default, as described in the Appendix Section 3.2.1.

[61] Table C.11 in the Appendix shows full results.

versus true brightness. If this is the case, growth in night-light intensity is underestimated in the upper range of pixel values, which in practice affects mostly urban centers.[62] Applying the top-coding approach to pixel values above DN55, point estimates are similar to the baseline.[63]

Data quality concerns also exist at the lower end of recorded light intensity. Henderson et al. (2012) discuss the underrepresentation of pixels below DN3. To tackle this, all pixels below DN3 are set to zero. Estimates suggest that the baseline results are robust in Panel B, Table 3.5 – except the contemporaneous treatment effect of storms turns insignificant.[64] Elvidge et al. (2009b) discuss in their methodology on the identification of gas flaring that pixel values below DN8 should potentially be ignored to "eliminate background noise present in the products". While the number of pixels below DN3 affects 0.1% of pixels in the data, the share of pixels between DN1 and DN8 is 7.5%. Masking all pixels in this range affects 23% of grid cells and eliminates all low-lit areas.[65] As this likely introduces sample selection, the following results should be interpreted with caution. For storms, contemporaneous treatment turns insignificant, lagged and spillover effects stay robust. Results on excessive precipitation are similar to the baseline when excluding low lit areas. For droughts, the contemporaneous positive treatment effect turns insignificant, while the lag and spillover structure remain unchanged. As droughts mainly affect rural areas – typically low lit – the absence of a local treatment effect indeed suggests that it is not possible to measure these local effects in light growth. For cold waves, contemporaneous treatment turns insignificant, while lagged treatment and spillover effects are robust. Overall, result remain broadly in line when considering top- and bottom-coding of night-time light emission data.

### 3.6.2 Time-Varying Country Characteristics

The baseline specification accounts for all time-constant unobservable cell characteristics and overall global trends (technological change, business cycles). This leaves country-specific fluctuations, such as country-wide policy decisions or institutional change, unaddressed. Thus, country-year fixed effects are applied to absorb unobserved country-time specific variation. Three mechanisms potentially affecting estimates are at play: (1) The smaller the country and hence its number of cells, the larger the share of variation in a cell's growth

[62] About 20 cells are lost when applying this wider masking range.

[63] Results are shown in Table C.12 in the Appendix.

[64] Table C.14 in the Appendix presents full results.

[65] See Table C.3 in the Appendix for summary statistics on the DN distribution of satellite-years. Full results for setting all pixel values below DN8 to zero are presented in Table C.13 in the Appendix.

rate that is absorbed by the country-year fixed effect; (2) within cell variation net of country-specifics only allows for identification of local treatment to the extent that this treatment does not affect a country as a whole (e.g., events which are particularly devastating or geographically dispersed may not be reflected in treatment estimates); and (3) 3,927 degrees of freedom are lost, potentially making identification more difficult. (1) and (2) point to the fact that this strategy favors larger countries over smaller ones and may work better for events that are explicitly local by nature.[66] It is known from the empirical literature that the most extreme events can have negative consequences for economic growth at the country level (Cavallo et al., 2013; Felbermayr and Gröschl, 2014). Therefore, point estimates are expected to attenuate.

Table 3.5, Panel C shows that results are qualitatively robust to the inclusion of country-year fixed effects and show an overall decline in magnitudes.[67] The local effect of storms turns insignificant. Note that hurricanes, typhoons and cyclones form the most extreme events in this category, which often hit small island states for which the cell effect is largely soaked up in the country-year fixed effect. Extreme precipitation results prove robust, with the lagged local treatment effect and current spatial spillovers somewhat reduced in size. The lagged spatial spillover turns weakly significant suggesting a higher precision of estimation. Point estimates on local treatment and spillover effects of droughts and cold waves are smaller – droughts turn insignificant.

### 3.6.3 Simple Annual Mean

In this part, the aggregation method is changed by taking the simple annual mean over all months within a year instead of the rolling average. Note that this may introduce systematic measurement error and bias by weighting events which occurred later in the year with the same weight as those that happened earlier. Table 3.5, Panel D shows very consistent results for all types of weather shocks.[68] While local treatment effects decrease slightly in magnitudes for storms, results are consistent for precipitation and increase by factor 2.9 for droughts and by factor 1.2 for cold waves. Spillover effects are consistent for storms, decrease slightly for precipitation and droughts and increase by one half for cold waves. Generally, results remain unchanged in sign and significance levels.

[66] Note that droughts, for example, typically stretch over large areas implying that they may well be ongoing in an entire country, albeit to a varying degree throughout its territory.

[67] For full results, see Table C.15 in the Appendix

[68] Table C.16 in the Appendix shows full results.

Table 3.5 : Sensitivity Results

**Dependent Variable:** $\Delta \ln(\text{lights}_t)$

| | wind | precip. | drought | cold |
|---|---|---|---|---|
| **PANEL A: Top-Coding: Excluding Top-Coded Pixels** | | | | |
| $\text{disaster}_t$ | −0.0019** | −0.0329*** | 0.0091* | −0.0752*** |
| | (0.0009) | (0.0070) | (0.0048) | (0.0152) |
| $\text{disaster}_{t-1}$ | −0.0090*** | 0.0222*** | 0.0012 | −0.0318** |
| | (0.0009) | (0.0069) | (0.0048) | (0.0149) |
| $W \cdot \text{disaster}_t$ | 0.0000 | 0.0052*** | −0.0046*** | 0.0219*** |
| | (0.0002) | (0.0013) | (0.0009) | (0.0027) |
| $W \cdot \text{disaster}_{t-1}$ | 0.0008*** | −0.0023* | 0.0011 | −0.0200*** |
| | (0.0002) | (0.0013) | (0.0009) | (0.0027) |
| **PANEL B: Bottom-coding: Setting Pixels <DN3 to Zero** | | | | |
| $\text{disaster}_t$ | −0.0007 | −0.0265*** | 0.0082* | −0.0852*** |
| | (0.0009) | (0.0070) | (0.0048) | (0.0154) |
| $\text{disaster}_{t-1}$ | −0.0106*** | 0.0290*** | 0.0015 | −0.0291* |
| | (0.0009) | −0.0069 | (0.0048) | (0.0150) |
| $W \cdot \text{disaster}_t$ | −0.0001 | 0.0042*** | −0.0041*** | 0.0242*** |
| | (0.0002) | (0.0013) | (0.0009) | (0.0027) |
| $W \cdot \text{disaster}_{t-1}$ | 0.0010*** | −0.0022* | 0.0007 | −0.0217*** |
| | (0.0002) | (0.0013) | (0.0009) | (0.0027) |
| **PANEL C: Time Varying Country Characteristics** | | | | |
| $\text{disaster}_t$ | 0.0004 | −0.0312*** | 0.0062 | −0.0360** |
| | (0.0010) | (0.0070) | (0.0049) | (0.0179) |
| $\text{disaster}_{t-1}$ | −0.0049*** | 0.0117* | 0.0009 | −0.0390** |
| | (0.0010) | (0.0069) | (0.0049) | (0.0175) |
| $W \cdot \text{disaster}_t$ | 0.0003** | 0.0043*** | −0.0041*** | 0.0165*** |
| | (0.0002) | (0.0013) | (0.0009) | (0.0029) |
| $W \cdot \text{disaster}_{t-1}$ | 0.0009*** | −0.0022* | 0.0017* | −0.0144*** |
| | (0.0002) | (0.0013) | (0.0009) | (0.0028) |
| **PANEL D: Simple Annual Mean of Disasters** | | | | |
| $\text{disaster}_t$ | −0.0032*** | −0.0289*** | 0.0243*** | −0.0613*** |
| | (0.0007) | (0.0055) | (0.0039) | (0.0137) |
| $\text{disaster}_{t-1}$ | −0.0064*** | 0.0011 | −0.0060 | −0.0540*** |
| | (0.0007) | (0.0055) | (0.0038) | (0.0133) |
| $W \cdot \text{disaster}_t$ | −0.0002 | 0.0018* | −0.0037*** | 0.0337*** |
| | (0.0001) | (0.0010) | (0.0007) | (0.0025) |
| $W \cdot \text{disaster}_{t-1}$ | 0.0008*** | 0.0030*** | 0.0000 | −0.0504*** |
| | (0.0001) | (0.0010) | (0.0007) | (0.0019) |

*Note:* ***, **, * denote significance at the 1%, 5% and 10% level. All specifications are SDEM and are estimated by Maximum Likelihood. Standard errors in parentheses. Cell and year fixed effects included but not reported in all specifications. Cell and country-year fixed effects included for the time-varying country characteristics analysis but not reported. Spatial radius is r=80 km. Yearly disaster intensities reflect time-weighted rolling averages over 12 subsequent monthly observations. Simple annual mean uses non-weighted mean over all monthly observations within a year. Full results are shown in Tables C.11 to C.16 in the Appendix.

## 3.7 Extension: Heterogeneity

Up to this point, focus has been on the global average of local weather shock impacts. In a next step, heterogeneity in income groups and across world regions is explored.

### 3.7.1 Income Groups

Cells are classified depending on whether they belong to high income or to low (and middle) income countries.[69] Equation (3.4) is an extension of the baseline model (3.2).

$$\begin{aligned}\Delta\boldsymbol{\ell}_t = \boldsymbol{\ell}_{t-1}\gamma + \boldsymbol{D}_t\boldsymbol{\beta^0} + \boldsymbol{X}_t\boldsymbol{\delta^0} + \boldsymbol{W}^r\boldsymbol{D}_t\boldsymbol{\beta^1} + \boldsymbol{W}^r\boldsymbol{X}_t\boldsymbol{\delta^1} \\ + [\boldsymbol{D}_t \times \textbf{low}]\boldsymbol{\beta^2} + [\boldsymbol{W}^r\boldsymbol{D}_t \times \textbf{low}]\boldsymbol{\beta^3} + \boldsymbol{\nu} + \boldsymbol{\pi} + \boldsymbol{u}_t \\ \boldsymbol{u}_t = \rho\boldsymbol{W}^r\boldsymbol{u}_t + \boldsymbol{\varepsilon}_t.\end{aligned} \tag{3.4}$$

It includes interaction terms of local disaster treatment and its spatial spillovers with a binary indicator **low**. This indicator flags cells in low- and middle income countries, compared to high income countries. Coefficients $\beta^2$ and $\beta^3$ identify by how much the treatment effects of cells in low and middle income countries differs from cells in high income countries, i.e., $\beta^0$ and $\beta^1$. Table 3.6 shows the combined effects obtained from these interaction regressions.

Estimates suggest that negative wind effects are driven by low income cells in the year of occurrence and thereafter. The lagged negative effect in low income cells is nearly three times as large as in high income cells. Positive lagged spillover effects occur in both types of cells, but are 1.5 times stronger for those that are poorer. Negative treatment and positive spillover effects for precipitation are entirely driven by low income cells. The positive local treatment effect on droughts shows only in cells of low income countries, as does the negative spillover effect. In line with the baseline, cold waves show a strong negative effect on light growth in low income cells, associated with a positive spillover effect. In high income cells, cold waves lead to more light growth in the period of occurrence and less thereafter, with negative spillovers in the preceding year. Overall, there is evidence that the baseline local average treatment and spillover effects are generally driven by cells in low and middle income countries. This relates well to findings in the literature that developing and poor countries are particularly vulnerable to the impact of extreme natural events (Raddatz, 2007; Noy and Nualsri, 2011).

[69] The binary categorization of income groups follows World Bank Lending Groups from year 2000. Cells in high income countries account for 31% of the sample, cells in low and middle income countries account for 69%.

Table 3.6 : Income Group Heterogeneity, Combined Effects

**Dependent Variable:** $\Delta \ln(\text{lights}_t)$

| | **wind** | **precip.** | **drought** | **cold** |
|---|---|---|---|---|
| **high income** | | | | |
| $\text{disaster}_t$ | −0.0015 | 0.0171 | −0.0120 | 0.2442*** |
| | (0.0016) | (0.0118) | (0.0093) | (0.0389) |
| $\text{disaster}_{t-1}$ | −0.0042*** | 0.0249** | 0.0081 | −0.0680* |
| | (0.0015) | (0.0117) | (0.0092) | (0.0384) |
| $W \cdot \text{disaster}_t$ | −0.0001 | 0.0015 | −0.0020 | 0.0077 |
| | (0.0003) | (0.0021) | (0.0016) | (0.0059) |
| $W \cdot \text{disaster}_{t-1}$ | 0.0006** | −0.0040* | 0.0029* | −0.0224*** |
| | (0.0003) | (0.0021) | (0.0016) | (0.0059) |
| **low income** | | | | |
| $\text{disaster}_t$ | −0.0021* | −0.0534*** | 0.0147*** | −0.1133*** |
| | (0.0011) | (0.0087) | (0.0056) | (0.0169) |
| $\text{disaster}_{t-1}$ | −0.0119*** | 0.0192** | −0.0010 | −0.0193 |
| | (0.0011) | (0.0085) | (0.0055) | (0.0165) |
| $W \cdot \text{disaster}_t$ | 0.0001 | 0.0064*** | −0.0052*** | 0.0191*** |
| | (0.0002) | (0.0016) | (0.0011) | (0.0031) |
| $W \cdot \text{disaster}_{t-1}$ | 0.0009*** | −0.0007 | 0.0000 | −0.0170*** |
| | (0.0002) | (0.0016) | (0.0010) | (0.0030) |
| Observations | 506,142 | 500,787 | 467,691 | 504,525 |

*Note:* ***, **, * denote significance at the 1%, 5% and 10% level. All specifications are SDEM and are estimated by Maximum Likelihood. Cell and year fixed effects and controls as in baseline included but not reported. Spatial radius is r=80 km. Yearly disaster intensities reflect time-weighted rolling averages over 12 subsequent monthly observations. Estimates represent combined effects from adding up coufficients from the interaction terms, significance levels are obtained with a two-sided t-test. Full regressions in Table C.18.

### 3.7.2 World Regions

Next, cells are categorized into world regions (see Figure C.13). Table 3.7 summarizes results from a set of split-sample regressions. Overall, results show that specific weather shocks are driven by some world regions. In line with the baseline, wind speeds show negative effects on night-light growth in Europe, North America, Latin America and the Caribbean (LATAM), as well as in South-East Asia and the Pacific (SEAP). Except for Europe, the lagged effect of wind persists throughout the following year. Middle Eastern and Northern African (MENA) and Central Asian cells show on average a positive effect in the year of occurrence and a negative effect with a lag. Spillover effects are generally positive in subsequent years (except SEAP) and positive in current years in North America and LATAM.

Table 3.7 : Heterogeneity Across World Regions

**Dependent Variable:** $\Delta \ln(\text{lights}_t)$

| | | Europe | North America | LATAM | SEAP | Central Asia & MENA | SSA |
|---|---|---|---|---|---|---|---|
| **wind** | $\text{disaster}_t$ | −0.0034* | −0.0076*** | −0.0048** | −0.0032* | 0.0061** | 0.0011 |
| | $\text{disaster}_{t-1}$ | 0.0042** | −0.0064*** | −0.0064*** | −0.0080*** | −0.0108*** | −0.0011 |
| | $W \cdot \text{disaster}_t$ | −0.0002 | 0.0007* | 0.0012** | −0.0001 | 0.0008 | −0.0003 |
| | $W \cdot \text{disaster}_{t-1}$ | 0.0005* | 0.0011*** | 0.0009* | 0.0001 | 0.0020*** | 0.0016* |
| **prec.** | $\text{disaster}_t$ | 0.0116 | 0.0026 | −0.0659*** | −0.0277* | −0.0348** | −0.0365 |
| | $\text{disaster}_{t-1}$ | 0.0046 | 0.0049 | 0.0483*** | 0.0021 | −0.0305* | 0.0200 |
| | $W \cdot \text{disaster}_t$ | 0.0033 | 0.0013 | −0.0022 | 0.0014 | 0.0062** | 0.0134* |
| | $W \cdot \text{disaster}_{t-1}$ | 0.0016 | −0.0037 | −0.0034 | 0.0078* | −0.0042 | 0.0038 |
| **drought** | $\text{disaster}_t$ | 0.0042 | −0.0245*** | 0.0373*** | 0.0021 | −0.0176 | 0.0102 |
| | $\text{disaster}_{t-1}$ | 0.0011 | 0.0049 | −0.0493*** | 0.0349*** | 0.0221** | 0.0454*** |
| | $W \cdot \text{disaster}_t$ | −0.0077*** | 0.0021 | −0.0008 | −0.0066** | −0.0024 | −0.0010 |
| | $W \cdot \text{disaster}_{t-1}$ | 0.0006 | 0.0045** | 0.0015 | −0.0047* | 0.0057*** | −0.0076 |
| **cold** | $\text{disaster}_t$ | 0.0906** | 0.0256*** | −0.1388*** | 0.1020*** | −0.2588*** | 0.1513** |
| | $\text{disaster}_{t-1}$ | −0.0858* | −0.1636*** | −0.0140 | 0.1289*** | −0.4732*** | −0.0437 |
| | $W \cdot \text{disaster}_t$ | 0.0295*** | 0.0111 | 0.0117** | −0.0104 | 0.0455*** | −0.0080 |
| | $W \cdot \text{disaster}_{t-1}$ | −0.0283*** | 0.0022 | 0.0086* | −0.0021 | −0.0196** | −0.0152 |

*Note:* ***, **, * denote significance at the 1%, 5% and 10% level. All specifications are SDEM and are estimated by Maximum Likelihood. Cell and year fixed effects and controls as in baseline included but not reported. Spatial radius is r=80 km. Yearly disaster intensities reflect time-weighted rolling averages over 12 subsequent monthly observations. Separate regressions for each disaster type and region. Full regressions in Tables C.19 – C.24.

Negative effects from excessive precipitation occur in LATAM, SEAP, MENA and Central Asia. A negative but statistically insignificant local treatment effect is found for Sub-Saharan Africa (SSA). Positive spillover effects stem from MENA, Central Asia and SSA.

Droughts reduce night-light growth in North America, while the positive baseline effect is driven by Latin American and Caribbean cells. Negative spillovers of droughts show up in Europe and SEAP. Already very dry regions, such as SSA or MENA show very little average effects on droughts.

In Europe, North America, SEAP and SSA, cold waves show positive local effects on night-light growth. While Europe and North America can generally afford the technology for coping with the cold, SEAP, as well as SSA benefit from cooler weather as overall warmer regions. Negative local effects from cold waves stem solely from LATAM, MENA and Central Asia. Positive spillover effects from cold waves are driven by Europe, LATAM, MENA and Central Asia.

## 3.8 Conclusion

This paper contributes to the emerging literature on the economic consequences of exogenous extreme natural events by taking the debate to the local level, asking how their economic effects propagate across space. Satellite night-time light data from 1992 to 2013 are used to proxy for local economic activity, which are proven to be highly correlated with GDP growth, and disaggregated seismologic, climatic and meteorologic data on natural disaster events are compiled. Available economic variables, such as light emission and population, are mapped together with the various disaster types on a balanced 0.5°×0.5° grid covering the whole world. Utilizing maximum likelihood techniques, the impact of various types of exogenous shocks on the growth of night-time light emissions is estimated in a spatial fixed effects setup, controlling for cell population and spatial autocorrelation in the error term. This setup allows explicit modeling and investigation of local average treatment effects but also of spatial spillover effects in nearby locations. With this setup, the problem of varying country sizes or subnational entities as the unit of observation is eliminated.

Results are heterogeneous across the various disaster types. Baseline results show that storms, cold waves and extreme precipitation events reduce local light growth and have positive contemporaneous or lagged spatial spillover effects within a geodesic radius of 80 km. Evaluated along the lights-to-GDP growth elasticity, a one standard deviation increase in wind speeds reduces contemporaneous income growth by 0.33 percentage points. In the next period, the effect quadruples and local spillovers from treatment of *one* neighboring cell increase lights growth by 1.48 percentage points. Likewise, a one standard deviation increase in excessive precipitation or cold waves decreases current income growth by 0.17 or 0.25 percentage points, respectively. In the next period, GDP growth increases on average by 0.12 percentage points due to high precipitation, but persistently decreases by 0.11 percentage points after a cold spell. Associated contemporaneous spillovers total 0.03 and 0.07 percentage points per neighbor treated, respectively. The link between light emission and droughts is rather weak as they mostly affect agricultural outcomes. Hence, negative spatial spillover effects of droughts are largely driven by rural rather than urban cells. Due to measurement error in the data or temporary relocation of activity into the open combined with reconstruction after an earthquake, a consistent pattern for earthquake events cannot be identified.

An important policy implication can be inferred from the assessment of alternative spillover specifications. Results suggest that that disaster spillovers are a rather local phenomenon,

which implies that adaptation policies aiming at supporting the temporary relocation of economic activity after a natural disaster should have a local focus. In an extension, some heterogeneity of disaster impacts across world regions and across income groups is shown. In particular, estimates suggest that cells in low and middle income countries drive the baseline results.

Finally, results are largely robust to top- and bottom-coding, the spatial radius, the temporal aggregation method, and the inclusion of time-varying country fixed effects.

# Appendix C.1 Technical Appendix

## C.1.1 Background Information: DMSP Night-Lights Data

The United States Air Force DMSP satellites were originally used to detect moonlit clouds, with lights from human settlements being a byproduct that is recorded by the DMSP Operational Linescan System sensor on-board. The sensor records light intensity with a DN between 0 and 63.

Satellites have been observing every location on the planet daily between 8.30 pm and 10 pm local time between 1992 and 2013. Each satellite orbits the earth 14 times a day and thus ensures global coverage every 24 hours (Doll, 2008).

The satellites have a 3000 km swath, from which data of the center half is used to produce images at a nominal resolution of 0.56 km. The data is smoothed on-board to produce an average of 5×5 pixel blocks resulting in a data resolution of approximately 2.7 kilometers at the equator. After smoothing, the data is delivered at a resolution of 30 arc seconds, representing half a minute, or 1/120th of a degree. This gives data for approximately 0.86 square kilometers at the equator, with surface area decreasing in absolute terms when moving away from the equator.

The Earth Observation Group of NOAA then processes the raw data using an advanced algorithm, which cleans the raw data as follows: lights from the center half of the 3000 km swath are selected since these have better geo-location, are smaller and have more consistent radiometry (Earth Observation Group, 2016).

Sunlit data and glare are then excluded based on the solar elevation angle and similarly moonlit data is excluded on basis of the moonlit half of the lunar cycle. Subsequently only cloud-free observations are included and lighting features from the aurora are excluded from the data (Baugh et al., 2010). The exclusion of lighting from auroral features, which concerns high-latitude zones, affects approximately 10,000 people or 0.0002% of the world population (Henderson et al., 2012).

Finally, ephemeral events such as forest fires and other background noise are removed to produce stable average visible light products that reflect annual average human produced light emission into space at a 30 arc second resolution between 65°South and 75°North (Earth

Observation Group, 2016). The average number of valid nights for a given pixel in the satellite-years is 39.2 (Keola et al., 2015) and typically ranges between 20 to 100 (Elvidge et al., 2009a).

The share of unlit pixels ranges from only 1% in the Netherlands to 99.47% and 99.89% for the sparsely populated countries Mozambique and Canada (Henderson et al., 2012, p. 1000). A contrasting example to Mozambique and Canada can be found when comparing Bangladesh and the Netherlands. Both have high population density, Bangladesh having twice the density of the Netherlands with an average of 1,080 people per square km between 1992-2008. Yet, average light intensity – the average digital number per country – is only 2 for Bangladesh, whereas it is 23.5 in the Netherlands (Henderson et al., 2012, p. 1000). With GDP per capita (purchasing power parity, constant 2005 dollars) being 35 times higher in the Netherlands, this indicates that light intensity informs not only about whether there is human life present in a certain area, but also about these areas' relative income per capita (see, e.g., Elvidge et al., 2009b; Ghosh et al., 2010).

Figure C.1 : Night Light Emission of Europe and 0.5° Grid Cells

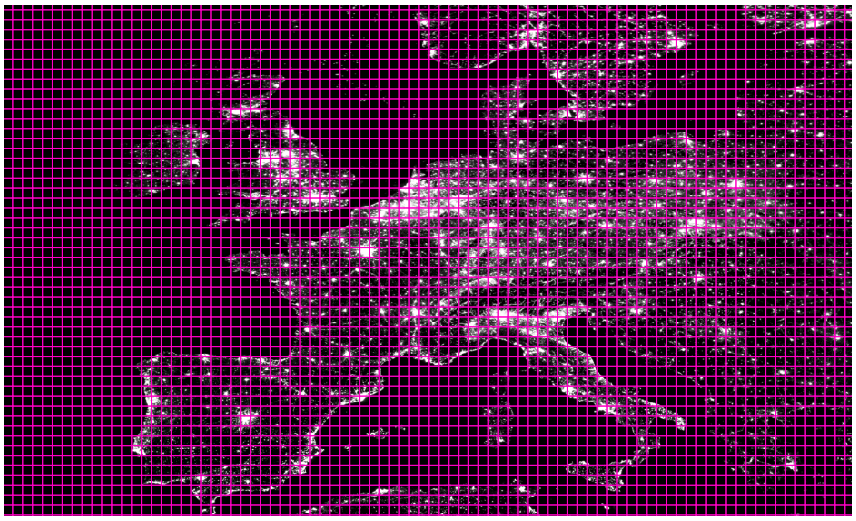

*Note:* Night light data cleaned and prepared as described. Raw data comes from satellite F182010.

Notwithstanding, a direct comparison of average light intensity can be misleading when not taking into account population size in a given area: The average light intensity of Canada is lower than that of Bangladesh while income per capita is much higher in Canada. Moreover, light usage per person may vary across countries due to cultural differences in night light use and customs of timing of economic activity across day and night. This is why Henderson et al. (2012) stress that night light intensity is better used as a proxy for income growth rather than income levels. Hence, this approach is followed.

### C.1.2 Interpolation of Wind Speeds

Using the algorithm by Hiemstra et al. (2008), the data are first classified into bins by breaking up distances $\boldsymbol{d}$ between all point locations of weather stations. For each distance bin $\bar{\boldsymbol{d}}$, the cross-sectional empirical (or experimental) semi-variance of observed maximum wind speeds across its $n$ observations at any given point in time is defined by equation (C.1). $z(x_i)$ is a random function defining a set of random variables, representing the respective wind speeds in any given location $x_i$. By assumption, the correlation between two random variables $z(x_i)$, $z(x_j)$ depends only on their bilateral spatial distance, irrespective of their location (i.e., stationarity of the second moment of $z(x_i)$). Thus, $z(x_i + \bar{\boldsymbol{d}})$ captures the wind speed realizations observed $\bar{\boldsymbol{d}}$ distance units away from location $x_i$.

$$\hat{\gamma}(\bar{\boldsymbol{d}}) = \frac{1}{2} \cdot \frac{1}{n(\bar{\boldsymbol{d}})} \sum_{i=1}^{n(\bar{\boldsymbol{d}})} (z(x_i + \bar{\boldsymbol{d}}) - z(x_i))^2 \tag{C.1}$$

Since the empirical semi-variogram cannot be computed at all possible distances $\boldsymbol{d}$, a model function is fit for each period, for which parameters are fully determined by the data. The best fit in line with the experimental semi-variogram is achieved by the Stein (1999) parametrization of the Matérn model[1] (C.2) with gamma function $\Gamma$ and a modified Bessel function $K_\nu$. The nugget (the intercept of the fit) is fixed at zero.[2] $\sigma^2$ is the so-called *sill* of the model, which under stationarity of the second moment is simply an estimate of the variance $Var\left[z(x_i)\right]$. $\nu$ and $\kappa$ are non-negative smoothing and range parameters, respectively. All parameters are determined by available global wind speed data for any given month.

$$\gamma(\boldsymbol{d}) = \begin{cases} 0 & \text{if } |\boldsymbol{d}| = 0 \\ \sigma^2 \left[ 1 - \frac{1}{2^{\nu-1}\Gamma(\nu)} \left( 2\frac{|\boldsymbol{d}|\sqrt{\nu}}{\kappa} \right)^{\nu} K_\nu \left( 2\frac{|\boldsymbol{d}|\sqrt{\nu}}{\kappa} \right) \right] & \text{if } 0 < |\boldsymbol{d}|,\ \nu > 0 \end{cases} \tag{C.2}$$

The resulting functional fit increases monotonically as a function of distance and is deployed to spatially interpolate the maximum wind speed for any location on the global grid. Note that this interpolation technique allows mapping recorded wind speeds to surrounding locations.

[1] Five different variogram models (spherical, exponential, Gaussian, Matérn, and M. Stein's parametrization of the Matérn model) are tested. Note that the Matérn model includes the exponential model as a special case and the Gaussian model as a limit case ($\nu \lim\inf$).

[2] A zero nugget constrains deviation of predicted from observed values at very short distances.

For areas that are very sparsely covered with weather stations, this inevitably results in a smoothing effect over larger distances. Note that this introduces a downward bias in the recorded wind speeds, such that obtained estimates may be considered a lower bound. Full global coverage is achieved by using all stations within a geodesic search radius of 2,000 km as predictors. Figure C.3 shows the semi-variogram obtained for June 2012. Figure C.4 visualizes the corresponding spatially interpolated maximum wind speeds and Figure C.5 assesses the fit of these predicted values, using a leave-one-out technique.

Figure C.2 : Balancing Wind Speeds

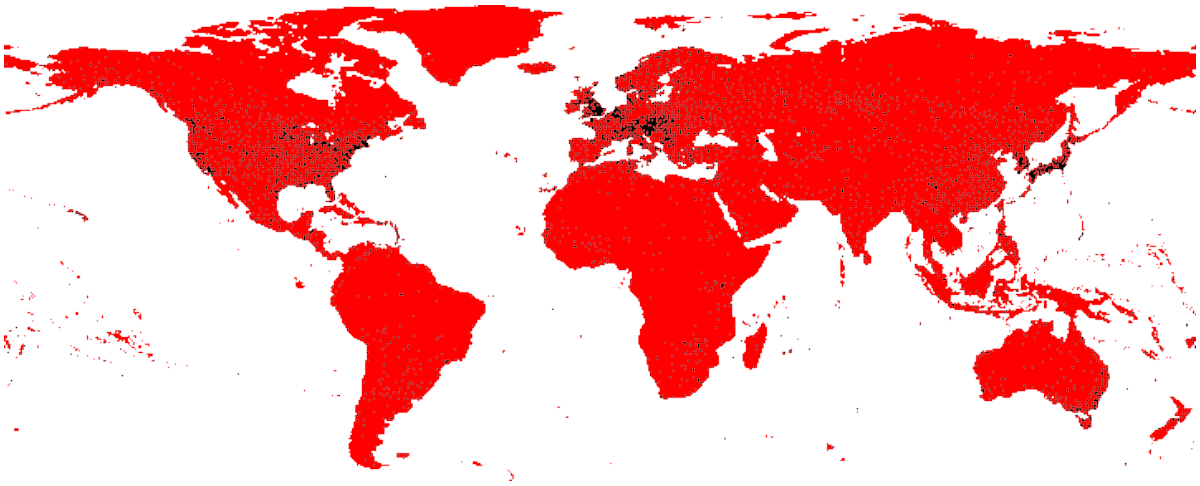

*Note:* Cells lost when balancing on non-interpolated wind speed data are shown in red.

Figure C.3 : Semi-Variogram for June 2012

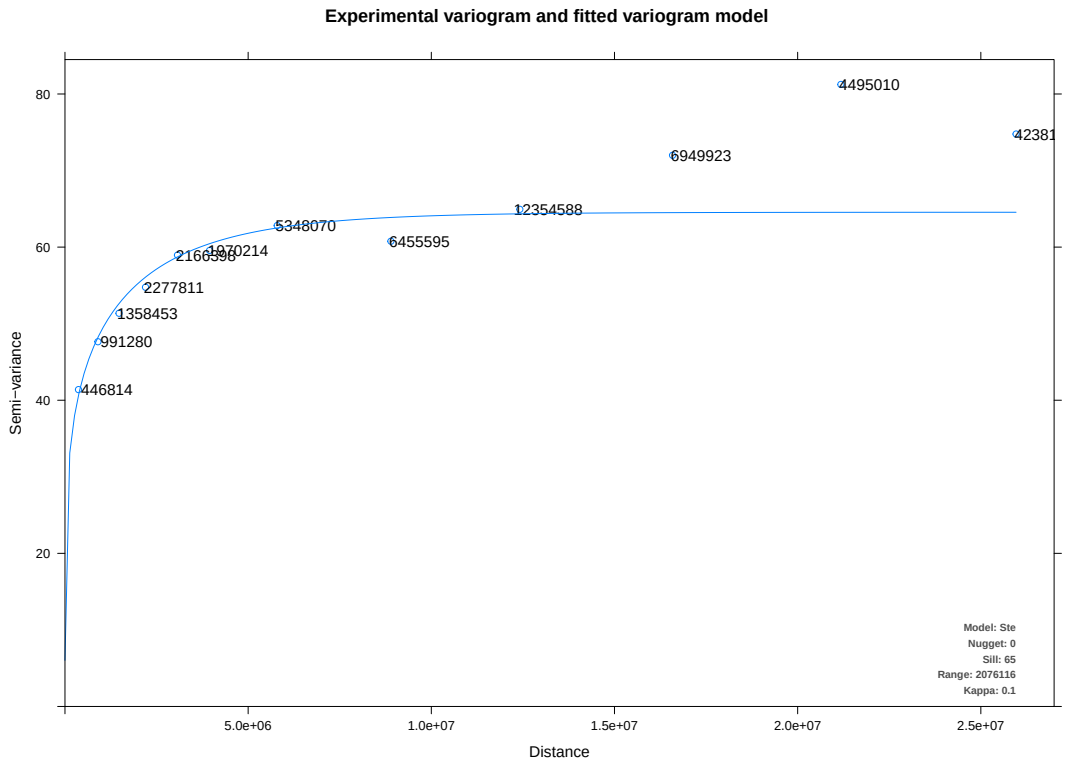


*Note:* Distance is in meters, value labels report the number of bilateral station-distance-pairs per bin.

Figure C.4 : Kriged Maximum Wind Speed in June 2012

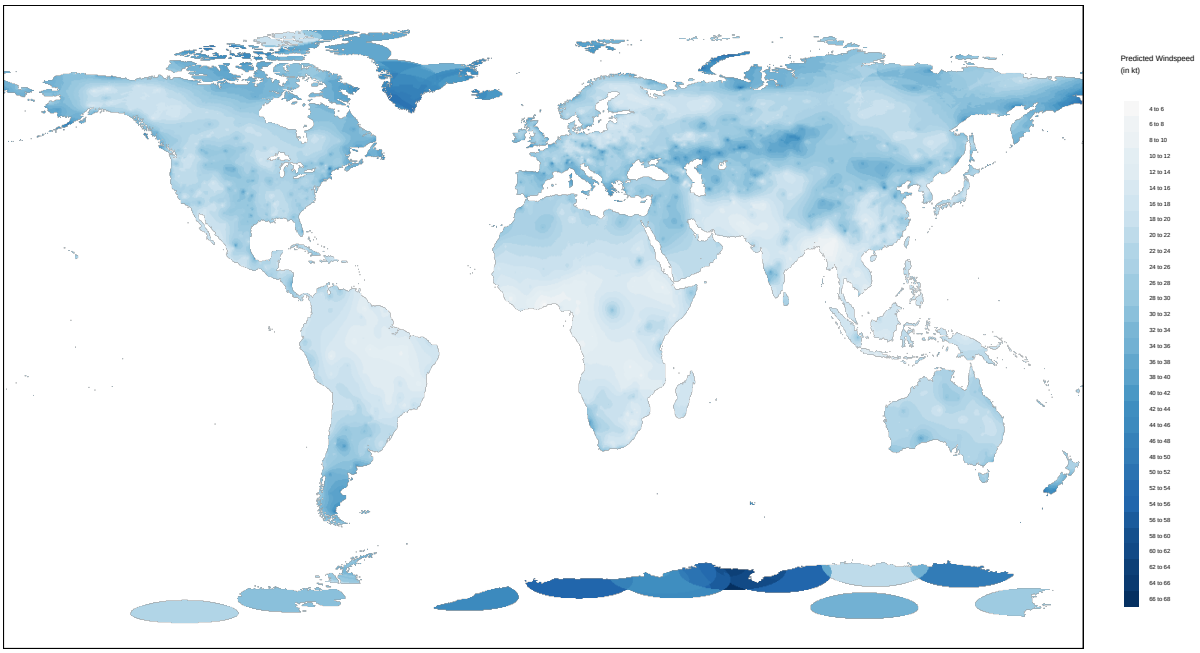

Figure C.5 : Goodness of Fit for Kriged Maximum Wind Speed in June 2012

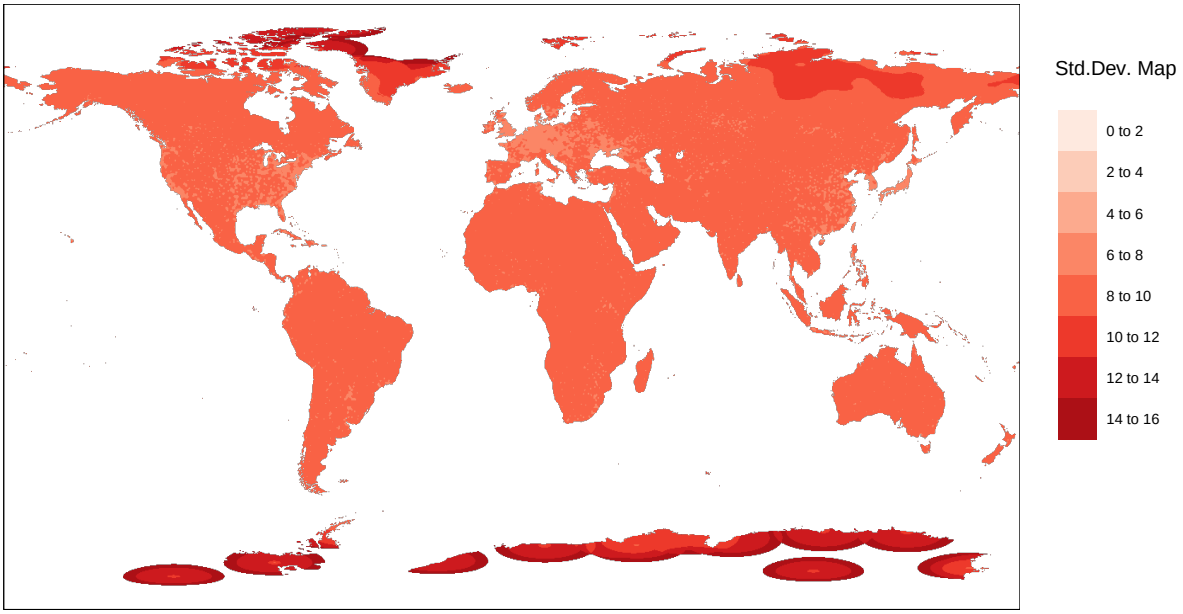


*Note:* Standard deviation of Kriged maximum wind speed (in kt) in June 2012, obtained using the 'leave one out' technique.

Figure C.6 : Inverse Distance Weighted Maximum Wind Speed in June 2012

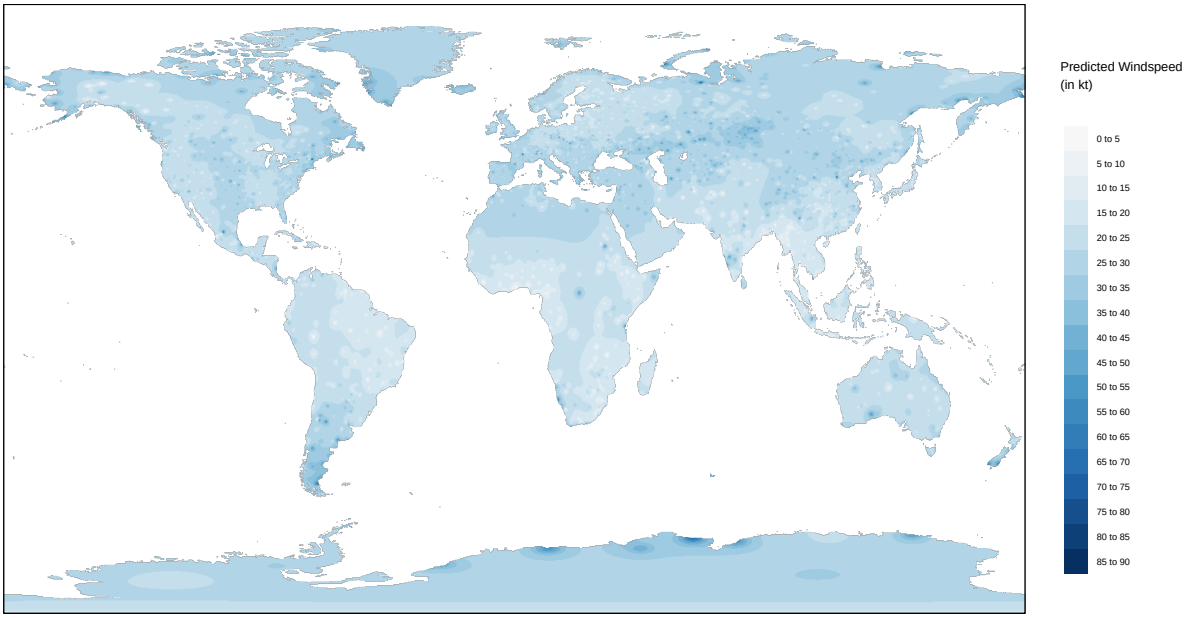


*Note:* Spiked pattern obtained with inverse distance weighting as alternative choice of wind speed interpolation.

### C.1.3 Balancing

Figure C.7 : Balanced Panel - Wind and Earthquake

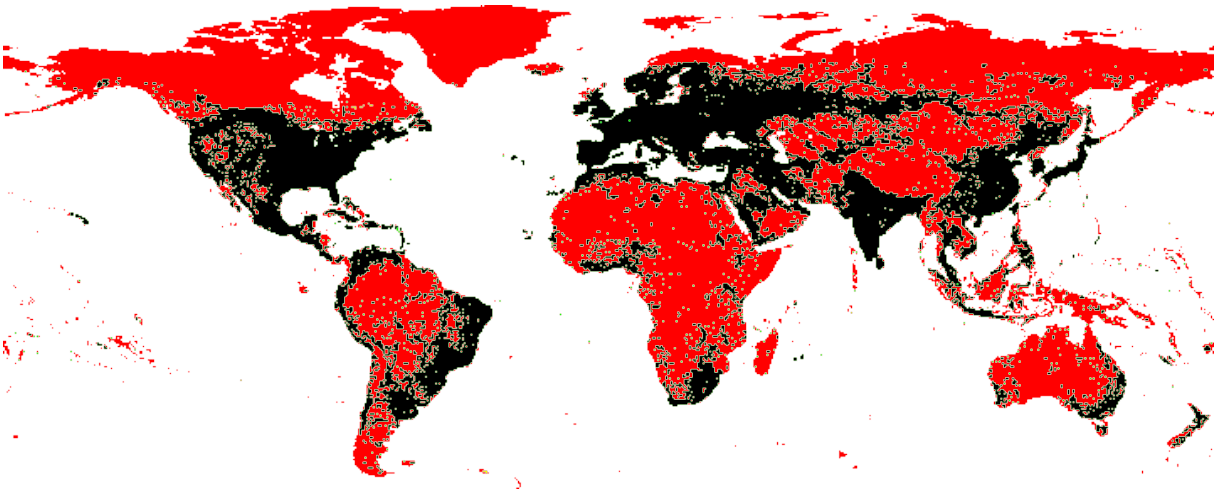

*Note:* Global distribution of grid cells preserved in balanced panel. Physical indicators used for balancing: Winds. Red: Dropped because of zero absolute light emission in at least one period. Yellow: Dropped because of zero population in at least one period. Green: Dropped because no neighbors found within 80 km radius, or because of singleton country. Black: Preserved, i.e., balanced and consecutive with at least one neighbor each and at least two cells per country. Number of years: 21. Number of preserved cells: 24,184.

Figure C.8 : Balanced Panel - Temperature

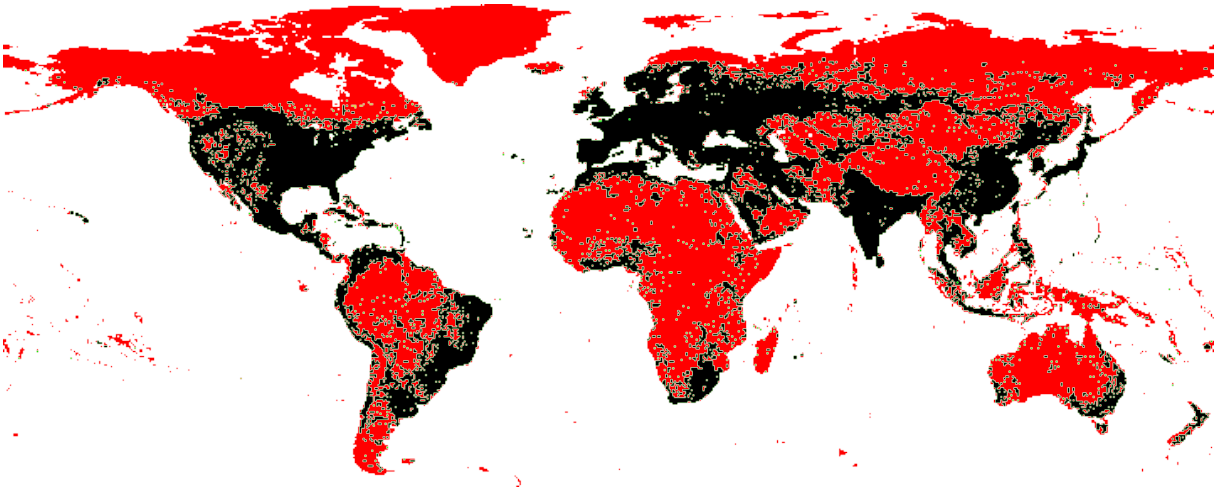

*Note:* Global distribution of grid cells preserved in balanced panel. Physical indicators used for balancing: Temperature. Red: Dropped because of zero absolute light emission in at least one period and because of missing values in the physical intensity measure. Yellow: Dropped because of zero population in at least one period. Green: Dropped because no neighbors found within 80 km radius, or because of singleton country. Black: Preserved, i.e., balanced and consecutive with at least one neighbor each and at least two cells per country. Number of years: 21. Number of preserved cells: 24,097.

Figure C.9 : Balanced Panel - Precipitation

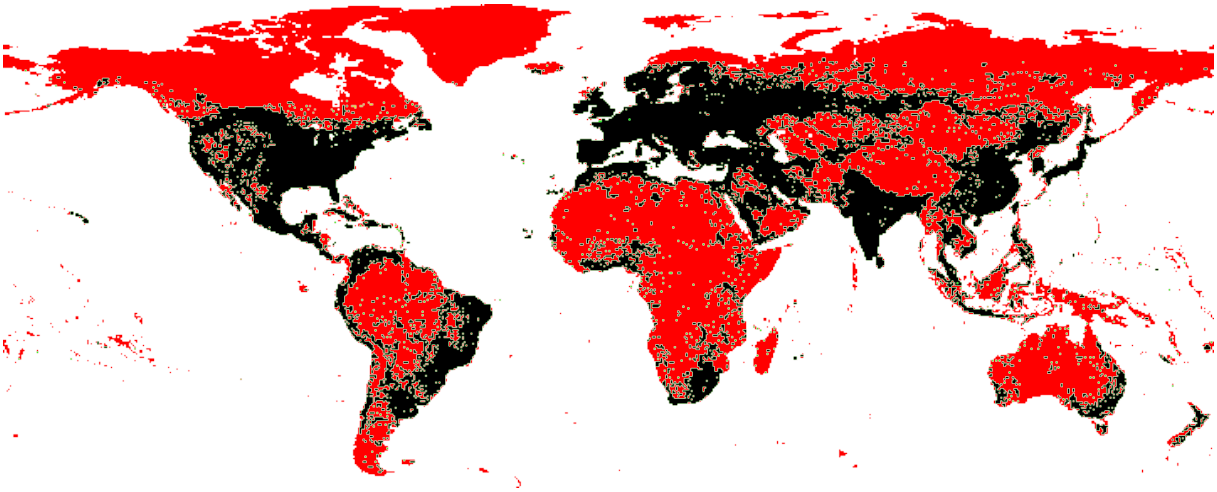

*Note:* Global distribution of grid cells preserved in balanced panel. Physical indicators used for balancing: Precipitation. Red: Dropped because of zero absolute light emission in at least one period and because of missing values in the physical intensity measure. Yellow: Dropped because of zero population in at least one period. Green: Dropped because no neighbors found within 80 km radius, or because of singleton country. Black: Preserved, i.e., balanced and consecutive with at least one neighbor each and at least two cells per country. Number of years: 21. Number of preserved cells: 23,906.

Figure C.10 : Balanced Panel - Drought

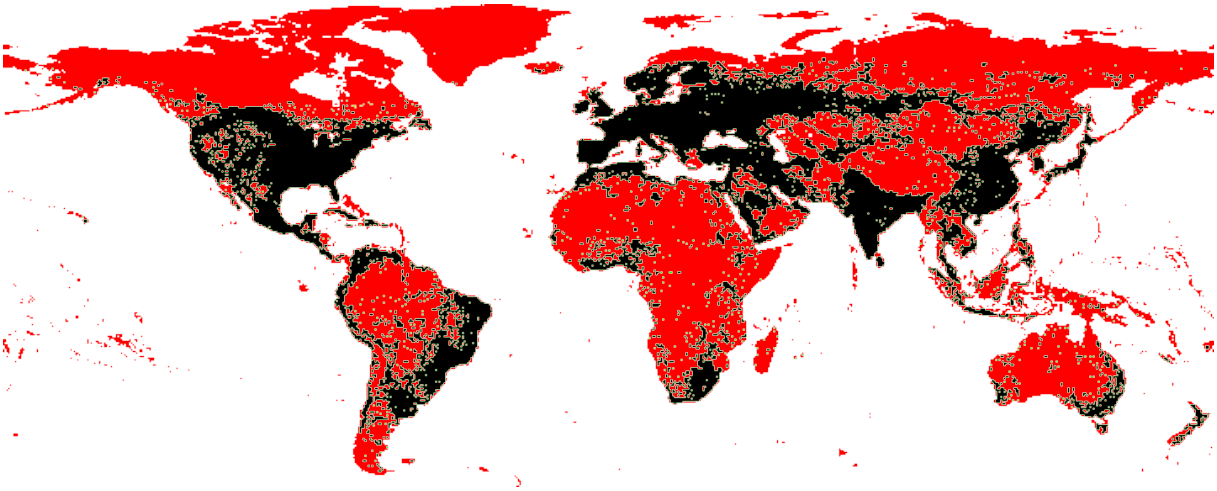

*Note:* Global distribution of grid cells preserved in balanced panel. Physical indicators used for balancing: Drought. Red: Dropped because of zero absolute light emission in at least one period and because of missing values in the physical intensity measure. Yellow: Dropped because of zero population in at least one period. Green: Dropped because no neighbors found within 80 km radius, or because of singleton country. Black: Preserved, i.e., balanced and consecutive with at least one neighbor each and at least two cells per country. Number of years: 21. Number of preserved cells: 22,294.

### C.1.4 Rural/Urban Classification

To test the hypothesis that the observed negative spillover effects of droughts are mainly driven by treated non-urban (potentially rural/agricultural) cells that negatively affect nearby urban (or residential) locations, cells must be classified into predominantly urban vs. non-urban ones. For this purpose, the MODIS Land-use Data provided by the FAO for year 2001 is used. This land-use data includes information on the extent of urban or crop areas at a spatial resolution of 15 arc-seconds (i.e., roughly 500 meters), obtained from MODIS satellite imagery using a supervised decision tree classification algorithm with region-specific parameters (Schneider et al., 2009). Urban land-use in particular comprises all human-constructed elements such as buildings and roads, while crop land-use comprises all kinds of cultivated fields. Pixel locations are defined according to the type of land-use they are *dominated* by (i.e., coverage of at least 50% of a given pixel unit). In particular, urban areas follow a defined minimum mapping unit approach, considering only contiguous patches of built-up land that are greater than one square kilometer (i.e., at least four adjacent pixels.). This data is aggregated to 0.5°×0.5°grid cell units by computing the cell level shares of each land-use pixel type.

As a next step, testing the hypothesis requires classifying each cell as either “urban” or “non-urban” in a mutually-exclusive fashion. Due to the presence of snow/ice and other vegetation, crops and urban shares do not sum up to one at the cell level. Moreover, cells with a relatively high share of urban pixels compared to the global distribution may simultaneously also have a relatively high share of rural pixels, and vice versa. Consequently, it is unclear ex-ante, what threshold should be imposed on land-use shares to make a binary distinction.

To solve this classification problem, an off-the-shelve unsupervised machine leaning algorithm provided by Scrucca et al. (2016) is applied, using three input components: The shares of urban, crop, and snow-ice pixels (vs. other vegetation) per cell in year 2001. Using the Bayesian Information Criteria (BIC), the algorithm picks the best fit across a range of classification models. The algorithm chooses an ellipsoidal, equal volume and shape (EEV) Gaussian finite mixture model fitted by expectation-maximization, to classify cells into three categories representing cells that are mostly urban (1,038), mostly non-urban/rural (21,163), and none (93). Thus, about 5% of ever-lit cells in the sample represent mostly urban areas. Figure C.11 depicts the classification outcome along the three input-dimensions.

Figure C.11 : Rural/Urban Classification

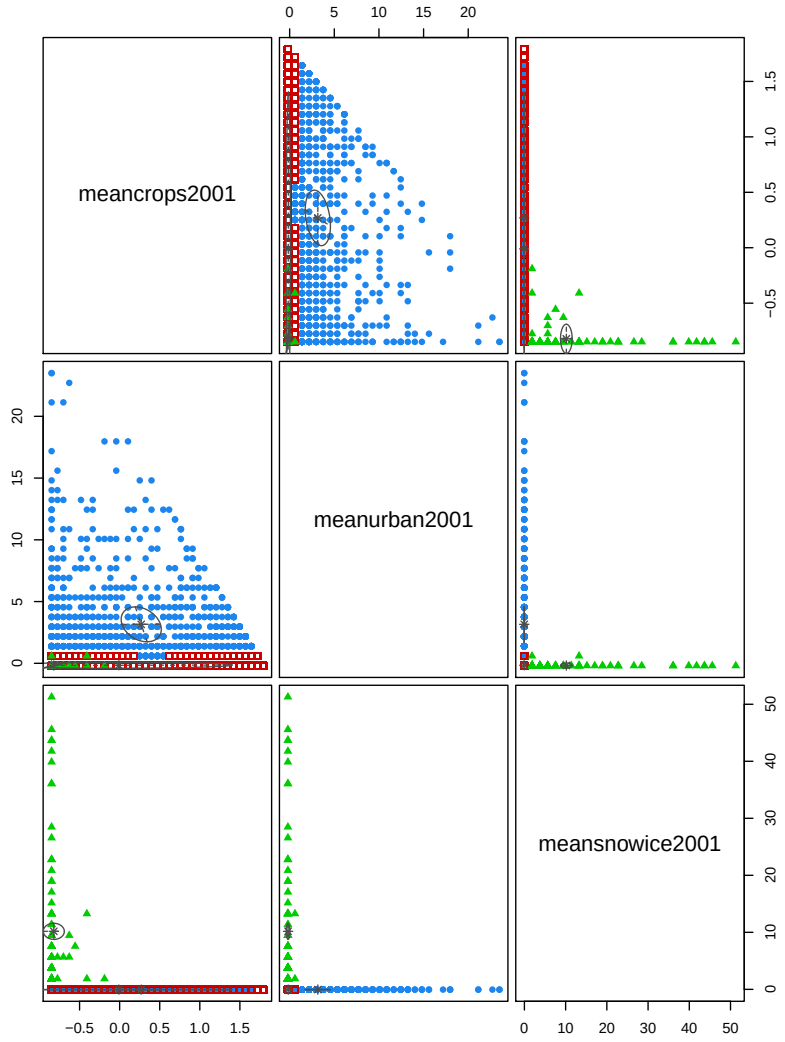


*Note:* Classification of Rural and Urban Cells in a Gaussian finite mixture model fitted by Expectation-Maximization (EM) algorithm. Ellipsoidal, equal volume and shape (EEV) model with 3 input components: Shares of urban, crop, and snow-ice pixels per cell in year 2001. All input components centered and scaled by their standard deviation for efficiency reasons. Log-Likelihood: 39,242.11, number of observations: 22,294 cells, number of estimated parameters: 23, Bayesian Information Criteria (BIC): 78,253.94, Integrated Complete-data Likelihood (ICL): 77,970.27. Best fit across range of classification models provided by 'mclust 5' R package (Scrucca et al., 2016), using BIC as selection criterion. 21,163 cells classified as rural (red), 1,038 as urban/residential (blue), 93 as none (green).

Figure C.12 depicts the distributions of key variables of interest for the obtained classes. The top two graphs are dedicated to the distribution of input components used by the classification algorithm. As it becomes clear, most cells classified as rural have no or only small urban pixel shares. The reverse conclusion is not true however: The graph on the top right suggests that

cells classified as urban may simultaneously have very high crop shares. This observation seems reasonable, given the arbitrary layout of the grid cells combined with the fact that cultivated croplands are often located in the outskirts of urban areas.

The lower two graphs turn to the distributions of the mean night light intensity (left) and of population (right). Neither of these two variables has been used as inputs for classification but are relevant for empirical identification and shall thus serve to asses the class validity. The plots suggest that both the mean night light intensity and the population size are overall higher for urban than for rural cells, which can be considered a reasonable finding.

Finally, to offer a more tractable alternative to the classification with non-supervised learning, a "simple" selection rule is tested, which baldly classifies all cells as urban that have a share of urban pixels which is larger than zero. This approach leads to about twice as many cells being classified as urban, potentially including also those that have only very small urban area. While it is reasonable to assume that about 10% urbanization at a global scale may be too high, results are qualitatively similar.

To decompose the local average treatment and spillover effects of droughts according to cell classification, the following model is estimated:

$$
\begin{aligned}
\Delta \boldsymbol{\ell}_t = \boldsymbol{\ell}_{t-1}\gamma &+ \boldsymbol{D}_t\boldsymbol{\beta^0} + [\boldsymbol{D}_t \times \text{urban}]\,\boldsymbol{\beta^1} \\
&+ \boldsymbol{W}^r_{\text{non-urban}}\boldsymbol{D}_t\boldsymbol{\beta^2} + [\boldsymbol{W}^r_{\text{non-urban}}\boldsymbol{D}_t \times \text{urban}]\,\boldsymbol{\beta^3} \\
&+ \boldsymbol{W}^r_{\text{urban}}\boldsymbol{D}_t\boldsymbol{\beta^4} + [\boldsymbol{W}^r_{\text{urban}}\boldsymbol{D}_t \times \text{urban}]\,\boldsymbol{\beta^5} \\
&+ \boldsymbol{X}_t\boldsymbol{\delta^0} + \boldsymbol{W}^r\boldsymbol{X}_t\boldsymbol{\delta^1} + \boldsymbol{\nu} + \boldsymbol{\pi} + \boldsymbol{u}_t \\
\boldsymbol{u}_t = \rho\boldsymbol{W}^r\boldsymbol{u}_t &+ \boldsymbol{\varepsilon}_t.
\end{aligned}
\tag{C.3}
$$

$\boldsymbol{W}^r_{\text{urban}}$ and $\boldsymbol{W}^r_{\text{non-urban}}$ represent mutually exclusive subsets of neighborhoods. Since these subsets potentially have systematic differences in the number of neighbors, spillover-components are standard-normalized to allow direct comparison of coefficient magnitudes. Results for both classifiers (clustering and simple) are summarized in Table C.1.

Results suggest that negative spillovers from non-urban to urban cells drive the aggregate spillover, with magnitudes about twice as strong as from non-urban to non-urban ones. This supports the hypothesis that negative drought spillovers are driven by the rural-to-urban channel. Spillovers within pairs of non-urban cells still persist, however, potentially due to

Figure C.12 : Distribution of Cell Properties Across Rural/Urban Clusters

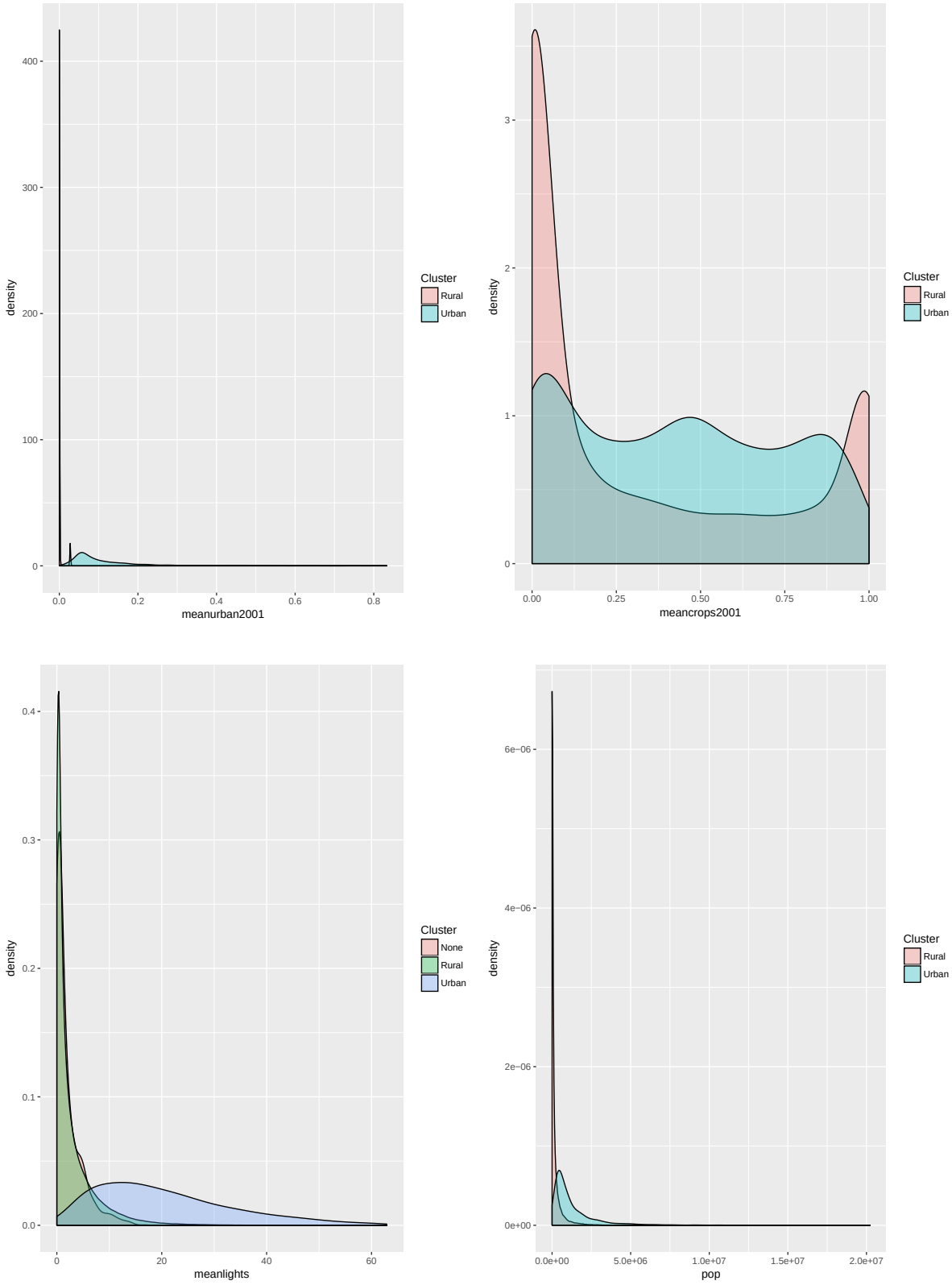

Table C.1 : Comparison of Drought-Effects Across Rural-Urban Neighborhoods

**Dependent Variable:** $\Delta \ln(\text{lights}_t)$

| | | | clustering | simple |
|---|---|---|---|---|
| **direct effects** | | **non-urban cells** | | |
| | | $\text{drought}_t$ | 0.0243*** | 0.0227*** |
| | | | (0.0039) | (0.0040) |
| | | $\text{drought}_{t-1}$ | −0.0046 | −0.0038 |
| | | | (0.0039) | (0.0039) |
| | | **urban cells** | | |
| | | $\text{drought}_t \times \text{urban}$ | 0.0593*** | 0.0463*** |
| | | | (0.0172) | (0.0123) |
| | | $\text{drought}_{t-1} \times \text{urban}$ | −0.0289* | −0.0204* |
| | | | (0.0172) | (0.0123) |
| **spillover effects** | **from non-urban cells** | **to non-urban cells** | | |
| | | $W_{\text{non-urban}} \cdot \text{drought}_t$ | −0.0080*** | −0.0079*** |
| | | | (0.0015) | (0.0015) |
| | | $W_{\text{non-urban}} \cdot \text{drought}_{t-1}$ | −0.0004 | −0.0006 |
| | | | (0.0015) | (0.0015) |
| | | **to urban cells** | | |
| | | $W_{\text{non-urban}} \cdot \text{drought}_t \times \text{urban}$ | −0.0094* | −0.0062* |
| | | | (0.0051) | (0.0036) |
| | | $W_{\text{non-urban}} \cdot \text{drought}_{t-1} \times \text{urban}$ | 0.0046 | 0.0037 |
| | | | (0.0051) | (0.0036) |
| | **from urban cells** | **to non-urban cells** | | |
| | | $W_{\text{urban}} \cdot \text{drought}_t$ | −0.0012 | −0.0004 |
| | | | (0.0011) | (0.0011) |
| | | $W_{\text{urban}} \cdot \text{drought}_{t-1}$ | −0.0005 | −0.0005 |
| | | | (0.0011) | (0.0011) |
| | | **to urban cells** | | |
| | | $W_{\text{urban}} \cdot \text{drought}_t \times \text{urban}$ | −0.0042** | −0.0050*** |
| | | | (0.0019) | (0.0019) |
| | | $W_{\text{urban}} \cdot \text{drought}_{t-1} \times \text{urban}$ | 0.0034* | 0.0025 |
| | | | (0.0019) | (0.0019) |
| | | **controls** | | |
| | | $\ln(\text{pop}_t)$ | 0.0276*** | 0.0276*** |
| | | | (0.0014) | (0.0014) |
| | | $W \cdot \ln(\text{pop}_t)$ | 0.0115*** | 0.0115*** |
| | | | (0.0006) | (0.0006) |
| | | $\ln(\text{lights}_{t-1})$ | −0.4329*** | −0.4329*** |
| | | | (0.0011) | (0.0011) |
| | | $\rho$ | 0.0676*** | 0.0676*** |
| | | | (0.0001) | (0.0000) |
| | | Observations | 468,174 | 468,174 |

*Note:* ***, **, * denote significance at the 1%, 5% and 10% level. All specifications are SDEM and are estimated by Maximum Likelihood. Standard errors in parentheses. Cell and year fixed effects included but not reported. Spatial radius is r=80 km. Yearly disaster intensities reflect time-weighted rolling averages over 12 subsequent monthly observations. $W_{\text{urban}}$ and $W_{\text{non-urban}}$ represent mutually exclusive subsets of neighborhoods. Spillover-Components standard-normalized to allow comparison across subsets within regressions.

residual urban structures in cells classified as non-urban. There is no evidence for spillovers from urban to non-urban cells and only weak spillovers within urban neighborhoods. Finally, the positive direct effect is nearly three times as large in urban cells compared to non-urban ones. Notably also, the relevant spillover effects from non-urban to urban cells are about a third higher with the machine-learning clustering approach than if the simple classification rule is used. This suggests that the distinction between urban and non-urban cells provided by machine-learning may be more precise but is not exclusively driving the qualitative findings.

# Appendix C.2 Supplementary Appendix

## C.2.1 Supplementary Descriptive Statistics

Table C.2 : Summary Statistics

| statistic | n | mean | st. dev. | min | max |
|---|---|---|---|---|---|
| $\Delta \ln(\text{lights})$ | 507,864 | 0.045 | 0.392 | −8.246 | 8.217 |
| $\Delta \ln(\text{lights NTC})$ | 468,111 | 0.046 | 0.394 | −8.139 | 8.109 |
| $\Delta \ln(\text{lights<=DN55})$ | 507,528 | 0.048 | 0.402 | −0.030 | 8.002 |
| $\Delta \ln(\text{lights>=DN3})$ | 507,024 | 0.045 | 0.397 | −8.246 | 8.217 |
| $\Delta \ln(\text{lights>=DN8})$ | 390,957 | 0.045 | 0.483 | −8.311 | 8.424 |
| $\ln(\text{lights})$ | 507,864 | 0.264 | 1.724 | −7.090 | 4.142 |
| $\ln(\text{lights NTC})$ | 468,111 | 0.135 | 1.672 | −7.090 | 4.093 |
| $\ln(\text{pop}_t)$ | 507,864 | 10.639 | 2.165 | −14.390 | 16.822 |
| **time-weighted physical intensities** | | | | | |
| wind | 507,864 | 20.766 | 4.486 | 5.478 | 46.528 |
| cold | 506,037 | 0.412 | 0.089 | 0.000 | 1.271 |
| precip. | 502,026 | 0.385 | 0.151 | 0.000 | 1.697 |
| drought | 468,174 | 0.387 | 0.242 | 0.000 | 2.305 |
| earthq. | 507,864 | 0.121 | 0.395 | −0.189 | 5.002 |
| **simple mean of yearly physical intensities** | | | | | |
| wind | 507,864 | 20.735 | 4.552 | 4.957 | 48.036 |
| cold | 506,037 | 0.410 | 0.093 | 0.000 | 1.372 |
| precip. | 502,026 | 0.386 | 0.182 | 0.000 | 1.841 |
| drought | 468,174 | 0.386 | 0.277 | 0.000 | 2.322 |
| earthq. | 507,864 | 0.120 | 0.405 | −0.317 | 5.342 |

Figure C.13 : Specification of World Regions

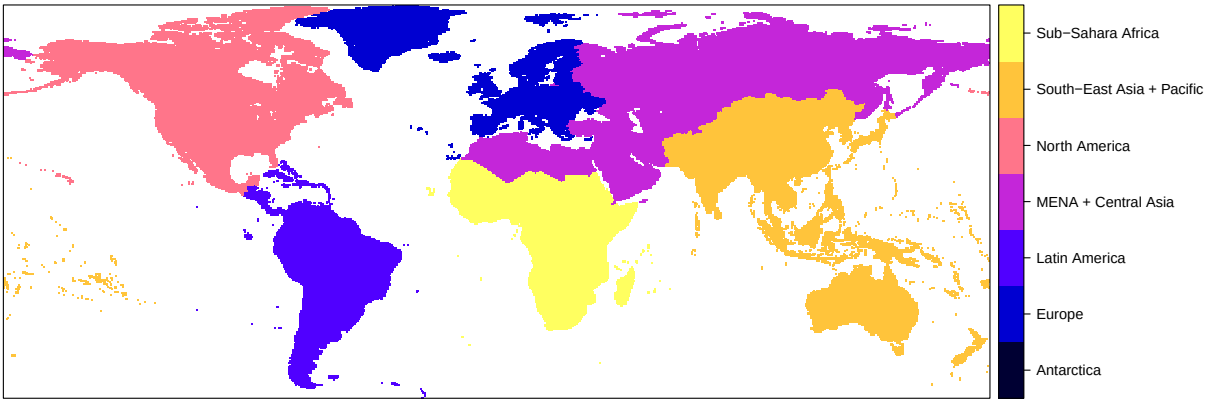

### Table C.3 : Summary Statistics of Satellite-Years for Night-time Lights

| Satellite-Year | DN | | | | | | | Cloud-Free Nights |
|---|---|---|---|---|---|---|---|---|
| | 0 | 1–2 | 3–8 | 9–15 | 16–25 | 26–62 | 63 | (Mean) |
| F101992 | 84.97% | 0.00% | 4.00% | 1.89% | 0.73% | 0.85% | 0.09% | 15.2 |
| F101993 | 86.34% | 0.00% | 6.19% | 1.65% | 0.70% | 0.86% | 0.00% | 31.2 |
| F101994 | 86.39% | 0.00% | 6.21% | 1.58% | 0.69% | 0.89% | 0.10% | 14.7 |
| F121995 | 84.97% | 0.00% | 6.26% | 1.92% | 0.84% | 1.08% | 0.10% | 40.9 |
| F121996 | 84.79% | 0.00% | 6.58% | 1.82% | 0.82% | 1.04% | 0.09% | 40.2 |
| F121997 | 84.81% | 0.00% | 5.90% | 1.99% | 0.85% | 1.10% | 0.11% | 36.3 |
| F121998 | 82.93% | 0.00% | 6.01% | 2.25% | 0.93% | 1.18% | 0.12% | 40.2 |
| F141999 | 78.35% | 0.03% | 7.65% | 1.45% | 0.66% | 0.89% | 0.08% | 37.1 |
| F152000 | 84.64% | 0.00% | 7.19% | 2.31% | 0.92% | 1.15% | 0.11% | 48.7 |
| F152001 | 81.82% | 0.00% | 7.49% | 2.11% | 0.89% | 1.15% | 0.09% | 47.1 |
| F152002 | 84.02% | 0.00% | 7.52% | 2.19% | 0.91% | 1.19% | 0.09% | 53.4 |
| F152003 | 82.19% | 0.19% | 8.24% | 1.30% | 0.63% | 0.86% | 0.06% | 45.8 |
| F152004 | 84.56% | 0.52% | 8.57% | 1.27% | 0.62% | 0.89% | 0.05% | 53.9 |
| F152005 | 83.91% | 0.61% | 8.90% | 1.37% | 0.69% | 0.95% | 0.06% | 59.4 |
| F152006 | 84.23% | 0.56% | 8.63% | 1.36% | 0.67% | 0.96% | 0.06% | 51.6 |
| F162007 | 84.16% | 0.00% | 8.16% | 1.99% | 0.87% | 1.20% | 0.09% | 53.7 |
| F162008 | 84.32% | 0.00% | 8.08% | 1.92% | 0.86% | 1.19% | 0.10% | 47.4 |
| F162009 | 85.55% | 0.00% | 6.74% | 1.90% | 0.87% | 1.17% | 0.12% | 32.0 |
| F182010 | 83.11% | 0.00% | 6.43% | 3.39% | 1.47% | 1.87% | 0.18% | 54.6 |
| F182011 | 83.56% | 0.00% | 7.85% | 2.44% | 1.06% | 1.44% | 0.14% | 54.6 |
| F182012 | 84.25% | 0.00% | 6.06% | 2.89% | 1.20% | 1.59% | 0.17% | 49.4 |
| F182013 | 84.61% | 0.00% | 6.16% | 2.83% | 1.16% | 1.57% | 0.16% | 58.8 |

*Note:* Summary statistics are provided for post-cleaning night light satellite-years. Light pixels are considered only on-land, not in gas-flaring zones and in vicinity of volcanoes (see Data Section). Exception: The mean number of cloud-free nights is constructed using the raw data product, as downloaded from NOAA.

### Table C.4 : Lights to GDP Growth Rate Elasticity

| Dependent Variable: | ln(GDP in const. LCU) | | ln(pop density) | |
|---|---|---|---|---|
| ln(light) | 0.348*** | 0.369*** | | 0.097*** |
| | (0.092) | (0.069) | | (0.015) |
| ln(GDP in const. LCU) | | | 0.132*** | |
| | | | (0.031) | |
| adj. $R^2$ | 0.999 | 0.998 | 0.997 | 0.997 |
| within $R^2$ | 0.240 | 0.273 | 0.073 | 0.080 |
| $N$ | 3,229 | 4,167 | 4,156 | 4,156 |

*Note:* ***, **, * denote significance at the 1%, 5% and 10% level. All models use panel OLS. Standard errors (in parentheses) are robust to heteroskedasticity. Country and year fixed effects included but not reported. Years 1992-2008 in first column, 1992-2013 in remaining columns. 197 countries in sample.

### Table C.5 : Test for Residual Spatial Autocorrelation

**Global Moran's $I$ Test for regression residuals of SLX model**

| | wind | precip. | drought | cold |
|---|---|---|---|---|
| **Sample Estimates** | | | | |
| Observed Moran's $I$ | 0.4466 | 0.4496 | 0.4530 | 0.4459 |
| Expected Moran's $I$ | −0.0001 | −0.0001 | −0.0001 | −0.0001 |
| **Test Statistics** | | | | |
| Moran's $I$ stat. s.d. | 596.16 | 596.66 | 579.01 | 594.28 |
| Two-sided p-value | 2.2e-16 | 2.2e-16 | 2.2e-16 | 2.2e-16 |

*Note:* Global Moran's $I$ Test for spatial autocorrelation in the residuals of estimated linear SLX models, compare column (3) of tables C.6–C.8. The Null Hypothesis of no residual spatial autocorrelation (RSA) is overwhelmingly rejected. Observed Moran's $I$ are positive throughout, suggesting positive RSA (i.e., spatial clustering).

Figure C.14 : Kernel Densities of Monthly Physical Intensities

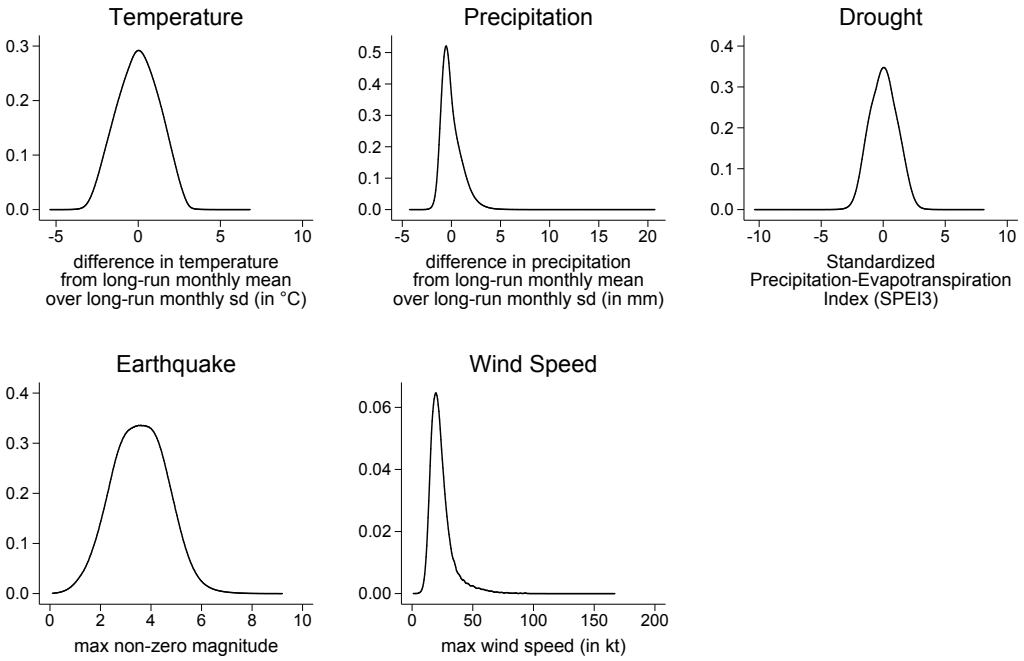


Figure C.15 : Kernel Densities of Monthly Temperature and Precipitation (raw data)

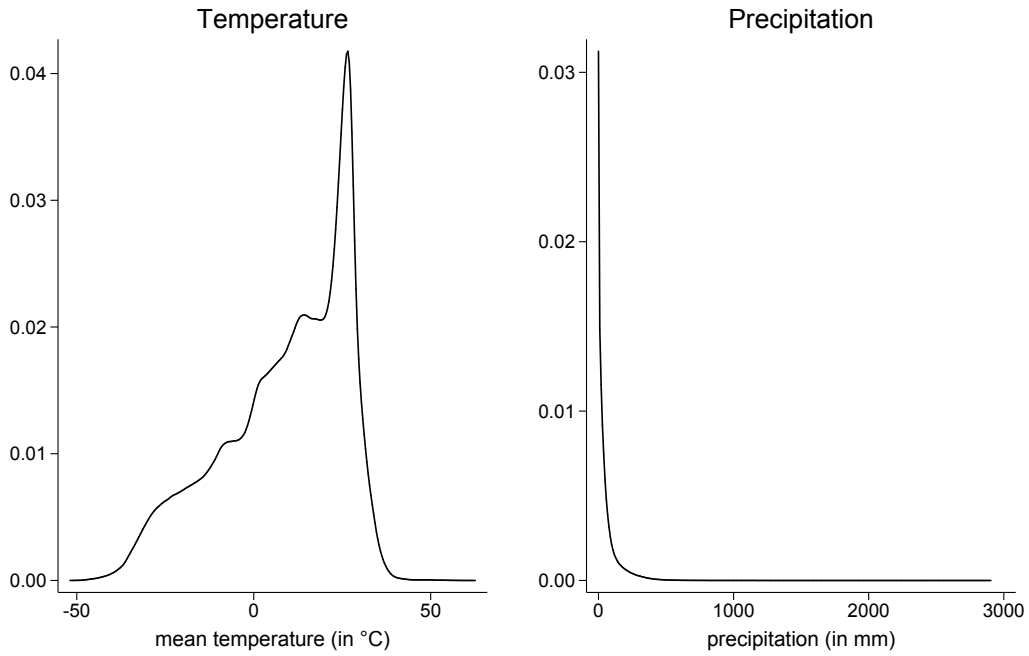

## C.2.2 Supplementary Tables

Table C.6 : Model Buildup: Impact of Droughts on Light Growth

| **Dependent Variable:** $\Delta \ln(\text{lights}_t)$ | | | | |
|---|---|---|---|---|
| | (1) | (2) | (3) | (4) |
| $\text{drought}_t$ | −0.0229*** | 0.0262*** | 0.0345*** | 0.0083* |
| | (0.0021) | (0.0055) | (0.0057) | (0.0048) |
| $\text{drought}_{t-1}$ | | | −0.0296*** | 0.0005 |
| | | | (0.0058) | (0.0047) |
| $W \cdot \text{drought}_t$ | | −0.0080*** | −0.0099*** | −0.0044*** |
| | | (0.0008) | (0.0008) | (0.0009) |
| $W \cdot \text{drought}_{t-1}$ | | | 0.0073*** | 0.0010 |
| | | | (0.0008) | (0.0009) |
| $\ln(\text{pop}_t)$ | 0.0432*** | 0.0267*** | 0.0266*** | 0.0276*** |
| | (0.0030) | (0.0029) | (0.0029) | (0.0014) |
| $W \cdot \ln(\text{pop}_t)$ | | 0.0149*** | 0.0149*** | 0.0115 |
| | | (0.0009) | (0.0009) | (0.0006) |
| $\ln(\text{lights}_{t-1})$ | −0.4054*** | −0.4086*** | −0.4084*** | −0.4329*** |
| | (0.0033) | (0.0033) | (0.0033) | (0.0011) |
| $\rho$ | | | | 0.676*** |
| | | | | (0.0000) |
| Method | OLS | SLX | SLX | SDEM |
| Observations | 468,174 | 468,174 | 468,174 | 468,174 |

*Note:* ***, **, * denote significance at the 1%, 5% and 10% level. Specifications (1), (2), and (3) are estimated by panel OLS, (4) is estimated by Maximum Likelihood. Standard errors (in parentheses) allow for heteroskedasticity and clustering at the cell level in specifications (1), (2), and (3). Cell and year fixed effects included but not reported. Spatial radius is r=80 km. Yearly disaster intensities reflect time-weighted rolling averages over 12 subsequent monthly observations.

Table C.7 : Model Buildup: Impact of Cold Waves on Light Growth

| **Dependent Variable:** $\Delta \ln(\text{lights}_t)$ | | | | |
|---|---|---|---|---|
| | (1) | (2) | (3) | (4) |
| $\text{cold}_t$ | 0.0134** | −0.1765*** | −0.1227*** | −0.0762*** |
| | (0.0068) | (0.0184) | (0.0194) | (0.0153) |
| $\text{cold}_{t-1}$ | | | −0.0293* | −0.0326** |
| | | | (0.0176) | (0.0149) |
| $W \cdot \text{cold}_t$ | | 0.0323*** | 0.0307*** | 0.0218*** |
| | | (0.0025) | (0.0026) | (0.0027) |
| $W \cdot \text{cold}_{t-1}$ | | | −0.0229*** | −0.0195*** |
| | | | (0.0024) | (0.0026) |
| $\ln(\text{pop}_t)$ | 0.0409*** | 0.0236*** | 0.0233*** | 0.0244*** |
| | (0.0028) | (0.0027) | (0.0027) | (0.0013) |
| $W \cdot \ln(\text{pop}_t)$ | | 0.0148*** | 0.0142*** | 0.0106*** |
| | | (0.0008) | (0.0008) | (0.0006) |
| $\ln(\text{lights}_{t-1})$ | −0.4097*** | −0.4141*** | −0.4138*** | −0.4379*** |
| | (0.0032) | (0.0032) | (0.0032) | (0.0011) |
| $\rho$ | | | | 0.0672*** |
| | | | | (0.0000) |
| Method | OLS | SLX | SLX | SDEM |
| Observations | 506,394 | 506,394 | 506,037 | 506,037 |

*Note:* ***, **, * denote significance at the 1%, 5% and 10% level. Specifications (1), (2), and (3) are estimated by panel OLS, (4) is estimated by Maximum Likelihood. Standard errors (in parentheses) allow for heteroskedasticity and clustering at the cell level in specifications (1), (2), and (3). Cell and year fixed effects included but not reported. Spatial radius is r=80 km. Yearly disaster intensities reflect time-weighted rolling averages over 12 subsequent monthly observations.

Table C.8 : Model Buildup: Impact of Earthquakes on Light Growth

**Dependent Variable:** $\Delta \ln(\text{lights}_t)$

| | (1) | (2) | (3) | (4) |
|---|---|---|---|---|
| $\text{earthq.}_t$ | 0.0107*** | 0.0055** | 0.0038 | 0.0044** |
| | (0.0018) | (0.0022) | (0.0023) | (0.0022) |
| $\text{earthq.}_{t-1}$ | | | 0.0032 | 0.0011 |
| | | | (0.0024) | (0.0022) |
| $W \cdot \text{earthq.}_t$ | | 0.0019*** | 0.0008 | 0.0005 |
| | | (0.0005) | (0.0006) | (0.0008) |
| $W \cdot \text{earthq.}_{t-1}$ | | | 0.0018*** | 0.0015* |
| | | | (0.0007) | (0.0008) |
| $\ln(\text{pop}_t)$ | 0.0406*** | 0.0243*** | 0.0243*** | 0.0251*** |
| | (0.0028) | (0.0027) | (0.0027) | (0.0013) |
| $W \cdot \ln(\text{pop}_t)$ | | 0.0148*** | 0.0147*** | 0.0111*** |
| | | (0.0008) | (0.0008) | (0.0006) |
| $\ln(\text{lights}_{t-1})$ | −0.4101*** | −0.4134*** | −0.4134*** | −0.4378*** |
| | (0.0032) | (0.0032) | (0.0032) | (0.0011) |
| $\rho$ | | | | 0.672*** |
| | | | | (0.0000) |
| Method | OLS | SLX | SLX | SDEM |
| Observations | 507,864 | 507,864 | 507,864 | 507,864 |

*Note:* ***, **, * denote significance at the 1%, 5% and 10% level. Specifications (1), (2), and (3) are estimated by panel OLS, (4) is estimated by Maximum Likelihood. Standard errors (in parentheses) allow for heteroskedasticity and clustering at the cell level in specifications (1), (2), and (3). Cell and year fixed effects included but not reported. Spatial radius is r=80 km. Yearly disaster intensities reflect time-weighted rolling averages over 12 subsequent monthly observations.

Table C.9 : Sensitivity of Baseline Results to Radius r=160km

**Dependent Variable:** $\Delta \ln(\text{lights}_t)$

| | **wind** | **precip.** | **drought** | **cold** |
|---|---|---|---|---|
| $\text{disaster}_t$ | −0.0016** | −0.0249*** | 0.0125*** | −0.0849*** |
| | (0.0007) | (0.0057) | (0.0041) | (0.0136) |
| $\text{disaster}_{t-1}$ | −0.0052*** | 0.0158*** | −0.0075* | −0.0129 |
| | (0.0007) | (0.0057) | (0.0040) | (0.0133) |
| $W \cdot \text{disaster}_t$ | 0.0000 | 0.0008** | −0.0015*** | 0.0061*** |
| | (0.0000) | (0.0004) | (0.0003) | (0.0009) |
| $W \cdot \text{disaster}_{t-1}$ | 0.0001* | 0.0000 | 0.0005* | −0.0060*** |
| | (0.0000) | (0.0004) | (0.0003) | (0.0008) |
| $\ln(\text{pop}_t)$ | 0.0245*** | 0.0252*** | 0.0264*** | 0.0240*** |
| | (0.0013) | (0.0013) | (0.0014) | (0.0013) |
| $W \cdot \ln(\text{pop}_t)$ | 0.0057*** | 0.0059*** | 0.0061*** | 0.0055*** |
| | (0.0003) | (0.0003) | (0.0003) | (0.0003) |
| $\ln(\text{lights}_{t-1})$ | −0.4375*** | −0.4360*** | −0.4328*** | −0.4371*** |
| | (0.0011) | (0.0011) | (0.0011) | (0.0011) |
| $\rho$ | 0.0220*** | 0.0221*** | 0.0226*** | 0.0220*** |
| | (0.0000) | (0.0000) | (0.0000) | (0.0000) |
| Observations | 515,130 | 509,166 | 475,083 | 513,282 |

*Note:* ***, **, * denote significance at the 1%, 5% and 10% level. All specifications are SDEM and are estimated by Maximum Likelihood. Standard errors in parentheses. Cell and year fixed effects included but not reported. Spatial radius is r=160 km. Yearly disaster intensities reflect time-weighted rolling averages over 12 subsequent monthly observations.

Table C.10 : Sensitivity of Baseline Results to Global Spillovers

**Dependent Variable:** $\Delta \ln(\text{lights}_t)$

| | wind | precip. | drought | cold |
|---|---|---|---|---|
| $\text{disaster}_t$ | −0.0046*** | −0.0279*** | −0.0016 | −0.0974*** |
| | (0.0007) | (0.0060) | (0.0041) | (0.0122) |
| | [−0.0044] | [−0.0259] | [−0.0029] | [−0.0794] |
| $\text{disaster}_{t-1}$ | −0.0095*** | 0.0198*** | 0.0017 | −0.0858*** |
| | (0.0007) | (0.0059) | (0.0041) | (0.0119) |
| | [−0.0093] | [0.0189] | [0.0017] | [−0.0908] |
| $W \cdot \text{disaster}_t$ | 0.0005*** | 0.0037*** | −0.0010* | 0.0217*** |
| | (0.0001) | (0.0009) | (0.0006) | (0.0017) |
| | [0.0000] | [0.0001] | [−0.0001] | [0.0010] |
| $W \cdot \text{disaster}_{t-1}$ | 0.0008*** | −0.0021** | −0.0001 | 0.0015 |
| | (0.0001) | (0.0009) | (0.0006) | (0.0017) |
| | [0.0000] | [−0.0001] | [0.0000] | [−0.0003] |
| $\ln(\text{pop}_t)$ | 0.0228*** | 0.0242*** | 0.0256*** | 0.0225*** |
| | (0.0014) | (0.0014) | (0.0015) | (0.0014) |
| | [0.0383] | [0.0397] | [0.0412] | [0.0383] |
| $W \cdot \ln(\text{pop}_t)$ | 0.0116*** | 0.0122*** | 0.0121*** | 0.0118*** |
| | (0.0004) | (0.0004) | (0.0005) | (0.0004) |
| | [0.0009] | [0.0009] | [0.0009] | [0.0009] |
| $\ln(\text{lights}_{t-1})$ | −0.3300*** | −0.3270*** | −0.3232*** | −0.3289*** |
| | (0.0009) | (0.0009) | (0.0009) | (0.0009) |
| $\lambda$ | 0.0671*** | 0.0671*** | 0.0675*** | 0.0671*** |
| | (0.0000) | (0.0000) | (0.0000) | (0.0000) |
| Observations | 508,158 | 502,320 | 468,384 | 506,394 |

*Note:* ***, **, * denote significance at the 1%, 5% and 10% level. All specifications are SDM and are estimated by Maximum Likelihood. Standard errors in parentheses. Average effects translated with spatial multiplier in square brackets. Cell and year fixed effects included but not reported. Spatial radius is r=80 km. Yearly disaster intensities reflect time-weighted rolling averages over 12 subsequent monthly observations.

Table C.11 : Sensitivity to Top-Coding: Excluding Top-Coded Pixels

**Dependent Variable:** $\Delta \ln(\text{lights}_t)$

| | wind | precip. | drought | cold |
|---|---|---|---|---|
| $\text{disaster}_t$ | −0.0019** | −0.0329*** | 0.0091* | −0.0752*** |
| | (0.0009) | (0.0070) | (0.0048) | (0.0152) |
| $\text{disaster}_{t-1}$ | −0.0090*** | 0.0222*** | 0.0012 | −0.0318** |
| | (0.0009) | (0.0069) | (0.0048) | (0.0149) |
| $W \cdot \text{disaster}_t$ | 0.0000 | 0.0052*** | −0.0046*** | 0.0219*** |
| | (0.0002) | (0.0013) | (0.0009) | (0.0027) |
| $W \cdot \text{disaster}_{t-1}$ | 0.0008*** | −0.0023* | 0.0011 | −0.0200*** |
| | (0.0002) | (0.0013) | (0.0009) | (0.0027) |
| $\ln(\text{pop}_t)$ | 0.0276*** | 0.0286*** | 0.0302*** | 0.0273*** |
| | (0.0013) | (0.0013) | (0.0014) | (0.0013) |
| $W \cdot \ln(\text{pop}_t)$ | 0.0113*** | 0.0117*** | 0.0119*** | 0.0110*** |
| | (0.0006) | (0.0006) | (0.0006) | (0.0006) |
| $\ln(\text{lights}_{t-1})$ | −0.4381*** | −0.4360*** | −0.4321*** | −0.4373*** |
| | (0.0011) | (0.0011) | (0.0011) | (0.0011) |
| $\rho$ | 0.0672*** | 0.0672*** | 0.0676*** | 0.0672*** |
| | (0.0000) | (0.0000) | (0.0000) | (0.0000) |
| Observations | 507,780 | 501,942 | 468,111 | 505,953 |

*Note:* ***, **, * denote significance at the 1%, 5% and 10% level. All specifications are SDEM and are estimated by Maximum Likelihood. Standard errors in parentheses. Cell and year fixed effects included but not reported. Spatial radius is r=80 km. Yearly disaster intensities reflect time-weighted rolling averages over 12 subsequent monthly observations. Dependent variable excludes top-coded pixels.

Table C.12 : Sensitivity to top-coding: masking all >DN55 pixels

**Dependent Variable:** $\Delta \ln(\text{lights}_t)$

| | wind | precip. | drought | cold |
|---|---|---|---|---|
| $\text{disaster}_t$ | −0.0019** | −0.0359*** | 0.0104** | −0.0784*** |
| | (0.0009) | (0.0070) | (0.0048) | (0.0153) |
| $\text{disaster}_{t-1}$ | −0.0091*** | 0.0227*** | 0.0024 | −0.0275* |
| | (0.0002) | (0.0069) | (0.0047) | (0.0150) |
| $W \cdot \text{disaster}_t$ | 0.0000 | 0.0056*** | −0.0049*** | 0.0229*** |
| | (0.0002) | (0.0013) | (0.0009) | (0.0027) |
| $W \cdot \text{disaster}_{t-1}$ | 0.0008*** | −0.0026** | 0.0012 | −0.0209*** |
| | (0.0002) | (0.0013) | (0.0009) | (0.0027) |
| $\ln(\text{pop}_t)$ | 0.0301*** | 0.0311*** | 0.0326*** | 0.0299*** |
| | (0.0013) | (0.0013) | (0.0014) | (0.0013) |
| $W \cdot \ln(\text{pop}_t)$ | 0.0114*** | 0.0118*** | 0.0120*** | 0.0111*** |
| | (0.0006) | (0.0006) | (0.0006) | (0.0006) |
| $\ln(\text{lights}_{t-1})$ | −0.4360*** | −0.4338*** | −0.4300*** | −0.4352*** |
| | (0.0011) | (0.0011) | (0.0011) | (0.0011) |
| $\rho$ | 0.0672*** | 0.0672*** | 0.0676*** | 0.0676*** |
| | (0.0000) | (0.0000) | (0.0000) | (0.0000) |
| Observations | 507,528 | 501,795 | 468,048 | 505,764 |

*Note:* ***, **, * denote significance at the 1%, 5% and 10% level. All specifications are SDEM and are estimated by Maximum Likelihood. Standard errors in parentheses. Cell and year fixed effects included but not reported. Spatial radius is r=80 km. Yearly disaster intensities reflect time-weighted rolling averages over 12 subsequent monthly observations.

Table C.13 : Sensitivity to Bottom-Coding: Setting Pixels <DN8 to Zero

**Dependent Variable:** $\Delta \ln(\text{lights}_t)$

| | wind | precip. | drought | cold |
|---|---|---|---|---|
| $\text{disaster}_t$ | 0.0009 | −0.0145* | −0.0032 | −0.0208 |
| | (0.0011) | (0.0084) | (0.0058) | (0.0186) |
| $\text{disaster}_{t-1}$ | −0.0093*** | 0.0215*** | 0.0063 | −0.1174*** |
| | (0.0011) | (0.0083) | (0.0058) | (0.0183) |
| $W \cdot \text{disaster}_t$ | −0.0011*** | 0.0066*** | −0.0040*** | 0.0172*** |
| | (0.0002) | (0.0017) | (0.0012) | (0.0035) |
| $W \cdot \text{disaster}_{t-1}$ | 0.0004** | −0.0031* | −0.0015 | −0.0206*** |
| | (0.0002) | (0.0017) | (0.0012) | (0.0035) |
| $\ln(\text{pop}_t)$ | 0.0201*** | 0.0204*** | 0.0236*** | 0.0188*** |
| | (0.0019) | (0.0019) | (0.0020) | (0.0019) |
| $W \cdot \ln(\text{pop}_t)$ | 0.0158*** | 0.0161*** | 0.0168*** | 0.0150*** |
| | (0.0009) | (0.0009) | (0.0009) | (0.0009) |
| $\ln(\text{lights}_{t-1})$ | −0.3756*** | −0.3738*** | −0.3700*** | −0.3742*** |
| | (0.0012) | (0.0012) | (0.0012) | (0.0012) |
| $\rho$ | 0.0679*** | 0.0680*** | 0.0684*** | 0.0679*** |
| | (0.0000) | (0.0000) | (0.0000) | (0.0000) |
| Observations | 390,957 | 388,227 | 362,607 | 390,201 |

*Note:* ***, **, * denote significance at the 1%, 5% and 10% level. All specifications are SDEM and are estimated by Maximum Likelihood. Standard errors in parentheses. Cell and year fixed effects included but not reported. Spatial radius is r=80 km. Yearly disaster intensities reflect time-weighted rolling averages over 12 subsequent monthly observations.

Table C.14 : Sensitivity to bottom-coding: setting pixels <DN3 to zero

| **Dependent Variable:** $\Delta \ln(\text{lights}_t)$ | | | | |
|---|---|---|---|---|
| | **wind** | **precip.** | **drought** | **cold** |
| $\text{disaster}_t$ | −0.0007 | −0.0265*** | 0.0082* | −0.0852*** |
| | (0.0009) | (0.0070) | (0.0048) | (0.0154) |
| $\text{disaster}_{t-1}$ | −0.0106*** | 0.0290*** | 0.0015 | −0.0291* |
| | (0.0009) | −0.0069 | (0.0048) | (0.0150) |
| $W \cdot \text{disaster}_t$ | −0.0001 | 0.0042*** | −0.0041*** | 0.0242*** |
| | (0.0002) | (0.0013) | (0.0009) | (0.0027) |
| $W \cdot \text{disaster}_{t-1}$ | 0.0010*** | −0.0022* | 0.0007 | −0.0217*** |
| | (0.0002) | (0.0013) | (0.0009) | (0.0027) |
| $\ln(\text{pop}_t)$ | 0.0265*** | 0.0275*** | 0.0296*** | 0.0262*** |
| | (0.0013) | (0.0013) | (0.0014) | (0.0013) |
| $W \cdot \ln(\text{pop}_t)$ | 0.0108*** | 0.0112*** | 0.0116*** | 0.0105*** |
| | (0.0006) | (0.0006) | (0.0006) | (0.0006) |
| $\ln(\text{lights}_{t-1})$ | −0.4395*** | −0.4376*** | −0.4338*** | −0.4388*** |
| | (0.0011) | (0.0011) | (0.0011) | (0.0011) |
| $\rho$ | 0.0672*** | 0.0672*** | 0.0676*** | 0.0672*** |
| | (0.0000) | (0.0000) | (0.0000) | (0.0000) |
| Observations | 507,024 | 501,228 | 467,460 | 505,197 |

*Note:* ***, **, * denote significance at the 1%, 5% and 10% level. All specifications are SDEM and are estimated by Maximum Likelihood. Standard errors in parentheses. Cell and year fixed effects included but not reported. Spatial radius is r=80 km. Yearly disaster intensities reflect time-weighted rolling averages over 12 subsequent monthly observations.

Table C.15 : Sensitivity of Baseline Results to Time Varying Country Characteristics

| **Dependent Variable:** $\Delta \ln(\text{lights}_t)$ | | | | |
|---|---|---|---|---|
| | **wind** | **precip.** | **drought** | **cold** |
| $\text{disaster}_t$ | 0.0004 | −0.0312*** | 0.0062 | −0.0360** |
| | (0.0010) | (0.0070) | (0.0049) | (0.0179) |
| $\text{disaster}_{t-1}$ | −0.0049*** | 0.0117* | 0.0009 | −0.0390** |
| | (0.0010) | (0.0069) | (0.0049) | (0.0175) |
| $W \cdot \text{disaster}_t$ | 0.0003** | 0.0043*** | −0.0041*** | 0.0165*** |
| | (0.0002) | (0.0013) | (0.0009) | (0.0029) |
| $W \cdot \text{disaster}_{t-1}$ | 0.0009*** | −0.0022* | 0.0017* | −0.0144*** |
| | (0.0002) | (0.0013) | (0.0009) | (0.0028) |
| $\ln(\text{pop}_t)$ | 0.0140*** | 0.0145*** | 0.0158*** | 0.0140*** |
| | (0.0013) | (0.0013) | (0.0014) | (0.0013) |
| $W \cdot \ln(\text{pop}_t)$ | 0.0040*** | 0.0041*** | 0.0044*** | 0.0039*** |
| | (0.0006) | (0.0006) | (0.0006) | (0.0006) |
| $\ln(\text{lights}_{t-1})$ | −0.4768*** | −0.4759*** | −0.4728*** | −0.4764*** |
| | (0.0011) | (0.0011) | (0.0012) | (0.0011) |
| $\rho$ | 0.0671*** | 0.0671*** | 0.0068*** | 0.0671*** |
| | (0.0000) | (0.0000) | (0.0000) | (0.0000) |
| Observations | 507,864 | 502,026 | 468,174 | 506,037 |

*Note:* ***, **, * denote significance at the 1%, 5% and 10% level. All specifications are SDEM and are estimated by Maximum Likelihood. Standard errors in parentheses. Cell and country-year fixed effects (with nested year fixed effects) included but not reported. Spatial radius is r=80 km. Yearly disaster intensities reflect time-weighted rolling averages over 12 subsequent monthly observations.

Table C.16 : Sensitivity of Baseline to Simple Annual Mean of Disasters

| **Dependent Variable:** $\Delta \ln(\text{lights}_t)$ | | | | |
|---|---|---|---|---|
| | **wind** | **precip.** | **drought** | **cold** |
| $\text{disaster}_t$ | −0.0032*** | −0.0289*** | 0.0243*** | −0.0613*** |
| | (0.0007) | (0.0055) | (0.0039) | (0.0137) |
| $\text{disaster}_{t-1}$ | −0.0064*** | 0.0011 | −0.0060 | −0.0540*** |
| | (0.007) | (0.0055) | (0.0038) | (0.0133) |
| $W \cdot \text{disaster}_t$ | −0.0002 | 0.0018* | −0.0037*** | 0.0337*** |
| | (0.0001) | (0.0010) | (0.0007) | (0.0025) |
| $W \cdot \text{disaster}_{t-1}$ | 0.0008*** | 0.0030*** | 0.0000 | −0.0504*** |
| | (0.0001) | (0.0010) | (0.0007) | (0.0019) |
| $\ln(\text{pop}_t)$ | 0.0247*** | 0.0257*** | 0.0276*** | 0.0245*** |
| | (0.0013) | (0.0013) | (0.0014) | (0.0013) |
| $W \cdot \ln(\text{pop}_t)$ | 0.0109*** | 0.0113*** | 0.0115*** | 0.0107*** |
| | (0.0006) | (0.0006) | (0.0006) | (0.0006) |
| $\ln(\text{lights}_{t-1})$ | −0.4385*** | −0.4367*** | −0.4329*** | −0.4376*** |
| | (0.0011) | (0.0011) | (0.0011) | (0.0011) |
| $\rho$ | 0.0672*** | 0.0672*** | 0.676*** | 0.0672*** |
| | (0.0000) | (0.0000) | (0.0000) | (0.0000) |
| Observations | 507,864 | 502,026 | 468,174 | 506,037 |

*Note:* ***, **, * denote significance at the 1%, 5% and 10% level. All specifications are SDEM and are estimated by Maximum Likelihood. Standard errors in parentheses. Cell and year fixed effects included but not reported. Spatial radius is r=80 km. Yearly disaster intensities reflect non-weighted mean over all monthly observations within a year.

Table C.17 : Spatial Error HAC Model following Hsiang (2010)

| **Dependent Variable:** $\Delta \ln(\text{lights}_t)$ | | | | |
|---|---|---|---|---|
| | **wind** | **precip.** | **drought** | **cold** |
| $\text{disaster}_t$ | −0.0010 | −0.0744*** | 0.0342*** | −0.1219*** |
| | (0.0014) | (0.0112) | (0.0080) | (0.0275) |
| $\text{disaster}_{t-1}$ | −0.0143*** | 0.0477*** | −0.0292*** | −0.0301 |
| | (0.0014) | (0.0108) | (0.0079) | (0.0253) |
| $W \cdot \text{disaster}_t$ | −0.0002 | 0.0137*** | −0.0098*** | 0.0306*** |
| | (0.0002) | (0.0019) | (0.0013) | (0.0043) |
| $W \cdot \text{disaster}_{t-1}$ | 0.0015*** | −0.0079*** | 0.0072*** | −0.0228*** |
| | (0.0002) | (0.0018) | (0.0013) | (0.0041) |
| $\ln(\text{pop}_t)$ | 0.0237*** | 0.0250*** | 0.0267*** | 0.0234*** |
| | (0.0020) | (0.0020) | (0.0021) | (0.0020) |
| $W \cdot \ln(\text{pop}_t)$ | 0.0142*** | 0.0149*** | 0.0149*** | 0.0141*** |
| | (0.0011) | (0.0011) | (0.0012) | (0.0011) |
| $\ln(\text{lights}_{t-1})$ | −0.4153*** | −0.4123*** | −0.4085*** | −0.4139*** |
| | (0.0035) | (0.0035) | (0.0037) | (0.0035) |
| Observations | 507,864 | 502,320 | 468,384 | 506,394 |

*Note:* ***, **, * denote significance at the 1%, 5% and 10% level. All specifications adapt the Spatial Error HAC Model methods by Conley (1999) as implemented by Hsiang (2010). Standard errors (in parentheses) allow for heteroskedasticity, spatial autocorrelation and temporal autocorrelation over 3 periods. Cell and year fixed effects included but not reported. Spatial radius is r=80 km. Yearly disaster intensities reflect time-weighted rolling averages over 12 subsequent monthly observations.

Table C.18 : Income Interaction

**Dependent Variable:** $\Delta \ln(\text{lights}_t)$

| | wind | | precip. | | drought | | cold | |
|---|---|---|---|---|---|---|---|---|
| | **estimate** | **combined** | **estimate** | **combined** | **estimate** | **combined** | **estimate** | **combined** |
| $\text{disaster}_t$ | −0.0015 | | 0.0171 | | −0.0120 | | 0.2442*** | |
| | (0.0016) | | (0.0118) | | (0.0093) | | (0.0389) | |
| $\text{disaster}_{t-1}$ | −0.0042*** | | 0.0249** | | 0.0081 | | −0.0680* | |
| | (0.0015) | | (0.0117) | | (0.0092) | | (0.0384) | |
| $W \cdot \text{disaster}_t$ | −0.0001 | | 0.0015 | | −0.0020 | | 0.0077 | |
| | (0.0003) | | (0.0021) | | (0.0016) | | (0.0059) | |
| $W \cdot \text{disaster}_{t-1}$ | 0.0006** | | −0.0040* | | 0.0029* | | −0.0224*** | |
| | (0.0003) | | (0.0021) | | (0.0016) | | (0.0059) | |
| $\text{disaster}_t \times$ low income | −0.0006 | −0.0021* | −0.0705*** | −0.0534*** | 0.0267** | 0.0147*** | −0.3575*** | −0.1133*** |
| | (0.0019) | (0.0011) | (0.0146) | (0.0087) | (0.0108) | (0.0056) | (0.0423) | (0.0169) |
| $\text{disaster}_{t-1} \times$ low income | −0.0076*** | −0.0119*** | −0.0057 | 0.0192** | −0.0092 | −0.0010 | 0.0484 | −0.0193 |
| | (0.0019) | (0.0011) | (0.0144) | (0.0085) | (0.0107) | (0.0055) | (0.0416) | (0.0165) |
| $W \cdot \text{disaster}_t \times$ low income | 0.0003 | 0.0001 | 0.0049* | 0.0064*** | −0.0032* | −0.0052*** | 0.0114* | 0.0191*** |
| | (0.0003) | (0.0002) | (0.0026) | (0.0016) | (0.0019) | (0.0011) | (0.0067) | (0.0031) |
| $W \cdot \text{disaster}_{t-1} \times$ low income | 0.0003 | 0.0009*** | 0.0033 | −0.0007 | −0.0029 | 0.0000 | 0.0054 | −0.0170*** |
| | (0.0003) | (0.0002) | (0.0026) | (0.0016) | (0.0019) | (0.0010) | (0.0066) | (0.0030) |
| $\ln(\text{pop}_t)$ | 0.0247*** | | 0.0258*** | | 0.0277*** | | 0.0241*** | |
| | (0.0013) | | (0.0013) | | (0.0014) | | (0.0013) | |
| $W \cdot \ln(\text{pop}_t)$ | 0.0109*** | | 0.0112*** | | 0.0115*** | | 0.0103*** | |
| | (0.0006) | | (0.0006) | | (0.0006) | | (0.0006) | |
| $\ln(\text{lights}_{t-1})$ | −0.4386*** | | −0.4366*** | | −0.4328*** | | −0.4382*** | |
| | (0.0011) | | (0.0011) | | (0.0011) | | (0.0011) | |
| $\rho$ | 0.0672*** | | 0.0672*** | | 0.0676*** | | 0.0672*** | |
| | (0.0000) | | (0.0000) | | (0.0000) | | (0.0000) | |
| Observations | 506,142 | | 500,787 | | 467,691 | | 504,525 | |

*Note:* ***, **, * denote significance at the 1%, 5% and 10% level. All specifications are SDEM and are estimated by Maximum Likelihood. Standard errors in parentheses. Cell and year fixed effects included but not reported. Spatial radius is r=80 km. Yearly disaster intensities reflect time-weighted rolling averages over 12 subsequent monthly observations.

Table C.19 : Region: Europe

**Dependent Variable:** $\Delta \ln(\text{lights}_t)$

| | **wind** | **precip.** | **drought** | **cold** |
|---|---|---|---|---|
| $\text{disaster}_t$ | −0.0034* | 0.0116 | 0.0042 | 0.0906** |
| | (0.0018) | (0.0161) | (0.0129) | (0.0442) |
| $\text{disaster}_{t-1}$ | 0.0042** | 0.0046 | 0.0011 | −0.0858* |
| | (0.0018) | (0.0160) | (0.0128) | (0.0442) |
| $W \cdot \text{disaster}_t$ | −0.0002 | 0.0033 | −0.0077*** | 0.0295*** |
| | (0.0003) | (0.0025) | (0.0019) | (0.0057) |
| $W \cdot \text{disaster}_{t-1}$ | 0.0005* | 0.0016 | 0.0006 | −0.0283*** |
| | (0.0003) | (0.0024) | (0.0019) | (0.0057) |
| $\ln(\text{pop}_t)$ | −0.0002 | 0.0010 | 0.0076 | −0.0008 |
| | (0.0054) | (0.0055) | (0.0062) | (0.0055) |
| $W \cdot \ln(\text{pop}_t)$ | 0.0011 | 0.0023 | 0.0042** | 0.0011 |
| | (0.0019) | (0.0019) | (0.0021) | (0.0019) |
| $\ln(\text{lights}_{t-1})$ | −0.5916*** | −0.5919*** | −0.5813*** | −0.5918*** |
| | (0.0031) | (0.0032) | (0.0034) | (0.0032) |
| $\rho$ | 0.0673*** | 0.0673*** | 0.0677*** | 0.0673*** |
| | (0.0000) | (0.0000) | (0.0000) | (0.0000) |
| Observations | 70,539 | 69,447 | 61,236 | 70,014 |

*Note:* ***, **, * denote significance at the 1%, 5% and 10% level. All specifications are SDEM and are estimated by Maximum Likelihood. Standard errors in parentheses. Cell and year fixed effects included but not reported. Spatial radius is r=80 km. Yearly disaster intensities reflect time-weighted rolling averages over 12 subsequent monthly observations.

Table C.20 : Region: North America

**Dependent Variable:** $\Delta \ln(\text{lights}_t)$

| | **wind** | **precip.** | **drought** | **cold** |
|---|---|---|---|---|
| $\text{disaster}_t$ | −0.0076*** | 0.0026 | −0.0245*** | 0.0256*** |
| | (0.0020) | (0.0132) | (0.0091) | (0.0428) |
| $\text{disaster}_{t-1}$ | −0.0064*** | 0.0049 | 0.0049 | −0.1636*** |
| | (0.0020) | (0.0130) | (0.0090) | (0.0421) |
| $W \cdot \text{disaster}_t$ | 0.0007* | 0.0013 | 0.0021 | 0.0111 |
| | (0.0004) | (0.0027) | (0.0019) | (0.0073) |
| $W \cdot \text{disaster}_{t-1}$ | 0.0011*** | −0.0037 | 0.0045** | 0.0022 |
| | (0.0004) | (0.0027) | (0.0019) | (0.0072) |
| $\ln(\text{pop}_t)$ | −0.0016 | −0.0026 | −0.0022 | −0.0025 |
| | (0.0020) | (0.0020) | (0.0021) | (0.0020) |
| $W \cdot \ln(\text{pop}_t)$ | 0.0013 | 0.0012 | 0.0007 | 0.0011 |
| | (0.0010) | (0.0010) | (0.0010) | (0.0010) |
| $\ln(\text{lights}_{t-1})$ | −0.5871*** | −0.5960*** | −0.5796*** | −0.5865*** |
| | (0.0027) | (0.0027) | (0.0028) | (0.0027) |
| $\rho$ | 0.0893*** | 0.0894*** | 0.0901*** | 0.0892*** |
| | (0.0004) | (0.0004) | (0.0004) | (0.0004) |
| Observations | 100,653 | 100,254 | 94,479 | 100,485 |

*Note:* ***, **, * denote significance at the 1%, 5% and 10% level. All specifications are SDEM and are estimated by Maximum Likelihood. Standard errors in parentheses. Cell and year fixed effects included but not reported. Spatial radius is r=80 km. Yearly disaster intensities reflect time-weighted rolling averages over 12 subsequent monthly observations.

Table C.21 : Region: Latin America and Caribbean

**Dependent Variable:** $\Delta \ln(\text{lights}_t)$

| | **wind** | **precip.** | **drought** | **cold** |
|---|---|---|---|---|
| $\text{disaster}_t$ | −0.0048** | −0.0659*** | 0.0373*** | −0.1388*** |
| | (0.0023) | (0.0154) | (0.0103) | (0.0239) |
| $\text{disaster}_{t-1}$ | −0.0064*** | 0.0483*** | −0.0493*** | −0.0140 |
| | (0.0023) | (0.0151) | (0.0101) | (0.0238) |
| $W \cdot \text{disaster}_t$ | 0.0012** | −0.0022 | −0.0008 | 0.0117** |
| | (0.0005) | (0.0032) | (0.0022) | (0.0046) |
| $W \cdot \text{disaster}_{t-1}$ | 0.0009* | −0.0034 | 0.0015 | 0.0086* |
| | (0.0005) | (0.0032) | (0.0022) | (0.0046) |
| $\ln(\text{pop}_t)$ | 0.0336*** | 0.0378*** | 0.0393*** | 0.0339*** |
| | (0.0037) | (0.0038) | (0.0040) | (0.0038) |
| $W \cdot \ln(\text{pop}_t)$ | 0.0178*** | 0.0173*** | 0.0166*** | 0.0156*** |
| | (0.0020) | (0.0020) | (0.0021) | (0.0020) |
| $\ln(\text{lights}_{t-1})$ | −0.4516*** | −0.4494*** | −0.4474*** | −0.4506*** |
| | (0.0028) | (0.0028) | (0.0029) | (0.0028) |
| $\rho$ | 0.0788*** | 0.0785*** | 0.0784*** | 0.0788*** |
| | (0.0008) | (0.0008) | (0.0008) | (0.0008) |
| Observations | 65,499 | 65,163 | 64,113 | 59,787 |

*Note:* ***, **, * denote significance at the 1%, 5% and 10% level. All specifications are SDEM and are estimated by Maximum Likelihood. Standard errors in parentheses. Cell and year fixed effects included but not reported. Spatial radius is r=80 km. Yearly disaster intensities reflect time-weighted rolling averages over 12 subsequent monthly observations.

Table C.22 : Region: Sout-East Asia and Pacific

**Dependent Variable:** $\Delta \ln(\text{lights}_t)$

| | **wind** | **precip.** | **drought** | **cold** |
|---|---|---|---|---|
| $\text{disaster}_t$ | −0.0032* | −0.0277* | 0.0021 | 0.1020*** |
| | (0.0017) | (0.0161) | (0.0115) | (0.0333) |
| $\text{disaster}_{t-1}$ | −0.0080*** | 0.0021 | 0.0349*** | 0.1289*** |
| | (0.0016) | (0.0159) | (0.0112) | (0.0324) |
| $W \cdot \text{disaster}_t$ | −0.0001 | 0.0014 | −0.0066** | −0.0104 |
| | (0.0004) | (0.0042) | (0.0027) | (0.0080) |
| $W \cdot \text{disaster}_{t-1}$ | 0.0001 | 0.0078* | −0.0047* | −0.0021 |
| | (0.0004) | (0.0042) | (0.0027) | (0.0078) |
| $\ln(\text{pop}_t)$ | 0.0378*** | 0.0388*** | 0.0443*** | 0.0378*** |
| | (0.0035) | (0.0035) | (0.0038) | (0.0035) |
| $W \cdot \ln(\text{pop}_t)$ | 0.0062*** | 0.0053** | 0.0062*** | 0.0065*** |
| | (0.0019) | (0.0019) | (0.0021) | (0.0019) |
| $\ln(\text{lights}_{t-1})$ | −0.4179*** | −0.4119*** | −0.4061*** | −0.4166*** |
| | (0.0022) | (0.0022) | (0.0024) | (0.0022) |
| $\rho$ | 0.0962*** | 0.0966*** | 0.0970*** | 0.0963*** |
| | (0.0004) | (0.0004) | (0.0004) | (0.0004) |
| Observations | 112,560 | 110,523 | 100,821 | 112,056 |

*Note:* ***, **, * denote significance at the 1%, 5% and 10% level. All specifications are SDEM and are estimated by Maximum Likelihood. Standard errors in parentheses. Cell and year fixed effects included but not reported. Spatial radius is r=80 km. Yearly disaster intensities reflect time-weighted rolling averages over 12 subsequent monthly observations.

Table C.23 : Region: MENA and Central Asia

| **Dependent Variable:** $\Delta \ln(\text{lights}_t)$ | | | | |
|---|---|---|---|---|
| | **wind** | **precip.** | **drought** | **cold** |
| $\text{disaster}_t$ | 0.0061** | −0.0348** | −0.0176 | −0.2588*** |
| | (0.0026) | (0.0161) | (0.0108) | (0.0496) |
| $\text{disaster}_{t-1}$ | −0.0108*** | −0.0305* | 0.0221** | −0.4732*** |
| | (0.0026) | (0.0160) | (0.0107) | (0.0487) |
| $W \cdot \text{disaster}_t$ | 0.0008 | 0.0062** | −0.0024 | 0.0455*** |
| | (0.0005) | (0.0032) | (0.0022) | (0.0081) |
| $W \cdot \text{disaster}_{t-1}$ | 0.0020*** | −0.0042 | 0.0057*** | −0.0196** |
| | (0.0005) | (0.0031) | (0.0022) | (0.0080) |
| $\ln(\text{pop}_t)$ | 0.0149*** | 0.0160*** | 0.0186*** | 0.0146*** |
| | (0.0026) | (0.0027) | (0.0027) | (0.0026) |
| $W \cdot \ln(\text{pop}_t)$ | 0.0101*** | 0.0113*** | 0.0116*** | 0.0102*** |
| | (0.0011) | (0.0011) | (0.0012) | (0.0011) |
| $\ln(\text{lights}_{t-1})$ | −0.4306*** | −0.4318*** | −0.4332*** | −0.4311*** |
| | (0.0022) | (0.0022) | (0.0022) | (0.0022) |
| $\rho$ | 0.0797*** | 0.0797*** | 0.0828*** | 0.0796*** |
| | (0.0001) | (0.0001) | (0.0002) | (0.0001) |
| Observations | 130,242 | 129,465 | 125,496 | 130,053 |

*Note:* ***, **, * denote significance at the 1%, 5% and 10% level. All specifications are SDEM and are estimated by Maximum Likelihood. Standard errors in parentheses. Cell and year fixed effects included but not reported. Spatial radius is r=80 km. Yearly disaster intensities reflect time-weighted rolling averages over 12 subsequent monthly observations.

Table C.24 : Region: Sub-Sahara Africa

| **Dependent Variable:** $\Delta \ln(\text{lights}_t)$ | | | | |
|---|---|---|---|---|
| | **wind** | **precip.** | **drought** | **cold** |
| $\text{Disaster}_t$ | 0.0011 | −0.0365 | 0.0102 | 0.1513** |
| | (0.0034) | (0.0281) | (0.0183) | (0.0618) |
| $\text{Disaster}_{t-1}$ | −0.0011 | 0.0200 | 0.0454*** | −0.0437 |
| | (0.0034) | (0.0274) | (0.0175) | (0.0588) |
| $W \cdot \text{Disaster}_t$ | −0.0003 | 0.0134* | −0.0010 | −0.0080 |
| | (0.0010) | (0.0073) | (0.0052) | (0.0166) |
| $W \cdot \text{Disaster}_{t-1}$ | 0.0016* | 0.0038 | −0.0076 | −0.0152 |
| | (0.0010) | (0.0072) | (0.0048) | (0.0158) |
| $\ln(\text{pop}_t)$ | 0.0410*** | 0.0444*** | 0.0385*** | 0.0453*** |
| | (0.0094) | (0.0094) | (0.0100) | (0.0094) |
| $W \cdot \ln(\text{pop}_t)$ | −0.0007 | −0.0040 | −0.0077 | −0.0072 |
| | (0.0048) | (0.0047) | (0.0050) | (0.0052) |
| $\ln(\text{lights}_{t-1})$ | −0.4132*** | −0.4131*** | −0.4180*** | −0.4133*** |
| | (0.0044) | (0.0045) | (0.0046) | (0.0044) |
| $\rho$ | 0.0802*** | 0.0800*** | 0.0815*** | 0.0799*** |
| | (0.0014) | (0.0014) | (0.0014) | (0.0014) |
| Observations | 28,140 | 27,993 | 26,082 | 28,035 |

*Note:* ***, **, * denote significance at the 1%, 5% and 10% level. All specifications are SDEM and are estimated by Maximum Likelihood. Standard errors in parentheses. Cell and year fixed effects included but not reported. Spatial radius is r=80 km. Yearly disaster intensities reflect time-weighted rolling averages over 12 subsequent monthly observations.

# 4 Illuminating the Spatial Connectivity of Disasters*

## 4.1 Introduction

The economic consequences of natural disasters and global warming have found soaring attention in recent years. Anthropogenic climate change could increase the frequency and severity of natural disasters which can result in dramatic economic shocks with consequences on human and economic development. To cope with the effects of climate change in the future, it is important to increase mitigation and adaptation capacities. Studying how past natural disasters have shaped economic outcomes may provide important insights into potential transmission channels to consider for reaching this objective.

A growing literature surveyed by Cavallo and Noy (2011) investigates the effect of natural disasters on economic growth. Typically, studies either use highly aggregated cross-country data (e.g., Felbermayr and Gröschl, 2013) or focus on very specific regions and episodes (e.g., Strobl, 2011). A number of problems have frequently occurred in the earlier literature. First, studies typically use information on the incidence of natural disasters from databases drawn from insurance records or news. This introduces reporting, selection and endogeneity biases, as both insurance penetration and damage are correlated with development (see Kahn, 2005; Toya and Skidmore, 2007; Felbermayr and Gröschl, 2014). To tackle these issues, Felbermayr and Gröschl (2014) propose a database which collects information on the physical intensities of geological and meteorological events from primary sources at country level. However, disasters are often local events and similar disasters affect small countries very differently from large ones (Noy, 2009). Mapping them to countries of heterogeneous size can result in measurement error and attenuation bias.[1]

*Grateful thanks apply to Vincent Stamer for able research assistance and to Andrew Bernard, Carsten Eckel, Jasmin Gröschl, Yoto Yotov and participants of the 2018 Annual Congress of the German Economic Association (Verein für Socialpolitik) for valuable comments and suggestions. The author gratefully acknowledges the compute and data resources provided by the Leibniz Supercomputing Centre (www.lrz.de).

[1] By aggregating to the country level, the difference between an event striking a densely populated coastal region or an empty desert is lost and countervailing treatment and geographic spillover effects may disguise the true local treatment effect. Strobl (2011) illustrates for the U.S. that hurricane effects are netted out at the state level and no effects are found on national economic growth rates.

Recently, Felbermayr et al. (2018) have addressed these issues by extending the empirical analysis to 24,000 geographical units in 197 countries over 21 years and by studying all natural disasters of a wide range of types, using detailed measures of physical disaster intensity. Employing satellite data on nighttime light emissions as a proxy for local economic activity (cf. Storeygard, 2016; Henderson et al., 2012, 2017) and adopting a spatial econometric fixed effects framework, the authors examine the local average treatment effects of natural disasters at the subnational level and assess potential spillovers. They find strong evidence for negative local average treatment effects and for the presence of spatial spillover effects. These spillovers are positive on average, suggesting that the relationship between locations is dominated by substitution effects rather than by complementarity.[2] While their findings suggest that these spillovers on average are local phenomena which phase out quickly over longer distances, their estimates represent simple mean effects across all neighboring cells. The exact mechanisms via which disaster effects propagate across space have been taken as a black box and are left open for research.

A key concern is the role of spillover propagation for mitigation and adaptation mechanisms (cf. Fisher et al., 2012; Deschênes and Greenstone, 2012; Burke and Emerick, 2016). Evidence on particular vehicles that facilitate mitigation include potential spillover determinants such as trade or financial openness (Felbermayr and Gröschl, 2014). Using a quantitative simulation model with high-resolution data on agricultural productivity predictions, Costinot et al. (2016) find that international trade attenuates the costs of climate change, but only weakly. Desmet and Rossi-Hansberg (2015) analyze climate change impacts on the spatial distribution of economic activity, trade, migration and welfare. Their results suggest that adaptation policies interact with innovation and the spatial pattern of economic activity. Finally, local geographic connectivity very likely plays a role in transmitting substitution or complementarity effects of disasters and thus may have implications for a location's mitigation and adaptation potential. Theory suggests that well-connected locations should find it easier to respond to shocks by importing more from other national regions or from abroad or by allowing people to escape the humanitarian and economic consequences of a disaster by relocating to less affected nearby places.

[2] If neighboring regions specialize in the same industries as the directly affected one, economic activity can shift towards them, increasing output or (in the absence of slack) the value of output there (see Hsieh and Ossa, 2016).

This study aims to explicitly assess the role of connectivity for the transmission of economic spillover effects at the grid cell level. Local spillover effects between two locations are likely to be smaller the less connected these places are with one another. Economic connectivity between grid cells can be driven by various aspects of economic life. A set of factors is provided by the gravity literature of international economics, which often uses bilateral proximity controls for given country pairs. In this literature, it is a well established empirical fact that the physical distance between two observational units reduces the amount of economic transactions between them (McCallum, 1995; Obstfeld and Rogoff, 2000; Anderson and Van Wincoop, 2003). Furthermore, economic transactions are known to be negatively affected by the need to cross national borders (Anderson and Van Wincoop, 2004; Chen, 2004). Another potential intermediating factor is provided by the literature on transport networks, focusing on the economic effects of the availability of highways (e.g., Banerjee et al., 2012; Faber, 2014). In a night-lights based study, Storeygard (2016) examines how road networks in Africa affect subnational economic growth upon oil price shocks. Closely related to this study, Amarasinghe et al. (2018) use a network model to examine how spatial spillovers from changes in mineral prices propagate through African road networks. Hence, the role of international borders and road networks for the transmission of spatial spillover effects in response to a natural disaster seems worthwhile to explore also at a global scale.

In the following, the empirical spatial spillover framework used by Felbermayr et al. (2018) is extended to unfold the black box of the spillover effects in a global analysis, by explicitly examining a selection of potential transmission channels which govern a location's connectivity with its neighbors. For this purpose, the cross-sectional variation in available geographic data on country borders and roads is exploited. Diversion of economic activity away from affected locations requires the mobility of goods and services or the mobility of people. The degree of connectivity of a disaster-struck location therefore is likely to be a driver of observed spatial spillovers. Good road networks can strengthen the effects, while limitations to connectivity (e.g., international borders) may hamper them. First, international border spillover effects are evaluated using information on the exact locations of country boundaries. Second, an infrastructure-based proxy capturing the overall ease of travel between cells is constructed using remote-sensed geographic information on road networks.

Estimates suggest that short run relocation of economic activity is subject to a border effect, a finding reminiscent of the empirical gravity literature on international trade. Spatial spillovers in the base period are driven by cells within national boundaries. For wind and extreme

precipitation events, domestic neighbors are on average the exclusive sources of statistically significant spillover effects. For droughts and cold waves, spillovers from foreign locations also matter, but magnitudes of domestic spillovers are about 2.5 times and 1.5 times the size respectively. This suggests that higher trade and migration costs hamper the short-run relocation of economic activity across international borders compared to relocation within countries. After one period, there is no evidence for statistically significant differences between domestic and foreign spillovers.

Moreover, higher connectivity along roads eases travel and lowers trade costs. Spillovers from cells that feature a connection by at least one major road are the sole driver of spatial spillovers for extreme precipitation events and feature spillover effects for droughts and cold waves that are 1.9 times and 3.5 times as strong as spillovers from cells that lack such a connection. Exploiting heterogeneity in the roads connectivity in terms of distance and the number of connections available, those neighbors with a connectivity index above the local neighborhood's median are the dominant drivers of spatial spillovers for precipitation events and cold waves, with no statistically significant difference for drought spillovers. Further distinguishing local neighbors along thirtiles of their connectivity distribution shows mixed evidence. All in all, results suggest that the overall availability of roads as well as connectivity differences at larger margins (i.e., upper vs. lower 50%) play a very important role, whereas connectivity differences at smaller margins seem less important.

The remainder of the paper is organized as follows: Section 4.2 describes the data used and discusses the proposed indicator for roads connectivity in detail. Section 4.3 presents the empirical strategy. Section 4.4 provides results, followed by a number of robustness checks in Section 4.5. The final section concludes.

## 4.2 Data

This study combines two types of data: First, it makes heavy use of the Gridded GAME Database on geological and meteorological events, including yearly information on global night-light emissions and population, as introduced by Felbermayr et al. (2018). Second, it matches this information with spatial polygon data on country borders and roads to analyze the impact of either factor on the transmission of spatial spillovers triggered by natural disasters. Section 4.2.1 briefly describes the gridded game data and its covariates. Sections 4.2.2 and 4.2.3 turn

to the polygon data and describe in detail how a new grid-cell level indicator on roads connectivity is extracted. Finally, section 4.2.4 presents descriptives and discusses the properties of this new indicator.

### 4.2.1 Natural Disasters and Economic Activity

This paper makes use of the Gridded GAME Database on geological and meteorological events described in detail by Felbermayr et al. (2018). The database partitions the globe into fields along latitude and longitude, an approach advocated by Nordhaus and Chen (2009) and Costinot et al. (2016). The balanced panel data set comprises 24,184 raster grid cells with a resolution of 0.5°×0.5° (approximately 55×55 km at the equator) spread across 197 countries from 1992 to 2013. Along with economic variables, it provides physical intensities of various weather shocks, namely wind speeds, extreme precipitation, droughts and cold waves. Wind speeds are measured by a combined indicator reflecting the maximum wind speeds from cyclone wind fields and spatially interpolated non-cyclone winds. Extreme precipitation events are identified by positive standardized precipitation anomalies above the local monthly long-run averages. Droughts are defined by negative realizations of the Standardized Precipitation Evapotranspiration Index (SPEI) which is a normalized indicator taking prolonged (3-month) periods of dryness and simultaneous potential evapotranspiration of water from the ground (e.g., due to heat) into account. Cold waves are identified by negative standardized temperature anomalies below the local monthly long-run average climatology. To align with the temporal resolution of the dependent variable, all monthly physical intensities are aggregated to the yearly level by computing time-weighted averages over a rolling window allowing each event to affect the outcome variable for exactly 12 months (compare Felbermayr et al., 2018).

Economic activity is used as the dependent variable, proxied by global night-light emissions, as included in the Gridded GAME Database. The data are obtained in the form of yearly composite satellite images from the US Air Force Defense Meteorological Satellite Program (DMSP), from which yearly mean light emissions can be extracted as a digital number (DN). The manipulation steps taken to prepare this data for econometric disaster analysis are described and discussed in detail by Felbermayr et al. (2018). In a nutshell, these steps include cropping all off-shore light pixels, masking misleading light sources like gas-flaring zones (Elvidge et al., 2009b) and active volcanoes, selecting satellite sources by coverage quality for years in which multiple satellites are available and masking pixels from the data for which the number of valid nights is zero. Finally, night-light pixels are aggregated to mean light intensity at 0.5°×0.5° grid

cell level. Night-light emission data has widely been used as a proxy for economic activity in empirical economic analyses. Henderson et al. (2012) and Storeygard (2016) find lights-to-GDP growth elasticity of around 0.3 at the country and the Chinese prefecture level, respectively. Felbermayr et al. (2018) reproduce this finding with the data at hand and in addition find strong similarity between the elasticities of lights to population density and of GDP to population density, fostering the adequacy of night-light emissions as a proxy for economic activity.

Grid cell level population is used as a control variable. 5-year target estimates at pixel level are obtained from the Gridded Population of the World (GPW) project by the Center for International Earth Science Information Network (CIESIN).[3] Summing up all pixel values within each cell yields grid cell level population numbers. These are interpolated exponentially to fill in the gaps between given 5-year periods.

### 4.2.2 Border Connectivity

To measure whether neighboring cells belong to the same or to a different country, the gridded dataset is mapped to countries along the 2011 global country boundaries defined in the high resolution Biogeo World Map Shape File provided by the Department of Environmental Science and Policy at the University of California, Davis.[4]

One grid cell coincides with at most four countries. The empirical strategy discussed in Section 4.3 requires an unambiguous mapping between cells and countries. Where a grid cell intersects more than one country, the main country is thus selected based on the relative size of its land area within a cell.

### 4.2.3 Roads Connectivity

To measure the roads connectivity of grid cells, a new globally consistent indicator is constructed by feeding remote-sensed information on global road networks into a modified Dijkstra (1959) search algorithm. Dijkstra's algorithm solves the problem of finding the shortest route between a start node and a goal node via an arbitrary number of intermediate nodes connected by paths on a predefined network. Each path has a non-negative cost weight. In the given case, nodes represent raster grid cells within a local neighborhood defined by a

[3] The data are based on census inputs collected at the lowest administrative units available, which are redistributed from their administrative census boundaries to a uniform grid by using aerial weights.

[4] `https://biogeo.ucdavis.edu/projects.html`, downloaded July 29, 2016.

constant metric search radius $r$. The cell in the neighborhood's center defines the starting node whereas all its neighbors serve as either intermediate or goal nodes. Paths represent distances between all pairs of adjacent nodes connected by roads.

Geographic information on road networks is obtained from the Environmental Systems Research Institute (Esri, 2016) who provide a globally consistent shape-file of important roads according to the DeLorme World Base Map.[5] It provides a global road network snapshot based on satellite images collected between 1999 and 2008.[6] The data includes 73,325 highways, 78,911 major roads, 3,373 local roads and 399 ferry connections.[7]

Since the separate road shapes are not always continuously connected, using them for direct routing along their shape paths is not feasible, at least at a global scale. Moreover, non-observed smaller road connections between the observed major roads are likely to exist. Both issues are addressed by not using the roads shapes as routing paths directly. Instead, the number of distinct roads leading from a cell to an adjacent neighbor is counted in terms of intersections between road shapes and cell-border polygons. For each intersection, one path is added to the network. Each path is associated with a distance proxy used as cost weight. This proxy should reflect the overall distance between the two cells, also accounting for potential intra-cell travel distance. Distances may vary across cells because of varying metric correspondence to one degree longitude $lon$ across latitude $lat$ (a result of the globe's curvature) and because of smaller land area $a$ typically associated with coastal cells.[8]

Hence, a cell's idiosyncratic distance weight is defined by the mean of its metric latitudinal dimension and the ratio between this dimension and its land area. To further approximate overall travel distance between two adjacent cells' centroids, the average between their

[5] This map is compiled by Garmin International, Inc. (formerly DeLorme Publishing Company, Inc.) from satellite imagery captured by Landsat 7 (Global Land Surveys 2000 and 2005) and the Shuttle Radar Topography Mission (SRTM).

[6] Global consistency is a key prerequisite for this research. Many available roads shape-files (e.g., Open Street Maps) are more detailed but have either strong coverage biases for certain regions of the world or are not cleaned, such that non-reasonable road patterns emerge in some locations.

[7] Ferries constitute an important source of connectivity especially for islands and will be treated as roads henceforth.

[8] While the longitudinal metric distance of 1° declines as one moves further away from the equator along latitudes, the latitudinal metric distance of 1° remains approximately constant at 110.57 km.

individual distance weights is computed. This results in the following proxy for the bilateral cell-distance $d^c$ of two adjacent cells:

$$d^c = \frac{1}{4} \sum_{i=1}^{2} \left( \frac{a^i \text{ km}^2}{lat^i \text{ km}} + lat^i \text{ km} \right) \tag{4.1}$$

For each goal cell within a local neighborhood, the search algorithm constructs a shortest-path tree from the start cell via all viable routes within this neighborhood. At each iteration, the algorithm picks the unvisited node with the lowest distance $d^c$, computes the distance through it to each of its unvisited adjacent cells. If the distance to reach any of these cells along this path is smaller than the one found in the previous iteration (or implied by the starting value), it is updated. The search algorithm stops iterating once the shortest path from the start cell to the goal cell has been found. The distance from the cell in the center to the goal cell is thus the sum of the bilateral cell distances over all nodes which jointly define the shortest path, $d = \sum_c d^c$.

If two adjacent cells are connected by multiple roads, this potentially increases the ease of transport between them and allows transport diversion if one of these roads should be congested or temporarily non-accessible. Thus, the number of roads should be reflected in the connectivity measure produced. For this reason, the algorithm allows two adjacent cells to be connected by multiple paths, whereby each path can only be part of one route for any pair of cells. The connectivity measure is then calculated as a mean over the distances $d_k$ along the $k$ shortest routes. If less than $k$ viable routes are identified for a connection between a given start and goal pair, a constant penalty distance $p$ is considered for each missing route. This penalty equals the local neighborhood radius $r$ plus half the neighborhood's circumference ($p = r + \pi r$) to represent the longest plausible geometric distance between the center of a circle and a point on its domain when initially setting out by 180° into the opposite direction.[9] The resulting indicator is defined as:

$$C = (1 - \bar{d}/p)\,, \tag{4.2}$$

where $\bar{d} = \frac{1}{k} \sum_{k=1}^{k} d_k$ is the mean distance along the $k$ shortest routes and $1/p$ is the inverse penalty for missing connections, which serves as a scaling factor. Consequently, $C$ is con-

[9] Technically, $p$ also serves as the starting value to be replaced on each routing iteration.

strained to the $[0, 1[$ interval.[10] For the baseline specification, $k = 3$ is defined to consider the availability of up to three separate routes in the indicator.[11] Finally, note that by confining nodes to cells within a given search radius, asymmetries are introduced into the connectivity matrix whenever a potential node that could lead to a shorter path between A and B lies just outside the search radius around A but within the search radius around B. Since the econometric strategy used requires symmetric weights matrices, asymmetric dyads are resolved by using the mean of the two deviating connectivity values. Section 4.2.4 examines the properties of the connectivity indicator constructed.

### 4.2.4 Descriptives

Figure 4.1 presents how the mean connectivity of each cell within an 80 km radius is distributed across the globe for the balanced estimation sample of economically active locations defined by Felbermayr et al. (2018). It can be seen that substantial heterogeneity exists across and within countries. Overall, local connectivity appears higher in highly developed countries, is especially clustered around economic centers and shows a natural decay around mountainous and desertified terrain and for islands which are disconnected by roads. These patterns are plausible and support the adequacy of the constructed connectivity measure.

Figure 4.2a depicts the cross-sectional correlation between overall cell connectivity and absolute economic activity at the end of the observed time period. The observed positive correlation suggests that economic activity tends to cluster in locations which are on average well-connected with their local neighbors by roads. The plot also shows that there is a significant amount of cells that are not connected by important roads but may still exhibit substantial economic activity. These observations account for about one fifth of the estimation sample.

Figure 4.2b compares the distribution of economic activity of cells that are completely unconnected by major roads within their local neighborhood (i.e., those with a zero connectivity in panel 4.2a) with those that are positively connected with at least one of their neighbors.

[10] A connectivity of $1$ by definition would apply only to the connectivity of each cell with itself, where distance is zero. This case however is ruled out by the need to disentangle local average treatment from spillover effects, which requires that a cell by itself must be excluded from its own set of neighbors. An index value of $0$ is obtained for $\bar{d} = p$, the longest possible mean distance.

[11] A smaller $k$ implies that more weight is given to the shortest route. A higher $k$ increases the right-skew of the connectivity distribution as it raises the likelihood of penalties. Descriptives are provided in Section 4.2.4. As part of the robustness checks in Section 4.5, $k = 1$ is considered as an alternative case.

Figure 4.1 : Global Connectivity Distribution

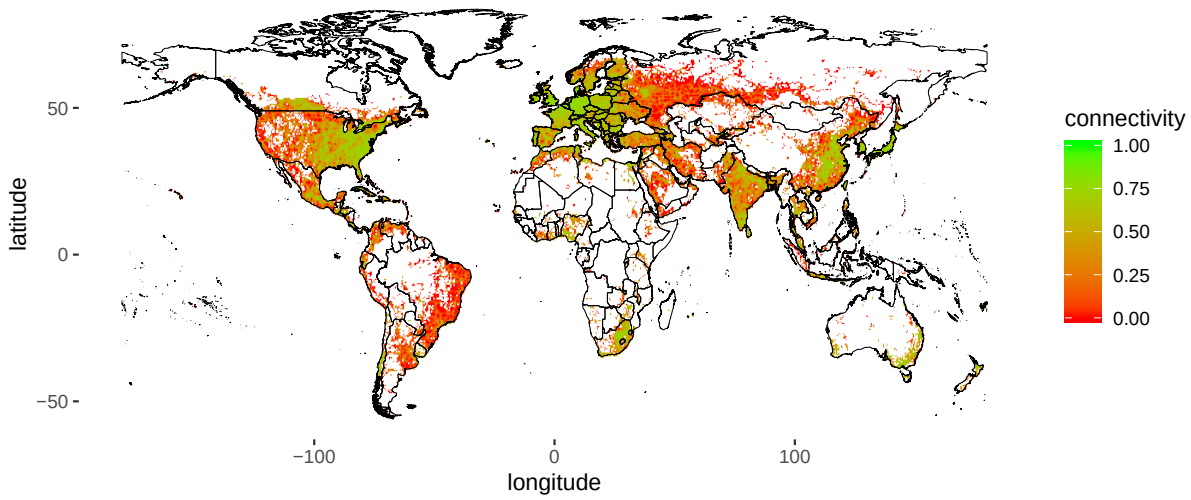


*Note:* Sources: Biogeo World Map Shape File (UC Davis), own calculations. Plotted values represent time-constant mean connectivity index realizations of locations within their local neighborhoods (80 km radius) for all observations included in the balanced estimation panel. Higher index values imply higher connectivity.

It can be seen that, while both distributions follow a bell-shape, connected cells comprise a greater relative mass of cells with stronger absolute night-light emissions than unconnected cells. Systematic differences in growth paths of connected versus unconnected cells can be controlled for in panel analysis using location fixed effects. Nevertheless, investigating potential differences in spillover effects originating in unconnected compared to connected cells appears as an interesting exercise.

Figure 4.2c shows the kernel densities of the mean connectivity by continent. It can be seen that the relative frequency of cells disconnected by roads is highest for South America and Asia. These regions also exhibit the lowest proportion of highly-connected cells. Interestingly, the proportion of disconnected cells in Africa is lower than in South America, Asia and also North America. This implies that, once a location in Africa is sufficiently active to be reflected in the night-light emissions data, its roads connectivity (in terms of overall travel distance and number of roads) within its local neighborhood is relatively good.[12] What is more, North America has a density function with two local maxima, representing the divide between many highly connected locations in the eastern states versus many lowly to intermediately connected cells in the west. Finally, the density function of Europe exhibits substantial left-skew, pointing at the continent's very advanced infrastructure and interconnectedness. This heterogeneity in

[12] Note however that information on the *quality* of given roads is not available.

Figure 4.2 : Connectivity Descriptives

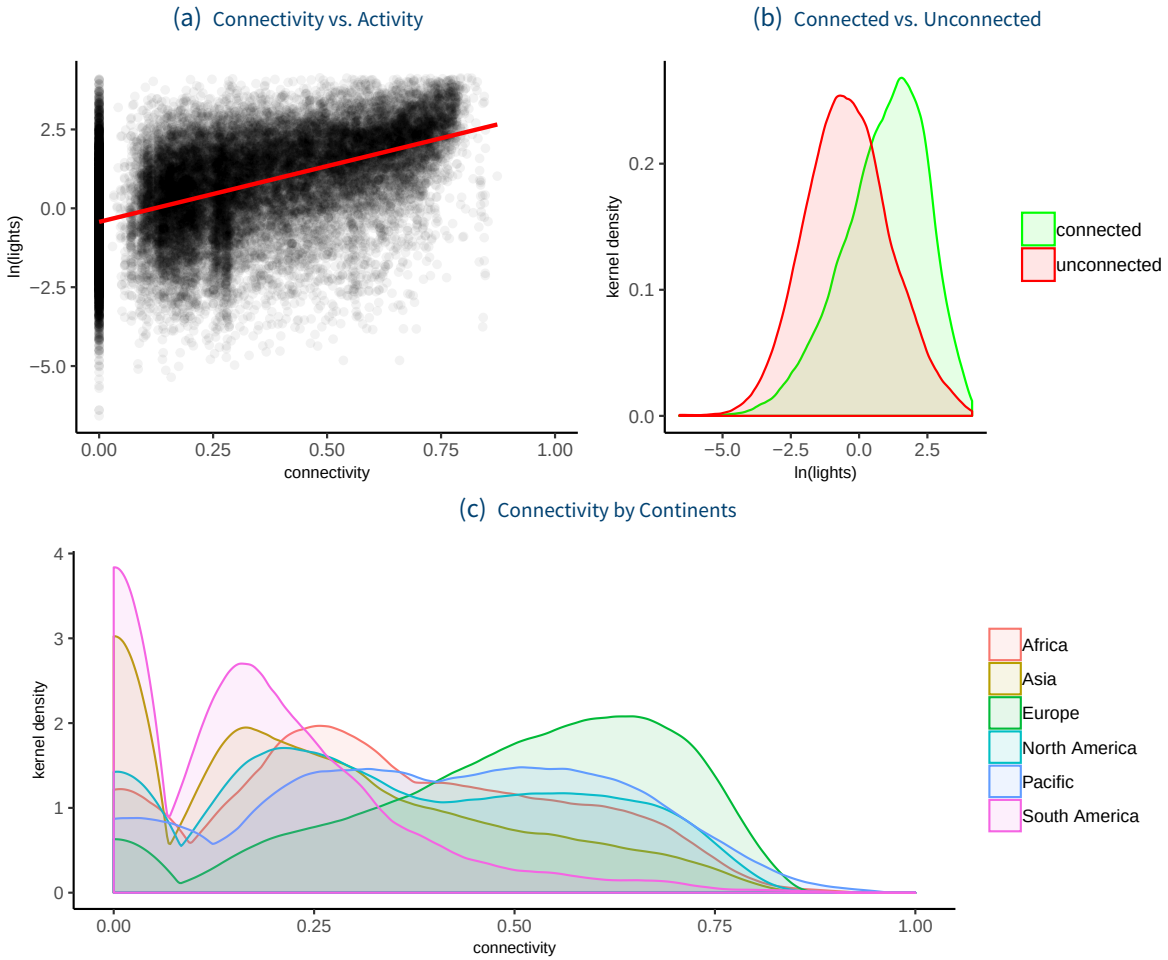


*Note:* Plotted $\ln(\text{lights})$ represent absolute logarithmic values at the end of the observational period (2013). Epanechnikov Kernel used to compute densities.

the connectivity distribution suggests that local rather than global summary statistics should serve as a reference when distinguishing local neighbors by their level of connectivity. Otherwise, identification will run the risk of capturing systematic differences across continents rather than the (relative) connectivity of locations within their neighborhood.

Figure 4.3 zooms in on selected locations to visualize the bilateral connectivity of each surrounding cell with the respective center-locations by example. Connectivity increases along the red-green spectrum with bright green representing the highest level of the connectivity index. Transparent off-center locations are not represented in the estimation panel due to the lack of economic activity (usually hinterland, desert or on-sea locations).

Figure 4.3 : Connectivity Examples

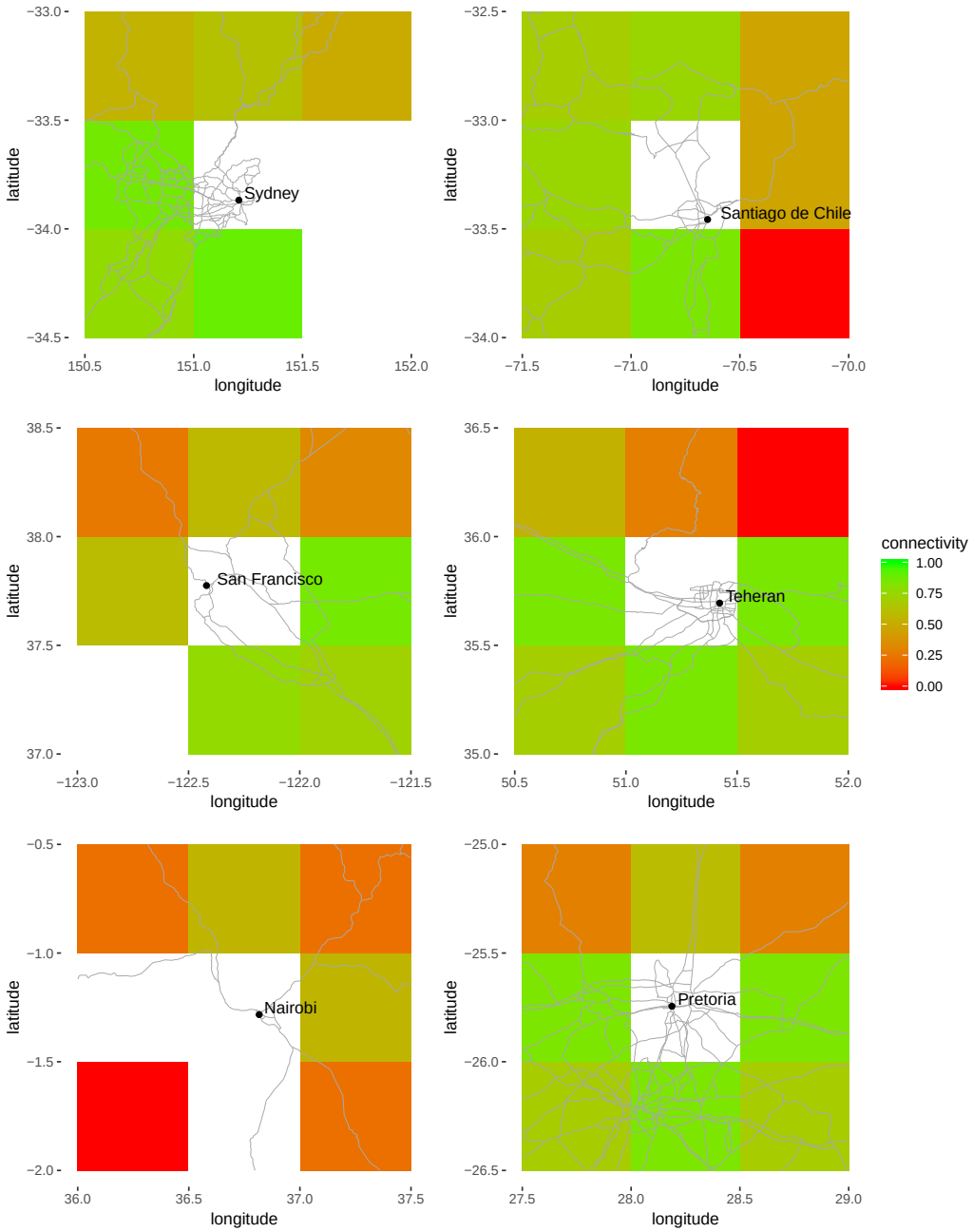


*Note:* Sources: Esri, Garmin International, Inc., own calculations. Colors reflect connectivity of cell with cell in the center. Transparent neighbors are excluded from the balanced estimation panel due to lack of economic activity.

In the case of Sydney, the highest connectivity exists with the cell to the West of the city center, to which the city extends to a large part, and to the southern cell which mostly contains ocean but also features some economically active land area in its upper left corner, which is closely connected to the city center. The South-West of Sydney's neighborhood contains the fairly

connected suburban areas around Campbelltown. In the North of the city, connectivity is lower. These cells mainly cover buildup areas in and beyond the Marramarra, Dharug, Yengo and Wollemi National Parks which impose limitations on road access.

For Santiago de Chile, the tightest connections exist with the cells in the immediate South, which includes parts of the city center and the connected towns San Bernardo and Puente Alto. The cells to the West of the city are also well connected, including a high density of small towns and linking Santiago de Chile to the seaside cities San Antonio in the south and Valparaíso and Viña del Mar in the North. The cells to the East of the city feature a relatively low connectivity, which is in line with them covering the hardly accessible Andean mountain range. For Denver on the other hand, the connections to the Rocky Mountains to the West, an economically important area during the Colorado gold rush in the 19th century, are much more pronounced than those leading into the Great Plains to the East.

To provide an example from the Middle East, Teheran is well-connected to the South, East and West, whereas it adjoins the Varjin Protected Area in the north, which is crossed exclusively by Chalus Road (visible in the top middle cell) which connects the capital to the Caspian Sea and to numerous settlements along the way. Finally, Nairobi and Pretoria serve to demonstrate the vast heterogeneity in terms of connectivity that can be found by comparing two African capital cities. While Pretoria is very well connected within its neighborhood, especially to its southern neighbor Johannesburg, the local neighborhood of Nairobi features a much less developed roads infrastructure and even contains two cells for which no economic activity is reflected in the night-lights data.

In general, holding the number of roads constant, corner cells tend towards lower connectivity index values than rook-pattern neighbors simply due to overall longer average distances along the diagonal. However, as shown by example of Denver and Teheran, variation in the number of available road connections can also lead to corner cells with higher index realizations than obtained for their contiguous rook-pattern counterparts.

Conclusively, the connectivity index provided is capable of generating plausible patterns in line with natural geographic features. It can thus be considered an adequate proxy for the true connectedness of locations.

## 4.3 Empirical Strategy

To study the relationship between natural disasters and economic growth, an empirical macroeconomic growth model à la Islam (1995) and Acemoglu et al. (2005) is used. Felbermayr et al. (2018) show that not accounting for the spatial dependence structure of the data results in omitted variable bias when analyzing the growth effects of natural disasters on local economic activity. Therefore, this study closely follows up on their approach by adopting a modified spatial Durbin error model (SDEM) with cell and year fixed effects.[13] This allows the dependent variable to be affected not only by own covariates but also by the covariates of neighboring observational units.

A fully specified panel model is estimated:

$$\Delta \boldsymbol{\ell}_t = \boldsymbol{\ell}_{t-1}\gamma + \boldsymbol{D}_t\boldsymbol{\beta^0} + \sum_i^k (\boldsymbol{C}^i \odot \boldsymbol{W}^r)\boldsymbol{D}_t\boldsymbol{\beta}^i + \boldsymbol{X}_t\boldsymbol{\delta^0} + \boldsymbol{W}^r\boldsymbol{X}_t\boldsymbol{\delta^1} + \boldsymbol{\nu} + \boldsymbol{\pi} + \boldsymbol{u}_t \quad (4.3)$$

$$\boldsymbol{u}_t = \rho\boldsymbol{W}^r\boldsymbol{u}_t + \boldsymbol{\varepsilon}_t$$

where $\Delta\boldsymbol{\ell}_t$ is a proxy for grid-cell level economic growth rates, measured by annual changes in the natural logarithm of mean night-light intensity $\Delta\boldsymbol{\ell}_t \equiv \ln\left(\overline{\textbf{light}}_t\right) - \ln\left(\overline{\textbf{light}}_{t-1}\right)$. $\boldsymbol{D}_t$ represents physical disaster intensities and temporal lags and $\boldsymbol{X}_t$ contains controls.

$\boldsymbol{\nu}$ is a vector of cell fixed effects controlling for time-constant local unobservables and required to account for systematic cross-latitude measurement error in night-lights due to aurora, the solar cycle, and stray light. Importantly, as pointed out by Felbermayr et al. (2018), these fixed effects take out location-specific baseline risk which determines the extent to which disasters occur unexpectedly. Thus, cell fixed effects restrict identification to the unexpected component of treatment variation, respecting that expected events should not affect economic behavior of rational agents which have already taken their occurrence into account. Other time-constant local characteristics comprise potential structural determinants of the relationship between light use and GDP growth, such as political, cultural, historical and geographic fundamentals. Since these fixed effects control for all time-constant structural fundamentals, estimates obtained from model (4.3) must be interpreted in terms of percentage point changes in economic activity above or below the local growth path.

[13] For a detailed description of the standard SDEM, see Anselin (2013) and Halleck Vega and Elhorst (2015).

$\pi$ represents a complete set of time fixed effects. These capture not only time variation in unobserved global characteristics, such as technological progress and the global business cycles, but are also required to control for systematic variation in the measurement of light emissions over time: The capacity of sensors on board the satellites varies systematically as they erode over their life-cycle or are replaced by newer models.[14] To allow for inter-temporal comparison of light intensities, Henderson et al. (2012) propose using time fixed effects to control for systematic temporal variation in sensor capacity.[15]

$\boldsymbol{W}^r$ is a time-invariant $K \times K$ dimensional spatial weights matrix with binary elements, filtering all neighboring observational units from the data which lie within a spatial radius $r$ around a given location, as recommended by Conley (2008).[16] A constant metric radius $r$ is chosen to ensure that the geodesic area of neighborhoods does not vary systematically across latitude.[17] In this study, $r$ is set to 80 km, which effectively respects eight adjacent cells at the equator.[18]

In principle, interacting $\boldsymbol{W}^r$ with treatment variables allows controlling for the treatment of neighbors and to explicitly assess associated spillovers. However, testing the more detailed hypothesis whether those spillover effects are transmitted via a specific connectivity channel demands for a more sophisticated approach. This demand is addressed in this study by constructing a set of $k$ connectivity matrices $\boldsymbol{C}^{\boldsymbol{i}}$, $i \in k$. Each matrix consists of binary elements assigning a weight of one to all neighbors satisfying a defined connectivity criterion and zero to all others. With respect to the selection criteria, all connectivity matrices from a joint set used to test a specific hypothesis must be mutually exclusive and collectively exhaustive (MECE) relative to the universe of neighbors defined by $\boldsymbol{W}^r$. Each connectivity matrix is multiplied element-wise with $\boldsymbol{W}^r$, such that $\boldsymbol{C}^i \odot \boldsymbol{W}^r$ provides a combined filter extracting groups of neighboring cells within radius $r$ that satisfy a common connectivity criterion $i$. Multiplying

[14] The rate of variation in sensor capacity is not documented.

[15] A different approach is proposed by Elvidge et al. (2009b, 2014), who inter-calibrate the original pixel data by normalizing all values to a base year for a reference area which they assume to have very little change in true light emission throughout the entire observational period. The fixed effects approach is a superior alternative in the sense that it does not require such assumptions on the stability of lights in any temporal or spatial window.

[16] This structure implies that the same set of neighbors must be used for each observational unit throughout the entire period of analysis, i.e., the panel must be balanced.

[17] The metric length of 0.5° longitude decreases with latitudinal distance to the equator due to earth's curvature, such that a varying number of cells are included into a neighborhood along the longitudinal axis.

[18] Felbermayr et al. (2018) extend this spatial radius to 160 km, finding that average spillovers from this greater neighborhood are significantly smaller. This suggests that spatial spillovers from natural disasters are a rather local phenomenon.

variables with this filter produces group-specific spatial lags. $\beta^i$ thus reflects the average local spillover effect of a marginal change in the natural disaster indicator in *one* neighboring cell that falls into a given group $i$.

Note that the matrix multiplications that represent the spillover terms essentially produce sums over treatments of particular groups of cells surrounding a location for which the dependent variable captures variation in economic activity. This has two implications.

First, even though it may seem suggestive, identification along a quasi difference-in-difference specification that compares the spillovers from a certain category of neighboring cells to a left-out base category and a spillover term capturing the full set of neighbors is econometrically unfeasible. In a standard difference-in-difference setup, identification relies on differences across observations where each observation belongs to only one difference group and variation in the dependent variable across these groups is exploited. In the given framework, this is clearly not the case. Instead, exogenous treatment of different neighboring groups is assumed to jointly affect the outcome of the *same* observational unit. This relationship can only be captured by explicitly defining treatments of different groups of neighbors as separate explanatory factors of the same outcome, hence the use of multiple MECE spillover terms.

Second, the sums over different groups of neighboring cells may follow different distributions. To make coefficient magnitudes directly comparable within the vector $\beta^i$, the spillover terms' distributions must be harmonized. This is done by computing z-scores, i.e., standard-normalizing all spillover terms by subtracting their arithmetic mean and dividing by their respective standard deviation. Note that spillover coefficient magnitudes from this specification cannot be interpreted in terms of physical disaster intensity. Nevertheless, the procedure serves its purpose by allowing testing for statistical equality of the spillover effects exerted by different groups of neighbors, using a Wald Chi-Squared Test. Also, the relation of both coefficients hinges at by how much the effects presented by Felbermayr et al. (2018) are driven by particular channels.

It must be acknowledged that entries of the connectivity matrix $\boldsymbol{C}^i$ may to some extent be endogenous, e.g., in the case of roads connectivity. First, this problem is alleviated by the use of cell fixed effects, which absorb all unobservable cell-specific links between economic growth and connectivity. Moreover, the term of interest is not $\boldsymbol{C}^i$ itself, but its interaction with the disaster treatment variable. As shown by Nizalova and Murtazashvili (2016) and Beverelli

et al. (2018), potential endogeneity vanishes upon interaction with an exogenous variable. Hence, as $C^i$ is multiplied with physical intensities of natural disasters, estimates will be consistent if disaster intensities are uncorrelated with the elements of $C^i$ or potential omitted variables.[19] This is the case, given the exogenous nature of the treatment variable.

Finally, the term $u_t$ allows for spatial auto-correlation in the residuals. Thus, model (4.3) accounts for spatial clustering and spillovers in unobserved characteristics, which potentially result from the fact that boundaries of superimposed grid cells arbitrarily intersect true economic units such that neighboring cells may share common business cycles and institutions.[20]

This model is estimated using the spatial Maximum Likelihood fixed effects estimator provided by Millo and Piras (2012) and Millo (2014).

## 4.4 Results

This section presents results on three different aspects of connectivity. Section 4.4.1 explores whether spillover effects are subject to the border effect known from the gravity literature of international economics. Section 4.4.2 will assess the role of infrastructure by examining whether the existence of important roads is driving spillover effects. Finally section 4.4.3 goes one step further by evaluating whether heterogeneity in roads connectivity, defined by a combination of the number and the approximate length of available road links, is relevant for explaining spillover magnitudes.

### 4.4.1 International Borders

In this section, the impact of country borders on the spillover effects of natural disasters is isolated. If national boundaries pose a friction to the relocation of economic activity, it can be expected that, at least in the short-run, spatial spillovers are confined within a country rather than crossing national borders. For this purpose, the connectivity term from equation (4.3) is

[19] Beverelli et al. (2018) employ an instrumental variable (IV) estimator to re-assure that IV estimates are not statistically different from estimates obtained without instrumenting for potentially endogenous institutions, which they use as an interaction variable.

[20] By comparing the baseline SDEM model with a spatial lag of X (SLX) model and conducting Moran's $I$ test, Felbermayr et al. (2018) show that accounting for residual spatial auto-correlation (RSA) is crucial in this context to obtain unbiased spatial estimates.

defined as $\sum_i^k \boldsymbol{C^i} = \boldsymbol{C}^{\text{same}} + \boldsymbol{C}^{\text{diff}}$, where $\boldsymbol{C}^{\text{same}}$ assigns a weight of one to all cells belonging to the same country and a weight of zero to all others, whereas $\boldsymbol{C}^{\text{diff}}$ does the exact opposite.

Table 4.1 : Border Effect

**Dependent Variable:** $\Delta \ln(\text{lights}_t)$

| | **wind** | **precip.** | **drought** | **cold** |
|---|---|---|---|---|
| $\text{disaster}_t$ | −0.0048*** | −0.0295*** | 0.0116** | −0.0562*** |
| | (0.0009) | (0.0069) | (0.0047) | (0.0133) |
| $\text{disaster}_{t-1}$ | −0.0068*** | 0.0181*** | −0.0017 | −0.0784*** |
| | (0.0009) | (0.0068) | (0.0046) | (0.0130) |
| $C^{\text{same}} \odot W^r \cdot \text{disaster}_t$ | 0.0405*** | 0.0071*** | −0.0090*** | 0.0240*** |
| | (0.0099) | (0.0019) | (0.0016) | (0.0030) |
| $C^{\text{diff}} \odot W^r \cdot \text{disaster}_t$ | −0.0006 | −0.0005 | −0.0036*** | 0.0162*** |
| | (0.0100) | (0.0016) | (0.0012) | (0.0034) |
| $C^{\text{same}} \odot W^r \cdot \text{disaster}_{t-1}$ | 0.0156 | −0.0019 | 0.0021 | −0.0120*** |
| | (0.0098) | (0.0018) | (0.0016) | (0.0030) |
| $C^{\text{diff}} \odot W^r \cdot \text{disaster}_{t-1}$ | 0.0332*** | 0.0003 | 0.0036*** | −0.0160*** |
| | (0.0099) | (0.0016) | (0.0012) | (0.0033) |
| $\ln(\text{pop}_t)$ | 0.0247*** | 0.0257*** | 0.0276*** | 0.0243*** |
| | (0.0013) | (0.0013) | (0.0014) | (0.0013) |
| $W^r \cdot \ln(\text{pop})_t$ | 0.0109*** | 0.0112*** | 0.0115*** | 0.0106*** |
| | (0.0006) | (0.0006) | (0.0006) | (0.0006) |
| $\ln(\text{lights}_{t-1})$ | −0.4387*** | −0.4367*** | −0.4329*** | −0.4380*** |
| | (0.0011) | (0.0011) | (0.0011) | (0.0011) |
| $\rho$ | 0.0672*** | 0.0672*** | 0.0676*** | 0.0672*** |
| | (0.0000) | (0.0000) | (0.0000) | (0.0000) |
| Observations | 507,864 | 502,026 | 468,174 | 506,037 |

*Note:* ***, **, * denote significance at the 1%, 5% and 10% level. All specifications are SDEM and are estimated by Maximum Likelihood. Standard errors in parentheses. Cell and year fixed effects included but not reported. Spatial radius is r=80 km. Yearly disaster intensities reflect time-weighted rolling averages over 12 subsequent monthly observations. $C^i \odot W^r \cdot \text{disaster}_t$ terms represent corresponding z-scores. Wald Chi-Squared Tests on equality of spillover estimates provided in Table D.4.

Results are presented in Table 4.1. Estimates of the core variables are broadly in line with the findings by Felbermayr et al. (2018). Results for wind speeds, extreme precipitation and cold waves suggest negative local average treatment effects on the growth rate in economic activity in the base period with heterogeneous persistence after one year. Spillover effects for these events are overall positive in the treatment period, suggesting that substitution effects outweigh complementarity of neighboring locations. Droughts show a different behavior, with a positive local average treatment effect and negative spillovers. Using a machine learning classification approach, Felbermayr et al. (2018) show that this pattern is driven by a rural/urban divide, according to which drought treatment of rural cells enacts a negative impact on nearby urban locations. Population sizes of cells and their neighbors show a positive impact on the growth in economic activity.

Concerning the impact of national borders on the transmission of spillover effects, it can be seen that for all disaster types regional economic linkages matter more than international ones in the short-run. Hence, spillovers in the base period $t$ are more pronounced for domestic neighboring cells than for cells in neighboring foreign countries. Domestic cells are the exclusive driver of spillover effects for wind and precipitation events and also exhibit significantly stronger effects than foreign cells for droughts and cold waves, with magnitudes about 2.5 times and 1.5 times the size, respectively. In the second period $t-1$, statistically significant effects can be also be observed for foreign neighbors.

Wald Chi-Squared Tests suggest that the similarity of spillover effects from domestic and foreign cells is overwhelmingly rejected in the treatment period for all disaster types but cannot be rejected for the temporal lags of spillovers. Test results are presented in Table D.4.

Thus, results provide evidence that short-run relocation of economic activity is mostly (if not exclusively) domestic, while over longer periods country borders are overcome possibly by international adaptation activities.[21]

### 4.4.2 Road Existence

In this section, the role of the general availability of transport infrastructure as a transmission channel for spatial spillovers is assessed. For about one fifth of observations in the sample the data does not suggest any major roads to connect them to their neighbors. However, these locations may still be subject to substantial economic activity, compare figure 4.2b. If the availability of major roads plays a significant role in the transmission of disaster spillovers, exploiting this cross-sectional feature of the data should provide the corresponding evidence.[22] The most straightforward way to assess the impact of infrastructure availability is to examine whether treatment period spillovers from those neighbors that are connected by roads are stronger than from those that are not. Moreover, if relocation of economic activity occurs towards locations lacking direct connections by major roads, it must be assumed that this relocation is more costly than it would be if locations had such a connection. Therefore, it can

[21] For example, international relocation of activity might take longer because cross-border transactions (i.e., international trade and migration) may be subject to bureaucratic and knowledge constraints that do not or to a lesser extent apply to domestic relocation. Where overcoming these constraints is a viable strategy, this potentially involves some adjustment time.

[22] Even in the absence of observed roads, spatial spillovers could theoretically be transmitted via small roads not captured by the data. Moreover, navigable waterways and railways could provide an alternative source of connectivity, which is beyond the scope of this paper and left for future research.

be expected that relocation of economic activity to unconnected locations is more likely to be reversed over time than for connected ones.

For this purpose, the connectivity term from equation (4.3) is defined as $\sum_i^k \boldsymbol{C}^i = \boldsymbol{C}^{\text{roads}} + \boldsymbol{C}^{\text{no-roads}}$, where $\boldsymbol{C}^{\text{roads}}$ assigns a weight of one to all neighbors connected by at least one road, whereas $\boldsymbol{C}^{\text{no-roads}}$ captures neighbors that lack such a connection. Results are presented in Table 4.2.

Table 4.2 : Road Existence

**Dependent Variable:** $\Delta \ln(\text{lights}_t)$

| | **wind** | **precip.** | **drought** | **cold** |
|---|---|---|---|---|
| $\text{disaster}_t$ | −0.0012 | −0.0301*** | 0.0126*** | −0.0338** |
| | (0.0009) | (0.0069) | (0.0047) | (0.0146) |
| $\text{disaster}_{t-1}$ | −0.0062*** | 0.0163** | −0.0054 | −0.0513*** |
| | (0.0009) | (0.0068) | (0.0047) | (0.0144) |
| $C^{\text{roads}} \odot W^r \cdot \text{disaster}_t$ | −0.0125 | 0.0106*** | −0.0105*** | 0.0280*** |
| | (0.0124) | (0.0021) | (0.0016) | (0.0041) |
| $C^{\text{no-roads}} \odot W^r \cdot \text{disaster}_t$ | −0.0086 | 0.0008 | −0.0055*** | 0.0080** |
| | (0.0120) | (0.0019) | (0.0014) | (0.0040) |
| $C^{\text{roads}} \odot W^r \cdot \text{disaster}_{t-1}$ | 0.0093 | −0.0008 | 0.0021 | −0.0212*** |
| | (0.0123) | (0.0021) | (0.0016) | (0.0040) |
| $C^{\text{no-roads}} \odot W^r \cdot \text{disaster}_{t-1}$ | 0.0197* | −0.0015 | 0.0059*** | −0.0255*** |
| | (0.0119) | (0.0019) | (0.0014) | (0.0040) |
| $\ln(\text{pop}_t)$ | 0.0249*** | 0.0258*** | 0.0276*** | 0.0244*** |
| | (0.0013) | (0.0013) | (0.0014) | (0.0013) |
| $W^r \cdot \ln(\text{pop})_t$ | 0.0109*** | 0.0113*** | 0.0116*** | 0.0106*** |
| | (0.0006) | (0.0006) | (0.0006) | (0.0006) |
| $\ln(\text{lights}_{t-1})$ | −0.4386*** | −0.4368*** | −0.4329*** | −0.4380*** |
| | (0.0011) | (0.0011) | (0.0011) | (0.0011) |
| $\rho$ | 0.0672*** | 0.0672*** | 0.0676*** | 0.0672*** |
| | (0.0000) | (0.0000) | (0.0000) | (0.0000) |
| Observations | 507,864 | 502,026 | 468,174 | 506,037 |

*Note:* ***, **, * denote significance at the 1%, 5% and 10% level. All specifications are SDEM and are estimated by Maximum Likelihood. Standard errors in parentheses. Cell and year fixed effects included but not reported. Spatial radius is r=80 km. Yearly disaster intensities reflect time-weighted rolling averages over 12 subsequent monthly observations. $C^i \odot W^r \cdot \text{disaster}_t$ terms represent corresponding z-scores. Wald Chi-Squared Tests on equality of spillover estimates provided in Table D.5.

All four regressions show very similar effects for all control variables as in Table 4.1. Moreover, direct treatment effects and their temporal lags are very similar, albeit with a loss of statistical significance for wind speeds in the base period. Concerning disaster spillovers, results show strong evidence that the availability of road connections is a key driver of the diversion of economic activity across space upon disaster treatment. For extreme precipitation events, estimates suggest that the spatial disaster spillover in the treatment period is driven exclusively by locations which are connected by roads. For droughts and cold waves, both connected and

unconnected cells are represented in the spillover patterns. Therein, connected neighbors account for drought and cold spillover effects twice and more than three times the magnitude of those from unconnected cells. For wind speeds, taking the existence of road connections into account results in negative point estimates for disaster spillovers. This may hint at complementarity rather than substitution effects to dominate the aggregate spillover. However, these point estimates are not statistically significant and and must therefore be taken with caution. With one year time lag, spillover estimates feature sign reversals for all disaster types, indicating that effects are to some extent reversed. In line with expectations, those reversals appear stronger for locations that lack a direct roads connection.

Wald Chi-Squared Tests suggest that the similarity of spillover effects from connected and unconnected cells is rejected in the treatment period for all disaster types but wind speeds. It cannot be rejected for the temporal lags of spillovers with the exception of droughts. Test results are presented in Table D.5.

### 4.4.3 Road Heterogeneity

This section attempts to provide a deeper understanding of the role of roads connectivity by further exploiting the cross-sectional variation in connectivity index magnitudes. Given that a higher connectivity of locations should simplify the relocation of economic activity upon exogenous shocks, findings should reflect a positive relationship between roads connectivity and spatial spillover effects not only for connected vs. unconnected locations, but also along the connectivity distribution. The connectivity measure described in Section 4.2.3 increases in inverse distance and in the number of up to 3 independent road connections to choose from.[23]

To allow assessing the role of connectivity in the transmission of spillovers, neighbors are classified into bins. For this matter it is important to define an appropriate selection criterion. Thereby, a relative notion of connectivity is implicitly assumed. Choosing a global or regional (beyond local) reference value induces a risk of undesired outcomes when constructing connectivity bins. For example, spillovers from highly connected cells may effectively

[23] If more roads are available, economic ties between locations are very likely more tight and routing of economic exchange can be diverted more easily if one connection is subject to destruction or congestion. Thus, the algorithm used is searching for the three shortest routes and adds a penalty if only less than three routes exist. The choice of this 3-routes-criterion is arbitrary. In the sensitivity analyses, it will therefore be relaxed, such that only the length of the single shortest connection is considered.

over-represent locations from Western Europe and the East Coast of the United States of America. Since these locations also stand out in terms of other characteristics which can be correlated with roads infrastructure, connectivity categories constructed using beyond-local reference values may result in confounded estimates capturing regional differences in the spillover mechanism due to unobserved characteristics rather than informing about the role of roads.

To circumvent this caveat, relative connectivity classes should be defined locally such that bins capture all neighboring cells by their relative connectivity compared to all other cells within the same neighborhood.[24] Therefore, the connectivity distribution within the local neighborhood will serve as as a reference for binning. Because the number of local neighbors is naturally limited by the fixed search radius, so is the number of bins to be constructed.

In a first step, two bins are considered, dividing neighbors into highly and lowly connected ones, $\sum_i^k \boldsymbol{C}^i = \boldsymbol{C}^{\text{high}} + \boldsymbol{C}^{\text{low}}$. The splitting criterion is the median of the local distribution, which ensures that each group can be represented in the neighborhood of each observational unit and that both groups are approximately equal in size.[25]

Results are presented in Panel A of Table 4.3. Estimates of the direct local disaster treatment effect are overall in line with the estimates obtained from previous specifications. Spillover estimates suggest that disaster spillovers from neighbors with above median connectivity are stronger than those from cells with below median connectivity for extreme precipitation, droughts and cold waves in the treatment period. Point estimates for wind speeds suggest negative spillovers (complementarity) for highly connected neighbors and positive spillovers (substitution) for lowly connected ones, albeit with a lack of statistical significance at the 10% level. After one period, spillover estimates exhibit sign reversals, suggesting that relocation of economic activity in the treatment period is partially temporary. To the extent that these time lags are statistically significant, they are more pronounced for neighbors with a low connectivity. This finding is in line with theoretical considerations, suggesting that transactions across worse connections tend to be more costly and might therefore not be upheld over an extended period.

[24] A neighboring location which is badly connected overall could still be relatively important for the spillover mechanism, if other nearby places feature connections that are even worse. Section 4.2.4 illustrates the heterogeneous distribution of roads connectivity across and within countries.

[25] Cells that have a connectivity which is exactly equal to the median are classified as highly connected. If however all cells in a neighborhood have a connectivity index of zero, these are defined as lowly connected. Robustness Section 4.5.1 provides estimates using the local mean as an alternative selection criterion.

Table 4.3 : Road Heterogeneity

| **Dependent Variable:** $\Delta \ln(\text{lights}_t)$ | | | | |
|---|---|---|---|---|
| | **wind** | **precip.** | **drought** | **cold** |
| **PANEL A: Connectivity above and below median** | | | | |
| $\text{disaster}_t$ | −0.0025*** | −0.0277*** | 0.0133*** | −0.0432*** |
| | (0.0009) | (0.0069) | (0.0047) | (0.0141) |
| $\text{disaster}_{t-1}$ | −0.0052*** | 0.0211*** | −0.0042 | −0.0776*** |
| | (0.0009) | (0.0068) | (0.0047) | (0.0138) |
| $C^{\text{high}} \odot W^r \cdot \text{disaster}_t$ | −0.0051 | 0.0074*** | −0.0067*** | 0.0213*** |
| | (0.0088) | (0.0015) | (0.0012) | (0.0028) |
| $C^{\text{low}} \odot W^r \cdot \text{disaster}_t$ | 0.0141 | 0.0012 | −0.0059*** | 0.0102*** |
| | (0.0087) | (0.0015) | (0.0013) | (0.0029) |
| $C^{\text{high}} \odot W^r \cdot \text{disaster}_{t-1}$ | −0.0030 | −0.0018 | 0.0003 | −0.0089*** |
| | (0.0087) | (0.0015) | (0.0012) | (0.0028) |
| $C^{\text{low}} \odot W^r \cdot \text{disaster}_{t-1}$ | −0.0004 | −0.0018 | 0.0042*** | −0.0107*** |
| | (0.0086) | (0.0015) | (0.0013) | (0.0028) |
| **PANEL B: Connectivity thirtiles** | | | | |
| $\text{disaster}_t$ | −0.0015* | −0.0266*** | 0.0135*** | −0.0350** |
| | (0.0009) | (0.0069) | (0.0047) | (0.0145) |
| $\text{disaster}_{t-1}$ | −0.0051*** | 0.0217*** | −0.0052 | −0.0675*** |
| | (0.0009) | (0.0069) | (0.0047) | (0.0142) |
| $C^{\text{high}} \odot W^r \cdot \text{disaster}_t$ | −0.0017 | 0.0057*** | −0.0058*** | 0.0113*** |
| | (0.0089) | (0.0015) | (0.0012) | (0.0031) |
| $C^{\text{medium}} \odot W^r \cdot \text{disaster}_t$ | −0.0072 | 0.0031** | −0.0028** | 0.0130*** |
| | (0.0090) | (0.0015) | (0.0012) | (0.0032) |
| $C^{\text{low}} \odot W^r \cdot \text{disaster}_t$ | −0.0018 | 0.0005 | −0.0054*** | 0.0086*** |
| | (0.0090) | (0.0015) | (0.0012) | (0.0030) |
| $C^{\text{high}} \odot W^r \cdot \text{disaster}_{t-1}$ | −0.0098 | −0.0018 | 0.0002 | −0.0049 |
| | (0.0088) | (0.0015) | (0.0012) | (0.0030) |
| $C^{\text{medium}} \odot W^r \cdot \text{disaster}_{t-1}$ | 0.0030 | −0.0001 | 0.0012 | −0.0078** |
| | (0.0089) | (0.0015) | (0.0012) | (0.0032) |
| $C^{\text{low}} \odot W^r \cdot \text{disaster}_{t-1}$ | 0.0015 | −0.0022 | 0.0041*** | −0.0146*** |
| | (0.0089) | (0.0015) | (0.0012) | (0.0030) |
| Observations | 507,864 | 502,026 | 468,174 | 506,037 |

*Note:* ***, **, * denote significance at the 1%, 5% and 10% level. All specifications are SDEM and are estimated by Maximum Likelihood. Standard errors in parentheses. Cell and year fixed effects included but not reported. Spatial radius is r=80 km. Yearly disaster intensities reflect time-weighted rolling averages over 12 subsequent monthly observations. $C^i \odot W^r \cdot \text{disaster}_t$ terms represent corresponding z-scores. Additional controls included but not reported. Full results are shown in Tables D.2 and D.3 in the Appendix. Wald Chi-Squared Tests on equality of spillover estimates provided in Tables D.6 and D.7.

Conducting Wald Chi-Squared Tests on the similarity of spillover effects from highly versus lowly connected cells shows that similarity is rejected in the treatment period for all disaster types except for droughts. In contrast, droughts feature the only statistically significant spillover difference after one period. Test results are provided in Table D.6.

In a second step, the number of bins is increased to distinguish high, medium and low connectivity neighbors, $\sum_i^k \boldsymbol{C^i} = \boldsymbol{C}^{\text{high}} + \boldsymbol{C}^{\text{medium}} + \boldsymbol{C}^{\text{low}}$. These are selected along the respective

thirtiles of the local neighborhoods' connectivity distributions. Results are presented in Panel B of Table 4.3. Again, the spillover effects of wind speeds turn out statistically insignificant. For the remaining disaster types, a mixed spillover pattern is observed. For extreme precipitation events, a clear hierarchy emerges, with spillover magnitudes gradually declining from high over middle to low connectivity neighbors. For drought events, spillovers are similar for highly and lowly connected cells, but are only half as high for cells with a medium connectivity. Finally, cold wave spillovers are weakest for lowly connected neighbors and in a similar order of magnitude for cells with a high and middle connectivity.[26] Again, as far as time lags of spatial spillovers have statistically significant estimates, these are more pronounced for neighbors with a lower connectivity.

Pairwise Wald Chi-Squared Test results on the similarity of spillovers between groups show mixed findings and are presented in Table D.7. Wind speeds do not show any statistically significant difference. For precipitation events, significant differences exist between spillovers from highly and lowly connected cells in the treatment period. Drought events stipulate significant differences between intermediately and lowly connected origins in the treatment period and for highly or intermediately connected cells compared to lowly connected cells after one period. For cold waves, equality can only be rejected for the temporal lag and between either highly or intermediately connected cells and lowly connected ones.

## 4.5 Robustness Analysis

In this section, a number of sensitivity checks are performed concerning the definition of connectivity. First, the splitting criterion for the assessment of lowly vs. highly connected neighbors is altered. Second, the sample composition is changed by removing observations which feature insufficient local neighbors to allow forming multiple groups. Finally, the connectivity index is modified to not incorporate the number of connections but only the length of the single shortest path.

### 4.5.1 Splitting Criterion: Local median vs. local mean

As a first check, the sensitivity of the results presented in Panel A of Table 4.3 with respect to the selection criterion for dividing neighbors into highly and lowly connected ones shall be

[26] While the point estimate is larger for neighbors with a medium compared to high connectivity, the difference is not statistically significant.

assessed. In the baseline, the median connectivity within the local neighborhood serves as a cutoff criterion between the two categories in order to separate the top half of neighboring observations from the bottom half. One advantage of this approach is that both neighboring groups should approximately be equal in size. To check whether results are sensitive to the exact definition of this reference criterion, the local median is replaced by the local arithmetic mean.

Table 4.4 : Connectivity Above and Below Local Mean

| **Dependent Variable:** $\Delta \ln(\text{lights}_t)$ | | | | |
|---|---|---|---|---|
| | **wind** | **precip.** | **drought** | **cold** |
| $\text{disaster}_t$ | −0.0025*** | −0.0276*** | 0.0131*** | −0.0471*** |
| | (0.0009) | (0.0069) | (0.0047) | (0.0143) |
| $\text{disaster}_{t-1}$ | −0.0050*** | 0.0211*** | −0.0043 | −0.0733*** |
| | (0.0009) | (0.0068) | (0.0047) | (0.0140) |
| $C^{\text{high}} \odot W^r \cdot \text{disaster}_t$ | −0.0056 | 0.0069*** | −0.0072*** | 0.0201*** |
| | (0.0090) | (0.0015) | (0.0012) | (0.0029) |
| $C^{\text{low}} \odot W^r \cdot \text{disaster}_t$ | 0.0145 | 0.0020 | −0.0059*** | 0.0143*** |
| | (0.0089) | (0.0015) | (0.0013) | (0.0030) |
| $C^{\text{high}} \odot W^r \cdot \text{disaster}_{t-1}$ | −0.0052 | −0.0019 | 0.0014 | −0.0109*** |
| | (0.0089) | (0.0015) | (0.0012) | (0.0029) |
| $C^{\text{low}} \odot W^r \cdot \text{disaster}_{t-1}$ | −0.0025 | −0.0018 | 0.0034*** | −0.0119*** |
| | (0.0088) | (0.0015) | (0.0013) | (0.0029) |
| $\ln(\text{pop}_t)$ | 0.0249*** | 0.0257*** | 0.0276*** | 0.0243*** |
| | (0.0013) | (0.0013) | (0.0014) | (0.0013) |
| $W^r \cdot \ln(\text{pop})_t$ | 0.0109*** | 0.0113*** | 0.0115*** | 0.0106*** |
| | (0.0006) | (0.0006) | (0.0006) | (0.0006) |
| $\ln(\text{lights}_{t-1})$ | −0.4386*** | −0.4367*** | −0.4329*** | −0.4380*** |
| | (0.0011) | (0.0011) | (0.0011) | (0.0011) |
| $\rho$ | 0.0672*** | 0.0672*** | 0.0676*** | 0.0672*** |
| | (0.0000) | (0.0000) | (0.0000) | (0.0000) |
| Observations | 507,864 | 502,026 | 468,174 | 506,037 |

*Note:* ***, **, * denote significance at the 1%, 5% and 10% level. All specifications are SDEM and are estimated by Maximum Likelihood. Standard errors in parentheses. Cell and year fixed effects included but not reported. Spatial radius is r=80 km. Yearly disaster intensities reflect time-weighted rolling averages over 12 subsequent monthly observations. $C^i \odot W^r \cdot \text{disaster}_t$ terms represent corresponding z-scores.

Results are shown in Table 4.4. All estimates remain qualitatively similar to Panel A of Table 4.3, with only small changes in magnitudes. Consequently, findings seem insensitive to the exact definition of this cutoff criterion.

### 4.5.2 Sampling: Exclude cells with less than three neighbors

As a second check, a potentially relevant aspect of the sample composition is addressed. The sample used to obtain the baseline estimates includes observations which feature only one

or two neighbors. Analyzing the impact of heterogeneity along the local distribution of road connectivity however requires constructing multiple neighbor groups. If, e.g., a cell has only one neighbor and this neighbor has a connectivity of zero, it will always fall into the low group whereas the high group will simply contain a zero value.[27] This means that the sample includes observations for which the treatment of one or two neighbor groups is zero by construction, simply because there are no neighbors to put into the respective bin. To assess whether this feature entails methodological issues related to identification, all observations which have less than three neighbors are excluded from the sample. This essentially removes cells which belong to small islands or otherwise remote locations, which are potentially more likely to appear in less developed countries (compare Figure 4.1). These observations account for about 10% of the sample.

Results are presented in Table 4.5. Panel A provides estimates for the specification distinguishing two groups of neighbors (high and low), Panel B distinguishes three groups (high, medium and low). In terms of magnitudes, findings are overall similar to the respective baseline but feature stronger local average treatment effects for cold waves. Qualitatively, findings do not change. Thus, inclusion of cells with a very small number of neighbors and their implications for the binning procedure does not seem to substantially affect overall results.[28]

[27] If the same neighbor has a non-zero connectivity, the requirement for the highly connected cell to have a connectivity larger or equal the (non-zero) local median will put it into the highly connected category instead.

[28] Appendix Tables D.10 and D.11 provide additional estimates from a sample excluding only observations with less than two neighbors. Results are very similar.

Table 4.5 : Exclude Observations With Less Than Three Neighbors

**Dependent Variable:** $\Delta \ln(\text{lights}_t)$

| | wind | precip. | drought | cold |
|---|---|---|---|---|
| **PANEL A: Connectivity above and below median** | | | | |
| $\text{disaster}_t$ | −0.0025** | −0.0211*** | 0.0099* | −0.0738*** |
| | (0.0011) | (0.0080) | (0.0056) | (0.0184) |
| $\text{disaster}_{t-1}$ | −0.0051*** | 0.0282*** | −0.0074 | −0.0889*** |
| | (0.0011) | (0.0079) | (0.0055) | (0.0182) |
| $C^{\text{high}} \odot W^r \cdot \text{disaster}_t$ | −0.0078 | 0.0060*** | −0.0056*** | 0.0241*** |
| | (0.0089) | (0.0015) | (0.0012) | (0.0030) |
| $C^{\text{low}} \odot W^r \cdot \text{disaster}_t$ | 0.0099 | 0.0006 | −0.0059*** | 0.0134*** |
| | (0.0088) | (0.0016) | (0.0013) | (0.0030) |
| $C^{\text{high}} \odot W^r \cdot \text{disaster}_{t-1}$ | −0.0032 | −0.0025* | 0.0003 | −0.0073** |
| | (0.0088) | (0.0015) | (0.0012) | (0.0030) |
| $C^{\text{low}} \odot W^r \cdot \text{disaster}_{t-1}$ | −0.0027 | −0.0035** | 0.0053*** | −0.0107*** |
| | (0.0087) | (0.0015) | (0.0013) | (0.0030) |
| **PANEL B: Connectivity thirtiles** | | | | |
| $\text{disaster}_t$ | −0.0009 | −0.0211*** | 0.0104* | −0.0583*** |
| | (0.0011) | (0.0080) | (0.0056) | (0.0189) |
| $\text{disaster}_{t-1}$ | −0.0051*** | 0.0287*** | −0.0084 | −0.0717*** |
| | (0.0011) | (0.0079) | (0.0055) | (0.0187) |
| $C^{\text{high}} \odot W^r \cdot \text{disaster}_t$ | −0.0071 | 0.0045*** | −0.0046*** | 0.0121*** |
| | (0.0087) | (0.0015) | (0.0012) | (0.0031) |
| $C^{\text{medium}} \odot W^r \cdot \text{disaster}_t$ | −0.0095 | 0.0029* | −0.0032*** | 0.0155*** |
| | (0.0088) | (0.0015) | (0.0012) | (0.0032) |
| $C^{\text{low}} \odot W^r \cdot \text{disaster}_t$ | −0.0085 | 0.0002 | −0.0054*** | 0.0110*** |
| | (0.0093) | (0.0016) | (0.0013) | (0.0033) |
| $C^{\text{high}} \odot W^r \cdot \text{disaster}_{t-1}$ | −0.0072 | −0.0023 | 0.0003 | −0.0053* |
| | (0.0086) | (0.0015) | (0.0012) | (0.0030) |
| $C^{\text{medium}} \odot W^r \cdot \text{disaster}_{t-1}$ | −0.0014 | −0.0012 | 0.0017 | −0.0068** |
| | (0.0087) | (0.0015) | (0.0012) | (0.0032) |
| $C^{\text{low}} \odot W^r \cdot \text{disaster}_{t-1}$ | 0.0009 | −0.0036** | 0.0049*** | −0.0155*** |
| | (0.0092) | (0.0015) | (0.0013) | (0.0033) |
| Observations | 459,669 | 453,831 | 421,953 | 457,947 |

*Note:* ***, **, * denote significance at the 1%, 5% and 10% level. All specifications are SDEM and are estimated by Maximum Likelihood. Standard errors in parentheses. Cell and year fixed effects included but not reported. Spatial radius is r=80 km. Yearly disaster intensities reflect time-weighted rolling averages over 12 subsequent monthly observations. $C^i \odot W^r \cdot \text{disaster}_t$ terms represent corresponding z-scores. Additional controls included but not reported. Full results are shown in Tables D.8 and D.9 in the Appendix.

### 4.5.3 Connectivity Index: Restrict to shortest connection

As a third check, the characteristics of the connectivity index are addressed. In the baseline, the index considers the mean distance of the three shortest connections, adding penalties if only one or two connections are available. Thus, the baseline indicator accounts for both distance and number of connections. In this section, this choice is revisited by dropping the latter component from the indicator. Instead, only the distance along the single shortest route will be considered. This choice potentially affects a cell's position on the local connectivity distribution and may thus result in different binning outcomes.

Results are presented in Table 4.6. Overall, results remain qualitatively similar. Coefficient magnitudes exhibit slight changes in Panel A, showing higher point estimates for spillovers from highly connected cells and smaller effects for lowly connected neighbors in the base period. This suggests that the importance of above-median relative to below-median connections increases if only the shortest route is considered, i.e., distance appears more important than the number of connections. If classification distinguishes three categories in Panel B, results show some differences to the baseline. The spillovers from intermediately connected neighbors lose statistical significance for extreme precipitation events, attributing all spillovers to highly connected neighbors. For droughts, a clear inverse pattern emerges, suggesting that spillovers increase in length of the shortest route. This finding is very likely related to the rural/urban divide. Felbermayr et al. (2018) find that negative spillovers of droughts mainly go from rural towards urban cells. To the extent that this rural/urban divide is more pronounced across relatively longer distances within the 80 km search radius, this relationship could be reflected in the the simple road distance bins.

Table 4.6 : Only Single Shortest Connection Considered

**Dependent Variable:** $\Delta \ln(\text{lights}_t)$

| | wind | precip. | drought | cold |
|---|---|---|---|---|
| **PANEL A: Connectivity above and below median** | | | | |
| $\text{disaster}_t$ | −0.0025*** | −0.0280*** | 0.0133*** | −0.0410*** |
| | (0.0009) | (0.0069) | (0.0047) | (0.0141) |
| $\text{disaster}_{t-1}$ | −0.0052*** | 0.0213*** | −0.0042 | −0.0775*** |
| | (0.0009) | (0.0068) | (0.0047) | (0.0138) |
| $C^{\text{high}} \odot W^r \cdot \text{disaster}_t$ | −0.0039 | 0.0082*** | −0.0069*** | 0.0221*** |
| | (0.0090) | (0.0015) | (0.0012) | (0.0029) |
| $C^{\text{low}} \odot W^r \cdot \text{disaster}_t$ | 0.0128 | 0.0006 | −0.0057*** | 0.0091*** |
| | (0.0088) | (0.0015) | (0.0013) | (0.0029) |
| $C^{\text{high}} \odot W^r \cdot \text{disaster}_{t-1}$ | −0.0065 | −0.0017 | 0.0003 | −0.0092*** |
| | (0.0089) | (0.0015) | (0.0012) | (0.0028) |
| $C^{\text{low}} \odot W^r \cdot \text{disaster}_{t-1}$ | 0.0021 | −0.0020 | 0.0042*** | −0.0106*** |
| | (0.0087) | (0.0015) | (0.0013) | (0.0028) |
| **PANEL B: Connectivity thirtiles** | | | | |
| $\text{disaster}_t$ | −0.0016* | −0.0275*** | 0.0130*** | −0.0355** |
| | (0.0009) | (0.0070) | (0.0048) | (0.0144) |
| $\text{disaster}_{t-1}$ | −0.0051*** | 0.0221*** | −0.0042 | −0.0723*** |
| | (0.0009) | (0.0069) | (0.0047) | (0.0141) |
| $C^{\text{high}} \odot W^r \cdot \text{disaster}_t$ | −0.0060 | 0.0064*** | −0.0039*** | 0.0150*** |
| | (0.0104) | (0.0017) | (0.0013) | (0.0036) |
| $C^{\text{medium}} \odot W^r \cdot \text{disaster}_t$ | 0.0006 | 0.0021 | −0.0047*** | 0.0082** |
| | (0.0105) | (0.0017) | (0.0013) | (0.0038) |
| $C^{\text{low}} \odot W^r \cdot \text{disaster}_t$ | −0.0015 | 0.0006 | −0.0054*** | 0.0085*** |
| | (0.0090) | (0.0015) | (0.0012) | (0.0030) |
| $C^{\text{high}} \odot W^r \cdot \text{disaster}_{t-1}$ | −0.0108 | −0.0017 | −0.0012 | 0.0017 |
| | (0.0103) | (0.0017) | (0.0014) | (0.0035) |
| $C^{\text{medium}} \odot W^r \cdot \text{disaster}_{t-1}$ | 0.0052 | −0.0002 | 0.0024* | −0.0149*** |
| | (0.0104) | (0.0016) | (0.0013) | (0.0037) |
| $C^{\text{low}} \odot W^r \cdot \text{disaster}_{t-1}$ | 0.0021 | −0.0023 | 0.0040*** | −0.0136*** |
| | (0.0089) | (0.0015) | (0.0012) | (0.0030) |
| Observations | 507,864 | 502,026 | 468,174 | 506,037 |

*Note:* ***, **, * denote significance at the 1%, 5% and 10% level. All specifications are SDEM and are estimated by Maximum Likelihood. Standard errors in parentheses. Cell and year fixed effects included but not reported. Spatial radius is r=80 km. Yearly disaster intensities reflect time-weighted rolling averages over 12 subsequent monthly observations. $C^i \odot W^r \cdot \text{disaster}_t$ terms represent corresponding z-scores. Additional controls included but not reported. Full results are shown in Tables D.12 and D.13 in the Appendix.

## 4.6 Conclusion

This study empirically investigates potential transmission channels of spatial spillovers caused by natural disasters, asking how the relocation of economic activity is affected by international borders and by available roads infrastructure. To answer this question, a global dataset recently introduced by Felbermayr et al. (2018) is exploited, which provides detailed measures of physical disaster intensity and local economic activity proxied by remotely-sensed night-light emissions for 24,000 geographical units in 197 countries over 21 years. To examine a selection of potential transmission channels for spillover effects, geographic data is used to provide new measures of local connectivity.

Theoretically, necessary preconditions for economic activity to divert away from affected locations are the mobility of goods and services or the mobility of people. This mobility depends on how connected locations are with one another. Hence, observed spatial spillovers are likely to be driven by the degree of connectivity of a disaster-struck location. Good road networks can strengthen relocation effects, while limitations to connectivity (e.g., international borders) may hamper them. In line with the literature on international transactions, empirical findings in this study suggest that connectivity of grid cells is a main driver of spatial spillovers.

Results indicate that short run relocation of economic activity is subject to a border effect. As the costs of relocation increases at international borders, spatial spillovers of natural disasters concentrate on cells within national boundaries in the base period. Domestic neighbors are, on average, the exclusive sources of statistically significant spillover effects of wind speeds and extreme precipitation events. For droughts and cold waves, estimates also suggest spillovers from foreign locations, but domestic spillovers are about 2.5 times and 1.5 times as strong. The difference between spillovers originating from domestic and foreign cells loses statistical significance after one period.

In addition, connections along major transport routes also matter for the spillover pattern of natural disasters, as higher connectivity via roads potentially eases travel and lowers trade costs. Spillovers from cells connected by at least one major road are exclusively driving spatial spillovers for extreme precipitation events. Moreover, spillover effects for droughts and cold waves are 1.9 times and 3.5 times as strong for connected compared to unconnected cells. Finally, heterogeneity in roads connectivity is exploited in terms of distance and the number of connections available. Estimates suggest that those neighbors with a connectivity index above

the local neighborhood's median have stronger spatial spillovers for precipitation events and cold waves. Further distinguishing neighbors along thirtiles of their local connectivity distribution provides mixed evidence. All in all, results suggest that connectivity differences at smaller margins seem less crucial whereas international borders, the overall availability of roads and local connectivity differences at larger margins (i.e., upper vs. lower 50%) play a very important role.

# Appendix D.1 Supplementary Appendix

## D.1.1 Supplementary Descriptive Statistics

Table D.1 : Summary Statistics

| statistic | n | mean | st. dev. | min | max |
|---|---|---|---|---|---|
| $\Delta \ln(\text{lights})$ | 507,864 | 0.045 | 0.392 | −8.246 | 8.217 |
| $\ln(\text{lights})$ | 507,864 | 0.264 | 1.724 | −7.090 | 4.142 |
| $\ln(\text{pop}_t)$ | 507,864 | 10.639 | 2.165 | −14.390 | 16.822 |
| **Physical Intensities** | | | | | |
| storm | 507,864 | 20.766 | 4.486 | 5.478 | 46.528 |
| precip. | 502,026 | 0.385 | 0.151 | 0.000 | 1.697 |
| drought | 468,174 | 0.387 | 0.242 | 0.000 | 2.305 |
| cold | 506,037 | 0.412 | 0.089 | 0.000 | 1.271 |
| **Roads Connectivity Index (cross-section)** | | | | | |
| bilat. connectivity (3 routes) | 169,626 | 0.326 | 0.230 | 0.000 | 0.913 |
| mean connectivity (3 routes) | 24,184 | 0.301 | 0.233 | 0.000 | 0.873 |
| bilat. connectivity (1 route) | 169,626 | 0.526 | 0.357 | 0.000 | 0.916 |
| mean connectivity (1 route) | 24,184 | 0.501 | 0.293 | 0.000 | 0.914 |

*Note:* Physical intensities represent time-weighted rolling averages over 12 subsequent months. Time-constant connectivity measures are reported for one year. 21 yearly periods included in the data.

Table D.2 : Roads Connectivity Above and Below Median

**Dependent Variable:** $\Delta \ln(\text{lights}_t)$

| | **wind** | **precip.** | **drought** | **cold** |
|---|---|---|---|---|
| $\text{disaster}_t$ | −0.0025*** | −0.0277*** | 0.0133*** | −0.0432*** |
| | (0.0009) | (0.0069) | (0.0047) | (0.0141) |
| $\text{disaster}_{t-1}$ | −0.0052*** | 0.0211*** | −0.0042 | −0.0776*** |
| | (0.0009) | (0.0068) | (0.0047) | (0.0138) |
| $C^{\text{high}} \odot W^r \cdot \text{disaster}_t$ | −0.0051 | 0.0074*** | −0.0067*** | 0.0213*** |
| | (0.0088) | (0.0015) | (0.0012) | (0.0028) |
| $C^{\text{low}} \odot W^r \cdot \text{disaster}_t$ | 0.0141 | 0.0012 | −0.0059*** | 0.0102*** |
| | (0.0087) | (0.0015) | (0.0013) | (0.0029) |
| $C^{\text{high}} \odot W^r \cdot \text{disaster}_{t-1}$ | −0.0030 | −0.0018 | 0.0003 | −0.0089*** |
| | (0.0087) | (0.0015) | (0.0012) | (0.0028) |
| $C^{\text{low}} \odot W^r \cdot \text{disaster}_{t-1}$ | −0.0004 | −0.0018 | 0.0042*** | −0.0107*** |
| | (0.0086) | (0.0015) | (0.0013) | (0.0028) |
| $\ln(\text{pop}_t)$ | 0.0249*** | 0.0258*** | 0.0276*** | 0.0244*** |
| | (0.0013) | (0.0013) | (0.0014) | (0.0013) |
| $W^r \cdot \ln(\text{pop}_t)$ | 0.0109*** | 0.0113*** | 0.0115*** | 0.0106*** |
| | (0.0006) | (0.0006) | (0.0006) | (0.0006) |
| $\ln(\text{lights}_{t-1})$ | −0.4386*** | −0.4367*** | −0.4329*** | −0.4380*** |
| | (0.0011) | (0.0011) | (0.0011) | (0.0011) |
| $\rho$ | 0.0672*** | 0.0672*** | 0.0676*** | 0.0672*** |
| | (0.0000) | (0.0000) | (0.0000) | (0.0000) |
| Observations | 507,864 | 502,026 | 468,174 | 506,037 |

*Note:* ***, **, * denote significance at the 1%, 5% and 10% level. All specifications are SDEM and are estimated by Maximum Likelihood. Standard errors in parentheses. Cell and year fixed effects included but not reported. Spatial radius is r=80 km. Yearly disaster intensities reflect time-weighted rolling averages over 12 subsequent monthly observations. $C^i \odot W^r \cdot \text{disaster}_t$ terms represent corresponding z-scores.

Table D.3 : Roads Connectivity Thirtiles

**Dependent Variable:** $\Delta \ln(\text{lights}_t)$

| | wind | precip. | drought | cold |
|---|---|---|---|---|
| $\text{disaster}_t$ | −0.0015* | −0.0266*** | 0.0135*** | −0.0350** |
| | (0.0009) | (0.0069) | (0.0047) | (0.0145) |
| $\text{disaster}_{t-1}$ | −0.0051*** | 0.0217*** | −0.0052 | −0.0675*** |
| | (0.0009) | (0.0069) | (0.0047) | (0.0142) |
| $C^{\text{high}} \odot W^r \cdot \text{disaster}_t$ | −0.0017 | 0.0057*** | −0.0058*** | 0.0113*** |
| | (0.0089) | (0.0015) | (0.0012) | (0.0031) |
| $C^{\text{middle}} \odot W^r \cdot \text{disaster}_t$ | −0.0072 | 0.0031** | −0.0028** | 0.0130*** |
| | (0.0090) | (0.0015) | (0.0012) | (0.0032) |
| $C^{\text{low}} \odot W^r \cdot \text{disaster}_t$ | −0.0018 | 0.0005 | −0.0054*** | 0.0086*** |
| | (0.0090) | (0.0015) | (0.0012) | (0.0030) |
| $C^{\text{high}} \odot W^r \cdot \text{disaster}_{t-1}$ | −0.0098 | −0.0018 | 0.0002 | −0.0049 |
| | (0.0088) | (0.0015) | (0.0012) | (0.0030) |
| $C^{\text{middle}} \odot W^r \cdot \text{disaster}_{t-1}$ | 0.0030 | −0.0001 | 0.0012 | −0.0078** |
| | (0.0089) | (0.0015) | (0.0012) | (0.0032) |
| $C^{\text{low}} \odot W^r \cdot \text{disaster}_{t-1}$ | 0.0015 | −0.0022 | 0.0041*** | −0.0146*** |
| | (0.0089) | (0.0015) | (0.0012) | (0.0030) |
| $\ln(\text{pop}_t)$ | 0.0249*** | 0.0258*** | 0.0276*** | 0.0244*** |
| | (0.0013) | (0.0013) | (0.0014) | (0.0013) |
| $W^r \cdot \ln(\text{pop}_t)$ | 0.0109*** | 0.0113*** | 0.0115*** | 0.0106*** |
| | (0.0006) | (0.0006) | (0.0006) | (0.0006) |
| $\ln(\text{lights}_{t-1})$ | −0.4386*** | −0.4367*** | −0.4329*** | −0.4380*** |
| | (0.0011) | (0.0011) | (0.0011) | (0.0011) |
| $\rho$ | 0.0672*** | 0.0672*** | 0.0676*** | 0.0672*** |
| | (0.0000) | (0.0000) | (0.0000) | (0.0000) |
| Observations | 507,864 | 502,026 | 468,174 | 506,037 |

*Note:* ***, **, * denote significance at the 1%, 5% and 10% level. All specifications are SDEM and are estimated by Maximum Likelihood. Standard errors in parentheses. Cell and year fixed effects included but not reported. Spatial radius is r=80 km. Yearly disaster intensities reflect time-weighted rolling averages over 12 subsequent monthly observations. $C^i \odot W^r \cdot \text{disaster}_t$ terms represent corresponding z-scores.

Table D.4 : Wald Chi-Squared Tests: Border Effect

**H0: Spillover from $C^{\text{same}}$ = Spillover from $C^{\text{diff}}$**

| | | wind | precip. | drought | cold |
|---|---|---|---|---|---|
| $t$ | $\chi^2$ | 11.3060 | 12.4590 | 9.2987 | 3.8703 |
| | $\Pr(>\chi^2)$ | 0.0008*** | 0.0004*** | 0.0023*** | 0.0492** |
| $t-1$ | $\chi^2$ | 2.0979 | 1.0715 | 0.6962 | 1.0028 |
| | $\Pr(>\chi^2)$ | 0.1475 | 0.3006 | 0.4041 | 0.3166 |

*Note:* ***, **, * denote significance at the 1%, 5% and 10% level. Tests based on regressions presented in Table 4.1.

Table D.5 : Wald Chi-Squared Tests: Road Existence

**H0: Spillover from $C^{\text{roads}}$ = Spillover from $C^{\text{no-roads}}$**

| | | wind | precip. | drought | cold |
|---|---|---|---|---|---|
| $t$ | $\chi^2$ | 0.1266 | 29.3600 | 13.0480 | 32.5250 |
| | Pr($>\chi^2$) | 0.7220 | 0.0000*** | 0.0003*** | 0.0000*** |
| $t-1$ | $\chi^2$ | 0.9441 | 0.1522 | 7.3717 | 1.5985 |
| | Pr($>\chi^2$) | 0.3312 | 0.6964 | 0.0066*** | 0.2061 |

*Note:* ***, **, * denote significance at the 1%, 5% and 10% level. Tests based on regressions presented in Table 4.2

Table D.6 : Wald Chi-Squared Tests: Road Heterogeneity (Two Groups)

**H0: Spillover from $C^{\text{high}}$ = Spillover from $C^{\text{low}}$**

| | | wind | precip. | drought | cold |
|---|---|---|---|---|---|
| $t$ | $\chi^2$ | 3.4094 | 12.0510 | 0.2801 | 10.6170 |
| | Pr($>\chi^2$) | 0.06483* | 0.0005*** | 0.5967 | 0.0011*** |
| $t-1$ | $\chi^2$ | 0.0626 | 0.0002 | 6.9959 | 0.2738 |
| | Pr($>\chi^2$) | 0.8025 | 0.9879 | 0.0082*** | 0.6008 |

*Note:* ***, **, * denote significance at the 1%, 5% and 10% level. Tests based on regressions presented in Panel A of Table 4.3.

Table D.7 : Wald Chi-Squared Tests: Road Heterogeneity (Three Groups)

| | | wind | precip. | drought | cold |
|---|---|---|---|---|---|
| **PANEL A: H0: Spillover from $C^{high}$ = Spillover from $C^{low}$** | | | | | |
| $t$ | $\chi^2$ | 0.0000 | 7.7980 | 0.0610 | 0.5153 |
| | $\Pr(>\chi^2)$ | 0.9955 | 0.0052*** | 0.8049 | 0.4728 |
| $t-1$ | $\chi^2$ | 1.0815 | 0.0705 | 6.8460 | 6.6952 |
| | $\Pr(>\chi^2)$ | 0.2984 | 0.7907 | 0.0089*** | 0.0097*** |
| **PANEL B: H0: Spillover from $C^{high}$ = Spillover from $C^{medium}$** | | | | | |
| $t$ | $\chi^2$ | 0.1437 | 1.0921 | 2.1989 | 0.1056 |
| | $\Pr(>\chi^2)$ | 0.7046 | 0.2960 | 0.1381 | 0.7452 |
| $t-1$ | $\chi^2$ | 0.7891 | 0.4490 | 0.2374 | 0.3136 |
| | $\Pr(>\chi^2)$ | 0.3744 | 0.5028 | 0.6261 | 0.5755 |
| **PANEL C: H0: Spillover from $C^{medium}$ = Spillover from $C^{low}$** | | | | | |
| $t$ | $\chi^2$ | 0.2350 | 1.7678 | 2.7717 | 1.3112 |
| | $\Pr(>\chi^2)$ | 0.6278 | 0.1836 | 0.0959* | 0.2522 |
| $t-1$ | $\chi^2$ | 0.0185 | 1.2671 | 3.7070 | 3.1560 |
| | $\Pr(>\chi^2)$ | 0.8920 | 0.2603 | 0.0542* | 0.0757* |

*Note:* ***, **, * denote significance at the 1%, 5% and 10% level. Tests based on regressions presented in Panel B of Table 4.3.

Table D.8 : Leaving Out Cells With Less Than Three Neighbors (2 Groups)

**Dependent Variable:** $\Delta \ln(\text{lights}_t)$

| | **wind** | **precip.** | **drought** | **cold** |
|---|---|---|---|---|
| $\text{disaster}_t$ | −0.0025** | −0.0211*** | 0.0099* | −0.0738*** |
| | (0.0011) | (0.0080) | (0.0056) | (0.0184) |
| $\text{disaster}_{t-1}$ | −0.0051*** | 0.0282*** | −0.0074 | −0.0889*** |
| | (0.0011) | (0.0079) | (0.0055) | (0.0182) |
| $C^{\text{high}} \odot W^r \cdot \text{disaster}_t$ | −0.0078 | 0.0060*** | −0.0056*** | 0.0241*** |
| | (0.0089) | (0.0015) | (0.0012) | (0.0030) |
| $C^{\text{low}} \odot W^r \cdot \text{disaster}_t$ | 0.0099 | 0.0006 | −0.0059*** | 0.0134*** |
| | (0.0088) | (0.0016) | (0.0013) | (0.0030) |
| $C^{\text{high}} \odot W^r \cdot \text{disaster}_{t-1}$ | −0.0032 | −0.0025* | 0.0003 | −0.0073** |
| | (0.0088) | (0.0015) | (0.0012) | (0.0030) |
| $C^{\text{low}} \odot W^r \cdot \text{disaster}_{t-1}$ | −0.0027 | −0.0035** | 0.0053*** | −0.0107*** |
| | (0.0087) | (0.0015) | (0.0013) | (0.0030) |
| $\ln(\text{pop}_t)$ | 0.0198*** | 0.0213*** | 0.0231*** | 0.0195*** |
| | (0.0015) | (0.0015) | (0.0016) | (0.0015) |
| $W^r \cdot \ln(\text{pop}_t)$ | 0.0097*** | 0.0103*** | 0.0104*** | 0.0096*** |
| | (0.0006) | (0.0006) | (0.0006) | (0.0006) |
| $\ln(\text{lights}_{t-1})$ | −0.4431*** | −0.4415*** | −0.4366*** | −0.4424*** |
| | (0.0011) | (0.0011) | (0.0012) | (0.0011) |
| $\rho$ | 0.0672*** | 0.0672*** | 0.0676*** | 0.0672*** |
| | (0.0000) | (0.0000) | (0.0000) | (0.0000) |
| Observations | 459,669 | 453,831 | 421,953 | 457,947 |

*Note:* ***, **, * denote significance at the 1%, 5% and 10% level. All specifications are SDEM and are estimated by Maximum Likelihood. Standard errors in parentheses. Cell and year fixed effects included but not reported. Spatial radius is r=80 km. Yearly disaster intensities reflect time-weighted rolling averages over 12 subsequent monthly observations. $C^i \odot W^r \cdot \text{disaster}_t$ terms represent corresponding z-scores.

Table D.9 : Leaving Out Cells With Less Than Three Neighbors (3 Groups)

**Dependent Variable:** $\Delta \ln(\text{lights}_t)$

| | **wind** | **precip.** | **drought** | **cold** |
|---|---|---|---|---|
| $\text{disaster}_t$ | −0.0009 | −0.0211*** | 0.0104* | −0.0583*** |
| | (0.0011) | (0.0080) | (0.0056) | (0.0189) |
| $\text{disaster}_{t-1}$ | −0.0051*** | 0.0287*** | −0.0084 | −0.0717*** |
| | (0.0011) | (0.0079) | (0.0055) | (0.0187) |
| $C^{\text{high}} \odot W^r \cdot \text{disaster}_t$ | −0.0071 | 0.0045*** | −0.0046*** | 0.0121*** |
| | (0.0087) | (0.0015) | (0.0012) | (0.0031) |
| $C^{\text{medium}} \odot W^r \cdot \text{disaster}_t$ | −0.0095 | 0.0029* | −0.0032*** | 0.0155*** |
| | (0.0088) | (0.0015) | (0.0012) | (0.0032) |
| $C^{\text{low}} \odot W^r \cdot \text{disaster}_t$ | −0.0085 | 0.0002 | −0.0054*** | 0.0110*** |
| | (0.0093) | (0.0016) | (0.0013) | (0.0033) |
| $C^{\text{high}} \odot W^r \cdot \text{disaster}_{t-1}$ | −0.0072 | −0.0023 | 0.0003 | −0.0053* |
| | (0.0086) | (0.0015) | (0.0012) | (0.0030) |
| $C^{\text{medium}} \odot W^r \cdot \text{disaster}_{t-1}$ | −0.0014 | −0.0012 | 0.0017 | −0.0068** |
| | (0.0087) | (0.0015) | (0.0012) | (0.0032) |
| $C^{\text{low}} \odot W^r \cdot \text{disaster}_{t-1}$ | 0.0009 | −0.0036** | 0.0049*** | −0.0155*** |
| | (0.0092) | (0.0015) | (0.0013) | (0.0033) |
| $\ln(\text{pop}_t)$ | 0.0198*** | 0.0213*** | 0.0231*** | 0.0196*** |
| | (0.0015) | (0.0015) | (0.0016) | (0.0015) |
| $W^r \cdot \ln(\text{pop}_t)$ | 0.0097*** | 0.0103*** | 0.0104*** | 0.0096*** |
| | (0.0006) | (0.0006) | (0.0006) | (0.0006) |
| $\ln(\text{lights}_{t-1})$ | −0.4431*** | −0.4415*** | −0.4366*** | −0.4424*** |
| | (0.0011) | (0.0011) | (0.0012) | (0.0011) |
| $\rho$ | 0.0672*** | 0.0672*** | 0.0676*** | 0.0672*** |
| | (0.0000) | (0.0000) | (0.0000) | (0.0000) |
| Observations | 459,669 | 453,831 | 421,953 | 457,947 |

*Note:* ***, **, * denote significance at the 1%, 5% and 10% level. All specifications are SDEM and are estimated by Maximum Likelihood. Standard errors in parentheses. Cell and year fixed effects included but not reported. Spatial radius is r=80 km. Yearly disaster intensities reflect time-weighted rolling averages over 12 subsequent monthly observations. $C^i \odot W^r \cdot \text{disaster}_t$ terms represent corresponding z-scores.

Table D.10 : Leaving Out Cells With Less Than Two Neighbors (2 Groups)

**Dependent Variable:** $\Delta \ln(\text{lights}_t)$

| | **wind** | **precip.** | **drought** | **cold** |
|---|---|---|---|---|
| $\text{disaster}_t$ | −0.0023** | −0.0256*** | 0.0147*** | −0.0753*** |
| | (0.0010) | (0.0075) | (0.0052) | (0.0161) |
| $\text{disaster}_{t-1}$ | −0.0052*** | 0.0284*** | −0.0114** | −0.0798*** |
| | (0.0010) | (0.0074) | (0.0051) | (0.0158) |
| $C^{\text{high}} \odot W^r \cdot \text{disaster}_t$ | −0.0079 | 0.0070*** | −0.0067*** | 0.0246*** |
| | (0.0089) | (0.0015) | (0.0012) | (0.0029) |
| $C^{\text{low}} \odot W^r \cdot \text{disaster}_t$ | 0.0116 | 0.0009 | −0.0064*** | 0.0145*** |
| | (0.0088) | (0.0015) | (0.0013) | (0.0030) |
| $C^{\text{high}} \odot W^r \cdot \text{disaster}_{t-1}$ | −0.0024 | −0.0026* | 0.0011 | −0.0083*** |
| | (0.0088) | (0.0015) | (0.0012) | (0.0029) |
| $C^{\text{low}} \odot W^r \cdot \text{disaster}_{t-1}$ | −0.0014 | −0.0029* | 0.0054*** | −0.0109*** |
| | (0.0087) | (0.0015) | (0.0013) | (0.0029) |
| $\ln(\text{pop}_t)$ | 0.0248*** | 0.0257*** | 0.0280*** | 0.0242*** |
| | (0.0014) | (0.0014) | (0.0015) | (0.0014) |
| $W^r \cdot \ln(\text{pop}_t)$ | 0.0105*** | 0.0110*** | 0.0112*** | 0.0104*** |
| | (0.0006) | (0.0006) | (0.0006) | (0.0006) |
| $\ln(\text{lights}_{t-1})$ | −0.4418*** | −0.4401*** | −0.4366*** | −0.4414*** |
| | (0.0011) | (0.0011) | (0.0011) | (0.0011) |
| $\rho$ | 0.0672*** | 0.0672*** | 0.0676*** | 0.0672*** |
| | (0.0000) | (0.0000) | (0.0000) | (0.0000) |
| Observations | 488,670 | 482,790 | 449,358 | 486,990 |

*Note:* ***, **, * denote significance at the 1%, 5% and 10% level. All specifications are SDEM and are estimated by Maximum Likelihood. Standard errors in parentheses. Cell and year fixed effects included but not reported. Spatial radius is r=80 km. Yearly disaster intensities reflect time-weighted rolling averages over 12 subsequent monthly observations. $C^i \odot W^r \cdot \text{disaster}_t$ terms represent corresponding z-scores.

Table D.11 : Leaving Out Cells With Less Than Two Neighbors (3 Groups)

**Dependent Variable:** $\Delta \ln(\text{lights}_t)$

| | **wind** | **precip.** | **drought** | **cold** |
|---|---|---|---|---|
| $\text{disaster}_t$ | −0.0010 | −0.0255*** | 0.0151*** | −0.0638*** |
| | (0.0010) | (0.0075) | (0.0052) | (0.0165) |
| $\text{disaster}_{t-1}$ | −0.0051*** | 0.0292*** | −0.0121** | −0.0668*** |
| | (0.0010) | (0.0074) | (0.0051) | (0.0163) |
| $C^{\text{high}} \odot W^r \cdot \text{disaster}_t$ | −0.0058 | 0.0059*** | −0.0057*** | 0.0134*** |
| | (0.0088) | (0.0015) | (0.0012) | (0.0031) |
| $C^{\text{medium}} \odot W^r \cdot \text{disaster}_t$ | −0.0086 | 0.0026* | −0.0031*** | 0.0151*** |
| | (0.0089) | (0.0015) | (0.0012) | (0.0032) |
| $C^{\text{low}} \odot W^r \cdot \text{disaster}_t$ | −0.0056 | 0.0005 | −0.0059*** | 0.0125*** |
| | (0.0092) | (0.0015) | (0.0013) | (0.0032) |
| $C^{\text{high}} \odot W^r \cdot \text{disaster}_{t-1}$ | −0.0107 | −0.0027* | 0.0009 | −0.0050* |
| | (0.0088) | (0.0015) | (0.0012) | (0.0030) |
| $C^{\text{medium}} \odot W^r \cdot \text{disaster}_{t-1}$ | 0.0038 | −0.0006 | 0.0017 | −0.0076** |
| | (0.0088) | (0.0015) | (0.0012) | (0.0031) |
| $C^{\text{low}} \odot W^r \cdot \text{disaster}_{t-1}$ | 0.0008 | −0.0032** | 0.0051*** | −0.0152*** |
| | (0.0091) | (0.0015) | (0.0013) | (0.0031) |
| $\ln(\text{pop}_t)$ | 0.0248*** | 0.0257*** | 0.0280*** | 0.0243*** |
| | (0.0014) | (0.0014) | (0.0015) | (0.0014) |
| $W^r \cdot \ln(\text{pop}_t)$ | 0.0105*** | 0.0110*** | 0.0112*** | 0.0104*** |
| | (0.0006) | (0.0006) | (0.0006) | (0.0006) |
| $\ln(\text{lights}_{t-1})$ | −0.4418*** | −0.4401*** | −0.4366*** | −0.4413*** |
| | (0.0011) | (0.0011) | (0.0011) | (0.0011) |
| $\rho$ | 0.0672*** | 0.0672*** | 0.0676*** | 0.0672*** |
| | (0.0000) | (0.0000) | (0.0000) | (0.0000) |
| Observations | 488,670 | 482,790 | 449,358 | 486,990 |

*Note:* ***, **, * denote significance at the 1%, 5% and 10% level. All specifications are SDEM and are estimated by Maximum Likelihood. Standard errors in parentheses. Cell and year fixed effects included but not reported. Spatial radius is r=80 km. Yearly disaster intensities reflect time-weighted rolling averages over 12 subsequent monthly observations. $C^i \odot W^r \cdot \text{disaster}_t$ terms represent corresponding z-scores.

Table D.12 : Consider Only Shortest Connection (2 Groups)

**Dependent Variable:** $\Delta \ln(\text{lights}_t)$

| | **wind** | **precip.** | **drought** | **cold** |
|---|---|---|---|---|
| $\text{disaster}_t$ | −0.0025*** | −0.0280*** | 0.0133*** | −0.0410*** |
| | (0.0009) | (0.0069) | (0.0047) | (0.0141) |
| $\text{disaster}_{t-1}$ | −0.0052*** | 0.0213*** | −0.0042 | −0.0775*** |
| | (0.0009) | (0.0068) | (0.0047) | (0.0138) |
| $C^{\text{high}} \odot W^r \cdot \text{disaster}_t$ | −0.0039 | 0.0082*** | −0.0069*** | 0.0221*** |
| | (0.0090) | (0.0015) | (0.0012) | (0.0029) |
| $C^{\text{low}} \odot W^r \cdot \text{disaster}_t$ | 0.0128 | 0.0006 | −0.0057*** | 0.0091*** |
| | (0.0088) | (0.0015) | (0.0013) | (0.0029) |
| $C^{\text{high}} \odot W^r \cdot \text{disaster}_{t-1}$ | −0.0065 | −0.0017 | 0.0003 | −0.0092*** |
| | (0.0089) | (0.0015) | (0.0012) | (0.0028) |
| $C^{\text{low}} \odot W^r \cdot \text{disaster}_{t-1}$ | 0.0021 | −0.0020 | 0.0042*** | −0.0106*** |
| | (0.0087) | (0.0015) | (0.0013) | (0.0028) |
| $\ln(\text{pop}_t)$ | 0.0249*** | 0.0258*** | 0.0276*** | 0.0244*** |
| | (0.0013) | (0.0013) | (0.0014) | (0.0013) |
| $W^r \cdot \ln(\text{pop}_t)$ | 0.0109*** | 0.0113*** | 0.0115*** | 0.0106*** |
| | (0.0006) | (0.0006) | (0.0006) | (0.0006) |
| $\ln(\text{lights}_{t-1})$ | −0.4386*** | −0.4367*** | −0.4329*** | −0.4380*** |
| | (0.0011) | (0.0011) | (0.0011) | (0.0011) |
| $\rho$ | 0.0672*** | 0.0672*** | 0.0676*** | 0.0672*** |
| | (0.0000) | (0.0000) | (0.0000) | (0.0000) |
| Observations | 507,864 | 502,026 | 468,174 | 506,037 |

*Note:* ***, **, * denote significance at the 1%, 5% and 10% level. All specifications are SDEM and are estimated by Maximum Likelihood. Standard errors in parentheses. Cell and year fixed effects included but not reported. Spatial radius is r=80 km. Yearly disaster intensities reflect time-weighted rolling averages over 12 subsequent monthly observations. $C^i \odot W^r \cdot \text{disaster}_t$ terms represent corresponding z-scores.

Table D.13 : Consider Only Shortest Connection (3 Groups)

**Dependent Variable:** $\Delta \ln(\text{lights}_t)$

| | **wind** | **precip.** | **drought** | **cold** |
|---|---|---|---|---|
| $\text{disaster}_t$ | −0.0016* | −0.0275*** | 0.0130*** | −0.0355** |
| | (0.0009) | (0.0070) | (0.0048) | (0.0144) |
| $\text{disaster}_{t-1}$ | −0.0051*** | 0.0221*** | −0.0042 | −0.0723*** |
| | (0.0009) | (0.0069) | (0.0047) | (0.0141) |
| $C^{\text{high}} \odot W^r \cdot \text{disaster}_t$ | −0.0060 | 0.0064*** | −0.0039*** | 0.0150*** |
| | (0.0104) | (0.0017) | (0.0013) | (0.0036) |
| $C^{\text{medium}} \odot W^r \cdot \text{disaster}_t$ | 0.0006 | 0.0021 | −0.0047*** | 0.0082** |
| | (0.0105) | (0.0017) | (0.0013) | (0.0038) |
| $C^{\text{low}} \odot W^r \cdot \text{disaster}_t$ | −0.0015 | 0.0006 | −0.0054*** | 0.0085*** |
| | (0.0090) | (0.0015) | (0.0012) | (0.0030) |
| $C^{\text{high}} \odot W^r \cdot \text{disaster}_{t-1}$ | −0.0108 | −0.0017 | −0.0012 | 0.0017 |
| | (0.0103) | (0.0017) | (0.0014) | (0.0035) |
| $C^{\text{medium}} \odot W^r \cdot \text{disaster}_{t-1}$ | 0.0052 | −0.0002 | 0.0024* | −0.0149*** |
| | (0.0104) | (0.0016) | (0.0013) | (0.0037) |
| $C^{\text{low}} \odot W^r \cdot \text{disaster}_{t-1}$ | 0.0021 | −0.0023 | 0.0040*** | −0.0136*** |
| | (0.0089) | (0.0015) | (0.0012) | (0.0030) |
| $\ln(\text{pop}_t)$ | 0.0249*** | 0.0258*** | 0.0276*** | 0.0244*** |
| | (0.0013) | (0.0013) | (0.0014) | (0.0013) |
| $W^r \cdot \ln(\text{pop}_t)$ | 0.0109*** | 0.0113*** | 0.0115*** | 0.0106*** |
| | (0.0006) | (0.0006) | (0.0006) | (0.0006) |
| $\ln(\text{lights}_{t-1})$ | −0.4386*** | −0.4367*** | −0.4329*** | −0.4380*** |
| | (0.0011) | (0.0011) | (0.0011) | (0.0011) |
| $\rho$ | 0.0672*** | 0.0672*** | 0.0676*** | 0.0672*** |
| | (0.0000) | (0.0000) | (0.0000) | (0.0000) |
| Observations | 507,864 | 502,026 | 468,174 | 506,037 |

*Note:* ***, **, * denote significance at the 1%, 5% and 10% level. All specifications are SDEM and are estimated by Maximum Likelihood. Standard errors in parentheses. Cell and year fixed effects included but not reported. Spatial radius is r=80 km. Yearly disaster intensities reflect time-weighted rolling averages over 12 subsequent monthly observations. $C^i \odot W^r \cdot \text{disaster}_t$ terms represent corresponding z-scores.

# References


Acemoglu, D., Johnson, S., Robinson, J.A., 2005. Institutions as a fundamental cause of long-run growth, Elsevier. volume 1 of *Handbook of Economic Growth*, pp. 385–472.

Ademmer, E., Barsbai, T., Lücke, M., Stöhr, T., 2015. 30 Years of Schengen: Internal Blessing, External Curse? Kiel Policy Brief 88.

Amarasinghe, A., Hodler, R., Raschky, P.A., Zenou, Y., 2018. Spatial Diffusion of Economic Shocks in Networks. CESifo Working Paper 7001.

Ambrosetti, E., Petrillo, E., 2016. Environmental Disasters, Migration and Displacement. Insights and Developments from L'Aquila's Case. Environmental Science & Policy 56, 80–88.

Anbarci, N., Escaleras, M., Register, C.A., 2005. Earthquake Fatalities: The Interaction of Nature and Political Economy. Journal of Public Economics 89, 1907–1933.

Anderson, J., 2009. Gravity, Productivity and the Pattern of Production and Trade. NBER Working Paper 14642.

Anderson, J., 2011. The gravity model. Annual Review of Economics 3, 133–160.

Anderson, J., Van Wincoop, E., 2003. Gravity with Gravitas: A Solution to the Border Puzzle. American Economic Review 93, 170–192.

Anderson, J., Van Wincoop, E., 2004. Trade Costs. Journal of Economic Literature 42, 691–751.

Anderson, J., Yotov, Y., 2015. Terms of Trade and Global Efficiency Effects of Free Trade Agreements, 1990–2002. Journal of International Economics 99, 279–298.

Anselin, L., 2013. Spatial Econometrics: Methods and Models. volume 4. Springer Science & Business Media.

Arkolakis, C., Costinot, A., Rodríguez-Clare, A., 2012. New Trade Models, Same Old Gains? American Economic Review 102, 94–130.

Aussilloux, V., Le Hir, B., 2016. The Economic Consequences of Rolling back Schengen. France Strategie Policy Brief.

Backhaus, A., Martinez-Zarzoso, I., Muris, C., 2015. Do Climate Variations Explain Bilateral Migration? A Gravity Model Analysis. IZA Journal of Migration 4.

Baier, S., Bergstrand, J., 2007. Do Free Trade Agreements Actually Increase Members' International Trade? Journal of International Economics 71, 72–95.

Baier, S., Bergstrand, J., 2009. Bonus vetus OLS: A Simple Method for Approximating International Trade-Cost Effects Using the Gravity Equation. Journal of International Economics 77, 77–85.

Baldwin, R., DiNino, V., Fontagné, L., De Santis, R., Taglioni, D., 2008. Study on the Impact of the Euro on Trade and Foreign Direct Investment. Directorate General Economic and Financial Affairs (DG ECFIN) Report. European Commission.

Baldwin, R., Taglioni, D., 2007. Trade Effects of the Euro: A Comparison of Estimators. Journal of Economic Integration 22, 780–818.

Baltagi, B.H., Song, S.H., Jung, B.C., Koh, W., 2007. Testing for Serial Correlation, Spatial Autocorrelation and Random Effects Using Panel Data. Journal of Econometrics 140, 5–51.

Banerjee, A., Duflo, E., Qian, N., 2012. On the Road: Access to Transportation Infrastructure and Economic Growth in China. NBER Working Paper 17897.

Barnett, J., Webber, M., 2010. Accommodating Migration to Promote Adaptation to Climate Change. World Bank Policy Research Working Paper 5270.

Barrios, S., Bertinelli, L., Strobl, E., 2006. Climatic Change and Rural-Urban Migration: The Case of Sub-Saharan Africa. Journal of Urban Economics 60, 357–371.

Baugh, K., Elvidge, C.D., Ghosh, T., Ziskin, D., 2010. Development of a 2009 Stable Lights Product Using DMSP-OLS Data. Proceedings of the Asia-Pacific Advanced Network 30, 114.

Beine, M., Bertoli, S., Fernández-Huertas Moraga, J., 2016. A Practitioners' Guide to Gravity Models of International Migration. The World Economy 39, 496–512.

Beine, M., Docquier, F., Özden, Ç., 2011. Diasporas. Journal of Development Economics 95, 30–41.

Beine, M., Parsons, C., 2015. Climatic Factors as Determinants of International Migration. Scandinavian Journal of Economics 117, 723–767.

Beine, M., Parsons, C., 2017. Climatic factors as determinants of international migration: Redux. CESifo Economic Studies 63, 386–402.

Berger, H., Nitsch, V., 2008. Zooming Out: The Trade Effect of the Euro in Historical Perspective. Journal of International Money and Finance 27, 1244–1260.

Bergin, P., Lin, C., 2012. The Dynamic Effects of a Currency Union on Trade. Journal of International Economics 87, 191–204.

Bergstrand, J.H., Larch, M., Yotov, Y., 2015. Economic Integration Agreements, Border Effects, and Distance Elasticities in the Gravity Equation. European Economic Review 78, 307–327.

Bertinelli, L., Strobl, E., 2013. Quantifying the Local Economic Growth Impact of Hurricane Strikes: An Analysis from Outer Space for the Caribbean. Journal of Applied Meteorology and Climatology 52, 1688–1697.

Bertoli, S., Fernández-Huertas Moraga, J., 2012. Visa Policies, Networks and the Cliff at the Border. IZA Discussion Paper 7094.

Beverelli, C., Keck, A., Larch, M., Yotov, Y., 2018. Institutions, Trade and Development: A Quantitative Analysis. CESifo Working Paper 6920.

Bleakley, H., Lin, J., 2012. Portage and Path Dependence. Quarterly Journal of Economics 127, 587–644.

Bluhm, R., Krause, M., 2017. Top Lights Bright Spots and Their Contribution to Economic Development. Mimeo University of Hamburg .

Boehmer, M., Limbers, J., Pivac, A., Weinelt, H., 2016. Departure from the Schengen Agreement – Macroeconomic Impacts of Germany and the Countries of the European Union. GED Study on behalf of Bertelsmann Foundation. Prognos AG.

Boeri, T., Brücker, H., 2005. Why are Europeans so Tough on Migrants? Economic Policy 20, 629–703.

Borjas, G., 1987. Self-Selection and the Earnings of Immigrants. American Economic Review 77, 531–553.

Borjas, G., 1989. Economic Theory and International Migration. International Migration Review 23, 457–485.

Bun, M., Klaassen, F., 2007. The Euro Effect on Trade is Not as Large as Commonly Thought. Oxford Bulletin of Economics and Statistics 69, 473–496.

Burke, M., Emerick, K., 2016. Adaptation to Climate Change: Evidence from US Agriculture. American Economic Journal: Economic Policy 8, 106–40.

Camarero, M., Gómez, E., Tamarit, C., 2014. Is the Euro Effect on Trade So Small After All? New Evidence Using Gravity Equations with Panel Cointegration Techniques. Economics Letters 124, 140–142.

Canuto, O., Ratha, D., 2011. Migration and Remittances Factbook 2011. The World Bank.

Cattaneo, C., Peri, G., 2016. The Migration Response to Increasing Temperatures. Journal of Development Economics 122, 127–146.

Cavallo, E., Galiani, S., Noy, I., Pantano, J., 2013. Catastrophic Natural Disasters and Economic Growth. Review of Economics and Statistics 95, 1549–1561.

Cavallo, E., Noy, I., 2011. Natural Disasters and the Economy — A Survey. International Review of Environmental and Resource Economics 5, 63–102.

Chang, S.E., 2010. Urban Disaster Recovery: A Measurement Framework and its Application to the 1995 Kobe Earthquake. Disasters 34, 303–327.

Chen, N., 2004. Intra-National Versus International Trade in the European Union: Why Do National Borders Matter? Journal of International Economics 63, 93–118.

Chen, N., Novy, D., 2011. Gravity, Trade Integration, and Heterogeneity across Industries. Journal of International Economics 85, 206–221.

Chen, X., Nordhaus, W., 2011. Using Luminosity Data as a Proxy for Economic Statistics. Proceedings of the National Academy of Sciences 108, 8589–8594.

Coniglio, N., Pesce, G., 2015. Climate Variability and International Migration: An Empirical Analysis. Environment and Development Economics 20, 434–468.

Conley, T.G., 1999. GMM Estimation with Cross Sectional Dependence. Journal of Econometrics 92, 1–45.

Conley, T.G., 2008. Spatial Econometrics, in: Durlauf, S.N., Blume, L.E. (Eds.), The New Palgrave Dictionary of Economics. Palgrave Macmillan.

Costinot, A., Donaldson, D., Smith, C., 2016. Evolving Comparative Advantage and the Impact of Climate Change in Agricultural Markets: Evidence from 1.7 Million Fields Around the World. Journal of Political Economy 124, 205–248.

Cox, D.R., 1958. Planning of Experiments. John Wiley & Sons, Inc.

Dai, M., Yotov, Y., Zylkin, T., 2014. On the Trade-Diversion Effects of Free Trade Agreements. Economics Letters 122, 321–325.

Davis, D., Gift, T., 2014. The Positive Effects of the Schengen Agreement on European Trade. World Economy 37, 1541–1557.

Deschênes, O., Greenstone, M., 2012. The Economic Impacts of Climate Change: Evidence from Agricultural Output and Random Fluctuations in Weather: Reply. American Economic Review 102, 3761–3773.

Desmet, K., Nagy, D.K., Rossi-Hansberg, E., 2018. The Geography of Development. Journal of Political Economy 126, 903–983.

Desmet, K., Rossi-Hansberg, E., 2015. On the Spatial Economic Impact of Global Warming. Journal of Urban Economics 88, 16–37.

Dijkstra, E.W., 1959. A Note on Two Problems in Connexion with Graphs. Numerische Mathematik 1, 269–271.

Docquier, F., Lodigiani, E., 2010. Skilled Migration and Business Networks. Open Economies Review 21, 565–588.

Docquier, F., Peri, G., Ruyssen, I., 2014. The Cross-Country Determinants of Potential and Actual Migration. International Migration Review 48, 37–99.

Doll, C., 2008. CIESIN Thematic Guide to Night-Time Light Remote Sensing and its Applications. Palisades, NY: Center for International Earth Science Information Network (CIESIN) of Columbia University.

Doll, C.N., Muller, J.P., Morley, J.G., 2006. Mapping Regional Economic Activity from Night-Time Light Satellite Imagery. Ecological Economics 57, 75–92.

Donaldson, D., Storeygard, A., 2016. The View from Above: Applications of Satellite Data in Economics. Journal of Economic Perspectives 30, 171–98.

Drabo, A., Mbaye, L.M., 2015. Natural Disasters, Migration and Education: An Empirical Analysis in Developing Countries. Environment and Development Economics 20, 767–796.

Earth Observation Group, 2016. Version 4 DMSP-OLS Night-Time Lights Time Series.

Eaton, J., Kortum, S., 2002. Technology, Geography, and Trade. Econometrica 70, 1741–1779.

Economist, 2012. Heated Debate: The Costs of Climate Change Can be Mitigated if Economic Activity Moves in Response. The Economist, Dec 8th 2012.

Egan, M., Guimarães, M.H., 2017. The Single Market: Trade Barriers and Trade Remedies. Journal of Common Market Studies 55, 294–311.

Egger, P.H., Larch, M., Staub, K.E., 2012. Trade Preferences and Bilateral Trade in Goods and Services: A Structural Approach. CEPR Discussion Paper DP9051.

Elliott, R., Strobl, E., Sun, P., 2015. The Local Impact of Typhoons on Economic Activity in China: A View from Outer Space. Journal of Urban Economics 88, 50–66.

Elvidge, C.D., Hsu, F.C., Baugh, K.E., Ghosh, T., 2014. National Trends in Satellite Observed Lighting. Global Urban Monitoring and Assessment through Earth Observation 23, 97–118.

Elvidge, C.D., Sutton, P.C., Ghosh, T., Tuttle, B.T., Baugh, K.E., Bhaduri, B., Bright, E., 2009a. A Global Poverty Map Derived from Satellite Data. Computers & Geosciences 35, 1652–1660.

Elvidge, C.D., Ziskin, D., Baugh, K.E., Tuttle, B.T., Ghosh, T., Pack, D.W., Erwin, E.H., Zhizhin, M., 2009b. A Fifteen Year Record of Global Natural Gas Flaring Derived from Satellite Data. Energies 2, 595–622.

Environmental Systems Research Institute, 2016. Data and Maps for ARCGIS - World, Europe, and United States: World Roads.

Faber, B., 2014. Trade Integration, Market Size, and Industrialization: Evidence from China's National Trunk Highway System. Review of Economic Studies 81, 1046–1070.

Fally, T., 2015. Structural Gravity and Fixed Effects. Journal of International Economics 97, 76–85.

Fan, Y., Van den Dool, H., 2008. A Global Monthly Land Surface Air Temperature Analysis for 1948–Present. Journal of Geophysical Research: Atmospheres 113.

Feenstra, R., 2004. Advanced International Trade: Theory and Evidence. Princeton University Press.

Felbermayr, G., Gröschl, J., 2013. Natural Disasters and the Effect of Trade on Income: A New Panel IV Approach. European Economic Review 58, 18–30.

Felbermayr, G., Gröschl, J., 2014. Naturally Negative: The Growth Effects of Natural Disasters. Journal of Development Economics 111, 92–106.

Felbermayr, G., Gröschl, J., Sanders, M., Schippers, V., Steinwachs, T., 2018. Shedding Light on the Spatial Diffusion of Disasters. CESifo Working Paper 7146.

Fisher, A.C., Hanemann, W.M., Roberts, M.J., Schlenker, W., 2012. The Economic Impacts of Climate Change: Evidence From Agricultural Output and Random Fluctuations in Weather: Comment. American Economic Review 102, 3749–3760.

Flam, H., Nordström, H., 2006. Trade Volume Effects of the Euro: Aggregate and Sector Estimates. Seminar Paper No. 746, Institute for International Economic Studies .

Geiger, T., Frieler, K., Bresch, D.N., 2017. A Global Historical Data Set of Tropical Cyclone Exposure (TCE-DAT). Earth System Science Data 10.

Ghil, M., Yiou, P., Hallegatte, S., Malamud, B., Naveau, P., Soloviev, A., Friederichs, P., Keilis-Borok, V., Kondrashov, D., Kossobokov, V., et al., 2011. Extreme Events: Dynamics, Statistics and Prediction. Nonlinear Processes in Geophysics 18, 295–350.

Ghosh, T., Elvidge, C.D., Sutton, P.C., Baugh, K.E., Powell, R.L., Anderson, S., 2010. Shedding Light on the Global Distribution of Economic Activity. Open Geography Journal 3.

Gibbons, S., Overman, H.G., Patacchini, E., 2015. Spatial Methods. Handbook of Regional and Urban Economics 5, 115–168.

Gibson, J., McKenzie, D., 2011. The Microeconomic Determinants of Emigration and Return Migration of the Best and Brightest: Evidence from the Pacific. Journal of Development Economics 95, 18–29.

Grogger, J., Hanson, G., 2011. Income Maximization and the Selection and Sorting of International Migrants. Journal of Development Economics 95, 42–57.

Halleck Vega, S., Elhorst, J.P., 2015. The SLX Model. Journal of Regional Science 55, 339–363.

Hallegatte, S., 2008. An Adaptive Regional Input-Output Model and its Application to the Assessment of the Economic Cost of Katrina. Risk analysis 28, 779–799.

Hallegatte, S., Hourcade, J.C., Dumas, P., 2007. Why Economic Dynamics Matter in Assessing Climate Change Damages: Illustration on Extreme Events. Ecological economics 62, 330–340.

Hallegatte, S., Przyluski, V., 2010. The Economics of Natural Disasters: Concepts and Methods. World Bank Policy Research Working Paper 5507.

Harris, I., Jones, P., Osborn, T., Lister, D., 2014. Updated High-Resolution Grids of Monthly Climatic Observations – The CRU TS3. 10 Dataset. International Journal of Climatology 34, 623–642.

Haslett, J., Raftery, A.E., 1989. Space-Time Modeling with Long-Memory Dependence: Assessing Ireland's Wind Power Resource. Applied Statistics , 1–50.

Head, K., Mayer, T., 2014. Gravity Equations: Workhorse, Toolkit, and Cookbook, Amsterdam: Elsevir. volume 4 of *Handbook of International Economics*, pp. 131–195.

Helpman, E., Melitz, M., Rubinstein, Y., 2008. Estimating Trade Flows: Trading Partners and Trading Volumes. The Quarterly Journal of Economics 123, 441–487.

Henderson, J.V., Squires, T., Storeygard, A., Weil, D., 2017. The Global Distribution of Economic Activity: Nature, History, and the Role of Trade. Quarterly Journal of Economics 133, 357–406.

Henderson, J.V., Storeygard, A., Weil, D., 2012. Measuring Economic Growth from Outer Space. American Economic Review 102, 994–1028.

Hiemstra, P., Pebesma, E., Twenhöfel, C., Heuvelink, G., 2008. Real-Time Automatic Interpolation of Ambient Gamma Dose Rates From the Dutch Radioactivity Monitoring Network. Computers & Geosciences .

Hodler, R., Raschky, P.A., 2014. Regional Favoritism. Quarterly Journal of Economics 129, 995–1033.

Hofstra, N., Haylock, M., New, M., Jones, P., Frei, C., 2008. Comparison of Six Methods for the Interpolation of Daily European Climate Data. Journal of Geophysical Research: Atmospheres 113.

Hsiang, S.M., 2010. Temperatures and Cyclones Strongly Associated with Economic Production in the Caribbean and Central America. Proceedings of the National Academy of Sciences 107, 15367–15372.

Hsieh, C.T., Ossa, R., 2016. A Global View of Productivity Growth in China. Journal of International Economics 102, 209–224.

INCCCD, 1994. The Almeria Statement on Desertification and Migration. Intergovernmental Negotiating Committee for a Convention to Combat Desertification, Switzerland.

IPCC, 2012. Managing the Risks of Extreme Events Disasters to Advance Climate Change Adaptation. Intergovernmental Panel on Climate Change, IPCC, Geneva, Switzerland.

IPCC, 2014. Climate Change 2014: Synthesis Report. Contribution of Working Groups I, II and III to the Fifth Assessment Report of the Intergovernmental Panel on Climate Change. [Core Writing Team, Pachauri, R.K., Meyer, L.A. (Eds.)]. IPCC, Geneva, Switzerland .

Islam, N., 1995. Growth Empirics: A Panel Data Approach. Quarterly Journal of Economics 110, 1127–1170.

Kahn, M.E., 2005. The Death Toll from Natural Disasters: The Role of Income, Geography, and Institutions. Review of Economics and Statistics 87, 271–284.

Keola, S., Andersson, M., Hall, O., 2015. Monitoring Economic Development from Space: Using Night-Time Light and Land Cover Data to Measure Economic Growth. World Development 66, 322–334.

Klomp, J., Valckx, K., 2014. Natural Disasters and Economic Growth: A Meta-Analysis. Global Environmental Change 26, 183–195.

Kocornik-Mina, A., McDermott, T., Michaels, G., Rauch, F., 2015. Flooded Cities. University of Oxford Department of Economics Discussion Paper Series 772.

Kraus, E., 1977. Subtropical Droughts and Cross-Equatorial Energy Transports. Monthly Weather Review 105, 1009–1018.

Krige, D.G., 1951. A Statistical Approach to Some Basic Mine Valuation Problems on the Witwatersrand. Journal of the Southern African Institute of Mining and Metallurgy 52, 119–139.

Kugler, M., Rapoport, H., 2007. International Labor and Capital Flows: Complements or Substitutes? Economics Letters 94, 155–162.

LeSage, J.P., Pace, R.K., 2009. Introduction to Spatial Econometrics. Taylor and Francis, Boca Raton, FL.

Letouzé, E., Purser, M., Rodriguez, F., Cummins, M., 2009. Revisiting the Migration-Development Nexus: A Gravity Model Approach. Human Development Research Papers 2009/44.

Lewer, J., Van den Berg, H., 2008. A Gravity Model of Immigration. Economics Letters 99, 164–167.

Marchiori, L., Schumacher, I., 2011. When Nature Rebels: International Migration, Climate Change, and Inequality. Journal of Population Economics 24, 569–600.

Mayda, A., 2010. International Migration: A Panel Data Analysis of The Determinants of Bilateral Flows. Journal of Population Economics 23, 1249–1274.

Mbaye, L., Zimmermann, K., 2015. Environmental Disasters and Migration. IZA Discussion Paper 9349.

McCallum, J., 1995. National Borders Matter: Canada-US Regional Trade Patterns. American Economic Review 85, 615–623.

McFadden, D., 1974. Conditional Logit Analysis of Qualitative Choice Behavior, Academic Press. Frontiers in Econometrics, pp. 105–142.

McKee, T., Doesken, N., Kleist, J., 1993. The Relationship of Drought Frequency and Duration to Time Scales, in: Proceedings of the 8th Conference on Applied Climatology, American Meteorological Society Boston, MA. pp. 179–183.

McLeman, R., Smit, B., 2006. Migration as an Adaptation to Climate Change. Climatic Change 76, 31–53.

Micco, A., Stein, E., Ordoñez, G., 2003. The Currency Union Effect on Trade: Early Evidence from EMU. Economic Policy 18, 315–356.

Michalopoulos, S., Papaioannou, E., 2013. Pre-Colonial Ethnic Institutions and Contemporary African Development. Econometrica 81, 113–152.

Michalopoulos, S., Papaioannou, E., 2014. National Institutions and Subnational Development in Africa. Quarterly Journal of Economics 129, 151–213.

Millo, G., 2014. Maximum Likelihood Estimation of Spatially and Serially Correlated Panels with Random Effects. Computational Statistics & Data Analysis 71, 914–933.

Millo, G., Piras, G., 2012. SPLM: Spatial Panel Data Models in R. Journal of Statistical Software 47, 1–38.

Mincer, J., 1978. Family Migration Decisions. Journal of Political Economy 86, 749–773.

Monar, J., 2014. Justice and Home Affairs. Journal of Common Market Studies 52, 141–156.

Moran, P.A., 1950. Notes on Continuous Stochastic Phenomena. Biometrika 37, 17–23.

Munshi, K., 2003. Networks in the Modern Economy: Mexican Migrants in the US Labor Market. Quarterly Journal of Economics 118, 549–599.

Munshi, K., 2014. Community Networks and Migration, in: The Oxford Handbook of the Economics of Networks. Oxford University Press.

Myers, N., Myers, N., 2002. Environmental Refugees: A Growing Phenomenon of the 21st Century. Philosophical Transactions of the Royal Society of London. Series B: Biological Sciences 357, 609–613.

Naudé, W., 2010. The Determinants of Migration from Sub-Saharan African Countries. Journal of African Economies 19, 330–356.

Nicholson, S.E., 1986. The Spatial Coherence of African Rainfall Anomalies: Interhemispheric Teleconnections. Journal of Climate and Applied Meteorology 25, 1365–1381.

Nizalova, O.Y., Murtazashvili, I., 2016. Exogenous Treatment and Endogenous Factors: Vanishing of Omitted Variable Bias on the Interaction Term. Journal of Econometric Methods 5, 71–77.

Nordhaus, W., Chen, X., 2009. Geography: Graphics and Economics. The BE Journal of Economic Analysis & Policy 9.

Nordhaus, W., Chen, X., 2015. A Sharper Image? Estimates of the Precision of Night-Time Lights as a Proxy for Economic Statistics. Journal of Economic Geography 15, 217–246.

Noy, I., 2009. The Macroeconomic Consequences of Disasters. Journal of Development Economics 88, 221–231.

Noy, I., Nualsri, A., 2011. Fiscal Storms: Public Spending and Revenues in the Aftermath of Natural Disasters. Environment and Development Economics 16, 113–128.

Obstfeld, M., Rogoff, K., 2000. The Six Major Puzzles in International Macroeconomics: Is There a Common Cause? NBER Macroeconomics Annual 15, 339–390.

Ortega, F., Peri, G., 2009. The Causes and Effects of International Migrations: Evidence from OECD Countries 1980-2005. NBER Working Paper 14833.

Ortega, F., Peri, G., 2015. Migration Policies: Recent Advances on Measurement, Determinants and Outcomes. CESifo Economic Studies 61, 521–526.

Patel, K., Vella, F., 2013. Immigrant Networks and their Implications for Occupational Choice and Wages. Review of Economics and Statistics 95, 1249–1277.

Pedersen, P., Pytlikova, M., Smith, N., 2008. Selection and Network Effects – Migration Flows Into OECD Countries 1990–2000. European Economic Review 52, 1160–1186.

Piermartini, R., Yotov, Y., 2016. Estimating Trade Policy Effects with Structural Gravity. WTO Staff Working Paper ERSD-2016-10.

Piguet, E., Pécoud, A., De Guchteneire, P., 2011. Migration and Climate Change: An Overview. Refugee Survey Quarterly 30, 1–23.

Pinkovskiy, M., Sala-i Martin, X., 2016. Lights, Camera … Income! Illuminating the National Accounts-Household Surveys Debate. Quarterly Journal of Economics 131, 579–631.

Raddatz, C., 2007. Are External Shocks Responsible for the Instability of Output in Low-Income Countries? Journal of Development Economics 84, 155–187.

Ratha, D., Shaw, W., 2007. South-South migration and remittances. The World Bank.

Rauch, J., Trindade, V., 2002. Ethnic Chinese Networks in International Trade. Review of Economics and Statistics 84, 116–130.

Reuveny, R., Moore, W., 2009. Does Environmental Degradation Influence Migration? Emigration to Developed Countries in the Late 1980s and 1990s. Social Science Quarterly 90, 461–479.

Rubin, D.B., 1980. Randomization Analysis of Experimental Data: The Fisher Randomization Test. Journal of the American Statistical Association 75, 591–593.

Samuelson, P.A., 1954. The Transfer Problem and Transport Costs, II: Analysis of Effects of Trade Impediments. The Economic Journal 64, 264–289.

Santos Silva, J., Tenreyro, S., 2006. The Log of Gravity. Review of Economics and Statistics 88, 641–658.

Santos Silva, J., Tenreyro, S., 2011. Further Simulation Evidence on the Performance of the Poisson Pseudo-Maximum Likelihood Estimator. Economics Letters 112, 220–222.

Schneider, A., Friedl, M.A., Potere, D., 2009. A New Map of Global Urban Extent from MODIS Satellite Data. Environmental Research Letters 4.

Schneider, F., 2005. Shadow Economies Around the World: What Do We Really Know? European Journal of Political Economy 21, 598–642.

Schneider, F., Enste, D.H., 2000. Shadow Economies: Size, Causes, and Consequences. Journal of Economic Literature 38, 77–114.

Scrucca, L., Fop, M., Murphy, T.B., Raftery, A.E., 2016. mclust 5: Clustering, Classification and Density Estimation Using Gaussian Finite Mixture Models. The R Journal 8, 205–233.

Sjaastad, L., 1962. The Costs and Returns of Human Migration. Journal of Political Economy 70, 80–93.

Skidmore, M., Toya, H., 2002. Do Natural Disasters Promote Long-Run Growth? Economic Inquiry 40, 664–687.

Stark, O., 1991. The Migration of Labor. Blackwell Oxford.

Stein, M., 1999. Interpolation of Spatial Data. Springer UK.

Stern, N., 2006. Stern Review on the Economics of Climate Change. Cambridge University Press.

Storeygard, A., 2016. Farther on Down the Road: Transport Costs, Trade and Urban Growth in Sub-Saharan Africa. Review of Economic Studies 83, 1263–1295.

Strobl, E., 2011. The Economic Growth Impact of Hurricanes: Evidence from US Coastal Counties. Review of Economics and Statistics 93, 575–589.

Strömberg, D., 2007. Natural Disasters, Economic Development, and Humanitarian Aid. Journal of Economic Perspectives 21, 199–222.

Tacoli, C., 2009. Crisis or Adaptation? Migration and Climate Change in a Context of High Mobility. Environment and Urbanization 21, 513–525.

Tanaka, K., Keola, S., 2017. Shedding Light on the Shadow Economy: A Night-Time Light Approach. Journal of Development Studies 53, 32–48.

Timmer, M., Dietzenbacher, E., Los, B., Stehrer, R., Vries, G., 2015. An Illustrated User Guide to the World Input–Output Database: the Case of Global Automotive Production. Review of International Economics 23, 575–605.

Tinbergen, J., 1962. Shaping the World Economy: Suggestions for an International Economic Policy. Twentieth Century Fund.

Tobler, W.R., 1970. A Computer Movie Simulating Urban Growth in the Detroit Region. Economic Geography 46, 234–240.

Toya, H., Skidmore, M., 2007. Economic Development and the Impacts of Natural Disasters. Economics Letters 94, 20–25.

Trauner, F., Ripoll Servent, A., 2016. The Communitarization of the Area of Freedom, Security and Justice: Why Institutional Change does not Translate into Policy Change. Journal of Common Market Studies 54, 1417–1432.

Vicente-Serrano, S.M., Beguería, S., López-Moreno, J.I., 2010. A Multiscalar Drought Index Sensitive to Global Warming: The Standardized Precipitation Evapotranspiration Index. Journal of Climate 23, 1696–1718.

Wooldridge, J., 2003. Introductory Econometrics: A Modern Approach. 2 ed., Thomson South-Western.

World Bank, 2012. Turn Down the Heat: Why a 4 Degree Celsius Warmer World Must be Avoided. International Bank for Reconstruction and Development / The World Bank.

World Bank, United Nations, 2010. Natural Hazards, UnNatural Disasters: The Economics of Effective Prevention. The World Bank.

Wu, J., Wang, Z., Li, W., Peng, J., 2013. Exploring Factors Affecting the Relationship Between Light Consumption and GDP Based on DMSP/OLS Night-Time Satellite Imagery. Remote Sensing of Environment 134, 111–119.

Yotov, Y., 2012. A Simple Solution to the Distance Puzzle in International Trade. Economics Letters 117, 794–798.

Yotov, Y., Piermartini, R., Monteiro, J.A., Larch, M., 2016. An Advanced Guide to Trade Policy Analysis: The Structural Gravity Model. World Trade Organization Geneva.

# Curriculum Vitae

Thomas Steinwachs
born 06/06/1986 in Fulda

| | |
|---|---|
| since 04/2014 | Junior Economist and Doctoral Student<br>ifo Institute – Leibniz Institute for Economic Research, Munich |
| 04/2014 – 01/2019 | Ph.D. Program in Economics (Dr. oec. publ.)<br>Munich Graduate School of Economics<br>Ludwig-Maximilians-Universität, Munich |
| 11/2013 – 01/2014 | Teacher in Economics and Business<br>BBZ Mitte GmbH, Petersberg |
| 04/2012 – 03/2013 | Research Assistant<br>Chair in International Economics, Eberhard Karls Universität, Tübingen |
| 05/2011 – 04/2013 | Master of Science in International Economics and European Studies<br>Eberhard Karls Universität, Tübingen |
| 02/2011 – 03/2012 | Student Assistant<br>Department for Business Relations, Faculty of Economics,<br>Eberhard Karls Universität, Tübingen |
| 11/2009 – 01/2013 | Volunteer in International Development Cooperation<br>Studieren Ohne Grenzen Deutschland e.V., Tübingen |
| 10/2006 – 04/2011 | Bachelor of Science in International Economics and European Studies<br>Eberhard Karls Universität, Tübingen and<br>University of Adelaide, South Australia |
| 07/2006 | Abitur<br>Modellschule Obersberg, Bad Hersfeld |